Electronic Thesis and Dissertation Repository

8-9-2017 12:00 AM

Fault Location in High Voltage Shunt Capacitor Banks

Hessamoddin Jouybari Moghaddam, *The University of Western Ontario*

Supervisor: Dr. Tarlochan Sidhu, *The University of Western Ontario*
A thesis submitted in partial fulfillment of the requirements for the Doctor of Philosophy degree in Electrical and Computer Engineering
© Hessamoddin Jouybari Moghaddam 2017

Follow this and additional works at: https://ir.lib.uwo.ca/etd

⚛ Part of the Power and Energy Commons

Abstract

This thesis is focused on developing and investigating methods for locating internal failures in High Voltage (HV) Shunt Capacitor Banks (SCBs). Integrating fault location algorithms into capacitor bank protective relays has become more vital with SCBs being more widely in use and unbalance being a major occurrence. Specifically, this is of importance for large (high voltage) SCBs, which have a wider search space in terms of the number of elements and units that comprise the bank. Localizing the fault location problem is an attempt towards reducing the outage (repair) time of SCBs with advantages such as planning preventive maintenance and reducing unscheduled outages of the SCBs.

The challenges for determining the location of internal failures and continuous monitoring of the SCBs for this application are: first, no outward indication for the common fusing technologies of SCBs (internally fused and fuseless), second, the offsetting (balancing) effect of subsequent failures against the low impact of the previous failures (i.e. ambiguous failures), third, compensating for other sources of unbalance, such as manufacturing tolerances, gradual capacitance changes, and system unbalances, and last, less than ideal number of available measurements.

In this thesis, first the ultra sensitive protection, unbalance protection, that is the conventional method for detecting internal failures is reviewed. This protection strategy would be the backbone for fault location methods. In the area of monitoring internal failures and fault location of SCBs very little research work has been reported in the literature. A chapter will cover the existing methods that are either directly related to this topic or indirectly perform the same application. Furthermore, a relevant method in the literature is investigated in more details.

Intimate connection exists between bank designs and unbalance protection methods. Therefore, different configurations have different advantages or shortcomings in terms of fault location. Having reviewed various connections, the ones that are more common or have more challenges in terms of available measurements are intended for proposing new methods for internal failure determination or enhancing the fault location algorithms.

In a separate chapter, first a new indicating quantity that employs automatic calibrating factors is proposed. The method overcomes the mentioned challenges and is further adapted to suit three of the common SCB grounding arrangements. The indicating quantity is referred to as Superimposed Reactance method and can be integrated into voltage-based unbalance protection functions to enhance the extracted information from detected failures. Then current-based unbalance protection methods for double wye banks are considered and a fault location method that applies a combination of self-tuning and auto-setting of k-factors is proposed for this type of banks.

In another part of the proposed method's chapter, envision of additional unbalance protection functions is discussed. While it is seldom economic to add voltage or current transducers for solely fault location purpose, two common protection philosophies with additional measurements are discussed in terms of fault location application.
In the last part of the chapter, provisions for the proposed algorithm security and also the proposed methods usage and information display are presented.

The performance of the investigated methods of the literature and the proposed methods are assessed in a separate chapter. Various internal failure scenarios and external

disturbances are studied to both examine the algorithm security and dependability. Simulations consider capacitor banks adapted from the literature and also actual banks in existing utility systems.

The work is extended by discussing other applications rather than only fault location determination for the proposed methods, accordingly online monitoring aspect is elaborated. In summarized tables the proposed method output operands are compared with the present methods in the literature. Fuse saving for externally fused banks is another application of the proposed methods which is verified using an illustrative scenario. A commercial relay is also tested by play back of COMTRADE files from PSCAD simulations to demonstrate the shortcomings of conventional unbalance relaying methods in terms of ambiguous failures online monitoring in comparison with the proposed methods.

Keywords: capacitor failure, condition monitoring, fault location, fault report, fuse, internal failure, online monitoring, preventive alarm, protective relays, shunt capacitor banks.

Dedication

To my parents, and my grandma

Acknowlegements

I would like to express my sincere gratitude to Dr. Tarlochan Singh Sidhu for his guidance, support, and continuous encouragement throughout the course of this research. It has been a great privilege to pursue my higher education under his supervision.

I give great thanks to my parents, Mr. A. Jouybari and Mrs. Z. Sani, and my grandma Mrs. S. Pouzesh for their love, support, encouragement and patience.

I am thankful to my friends in London, ON for helping me through the difficult times and for their support and care.

Contents

List of Figures

List of Tables

List of Appendices

Chapter 1

Introduction

1.1 Problem statement and research objectives

Today, complex transmission systems demand increasing amount of reactive power support which is to be supplied by transmission providers. Shunt Capacitor Banks (SCBs), Figure 1.1, are critical power system apparatus that are mainly installed for this VAR demand. Benefits from installation of SCBs includes: relatively inexpensive voltage support, power factor correction, providing VAR support for distributed energy resources, and keeping FACTS devices within their capacity limits. Relieving reactive power requirements itself leads to reduction of losses and can also help to postpone investments in transmission and generation capacities. Although SCBs are not new in terms of application and their introduction to power system, there has been little research on advanced methods for their protection. The reason for less interest in development of SCBs advanced dedicated relays is because SCBs are historically considered a relatively low-volume market [6]. Referring back to early research on SCBs monitoring and protection, papers and patents include discussing the general protection methods [7–9], special logics for discrimination between an internal fault and a system fault for a capacitor battery [10], effects of system disturbances on security of protection functions for SCBs [11, 12], detection of high impedance ground faults within a SCB that benefits from perphase voltage differential protection [13], and direct impedance measurements for unbalance detection [14].

Fault location for various power apparatus is different in the level of selectivity and search space reduction. For example for transmission lines fault location can point out the exact distance at which the fault has occurred. For SCBs the less than ideal number of available measurements limits the fault location to the affected phase detection and in case of double wye connections to the affected wye section. There are a few recent publications for fault location in SCBs. The faulted phase determination is adequate enough to narrow the search area and reduce the investigation time for locating the fault by at least 66.6 %. In addition, in single wye SCBs with tapped potential transformers (PT) or in double wye SCBs with neutral current transformers (CT), this search area can be reduced by 83.3 % because in these configurations each phase has two sections that are distinguishable in terms of failure location. As a result, IEEE guide for pro-

Figure 1.1: High Voltage Shunt Capacitor Banks (Scale Illustration).

tection of SCBs [2] recommends fault location logics as effective methods to speed up troubleshooting and repair of the banks. Summing up, higher availability of supporting reactive power is an advantage that the current research is looking for.

1.1.1   Challenges

Failure of an element/unit will increase the voltage stress on the remaining series elements/units. The more the number of the failed units, the greater the stress and thus less time between the failures. As a result, cascading failure is the condition that must be taken care of by not missing the detection of any failure inside the SCB.

Knowing the location of the failure (i.e. the phase and, for double wye configurations, the wye section containing the fault) would eventually result in increasing the total in-service time of SCBs. This is realized by either minimizing the searching time for the failed elements in the repair process or by enabling advance preventive maintenance schedules. Few available measurements and metering accuracies make the fault location techniques to be challenging especially when considering the effect of a single element failure among hundreds of elements in the measured signals.

Another challenge is the masking or offsetting effect which stands for the condition at which a subsequent failure cancels out the unbalance seen by the relay and thus makes the failure location detection false or insensitive. For H-bridge SCBs, the masking happens when a second failure occurs in the opposite diagonal of an existing failure. For double wye SCBs, same phase faults on both sections may become hidden from the relay. Similarly, same number of element failures on all three phases in a section are the cases that may not be detected. Also, failures on two phases in a section can be mis-detected for a failure in the other phase of the other section. Comparably, in single wye SCBs, when failures exist in all three phases the bank might seem balanced to the relay and failures in two phases may become mis-detected for an unbalance in the other phase. Figure 1.2 illustrates these scenarios.

In order to introduce highly sensitive fault location methods, the technique must also be able to accurately and completely compensate for the inherent unbalances in the SCB and the system voltage unbalances. In addition, gradual capacitance changes due to temperature variations and aging should be compensated. Shading effect is also another similar case which occurs at times that part of the SCB may be under direct sunlight while the other part is in the shade. Compensating for these slight and low rate changes at regular time interval has to be considered in a fault location method.

1.1.2   Motivation

In the following parts it is explained why the fault location function is an emerging crucial requirement for capacitor bank protection and monitoring relays in the modern electrical power systems.

The popular design requires sensitive relaying

Single phase capacitor units constitute a shunt capacitor bank. With these units connected in parallel and series, the desired voltage rating and reactive power rating would be achieved. In a similar way, capacitor elements form a capacitor unit with their parallel and series combination.

Capacitor units in their early generation needed fuses because they were very vulnerable to case rupture (as there was no control over minor internal faults until they became a major fault). These *Externally fused* banks are known for higher operating costs and bank unavailability. A capacitor unit with a blown fuse requires the capacitor bank to be taken out of service and hence, reduces the time that SCB is available and benefits the system. Because pollution, corrosion, and fluctuating climatic conditions reduce the reliability of external fuses, they have to be checked and replaced periodically [1]. Figure 1.3 shows an externally fused capacitor unit.

In another fusing method called *Internally fused*, the isolation of a failed capacitor element allows the capacitor bank to remain in service. The design reduces the vulnerability to faults from animals climbing inside the bank. Figure 1.4 demonstrates an internally fused design for capacitor units.

High quality insulating materials has made the role played by SCB fuses to become secondary. The prevalent dielectric type for the HV power capacitors is polypropylene

Single Wye

Double Wye

H-Bridge
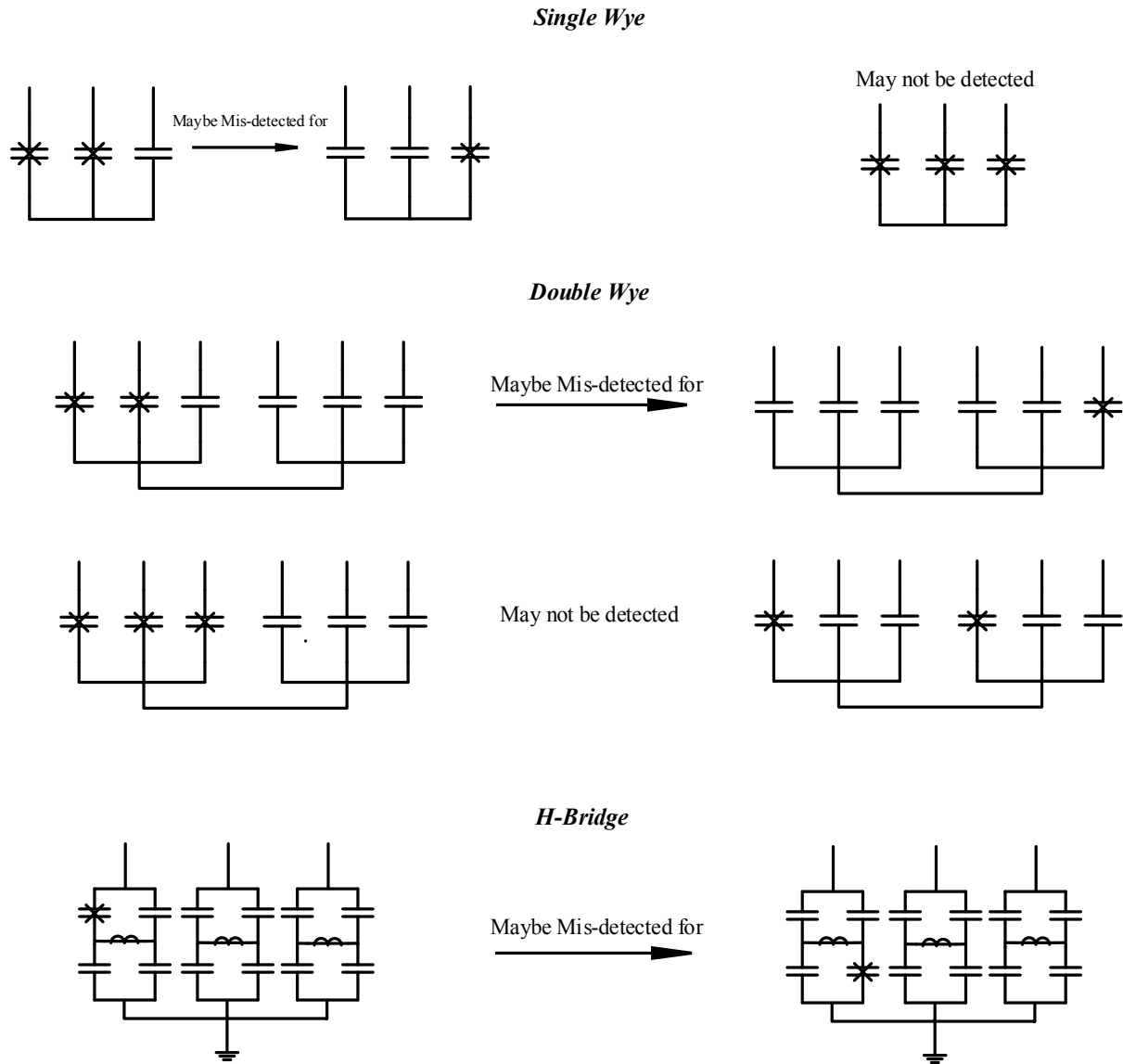
Figure 1.2: Masking or offsetting effect.
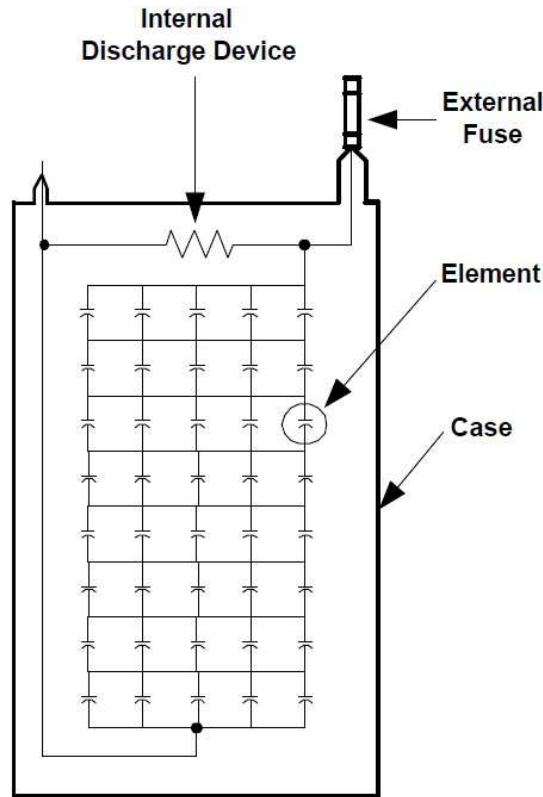
Figure 1.3: Externally fused capacitor unit [1].

film. These films are impregnated with synthetic fluid such as Faradol 810 or other biodegradable PCB free oils [15]. As a result, fuseless designs have been introduced. They have the advantage of being cheaper and having lower losses, i.e. RI^2 losses associated with capacitor can as capacitor fuses are not present in these bank designs. Heavy duty welding of the two foil electrodes within the failed element minimizes the chance of continued arcing [16]. Figure 1.5 illustrates this design. Depending on whether the groups of capacitor units are connected in series or in series/parallel from phase to neutral, capacitor banks without fuse may also be called unfused instead of fuseless [17]. The operating voltage level changes according to the arrangement of units [3], i.e. unfused banks are normally used for systems with voltages below 34.5 kV, for voltages equal or higher than this value fuseless banks are in service.

In short, while the fuseless units are superior in terms of lower losses associated with fuses, both of fuseless and internally fused technologies are advantageous to the externally fused designs. With instantaneous disconnection/shorting out of the faulty element, these designs prevent from cascading element failures inside the capacitor units. Although manufacturers have adopted these technologies for higher availability of the SCB and lower maintenance costs, but internally protected capacitor units have the disadvantage of low transient withstand capability of their low rating fuses [18] and no visual indication for the unit with failed elements– all film capacitors even do not bulge when a failure occurs [19]. Historically, SCB's maintenance is a time-consuming task
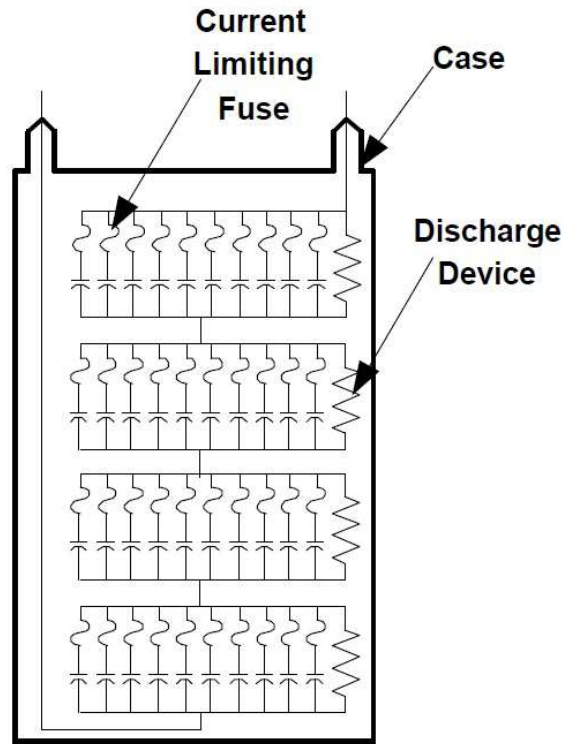
Figure 1.4: Internally fused capacitor unit [1].
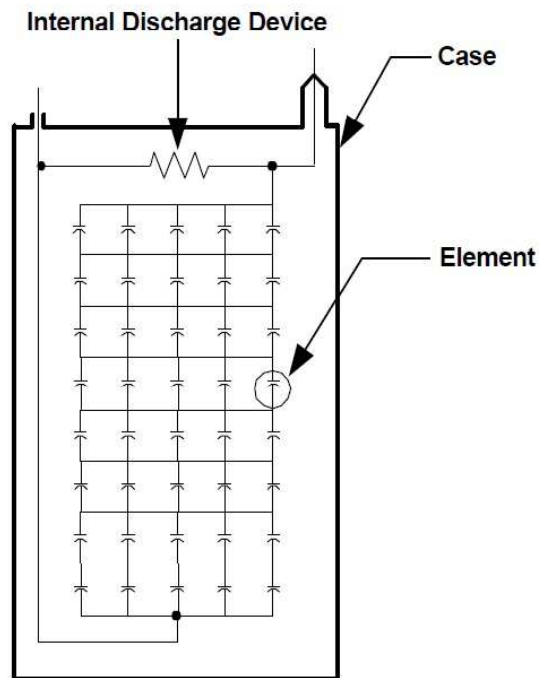
Figure 1.5: Fuseless capacitor unit [1].

for utilities [20]. With unbalance being a major occurrence due to the dielectric failure, developing methods for determining the involved phase is an advancement for SCB protection and control relays. This helps the crew by reducing the search space to a particular phase for repair and preparing the bank faster for service.

The increased frequency of failures in today's grid

Modern grids work close to their operation limits, and over-voltage duty is placed on transmission systems by today's load flow requirements. Utilities have also reported an increase in the frequency of failures in SCBs in recent years [21]. Integrating fault location algorithms into capacitor bank protective relays has become more vital with SCBs being more widely in use. Specifically, this is of importance for large (high voltage) SCBs which have a larger search space in terms of the number of elements and units that comprise the bank.

Outage times and incidents in Canada

The Canadian Electricity Association reports major transmission equipment statistics annually. For shunt capacitor banks, considering failures of capacitors, bushings, and insulation, SCBs at different voltage levels have had time consuming repair and recovery of service. For banks with 60 kV-109 kV voltage rating, the average repair time (forced unavailable time) studied over a period of five years, 1998-2002, has been reported to be 555.2 hours- same statistic for banks of 200 kV-299 kV has been 140.6 hours. The total outage time over this interval at 60 kV-109 kV has been 231,520 hours for 417 SCB outages. A single bank outage incident at extra high voltage level, 600 kV- 799 kV, has resulted in 10 hours of repair or replacement time [22]. The recent SCB installations in south western Ontario and a recent incident in greater Toronto area originating from SCB switching and grounding issues can also be mentioned as local examples that motivate research topics on protection and monitoring of SCBs. For details on installation of seven 230 kV SCBs in transmission stations across south western Ontario see [23]. For the incident at Richview Transformer station that resulted in substantial damage to the 230 kV SCBs and their breakers see [24].

1.1.3   Research objectives

The thesis objectives are:

- To investigate a relevant commercial fault location method and to do performance analysis for that, under special challenging scenarios

- To develop an enhanced fault location technique for SCBs protected with neutral current unbalance protection (both grounded and ungrounded), in order to prevent ambiguous indications and provide live report of number of failures

- To introduce a new fault location indicating quantity for banks with voltage based unbalance protection, in order to detect consecutive failures and provide live report of number of failed elements. The method is intended to be applicable to different grounding arrangements

- To expand the concept of fault location to online monitoring for fuse saving in externally fused banks

- To apply self-tuning and auto-setting to voltage differential unbalance protection

- To investigate and discuss applicability of neutral voltage unbalance estimation for fault location of double wye SCBs

- To discuss the proposed methods advantages to a conventional unbalance protection method alarms by testing a commercial relay

Furthermore, all of the developed fault location methods have the following properties:

- Making the best out of the available measurements

- Deploying k-factor auto-setting and self-tuning concept

- Compensating for pre-existing inherent unbalance in the SCB (manufacturing tolerances) and system voltage unbalance

- Compensating for gradual changes in the capacitance (aging, temperature impacts)

- Determining consecutive failures location

- Determining number of failed capacitor elements

- Verified for reliable operation considering system harmonics, system voltage unbalance, measurement noise, and power system disturbances

1.2   Thesis outline

Chapter 2 gives an overview of the unbalance protection methods whose purpose is to remove the bank from service for any fault that is likely to cause further damage. Dependent on the connection type and available transducers several unbalance protection methods exist. The chapter covers these methods and explains the theory of them. In case there are adjustments for the methods that increase their sensitivity it is explained in this chapter to help in forming the basis for fault location algorithm development. The conventional operating functions that help in discriminating internal failures from other unbalance signals are elaborated in this chapter.

Chapter 3 presents the current literature in the area of fault location in SCBs. The chapter includes investigation of the relevant methods theories. Because the present methods are restrictively disclosed, only in the form of patents, rather than academic papers; where applicable, this chapter is intended to find out the assumptions and derivation approach of these existing methods in the literature.

Chapter 4 introduces the proposed methods in this thesis. The chapter includes fault location principle development equations and any other estimation/calculation that is

used to add a property, such as detection of number of failed elements, to the proposed methods. The proposed methods cover different connections and fusing technologies: internally fused, and fuseless designs as well as both grounded and ungrounded configurations. Algorithm application settings, margins and blinder settings are discussed in this chapter as well. A discussion on additional measurements application is also provided.

Chapter 5 presents the simulation study and validation of the proposed fault location techniques. Power System Computer Aided Design (PSCAD) software is used for generating the voltage and current signals and then a relay model developed in MATLAB is used to playback and process the signals for fault location purpose. Evaluations are categorized to two different sections, the ones that focus on various internal failure scenarios and the ones that are for validation under special conditions like external unbalances.

Chapter 6 discusses applications of the proposed methods, such as fuse saving for externally fused SCBs, and extending the fault location function to an online monitoring system. A commercial relay's conventional unbalance protection is tested by play back of the PSCAD records to demonstrate the advantage of the proposed methods features for integration into this conventional unbalance relaying.

Chapter 7 summarizes the presented work. This chapter is followed by a list of references. Appendix A gives a more detailed information on software settings for the simulation study. Appendix B provides the simulated system and SCB specifications. Appendix C presents some additional plots for the algorithm evaluation. Appendix D provides additional results on measurement and phasor estimation accuracy. Appendix E gives further information for interested readers on capacitor banks and their protection.

1.3   Summary

This chapter has briefly introduced the role and importance of high voltage shunt capacitor banks in power systems. The problem of fault location and its application have been explained. Challenges and motivation for the present research have been outlined followed by the thesis organization. A literature review and investigation of a relevant fault location method will be discussed in the following chapter.

Chapter 2

Fault Location Fundamentals: Unbalance Protection

2.1   Introduction

SCBs protection consists of system protection schemes and bank protection schemes [2]. System protection schemes are required to handle abnormal system conditions, such as over/undervoltages and excessive transient overcurrents within a system and to disconnect the entire shunt capacitor bank in order to prevent further damage to the capacitors. On the other hand, bank protection schemes are required to protect faults within the capacitor bank. The main concerns in bank protection are unbalance problems within the bank due to faulted capacitor units or elements [13]. This is due to the fact that mild internal faults do not render high currents for external fuses or over current protection operation. Accordingly, unbalance relaying would be the proper sensitive solution for protection against internal failures and it can trip the element failures much faster [18]. This chapter presents the theory of unbalance protection methods as the main existing schemes that are in connection with internal failures in SCBs. Unbalance protection methods are the backbone of fault location methods. They use the evaluated unbalance for detection of abnormalities in a device. The known relationships among the measured voltages/currents taken around the SCB are used to monitor the changes in impedances indirectly. Unbalance protection methods have to be designed to eliminate or reduce unbalances due to capacitor tolerances and temperature drifts [2]. The rest of the chapter introduces various unbalance relaying methods. It should be noted that unbalance relaying methods with particular fault location schemes proposed in the literature will be covered in a separate, literature review, chapter. More information on protection and design of SCBs is presented in Appendix E.

2.2   Phase voltage differential

The phase voltage differential protection is selected to illustrate how phase difference between electrical quantities can determine whether an internal failure has occurred. Assume a solidly grounded wye SCB with potential transformer in each phase at a tap

point, Figure 2.1.
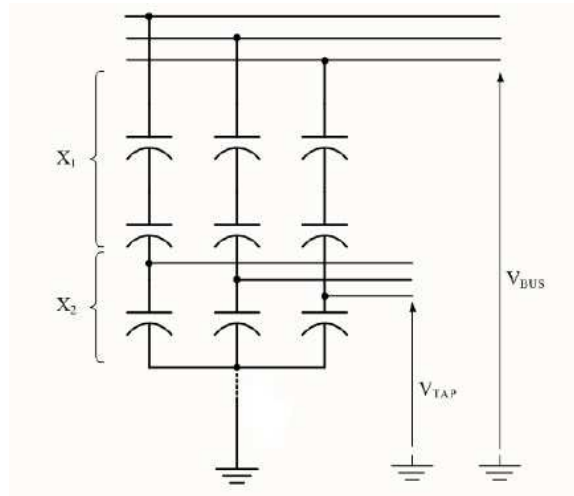
Figure 2.1: SCB with phase voltage differential protection [2].

For each phase of the bank the following equation would be true:

$$V_{TAP} = \frac{X_2}{X_1 + X_2} V_{BUS} \tag{2.1}$$

Note that to date all-film capacitor units losses combined with buswork losses are so low [25] that in references and also in IEEE Std C37.99-2012 [2] the impedance of the capacitor bank is considered to be purely negative reactive. Following the previous equation, a constant is defined as:

$$K = \frac{X_2}{X_1 + X_2} \tag{2.2}$$

The protection operating signal and the self-set value for the constant are defined as:

$$V_{OP} = V_{TAP} - K \, V_{BUS} \tag{2.3}$$

$$K_{SET} = \mid \frac{V_{TAP}}{V_{BUS}} \mid \tag{2.4}$$

It is worth noting that for ungrounded SCBs the voltage terms in (2.3), which are usually magnitudes, will be replaced with phasors measured with respect to the neutral voltage [3]. The actual value for the constant, K_{ACT}, in the operating signal equation will change as a result of an internal failure. Therefore, by replacing the actual tap voltage in terms of this k-factor, the following equation can be derived for the operating signal:

$$V_{OP} = (K_{ACT} - K_{SET}) \times V_{BUS} \tag{2.5}$$

By analyzing the vectorial position of the operating signal with the bus voltage (in phase or out of phase) it can be determined that the failure is in the upper side of the

tapped point or the lower. In some references the differential voltage, (2.3), is formed from magnitudes of the voltage phasors [26], while in other references the operating voltage is the vectorial difference [27]. Considering the k-factor nature, (2.4), which must be an absolute value to make the fault location based on (2.5) valid, in the vectorial difference case, the phase angle difference between the tap voltage and the bus voltage can introduce standing unbalance in the operating signal. For fuseless SCBs instead of a midpoint tap voltage, the voltage across low voltage capacitors forms the tap voltage. This is because strings are not connected at the midpoints in multi-string fuseless designs. The described unbalance protection is phase segregated and very simple that can also be used for locating an internal failure. This is applicable only for wye connected SCBs with tapped potential transformer. Voltage difference between the tap voltages of the parallel banks for double wye grounded SCBs is also an alternative similar unbalance protection, in which again three separate single phase voltage differential relays are used to detect unbalance for each phase independently. Special configurations with the tapped voltage transformers connected at the phase side of grounding capacitors also exist [2], [1]. The principles of the other fault location detection algorithms are similar in basics to the explained method.

2.3   Unbalance method for capacitor banks grounded through a neutral capacitor

In IEEE Std C37.99 [2] unbalance protection of a bank grounded via a capacitor is explained. Depending on the grounding impedance, the configuration could either be considered as an ungrounded SCB (relatively large grounding impedance), or a grounded SCB with relatively small grounding impedance. The first case is discussed thoroughly in the next sections. The latter is the same as the presented phase voltage differential protection.

For the sake of brevity, only the equation set which explains the operating signal assuming equal phase reactances is brought here.
By Ohm's law in the SCB shown in Figure 2.2, we have

$$(\frac{V_A - V_N}{-jX} + \frac{V_B - V_N}{-jX} + \frac{V_C - V_N}{-jX}) \times (-jX_N) = V_N \tag{2.6}$$

which is equivalent to

$$3V_0 \times jX_N = jX \times V_N + jX_N \times 3V_N \tag{2.7}$$

which allows for introducing the following protection function:

$$V_{op} = \mid 3V_0 - (\frac{X}{X_N} + 3) \times V_N \mid \tag{2.8}$$

This protection function is a neutral voltage unbalance protection with a ratio compensation. In the upcoming section for the proposed methods, we will show that this ratio of neutral reactance to phase reactance adds a third factor to the fault location principle.
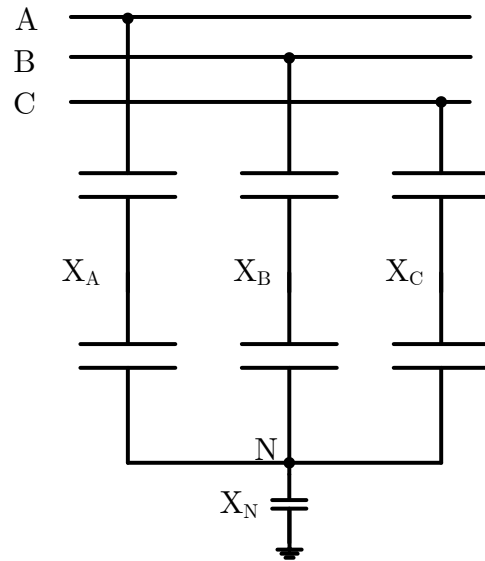
Figure 2.2: Single wye SCB grounded through a capacitor

2.4 Unbalance method for capacitor banks grounded through a CT with resistive burden

In IEEE Std C37.99 [2] unbalance protection of a bank grounded via CT with a resistive burden is explained.
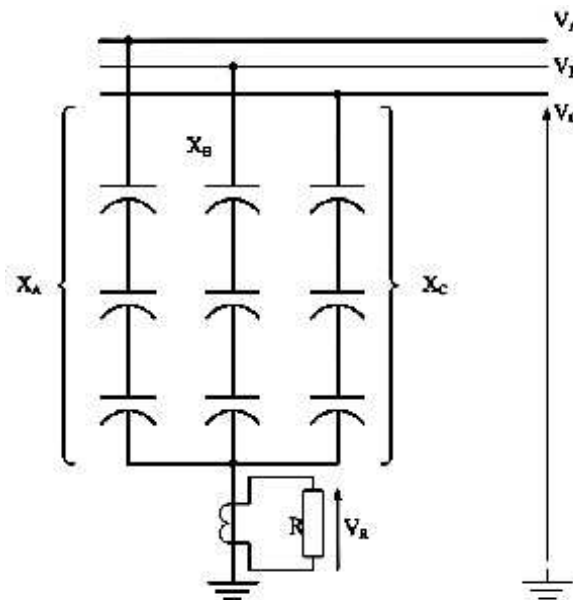
Figure 2.3: Single wye SCB grounded via CT with a resistive burden.

Again we assume that the three phase reactances are equal, and thus denoted by X. Another assumption, for the sake of simplicity, would be the CT ratio of 1:1. In [2]

instead of the primary value of the ground current, its secondary value, based on the burden and the voltage across it, is used for deriving the protection function.

Considering a SCB as in Figure 2.3, the following balance equation holds true:

$$\left(\frac{V_A}{-jX} + \frac{V_B}{-jX} + \frac{V_C}{-jX}\right) \times R = V_R \tag{2.9}$$

which can be simplified as

$$3V_0 + j\frac{X}{R} \times V_R = 0 \tag{2.10}$$

which demonstrates that the neutral voltage at the bus, V_0, is balanced by a voltage associated with the bank neutral (shifted and with a compensation ratio, $j\frac{X}{R} \times V_R$). Thus, a neutral voltage unbalance relay can be used for implementation of such a protection scheme, see Figure 2.4.
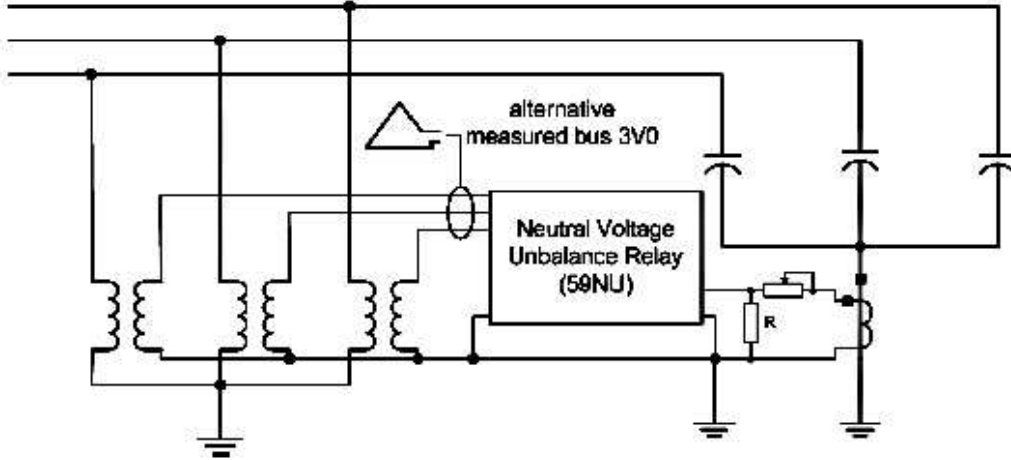
Figure 2.4: Single wye SCB grounded via CT with a resistive burden: application of a neutral unbalance relay capable of ratio compensation, and phase shifting.

To further simplify the operating function, knowing that $\frac{V_R}{R} = 3I_0$, and defining a simple pickup value, V_{pickup}, the protection function actuation can be describe as

$$\mid 3V_0 + 3j\,X\,I_0 \mid > V_{pickup} \tag{2.11}$$

which is more simplified in (2.12)

$$\mid Z_0 - (-jX) \mid > \frac{V_{pickup}}{3 \mid I_0 \mid} \tag{2.12}$$

This relates the protection function to the apparent zero sequence monitoring of the bank. The zero sequence impedance can be measured having the ground current and the bus voltages; however, the protection assumes a fixed and equal reactance for the three phases of the bank. It is worthwhile to note that no reference in the current literature has discussed fault location for this scheme. Thus, we have addressed this in the proposed methods chapter.

2.5 Phase current unbalance protection for fault location

Figure 2.5 illustrates application of phase unbalance for protection of different capacitor units connections inside a capacitor bank.
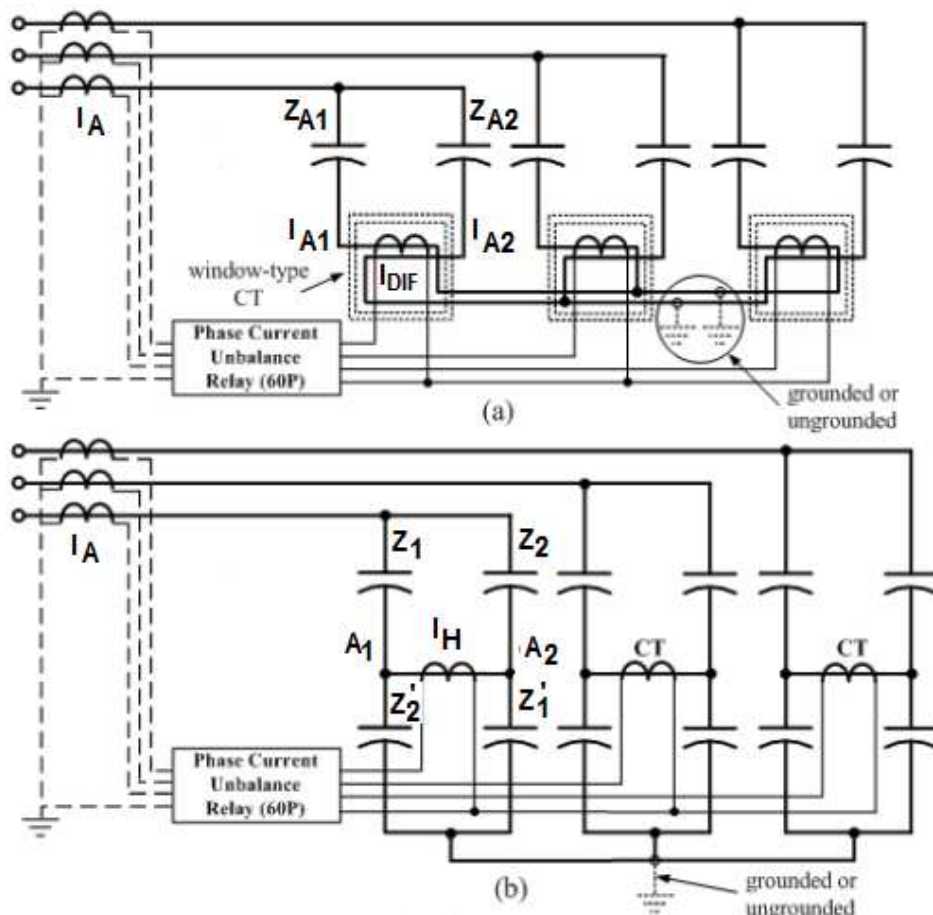
Figure 2.5: Phase current unbalance protection,(a) SCB with window type CTs at neutral connection (b) SCB with H-bridge configuration [2].

Because phase unbalance provides unbalance measurement per phase, deriving the equation sets and logics that can be used for fault location is rather straight forward. For two parallel banks with window CT at the neutral of each phase, the differential currents measured per phase will be useful for sensitive unbalance protection and fault location when compared to two individual CTs, per phase, summated electrically. With reference to Figure 2.5 part (a), the following can be written for phase A:

$$\begin{cases} I_{DIF} = I_{A1} - I_{A2} \\ I_A = I_{A1} + I_{A2} \end{cases} \qquad (2.13)$$

Using the identical voltage that the two parallel banks are working with, we have

$$\begin{cases} I_{DIF} = V_A \frac{Z_{A2}-Z_{A1}}{Z_{A2}Z_{A1}} \\ I_A = V_A \frac{Z_{A2}+Z_{A1}}{Z_{A2}Z_{A1}} \end{cases} \tag{2.14}$$

Before the failure, the vectorial relationship between phase current and the differential neutral current of the same phase is

$$\begin{cases} I_{DIF} = I_A \frac{Z_{A2}-Z_{A1}}{Z_{A2}+Z_{A1}} \quad \text{or} \\ I_{op} = I_{DIF} - I_A K_A = 0 \end{cases} \tag{2.15}$$

where I_{op} is the operating protection signal, which is nulled by compensating the inherent unbalance via the K_A. By approximating the impedances with their pure reactance this k factor can be expressed as

$$K_A \approx \frac{X_{A2}-X_{A1}}{X_{A2}+X_{A1}} \tag{2.16}$$

Failure of any capacitor element in either of the strings, 1 or 2, changes the value of K_A to, say, K_{A_f}. If we represent the new differential current with $K_f I_A$, then the operating signal would become

$$I_{op} = I_A(K_{A_f} - K_A) \tag{2.17}$$

According to (2.16), and Figure 4.1, the phase angle difference between the phase current and the operating current, defined by (2.17), can only be 180° or 0°, dependent on the fusing and the string that involves the failed element. Thus, the location of the internal failure can be found for each phase, (string 1 or 2). Note that phase B and C are respectively duplicated in the equations and explanations.

Same idea applies for H-configured banks. This time the operating signal will be the difference between line current and the bridge current with a correlating k factor defined by circuitry laws. In Figure 2.5 (b), I_H will be zero if the voltage difference between the two points of A_1, and A_2 is zero. For phase A, using the identical voltage that the two parallel strings are working with, and by voltage division, one can find out that this zero voltage difference implies the following balance equation:

$$\frac{Z_2'}{Z_1 + Z_2'} = \frac{Z_1'}{Z_2 + Z_1'} \tag{2.18}$$

Any unbalance will make the bridge current non-zero as

$$I_H = I_A\left(\frac{Z_2'}{Z_1 + Z_2'} - \frac{Z_1'}{Z_2 + Z_1'}\right) \tag{2.19}$$

As a result, failures in the upper left section (Z_1) of the bridge, and failures in lower right section (Z_1') of the bridge will cause same phase relation between the phase current and the bridge current. Same story applies for upper right (Z_2) and lower left sections (Z_2'). Note that phase B and C are respectively duplicated in the equations and explanations.

2.6 Neutral voltage unbalance for double wye ungrounded configurations with isolated neutrals

Figure 2.6 illustrates another unbalance protection method for double wye banks. The two sections in this protection scheme are not parallel. Applying fault location considering pre-existing inherent unbalance for such a protection scheme is not applicable. This is due to the fact that as the neutrals of the two sections are isolated, no relation could be found between the phase reactances. Thus, the number of unknown k factors will be more than the known equations. With regard to this configuration, in the next chapter we will discuss the proposed method of [27], which is based on some simplifying assumptions.
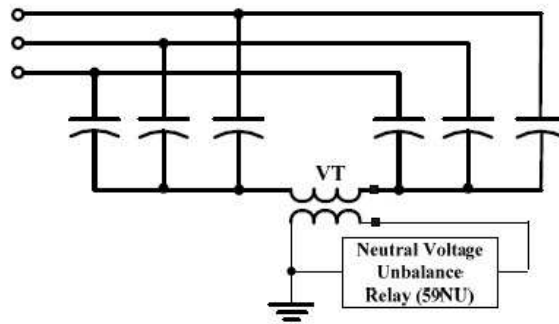
Figure 2.6: Neutral Voltage Unbalance Protection for Double Wye Ungrounded Configurations with Isolated Neutrals [2].

2.7 Neutral voltage unbalance for double wye ungrounded configurations with tied neutrals

Figure 2.7 illustrates another unbalance protection method for double wye banks. This
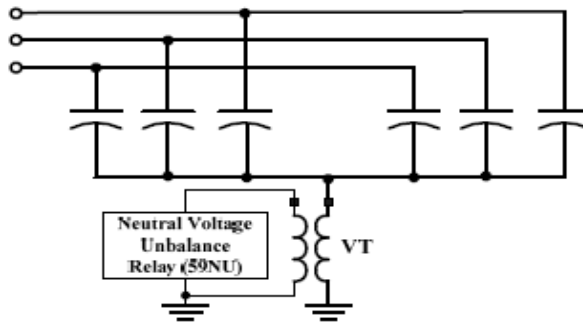
Figure 2.7: Neutral Voltage Unbalance Protection for Double Wye Ungrounded Configurations with Tied Neutrals [2].

unbalance protection is not sensitive to third harmonic components or system voltage unbalance [2]. However, it does not address bank inherent unbalance and thus it is not as common as the unbalance protection with neutral current. Again this protection scheme is not favorable in terms of fault location. Which is because unlike the double wye connections with a CT in the tied neutral, the neutral quantity does not help to discriminate between failures in the right/left sections i.e., there is no phase angle difference in the neutral voltage phasor. We will elaborate more on this in neutral voltage estimation Section 4.7.2.

2.8   Summary

This chapter introduced the fundamentals of detection of problems within the capacitor units. Known relations of currents and voltages based on presumed symmetry in the impedances of the bank are used in developing operating functions whose level is evaluated against thresholds for tripping the bank and preventing from cascading failures. The chapter mainly introduced unbalance protection basics for configurations that already have per phase unbalance measurements to give an idea of the fundamentals of fault location. Various unbalance relaying methods were introduced including some uncommon unbalance protection schemes. In the following chapter a survey and theory investigation will be presented for the patents and publications for SCBs fault location. The focus of the present thesis would be on configurations that do not have per phase unbalance indication, common connections will be studied in more detail.

Chapter 3

SCBs Fault Location Literature Survey

3.1 Introduction

This literature survey reviews the existing approaches in locating internal element failures for HV-SCBs. The review has two parts. The first part will cover explanation of the properties and application of existing fault location methods. The second part investigates one of the references in more detail as the relevant and fairly disclosed fault location method in the literature.

3.2 Literature Survey

Detection of unbalances inside power coupling devices has been a concern for the industry in the past decades. The aim has been disconnecting the device, e.g. SCB, to prevent from cascading failures [28]. Particularly, several patents and papers on the protection of SCBs have been published [7–10,29,30]. However, the issue of fault location detection for three phase SCBs have recently attracted more attention. Identifying the failed element among the numerous elements constituting the bank requires measurement of voltage across the capacitors or calculation of the impedance or current flow by deploying several CTs. This simple idea of direct measurements is complex for application and roughly speaking is an impractical approach. Therefore, research to at least identify the involved phase has emerged in the recent years.

Fault location determination is complex for configurations that do not benefit from phase segregated protection methods, i.e. where the unbalance is not measured per phase. Examples of these are, single wye and double wye configurations with neutral voltage unbalance protection or neutral current unbalance protection, respectively. As discussed in the former chapter, configurations that apply per-phase unbalance measurements do not introduce a concern in terms of fault location. For example, phase current unbalance and H-bridge current unbalance both imply *measured unbalance in each phase* via CTs. The H-bridge configuration can even include potential transformers at tap points to make its simple fault location immune to ambiguous failures [27]. Fault location for solidly

19

grounded single wye banks is also reported to be straight forward, because normally they are protected with voltage differential function across each phase, that inherently determines the faulted phase [31], see section 2.

In [4] a string differential current based approach is presented which in fact is only applicable for specially designed banks with extra available measurement points. The configuration discussed in [4] has 4 strings per phase. Each string current is compared twice, i.e. with its two adjacent strings. In addition to this intra phase current unbalance protection, a common string (zero sequence) current unbalance protection has also been introduced in [4]. This zero sequence measurement is accomplished using 4 separate summing blocks and helps in finding the involved string for cases that there are equal number of failed elements in two adjacent strings of the intra phase unbalance protection.

The method presented in [25, 32, 33] is an impedance measurement based approach that benefits from compensating temperature effects on impedance variation. Real time measured impedances are averaged to fine tune the nameplate values. A mho characteristic in the impedance plane is used for detecting changes in impedance of strings. To maintain the sensitivity of the method the radii of the offset mho adapts with changes in the temperature. For security reason in case of large scale system disturbances the function is blocked. Such an approach for fault location and the method of [4] can be categorized in a separate group of methods as they require measurement of all string currents which is not usually the case in terms of availability of measurement points and installed CTs. The basis of the rest of the fault location methods for SCBs is phase angle comparison [10] which is employed to determine the involved phase [26, 34].

The method introduced in [26, 31, 34] is faulted phase identification for ungrounded wye SCBs and faulted phase and section identification for ungrounded double wye SCBs. The idea is further discussed in [27, 35] for several other simple connections. A fixed reference, i.e. positive sequence voltage for SCBs with neutral voltage protection, and positive sequence current for SCBs with neutral current measurement, has been defined for the phase angle evaluation of a determined compensated quantity. The suggested methods of these references neglect the negative sequence component of the voltage or current to derive the expected value for each phase's fault. Furthermore, in these references, detection of number of failed elements, consecutive failures and compensation for partial shading and gradual changes in the capacitance, as a result of aging and temperature variations, is not discussed. Details of these methods will be elaborated in the next part of this chapter.

In the reference [36], a method which does not use the neutral measurements and thus is applicable to both ungrounded and grounded SCBs is introduced. The method compromises the simplicity of unbalance protection and instead of four measurements deploys all three phase currents and voltages for SCB protection. Also the fault location basis is very similar to [34] with the only difference of comparing current based operating quantity angle to positive sequence voltage phase angle presuming the 90 degree phase shift between phase currents and bus voltages for ideal capacitors. In the mentioned reference, compensated negative sequence current cancels out the effect of imbalances not related to internal capacitor failures. Having the present time measurements and the measurements from commissioning time, the predetermined factor indirectly takes into account the temperature variations. However, such an approach does not address the

shading effect. Moreover, consecutive failure detection and determination of number of failed elements have not been considered in [36].

In [37] an algorithm for fault location is presented for double wye connected SCBs which relies on comparison between consecutive measurements of the normalized unbalance current phase angle with respect to *one* of the phases. In terms of the choice of only one phase current, considerations rise for algorithm security. Because in case steady state changes in the network symmetry are expected, then per-unitizing based on a single phase current is not the proper choice. The compensation method in [37] for pre-existing unbalance and consecutive failures is based on determining step changes in the per-unitized neutral current. This implies that by consecutive measurements the goal of compensation is achieved indirectly. The start tracking and end tracking moments have not been clarified for these consecutive measurements. Detection of the number of failed elements is reported to be done by scaling the rms of neutral current to the rms of a selected phase current (perunit) for an offline simulation based look-up table. Details on how such an algorithm can be adapted to suit commercial relaying functions are not provided. Moreover, in [37] it is claimed that by using the per unit value of the neutral current it becomes independent of system transients and less dependent of the temperature changes; however, such a method can not address the shading effect. Same idea of measurement of step changes has also been developed in [21] for H-bridge banks. The proposed method in [37] is unproven in terms of angle of the step change. The angle of the neutral current referenced to the phase current per se can not identify consecutive failures and also it is not immune to pre-existing unbalance. In this reference, angle of the step change is a vague term as the angle between the two subsequent unbalance currents would be close to zero. In addition, the method does not introduce any compensation or resetting procedure.

In conclusion, because the details of the operating equations are also not disclosed for [37], method of SEL [31] was chosen for comparison and review. The following section provides the calculations required to prove the derivation approach for the SEL method discussed in [27, 34].

3.3 Investigation and review of the SEL method

The explanations in this section are mainly from references [27, 34]. But we have investigated the details on derivation of the equations and assumptions, because they were not disclosed. We refer to these references' approach for fault location as the "SEL method" throughout this thesis, by this we mean the method of SEL Inc.

3.3.1 Single Wye Ungrounded SCB

Figure 3.1 shows the respective measurements, SEL's compensated voltage term (introduced as *unbalance quantity*) is defined as follows:

$$\Delta V_G = V_A^{BUS} + V_B^{BUS} + V_C^{BUS} - 3\,V_N - \left(\eta_1\left(V_B^{BUS} - V_N\right) + \eta_2\left(V_C^{BUS} - V_N\right)\right) \quad (3.1)$$

η_1 and η_2 are defined as scale factor settings based on the relay measurements that reset the unbalance quantity.

By comparing the phase angle of the ΔV_G with the phase angle of the positive sequence voltage the involved phase will be determined through the logic shown in Figure 3.2. Note that the phase differences include a 15° blinder to avoid mis-detection of unbalances not resulting from capacitor failures. The first inputs of the OR gates are for fuseless banks and the second ones stand for fused banks cases (implying 180° phase shift for change in the sign of reactance variation in case of failure).
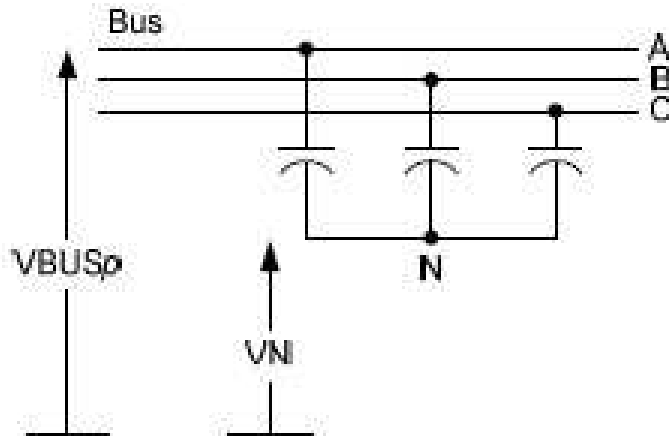
Figure 3.1: The SEL method's single Y configuration and available measurements.
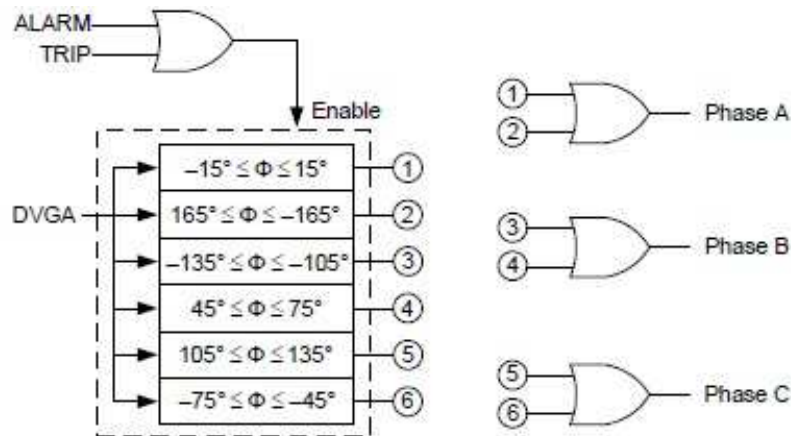
Figure 3.2: The SEL method fault location logic for single wye.

Here we will investigate how they have come up with this equation and fault location method. For fault location purpose, we have to write the equations while assuming a failure. The assumption is that capacitor bank impedances can be approximated as pure reactances. Also, at this point, it is assumed that all three phases have the same

reactance (X) before the failure takes place. We start by writing a KCL at the neutral of Figure 3.1

$$\frac{V_A - V_N}{X} + \frac{V_B - V_N}{X} + \frac{V_C - V_N}{X} = 0 \tag{3.2}$$

where the bus voltages are denoted without the BUS superscript. Considering a failure in phase A and rewriting the equations in another form we have

$$-3V_N = 3 \times \frac{-\frac{V_A}{X_f} - \frac{V_B}{X} - \frac{V_C}{X}}{\frac{1}{X_f} + \frac{2}{X}} \tag{3.3}$$

where the reactance of phase A after failure is denoted by X_f. Adding and subtracting the underlined terms in the nominator results in

$$-3V_N = 3 \times \frac{-\frac{V_A}{X_f} - \underline{\frac{V_A}{X}} + \underline{\frac{V_A}{X}} - \frac{V_B}{X} - \frac{V_C}{X}}{\frac{1}{X_f} + \frac{2}{X}} \tag{3.4}$$

$$\Rightarrow -3V_N = 3 \times \frac{V_A(\frac{1}{X} - \frac{1}{X_f}) - \frac{3V_0}{X}}{\frac{1}{X_f} + \frac{2}{X}}$$

Multiplying the nominator and denominator of the right side by X and then adding $3V_0$ to both sides gives

$$3V_0 - 3V_N = 3 \times \frac{V_A(1 - \frac{X}{X_f}) - 3V_0}{2 + \frac{X}{X_f}} + 3V_0 \tag{3.5}$$

$$\Rightarrow 3V_0 - 3V_N = 3 \times \left(\frac{V_A(1 - \frac{X}{X_f}) - 3V_0 + V_0\frac{X}{X_f} + 2V_0}{2 + \frac{X}{X_f}} \right)$$

, and consequently we derive

$$3V_0 - 3V_N = 3 \times \frac{(V_A - V_0)(1 - \frac{X}{X_f})}{\frac{X}{X_f} + 2} \tag{3.6}$$

$3V_0$ can be replaced with sum of the bus voltages. Also, the denominator on the right side of the equation is a positive number as $\frac{X}{X_f} \approx 1$. It is also clear that $V_A - V_0 = V_A^+ + V_A^-$. Considering that $V_A^- \ll V_A^+$ in a normal power system operation, we can fairly approximate that $\angle(V_A - V_0) = \angle V_A^+$. By employing the same approach for phases B and C, we can write:

$$\angle \Delta V_G = \angle(3(V_A + V_B + V_C) - 3V_N) = \angle(V_p^+) + \angle(1 - \frac{X}{X_f}) \tag{3.7}$$

where V_p^+ denotes the positive sequence component of the voltage of the involved phase (p). For fuseless SCBs, $X > X_f$, and for fused ones $X_f > X$. Therefore, the algorithm of Figure 3.2 can be verified. However, the assumption of equal reactances in (3.2) makes

the method vulnerable to inherent unbalance in the SCB. Thus, to increase the security of the method, the authors of [27,34] have subtracted a compensating factor of the following form $\eta_1 \left(V_B^{BUS} - V_N \right) + \eta_2 \left(V_C^{BUS} - V_N \right)$ from $V_A + V_B + V_C - 3V_N$ to define ΔV_G as (3.1). To determine η_1 and η_2 in (3.1), we write a KCL at the neutral of Figure 3.1:

$$\frac{V_A - V_N}{X_A} + \frac{V_B - V_N}{X_B} + \frac{V_C - V_N}{X_C} = 0 \tag{3.8}$$

where the bus voltages are denoted without the BUS superscript. By multiplying this equation by X_A, we have

$$V_A - V_N + \frac{X_A}{X_B}(V_B - V_N) + \frac{X_A}{X_C}(V_C - V_N) = 0 \tag{3.9}$$

By adding and subtracting the underlined terms as follows:

$$V_A + \underline{V_B} + \underset{\sim}{V_C} - V_N - \underline{\underline{2V_N}} + \underline{\underline{V_N}} - \underline{V_B} + \underline{\underline{V_N}} - \underset{\sim}{V_C} + \frac{X_A}{X_B}(V_B - V_N) + \frac{X_A}{X_C}(V_C - V_N) = 0 \tag{3.10}$$

By further simplification and factoring appropriate terms, we have

$$V_A + V_B + V_C - 3V_N - \left(\left(\frac{X_A}{X_B} - 1 \right)(V_B - V_N) + \left(\frac{X_A}{X_C} - 1 \right)(V_C - V_N) \right) = 0 \tag{3.11}$$

By comparing 3.1 and 3.11, we can determine

$$\eta_1 = \frac{X_A}{X_B} - 1 \tag{3.12}$$

$$\eta_2 = \frac{X_A}{X_C} - 1$$

It is important to note here that (3.7) can not be simply derived assuming the general case where the capacitors of three phases are not equal.

3.3.2 Double Wye Ungrounded SCB with Neutral Current Measurement

For a failed capacitor to withstand the discharge transient current flow from parallel capacitors there is a limit for the total stored energy in a parallel connected group. To keep the sensitivity of unbalance protection schemes while not violating this limit, splitting the bank into two wye sections is the preferred solution. This makes double wye banks a common connection in HV-SCBs.

For the double wye configuration, the SEL unbalance quantity is defined as:

$$60K_N = I_N - (K_1 \cdot I_B^{CAP} + K_2 \cdot I_C^{CAP}) \tag{3.13}$$

variables of which are measured currents according to Figure 3.3. By comparing the phase angle of the $60K_N$ with phase angle of the positive sequence current the faulted phase will be identified through the logic shown in Figure 3.4. For double wye configuration

depending on the CT polarity and the direction of the neutral current, the phase angle relationship with failures in the left bank and right bank is distinguished. Figure 3.4 is based on the assumption that the phase CT matches the neutral CT polarity and is for fuseless banks. In case of fused banks, the legend would be reverse for right and left section faults.

The way that such a method has been derived can be explained through the following equations:

Writing KCL at the left neutral node (Figure 3.3)

$$I_N = I_A^l + I_B^l + I_C^l \tag{3.14}$$

where the superscript l denotes the left section current in the corresponding phase. By performing a current division this KCL can be written in terms of the phase currents as

$$I_N = K_A I_A + K_B I_B + K_C I_C \tag{3.15}$$

where we have omitted the "CAP" from notation of the phase currents, and

$$K_p = \frac{X_p^r}{X_p^l + X_p^r} \qquad p : A, B \ or \ C \tag{3.16}$$

in which, the superscripts r and l denote the corresponding right section and left section reactances. In order to find the k-factors that should be set for inherent unbalance compensation, the KCL equation can be rewritten in the following way:

$$I_N = K_A I_A + \underset{\sim}{K_A I_B} - \underset{\sim}{K_A I_B} + K_B I_B + \underline{\underline{K_A I_C}} - \underline{\underline{K_A I_C}} + K_C I_C \tag{3.17}$$

Because I_0 would be zero, as there is no path to ground in this configuration, we have:

$$I_N = (K_B - K_A)I_B + (K_C - K_A)I_C = \alpha_A I_B + \beta_A I_C \tag{3.18}$$

which is in fact the neutral current prior to an internal failure, that is caused by any other unbalance, i.e. pre-existing unbalance.

As a result, and by simply changing the way k-factors are denoted, the SEL fault location principle constants, (3.13), are found to have the following values:

$$\begin{cases} K_1 = K_B - K_A \\ K_2 = K_C - K_A \end{cases} \tag{3.19}$$

Assuming an element failure in the left section of phase A, which causes the k-factor in phase A to get a new value of K_{A_f}, namely *after failure k-factor*:

$$K_{A_f} = \frac{X_A^r}{X_{A_f}^l + X_A^r} \tag{3.20}$$

the neutral current becomes

$$I_N = K_{A_f} I_A + K_B I_B + K_C I_C$$
$$= K_{A_f} I_A - \underline{\underline{K_A I_A}} + \underline{\underline{K_A I_A}} + K_B I_B + K_C I_C \tag{3.21}$$

the compensated neutral current is then defined to be

$$
\begin{aligned}
I_{N_{compensated}} = I_N - I_{N_{pre-failure}} &= I_N - (K_1 I_B + K_2 I_C) \\
= (K_{A_f} I_A + K_B I_B + K_C I_C) &- (K_A I_A + K_B I_B + K_C I_C) \\
&= (K_{A_f} - K_A) I_A \\
&= I_A X_A^r \frac{X_A^l - X_{A_f}^l}{(X_A^l + X_A^r)(X_{A_f}^l + X_A^r)}
\end{aligned}
\tag{3.22}
$$

Having this equation derived, the logic of Figure 3.4 can be explained through the following notes:

First of all, considering that $I_A^- \ll I_A^+$ in a normal power system operation, we can fairly approximate that $\angle I_A = \angle I_A^+$. Second, the positive sequence component of different phases have 120° phase shift with respect to each other. Third, (3.22) implies that the phase angle of the compensated neutral current has zero or 180° phase shift (depending on the section of the failure location) with respect to the phase angle of the phase in which the element/unit has failed. The phase angle difference between the compensated neutral current and the phase current is also dependent on the fusing method (i.e. impedance change direction in case of failure, see Figure 4.1). Putting these together, the phase comparison demonstrated in Figure 3.4 has been devised by SEL Inc. to determine the internal failure location. Note that for a fused bank the legend for the right section and the left section will replace each other.
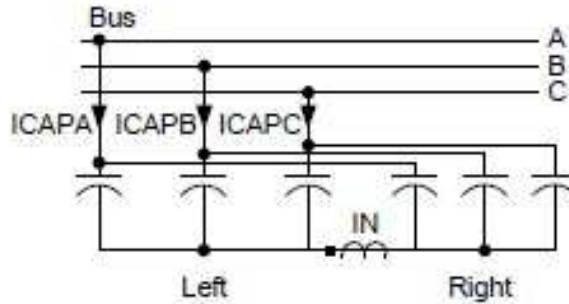
Figure 3.3: The SEL method's double wye configuration and available measurements.

3.3.3 Double Wye Ungrounded SCB with Isolated Neutrals

Fig. 3.5 shows the measurements that are available based on the neutral voltage unbalance protection (59NU) for this configuration.
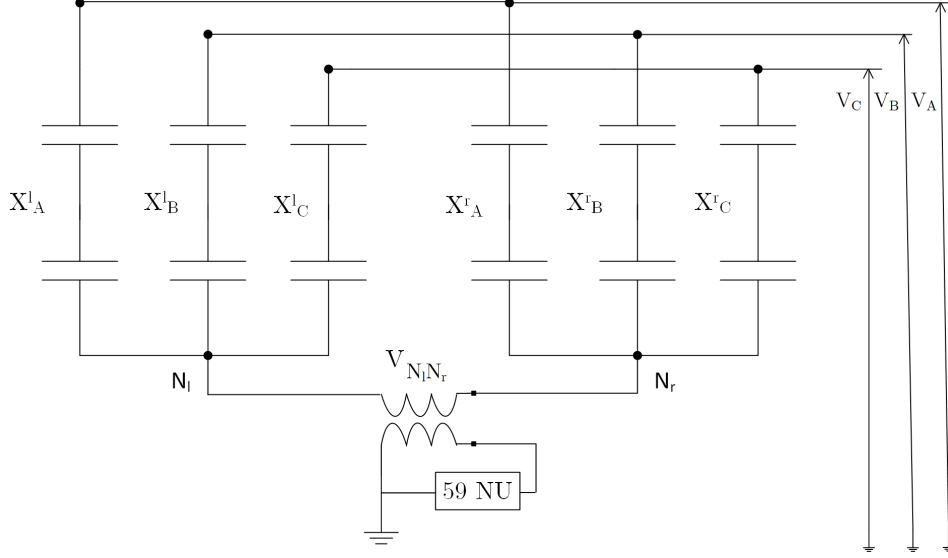
Figure 3.5: Double Wye Ungrounded Configurations with Isolated Neutrals.

Similar to ungrounded double wye banks with neutral current unbalance protection, the measured neutral quantity is expected to be zero for two healthy bank sections. This is because both neutrals will have the same value which is equal to V_0. Therefore, by design, the two sections could be of different rated reactances, which is not considered by the SEL method. Here we will investigate the SEL method for this configuration, i.e. the equations are developed for this purpose. The final assumptions concluded for this method will be used to clarify why this particular SEL method is susceptible to external disturbance case studies in the future chapters.

Assume that all phase reactances are equal to X. With a failure in the left section of phase A that makes the reactance X_f, we can write two KCLs at the neutrals.

$$\frac{V_A - V_{N_l}}{X_f} + \frac{V_B - V_{N_l}}{X} + \frac{V_C - V_{N_l}}{X} = 0 \tag{3.23}$$

$$\frac{V_A - V_{N_r}}{X} + \frac{V_B - V_{N_r}}{X} + \frac{V_C - V_{N_r}}{X} = 0 \tag{3.24}$$

Subtracting the later equations from each other, we can express the result in terms of the neutral voltage difference, defined by (3.25)

$$V_{N_l N_r} = V_{N_l} - V_{N_r} \tag{3.25}$$

$$\frac{V_A}{X_f} - \frac{V_{N_l}}{X_f} - \frac{V_A}{X} + \frac{V_{N_r}}{X} - \frac{V_{N_l}}{X} + \frac{V_{N_r}}{X} - \frac{V_{N_l}}{X} + \frac{V_{N_r}}{X} + \frac{V_{N_l}}{X} - \frac{V_{N_l}}{X} = 0 \tag{3.26}$$

Simplifying the later equation gives:

$$V_{N_l N_r} \frac{3}{X} = (\frac{1}{X_f} - \frac{1}{X})(V_A - V_{N_l}) \tag{3.27}$$

If we multiply both sides by X, and using the following notation

$$X^{Spu} = \frac{X - X_f}{X_f} \tag{3.28}$$

we can express the identity as

$$3V_{N_l N_r} = X^{Spu}(V_A - V_{N_l}) \tag{3.29}$$

By defining an unbalance quantity from (3.29):

$$\Delta V_G = V_{N_l N_r} - \frac{X^{Spu}}{3}(V_A - V_{N_l}) \tag{3.30}$$

one can get an idea of the parameter estimations in the SEL operating quantity which is:

$$\Delta V_G = V_{N_l N_r} - K V^+ \tag{3.31}$$

where K is the phasor setting that resets the principle.

The SEL fault location logic assuming a 15° blinder is shown in Figure 3.6. The principle phase angle is referenced to the positive sequence bus voltage phase angle, denoted as $DVGA$. As a result, the concluded assumptions are as follows:

For a normal power system operation, when assuming $V_{N_l} \ll V_A$, fairly it can be approximated that $\angle(V_A - V_{N_l}) = \angle V_A^+$ (because the neutral voltage is almost equal to residual voltage when pre-existing unbalance is neglected). Similar idea is true for other phases and therefore a general phase angle relationship can be written for (3.29):

$$\angle V_{N_l N_r} = \angle(V_p^+) + \angle(1 - \frac{X}{X_f}) \tag{3.32}$$

where V_p^+ denotes the positive sequence component of the faulted phase voltage. For fuseless SCBs, $X > X_f$, and for fused ones $X_f > X$.
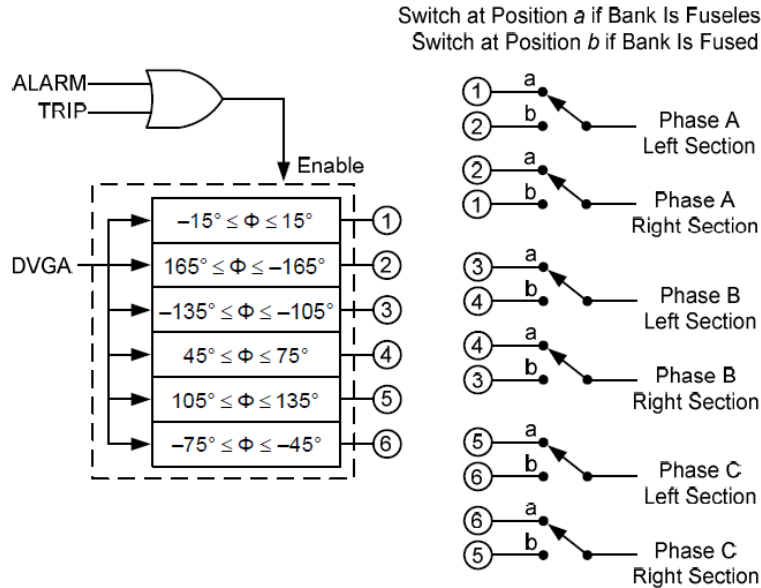
Figure 3.6: The SEL fault location logic for double wye with isolated neutrals.

Because K is expected to get a small value, the phase angle of the compensated quantity referenced to positive sequence voltage phase angle is approximately the same as its uncompensated referenced phase angle, which was verified in (3.32). In equation form this is:

$$\angle(\frac{V_{N_l N_r} - KV^+}{V^+}) = \angle(\frac{V_{N_l N_r}}{V^+} - K) \simeq \angle\frac{V_{N_l N_r}}{V^+} = \angle V_{N_l N_r} - \angle V^+ \qquad (3.33)$$

3.3.4   H-bridge banks with CT in each phase and PT at the tap point

In accordance with the descriptions in section 2.5, the fault location principle using the bridge unbalance current is expressed as follows in [27]:

$$60p = I_{H_p} - K_p I_p \qquad (3.34)$$

Which is derived from (2.17), and (2.19).

In order to determine which quadrant of each phase of an H-bridge has the failed element, both phase voltage and phase current unbalance protections should be applied. The reason is, as per section 2.2, voltage differential protection can distinguish whether the upper part of a tap is faulty or the lower part. Also, as per section 2.5, the phase current unbalance itself can only distinguish between the failure of the two diagonals of the bridge.

Figures 3.7, and 3.8 demonstrate the configuration measurements and the fault location logic based on a 15° blinder, respectively. It is worthy to note that in Figure(3.8), DVA points out to (2.3).

3.4   Summary

This chapter covered the current fault location methods and where applicable elaborated on some of them in detail. Assumptions and properties of the methods were extracted to help out in proposing new methods for fault location in HV SCBs. Next chapter will present the proposed ideas and algorithms.
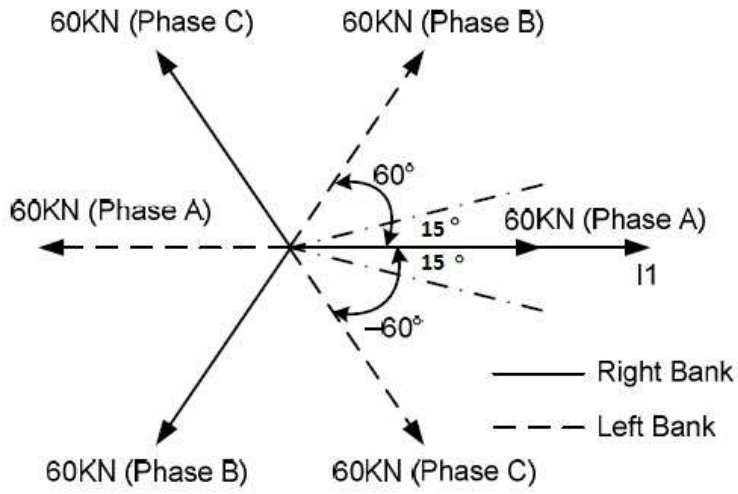
Figure 3.4: The SEL method's fault location logic for double wye (fuseless).
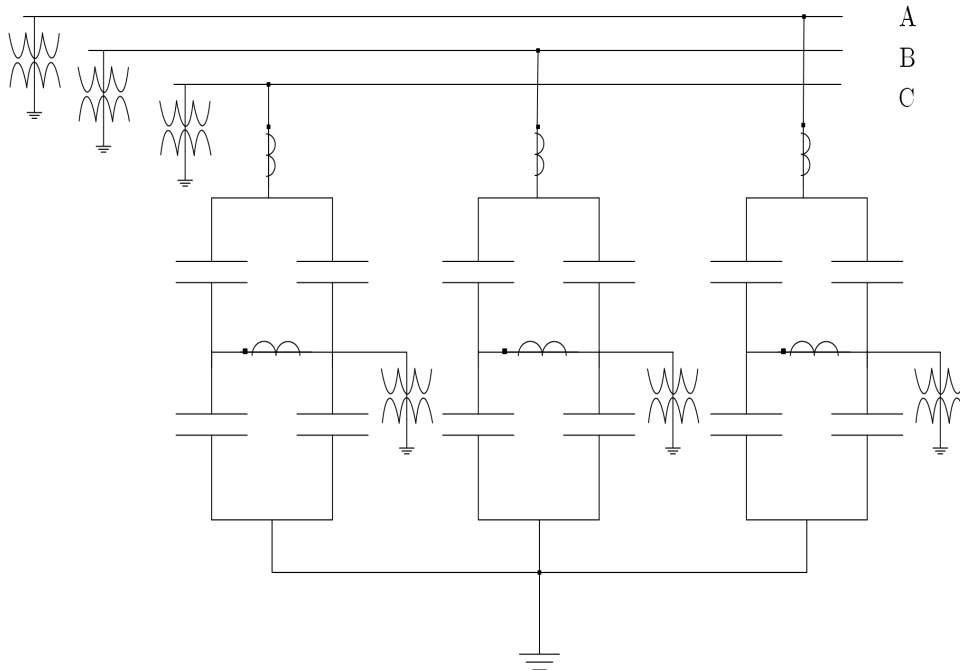
Figure 3.7: Measurements for fault location of H-bridge banks
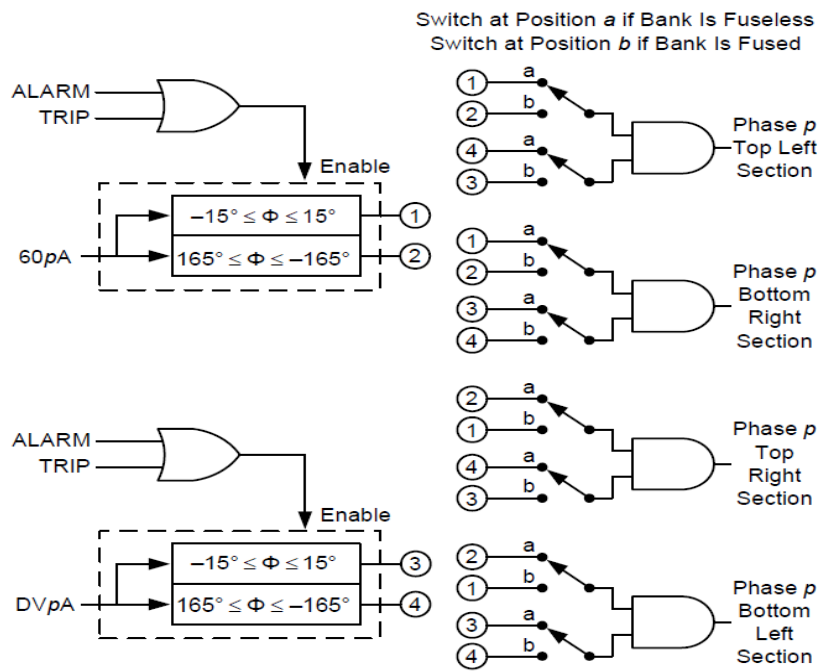
Figure 3.8: The SEL fault location logic for H-bridge banks

Chapter 4

The Proposed Fault Location Methods

4.1   Introduction

This chapter presents the proposed methods for fault location in HV SCBs. The configurations for which new ideas have been developed or the fault location is proposed for the first time are introduced and the equation sets that form the fault location principles are elaborated. Flowchart of the algorithms and application settings are also explained.

Accuracy of an internal failure detection method is directly related to how it can discriminate between pre-existing unbalances in the bank and the subsequent failures. Accordingly, operating function k-factors are determined to develop sensitive fault location methods.

Although the initial difference between reactances of different phases is minimized through manufacturing methods [4], see Section 5.1, but still there would be a difference in the total phase reactances. Thus, different reactances need to be assumed for the three phases. Because temperature affects the reactance, and even at times part of the SCB may be under direct sunlight while the other part is in the shade (a.k.a. shading effect), k-factors should be updated at regular time intervals. This helps to compensate for the gradual changes. A separate section in this chapter will explain this algorithm property.

Common connections and fusing technologies are considered in the proposed fault location methods development. The selected configurations are complex in terms of derivation of the unbalance equations with the expected available measurements. The proposed logics consider whether the bank is internally fused or fuseless to account for the increase or decrease in the magnitude of the reactance after the fault, see Figure 4.1.

In the following sections of this chapter, first a new indicating quantity is defined based on the measured voltages around single wye SCBs and it is denoted as superimposed reactance. This complex value forms the basis for the proposed fault location methods in three different grounding arrangements. Originally the principle is developed for single wye ungrounded SCBs with neutral voltage unbalance protection and then it is adapted to become suitable for two other connections, grounded through CT and grounded through capacitor. After these, an enhanced fault location method is intro-
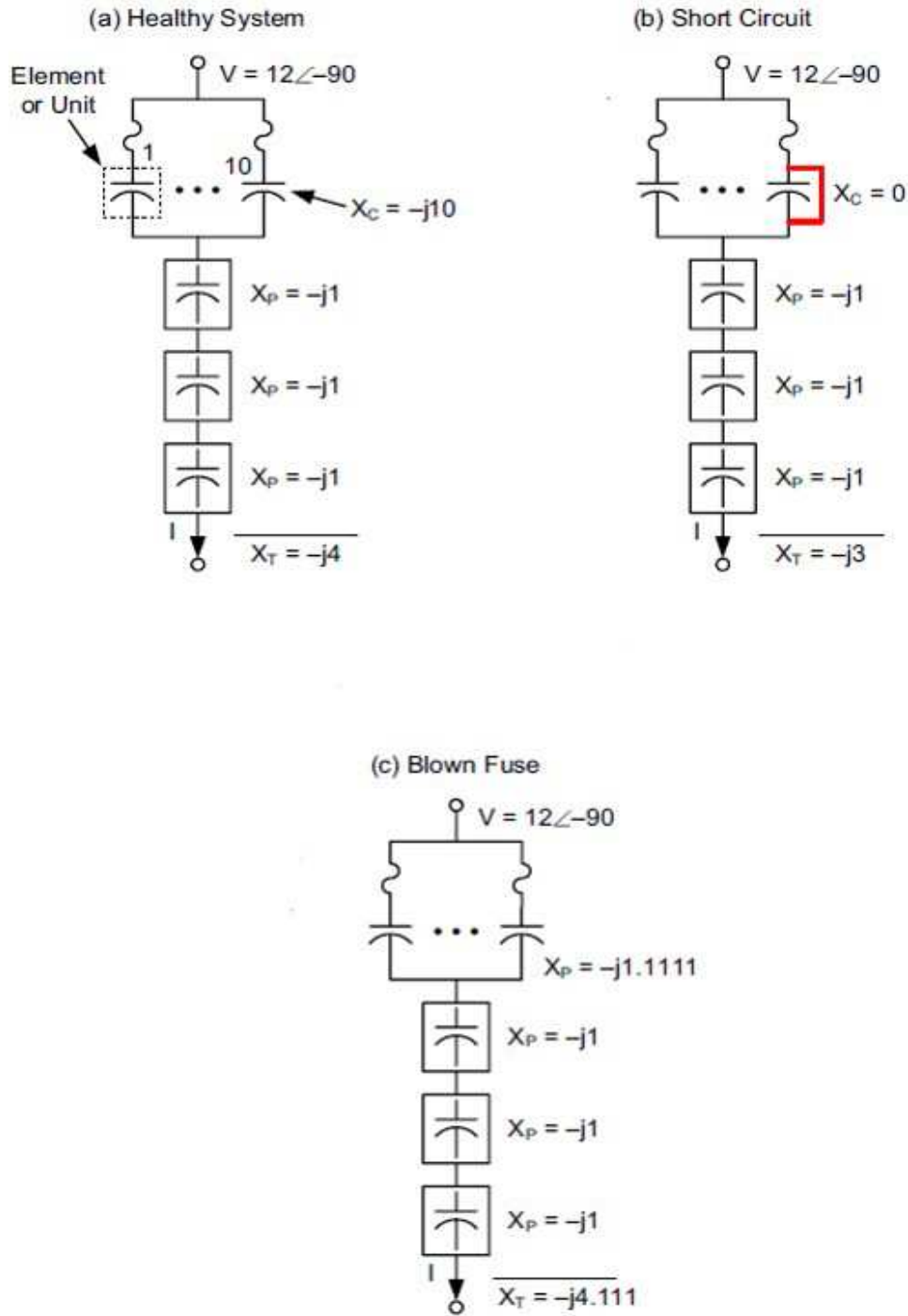
Figure 4.1: Effect of fusing on the change of reactance

duced for grounded and ungrounded double wye SCBs with neutral current unbalance protection. The proposed fault location methods not only incorporate the properties of the present methods in the literature but also put forth solutions for more application issues while making the most out of the in-use measurements. This is in consistent with the

common practical unbalance protection functions. The algorithm development includes assumption of different phase and section reactances due to manufacturing tolerance. The proposed methods are devised with less simplifications to keep the fault location sensitive to slightest failures while it is immune to noise, harmonics, and external unbalances.

4.2 Superimposed Reactance (SR) for Ungrounded Single Wye SCB

4.2.1 Determining the involved phase
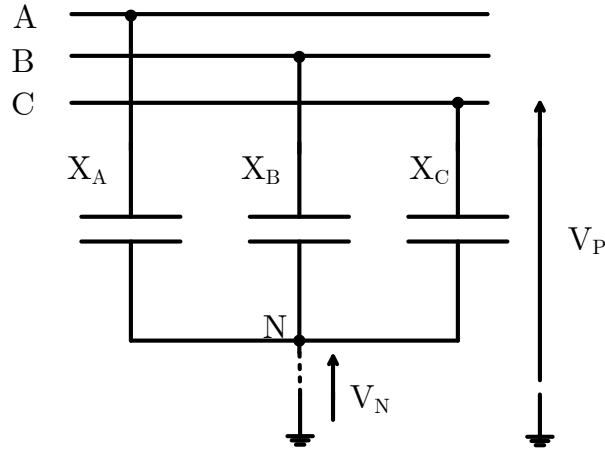
Figure 4.2: Ungrounded single wye shunt capacitor bank

Assume a single wye ungrounded SCB, Figure. 4.2. Writing KCL at the neutral node considering a failure in phase A gives

$$V_N\left(\frac{1}{X_{A_f}} + \frac{1}{X_B} + \frac{1}{X_C}\right) = \frac{V_A}{X_{A_f}} + \frac{V_B}{X_B} + \frac{V_C}{X_C} \tag{4.1}$$

where X_{A_f} denotes the reactance of phase A after the element/unit failure. Adding and subtracting the underlined terms will simplify this very first equation

$$V_N\left(\frac{1}{X_{A_f}} + \underaccent{\sim}{\frac{1}{X_A}} - \underaccent{\sim}{\frac{1}{X_A}} + \frac{1}{X_B} + \frac{1}{X_C}\right) = \frac{V_A}{X_{A_f}} + \underline{\underline{\frac{V_A}{X_A}}} - \underline{\underline{\frac{V_A}{X_A}}} + \frac{V_B}{X_B} + \frac{V_C}{X_C} \tag{4.2}$$

Multiplying both sides by X_A, will give

$$V_N = \frac{\left(V_A \frac{X_A}{X_{A_f}} - V_A\right) + V_A + K_B^A V_B + K_C^A V_C}{\left(\frac{X_A}{X_{A_f}} - 1\right) + 1 + K_B^A + K_C^A} \tag{4.3}$$

where we have defined two pre-failure reactance ratios as follows:

$$K_B^A = \frac{X_A}{X_B} \tag{4.4}$$

$$K_C^A = \frac{X_A}{X_C}$$

Having (4.3), we can add and subtract V_B and V_C to the numerator. The *internal* unbalance of the SCB makes the neutral voltage to change from the zero sequence voltage. Also, V_0 can be considered to be a representative of the *power system* (voltage) unbalance. Thus, to account for the power system unbalance, it is tried to abstract the difference between the residual voltage, V_0, and the neutral voltage by adding and subtracting V_0 from (4.3).

$$V_N = \frac{V_A\frac{X_A - X_{A_f}}{X_{A_f}} + V_A + K_B^A V_B + V_B - V_B + K_C^A V_C + V_C - V_C}{\frac{X_A - X_{A_f}}{X_{A_f}} + 1 + K_B^A + K_C^A} - V_0 + V_0 \qquad (4.5)$$

Simplifying the previous equation, one can derive

$$V_N = \frac{(V_A - V_0)\frac{X_A - X_{A_f}}{X_{A_f}} + (K_B^A - 1)(V_B - V_0) + (K_C^A - 1)(V_C - V_0)}{\frac{X_A - X_{A_f}}{X_{A_f}} + 1 + K_B^A + K_C^A} + V_0 \qquad (4.6)$$

For auto-setting of the constants in (4.6), and thus representing the inherent unbalance in the SCB, we have to evaluate this equation prior to an internal failure. By assuming:

$$X_{A_f} = X_A \qquad (4.7)$$

we will have:

$$V_{N_{est}} = \alpha_A (V_B - V_0) + \beta_A (V_C - V_0) + V_0 \qquad (4.8)$$

where

$$\alpha_A = \frac{K_B^A - 1}{1 + K_B^A + K_C^A} \qquad (4.9)$$

and

$$\beta_A = \frac{K_C^A - 1}{1 + K_B^A + K_C^A} \qquad (4.10)$$

In (4.8), the neutral voltage is denoted by $V_{N_{est}}$, as it is an estimation of neutral voltage without direct measurement of it. Using (4.8) we can solve for α_A and β_A.
For a failure in phase A of the SCB, the corresponding k-factors in terms of their relative α_A and β_A are:

$$K_C^A = \frac{1 + 2\beta_A - \alpha_A}{1 - \beta_A - \alpha_A} \qquad (4.11)$$

$$K_B^A = \frac{\alpha_A + \alpha_A K_C^A + 1}{1 - \alpha_A} \qquad (4.12)$$

The k-factors can also be set directly using the following equations. A simple KCL at the neutral point implies

$$\frac{V_A - V_N}{X_A} + \frac{V_B - V_N}{X_B} + \frac{V_C - V_N}{X_C} = 0 \qquad (4.13)$$

or equivalently

$$\frac{V_A - V_N}{X_A/X_A} + \frac{V_B - V_N}{X_B/X_A} + \frac{V_C - V_N}{X_C/X_A} = 0 \tag{4.14}$$

Thus for each phase, the k-factors can be set separately, e.g. for phase A we can write

$$(V_B - V_N)K_B^A + (V_C - V_N)K_C^A = V_N - V_A \tag{4.15}$$

Equation (4.15) is a set of two equations for real and imaginary parts of the voltage terms. Hence, the two unknowns, k-factors, can be found and set for fault location. After setting the k-factors, the following terms can be defined to simplify (4.6):

$$\gamma_A = (K_B^A - 1)(V_B - V_0) + (K_C^A - 1)(V_C - V_0) \tag{4.16}$$

$$\lambda_A = 1 + K_B^A + K_C^A \tag{4.17}$$

$$X_p^{Spu} = \frac{X_p - X_{p_f}}{X_{p_f}} \tag{4.18}$$

Note that γ is not a constant but a continuously monitored factor for each phase. X^{Spu} denotes the superimposed reactance and both its magnitude and phase angle will be monitored. Therefore, the general form for (4.6) becomes:

$$(X_p^{Spu} + \lambda_p)(V_N - V_0) = (V_A - V_0)X_p^{Spu} + \gamma_p \tag{4.19}$$

which implies

$$X_p^{Spu} = \frac{\gamma_p - \lambda_p(V_N - V_0)}{V_N - V_p} \tag{4.20}$$

By applying the same procedure when assuming failures in phase B or C, the equation for k-factors, γ, and λ of the two other phases can be found as follows:

For phase B:

$$\begin{cases} K_C^B = \frac{K_C^A}{K_B^A} \\ K_A^B = (K_B^A)^{-1} \\ \gamma_B = (K_C^B - 1)(V_C - V_0) + (K_A^B - 1)(V_A - V_0) \\ \lambda_B = 1 + K_A^B + K_C^B \end{cases} \tag{4.21}$$

For phase C:

$$\begin{cases} K_A^C = (K_A^A)^{-1} \\ K_B^C = \frac{K_B^A}{K_C^A} \\ \gamma_C = (K_A^C - 1)(V_A - V_0) + (K_B^C - 1)(V_B - V_0) \\ \lambda_C = 1 + K_A^C + K_B^C \end{cases} \tag{4.22}$$

The latter equation-sets for the two other phases, demonstrate that the k-factors are relative to each other. As a consequence, upon a failure the magnitude of the two other phase principles also will change. Fault location using X^{Spu} implies that measuring the

equivalent reactance in terms of the measured voltages introduces an accurate way to locate the internal unbalance caused by element failures.

With reference to (4.18), and the sign of the reactance difference (before and after an internal failure), we know the expected phase angle of the perunit superimposed reactance. For fuseless banks, because $X_p > Xp_f$ it is expected that in case of failure, the angle of X^{Spu} for the faulted phase would be around $0°$, we will consider a tolerance for security reason as it will be explained in Section 4.8.4. Similarly, for fused banks the expected phase angle for X^{Spu} is (about) $180°$ because $X_p < Xp_f$. In order to make a unique phase angle boundary for both fused and fuseless banks, it is proposed to incorporate a sign factor to (4.18). This factor is defined as follows:

$$K_{sg} = \begin{cases} +1 & \text{for fuseless banks} \\ -1 & \text{for fused banks} \end{cases} \tag{4.23}$$

Therefore, after failures, the phase angle of the superimposed reactance will lie around zero. As a result, the superimposed reactance would be

$$X_p^{Spu} = K_{sg} \frac{\gamma_p - \lambda_p(V_N - V_0)}{V_N - V_p} \tag{4.24}$$

4.2.2   Estimating the number of failed elements

For detection of the number of failed elements and also activation of the phase angle comparison logic, a reference/threshold value can be set simply using the superimposed reactance magnitude based on (4.18). Accordingly, one advantage of the proposed principle is that there is no need for derivative calculation to find a base for number of element failures detection. The defined superimposed reactance as per (4.18) can be set as a base for this purpose using the SCB nameplate values assuming failure of a single element. See Section 4.8.2 for more detailed equations.

4.3   Adapted SR for Single Wye SCB Grounded through a Capacitor

4.3.1   Determining the involved phase

We will investigate application of the proposed superimposed reactance concept for fault location of single wye SCBs grounded through a capacitor. Applying KCL at the neutral point of the shown SCB in Figure 4.3, with a presumed internal failure in phase A, results in the following balance equation:

$$\frac{V_A}{X_{A_f}} + \frac{V_B}{X_B} + \frac{V_C}{X_C} = V_N\left(\frac{1}{X_{A_f}} + \frac{1}{X_B} + \frac{1}{X_C} + \frac{1}{X_N}\right) \tag{4.25}$$

Adding and subtracting the following underlined terms results in:
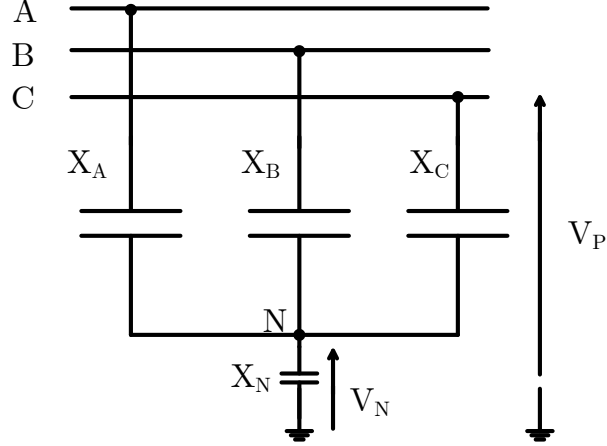
Figure 4.3: Measurements available for single wye SCB grounded through a capacitor.

$$\frac{V_A}{X_{A_f}} - \frac{V_A}{\underline{\underline{X_A}}} + \frac{V_A}{\underline{\underline{X_A}}} + \frac{V_B}{\underline{\underline{X_A}}} + \frac{V_C}{\underline{\underline{X_A}}} + \frac{V_B}{X_B} - \frac{V_B}{\underline{\underline{X_A}}} + \frac{V_C}{X_C} - \frac{V_C}{\underline{\underline{X_A}}} = V_N(\frac{1}{X_{A_f}} - \frac{1}{\underline{\underline{X_A}}} + \frac{1}{\underline{\underline{X_A}}} + \frac{1}{X_B} + \frac{1}{X_C} + \frac{1}{X_N})$$

(4.26)

Multiplying both sides by X_A, reintroducing the superimposed reactance as per (4.18), and defining the k-factors as per (4.4), with a third k-factor introduced by the following definition:

$$K_N^A = \frac{X_A}{X_N}$$

(4.27)

gives

$$V_A X_A^{Spu} + 3V_0 + V_B (K_B^A - 1) + V_C (K_C^A - 1) = V_N(1 + K_B^A + K_C^A + K_N^A + X_A^{Spu}) \quad (4.28)$$

Adding and subtracting three terms of $K_p^A V_0$ for the three k-factors, can introduce an equation which looks similar to the proposed principle for ungrounded banks as per (4.24):

$$(V_N - V_A)(X_A^{Spu}) = (V_B - V_0)(K_B^A - 1) + (V_C - V_0)(K_C^A - 1) - (V_N - V_0)(1 + K_B^A + K_C^A + K_N^A) - K_N^A V_0$$

(4.29)

The following terms can be defined to simplify the last equation:

$$\gamma_A' = (K_B^A - 1)(V_B - V_0) + (K_C^A - 1)(V_C - V_0)$$

(4.30)

$$\lambda_A' = 1 + K_B^A + K_C^A + K_N^A$$

(4.31)

Comparing with the γ and λ terms derived for ungrounded wye SCBs, (4.16), and (4.17), it can be shown that

$$\begin{cases} \gamma_A' = \gamma_A \\ \lambda_A' = \lambda_A + K_N^A \end{cases}$$

(4.32)

Therefore, the resultant fault location principle would be

$$X_p^{Spu} = \frac{\gamma_p' - \lambda_p'(V_N - V_0) - K_N^p V_0}{V_N - V_p} \tag{4.33}$$

where the superscript, p, denotes the phase for which the superimposed reactance is estimated.

To derive the self-setting equations, KCL is applied at the neutral point of the SCB shown in Figure 2.2, which results in the following balance equation:

$$\frac{V_A}{X_A} + \frac{V_B}{X_B} + \frac{V_C}{X_C} = V_N(\frac{1}{X_A} + \frac{1}{X_B} + \frac{1}{X_C} + \frac{1}{X_N}) \tag{4.34}$$

this can be rewritten as

$$V_A + K_B^A V_B + K_C^A V_C = V_N(1 + K_B^A + K_C^A + K_N^A) \tag{4.35}$$

a more organized presentation of the later equation is

$$V_N(1 + K_N^A) - V_A = K_B^A(V_B - V_N) + K_C^A(V_C - V_N) \tag{4.36}$$

As can be seen, the number of k-factors is three but only two equations, i.e. real and imaginary segments of (4.36), exist for deriving them (all of the k-factors are real numbers representing reactance ratios). Accordingly, since the grounding capacitive reactance is smaller than phase equivalent capacitive reactance, the K_N^p would be much larger than the phase k-factors, which are normally about unity. Based on the neutral capacitor and the phase capacitor values [3], a typical phase to neutral k-factor would be around 10. As a result, even with element failures development in any of the three phases the change in the third k-factor from its pre-set value would be trivial, and thus it is assumed that this k-factor is constant for the fault location purpose, i.e. there is no need to update this quantity once it is set based on rated capacitor values. It should be noted that according to IEEE Std C37.99 [2], the ratio of phase reactance to grounding reactance (the third k-factor) does also appear as a ratio compensation property in the operating voltage for neutral voltage unbalance protection of this configuration and it is set constant using the capacitor rated values.

4.3.2 Estimating the number of failed elements

To determine the number of failed elements and also to trigger the phase angle comparison logic, a reference value can be set for superimposed reactance magnitude using (4.33). It is an advantage of this proposed principle that there is no need for derivative calculation in quantifying element failures with a reference index. The defined superimposed reactance as per (4.33) can be set as a base for this purpose using the SCB nameplate values assuming the minimum failure of one element. See Section 4.8.2 for more detailed equations.

4.4   Adapted SR for Single Wye SCB Grounded through a CT

4.4.1   Determining the involved phase

We will investigate application of superimposed reactance for fault location of this configuration. Figure 4.4 illustrates the corresponding SCB unbalance protection scheme. Faults will cause residual current to flow through the low ratio grounding CT and the
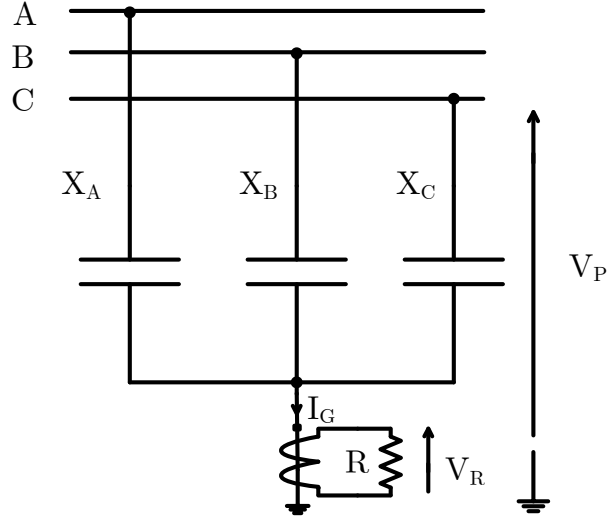
Figure 4.4: Single wye bank grounded through a CT.

resistive burden will develop an associated voltage, V_R. For the sake of simplicity, a CT ratio (CTR) equal to the aforementioned resistance is assumed. This way, V_R and the primary ground current (I_G) values can be equivalently expressed in the equations. Same assumption has been applied in the technical data provided in [2].

$$I_G = \frac{V_R}{R} \ CTR = V_R \tag{4.37}$$

Same assumption has been applied in the technical data provided in [2], CTR of 50/5 and R of 10 Ω.
Applying KCL at the neutral point gives the following equation:

$$\left(\frac{V_A}{-jX_A} + \frac{V_B}{-jX_B} + \frac{V_C}{-jX_C}\right) = I_G \tag{4.38}$$

Considering an internal failure in phase A that changes the phase A reactance to X_{A_f}, plus adding/subtracting the specified terms will simplify the previous equation

$$\frac{V_A}{X_{A_f}} - \frac{V_A}{X_A} + \frac{V_A}{X_A} + \frac{V_B}{X_A} + \frac{V_C}{X_A} + \frac{V_B}{X_B} - \frac{V_B}{X_A} + \frac{V_C}{X_C} - \frac{V_C}{X_A} = -jV_R \tag{4.39}$$

With the same definition for superimposed reactance as per (4.18), and the k-factors as per (4.4), the rearranged balance equation would be

$$V_A(X_A^{Spu}) + 3V_0 + V_B(K_B^A - 1) + V_C(K_C^A - 1) = -jX_A V_R \tag{4.40}$$

In (4.40), the before failure phase reactance, X_A, can be approximated with its rated value, denoted by X. In terms of algorithm reliability, the applicability of this assumption for consecutive failures will be investigated in Chapter 5. Nevertheless, this assumption is considered to be acceptable as the rated reactance is similarly applied in the operating voltage of the corresponding protection method defined in IEEE Std C37.99 [2]. To give an example, for a 230 kV, 84.37 Mvar SCB with a value of $627\,\Omega$ for X, a change of less than 0.1% after an element failure and less than 1.8% upon a unit failure was observed in the phase reactance. Therefore, even for detecting consecutive failures the assumption should still hold true.

The general equation for the SR, developed from (4.40) and considering phase sequence as: p, $p\prime$, and $p\prime\prime$, would become

$$X_p^{Spu} = \frac{V_p + V_{p\prime} K_{p\prime}^p + V_{p\prime\prime} K_{p\prime\prime}^p + jXV_R}{-V_p} \tag{4.41}$$

For self-setting the k-factors, we have to evaluate the former equation prior to an internal failure, e.g. when $X_{A_f} = X$. This results in nulling out the superimposed reactance. Therefore, the real and imaginary parts of the following identity can be solved for finding the two k-factors.

$$K_B^A V_B + K_C^A V_C = -jXV_R - V_A \tag{4.42}$$

The equation sets for phase B and C are analogous to (4.42). The final fault location logic would be the same as the one explained for ungrounded wye SCBs. Also, it is worth noting that like the ungrounded wye case, the principle should be multiplied by a sign factor as per (4.23). This makes the angle boundary become unique for both fused and fuseless banks.

4.4.2 Estimating the number of failed elements

For detection of the number of failed elements and also activation of the phase angle comparison logic, a reference value can be defined to be compared with the superimposed reactance magnitude using (4.41). Accordingly, unit and phase construction (number of series and parallel connections, ratings of elements and the bank) are the required information for estimating pre-fault and post-fault phase reactances. It is worthy to note that as the proposed SR is a per unit quantity, the thresholds are not susceptible to aging of the capacitors.

4.5   Enhanced Compensated Neutral Current for Ungrounded Y-Y SCB

Double wye connection is a prevalent connection in HV-SCBs which helps to keep the total stored energy in a parallel connected group of capacitors within the limits, while maintaining the sensitivity of unbalance protection. Neutral current unbalance protection (ANSI 60N) is selected for development of the proposed fault location method since this is the most common unbalance protection used for double wye banks. Also, this unbalance protection does not benefit from per phase unbalance quantity measurement which makes it challenging in terms of fault location.

4.5.1   Determining the involved phase and section
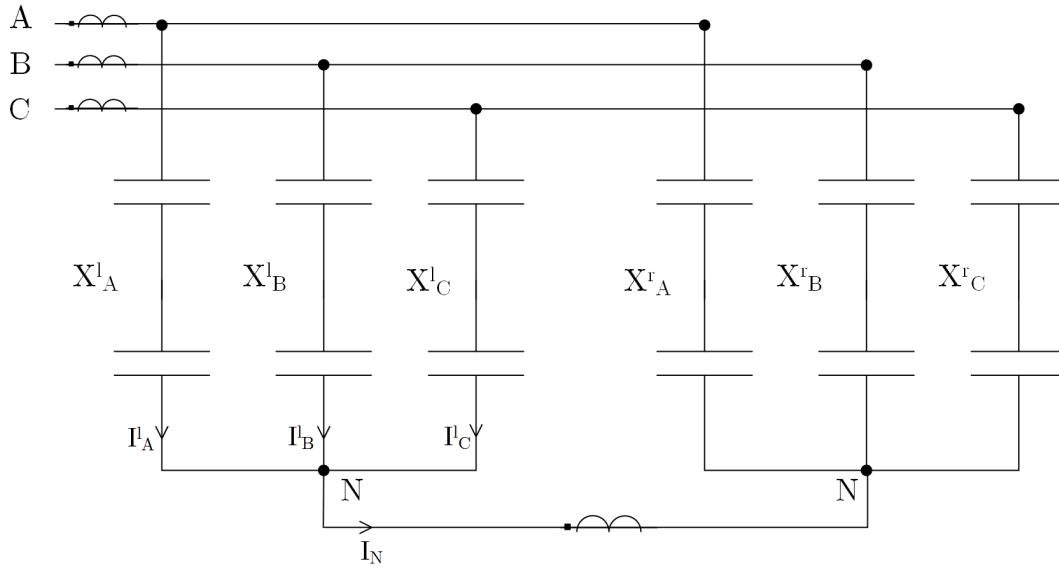
Figure 4.5: Ungrounded double wye shunt capacitor bank

Figure 4.5 illustrates the circuit diagram and available measurements for an un-grounded double wye SCB with neutral current unbalance protection. Using the left section currents, denoted by superscript l, the measured neutral current is identical to

$$I_N = I_A^l + I_B^l + I_C^l \tag{4.43}$$

Performing current division helps to relate the left section currents to measured phase currents

$$I_N = K_A I_A + K_B I_B + K_C I_C \tag{4.44}$$

where the phase coordinate k-factors are defined as

$$K_p = \frac{X_p^r}{X_p^l + X_p^r} \qquad p : A, B \ or \ C \tag{4.45}$$

in which the superscripts r and l denote the corresponding right section and left section reactances.

Assuming an element failure in the left section of phase A, that changes the left section reactance of this phase to X_{Af}^l, and thus yielding to a new k-factor for phase A signified by K_{Af}

$$K_{Af} = \frac{X_A^r}{X_{Af}^l + X_A^r} \tag{4.46}$$

the neutral current would change to:

$$I_N = K_{Af}I_A + K_B I_B + K_C I_C \tag{4.47}$$

Subtracting (4.47) from (4.44) nulls out any pre-existing unbalance and helps the neutral current change caused by the internal failure to stand out. The result is noted by compensated neutral current, I_N^{Comp}:

$$\begin{aligned} I_N^{Comp} &= (K_{Af}I_A + K_B I_B + K_C I_C) \\ &\quad -(K_A I_A + K_B I_B + K_C I_C) \\ &= (K_{Af} - K_A)I_A \end{aligned} \tag{4.48}$$

which evolves to

$$I_N^{Comp} = I_A X_A^r \frac{X_A^l - X_{Af}^l}{(X_A^l + X_A^r)(X_{Af}^l + X_A^r)} \tag{4.49}$$

Equation (4.49) clarifies that for the phase in which the element has failed, the I_N^{Comp} would be either in phase or out of phase with the corresponding phase current, depending on direction of change in the affected reactance, see (4.50).

$$\angle I_N^{Comp} = \angle I_A + \angle(X_A^l - X_{Af}^l) \tag{4.50}$$

However, I_N^{Comp} should be expressed in terms of the measured current and adjustable setting. In this regard, the neutral current of (4.44) is re-written in terms of symmetrical components. Note that as there is no path to ground, I_0 is zero for this configuration, thus we have:

$$I_N = K_1 I_1 + K_2 I_2 \tag{4.51}$$

Interestingly, the k-factors are found to be complex conjugates of each other, which can be proved as follows:
Rewriting the KCL equation of (4.44) in terms of symmetrical components gives

$$\begin{aligned} I_N = K_A(I_1 + I_2) + K_B(a^2 I_1 + a I_2) + K_C(a I_1 + a^2 I_2) = \\ I_1(K_A + a^2 K_B + a K_C) + I_2(K_A + a K_B + a^2 K_C) \end{aligned} \tag{4.52}$$

where $a = e^{j\frac{2\pi}{3}}$. Since $K_{A,B,C}$ are real values and $a^2 = a^*$, the two k-factors are proved to be complex conjugates of each other. In order to solve for K_1, the following approach has been applied:

First equation (4.51) is multiplied by I_1^* and then the conjugate of equation (4.51) is multiplied by I_2:

$$I_1^* \cdot I_N = I_1^* \cdot (K_1 I_1 + K_1^* I_2) \tag{4.53}$$

$$I_2 \cdot I_N^* = I_2 \cdot (K_1^* I_1^* + K_1 I_2^*) \tag{4.54}$$

subtracting the results gives:

$$I_1^* I_N - I_2 I_N^* = K_1 |I_1|^2 - K_1 |I_2|^2 \tag{4.55}$$

therefore, we have:

$$K_1 = \frac{I_1^* I_N - I_2 I_N^*}{|I_1|^2 - |I_2|^2} \tag{4.56}$$

Equation (4.56) uses the current measurements to auto-set the k-factors. To ensure dependability of the unbalance k-factors, the auto-set can be done using the average of several successive measurements of phase and neutral currents.

By replacing the derived k-factors in the compensating term of $K_1 I_1 + K_2 I_2$, and subtracting it from the neutral current, one can use the phase angle difference between the calculated quantity and the phase currents to determine the faulted phase and section. To make the phase comparison, demonstrated in (4.49), adjustable for internally fused and fuseless banks, a sign factor, K_{sg}, is defined that makes the final fault location principle to be expressed as

$$I_N^{Comp} = K_{sg}\left(I_N - (K_1 I_1 + K_2 I_2)\right) \tag{4.57}$$

Moreover, depending on whether the element has failed in the left section or right section of the SCB, (4.49) will get an additional negative sign. As a result, to make the decision boundary uniquely around $0°$ phase angle difference between I_N^{Comp} and the faulted phase current, K_{sg} is defined as follows.
For fuseless SCBs:

$$K_{sg} = \begin{cases} +1 & \text{Left Section Evaluation} \\ -1 & \text{Right Section Evaluation} \end{cases} \tag{4.58}$$

For internally fused SCBs:

$$K_{sg} = \begin{cases} -1 & \text{Left Section Evaluation} \\ +1 & \text{Right Section Evaluation} \end{cases} \tag{4.59}$$

4.5.2   Estimating the number of failed elements

The consequence of an element failure in one of the sections is the change in the reactance value. The effect on the neutral current magnitude should therefore be evaluated to set a reference for fault location application. With reference to (4.44) and (4.45), the derivative of the neutral current can be used to derive the required setting. The procedure would be similar to neutral current unbalance pickup setting calculations [3]. It is worthy to note that as in the common design for double wye *ungrounded* SCBs, the left and right section of the bank may not have the same reactance, so the reference value for detection

of number of failed elements should be set separately for each section. To find the change in the neutral current with development of a single element failure in the left section, a failure is assumed in one of the phases, say phase A:

$$\frac{d\,I_N}{dX_A^l} = \frac{d(K_A I_A + K_B I_B + K_C I_C)}{dX_A^l} = \frac{dK_A}{dX_A^l} I_A \qquad (4.60)$$

which gives the following identity

$$\frac{d\,I_N}{dX_A^l} = \frac{-X_A^r}{(X_A^l + X_A^r)^2} I_A \qquad (4.61)$$

Similarly for a failure in the right section of phase A, one can derive:

$$\frac{d\,I_N}{dX_A^r} = \frac{X_A^l}{(X_A^l + X_A^r)^2} I_A \qquad (4.62)$$

Same equations hold true for phase B and C. To form the derived equations as a setting, the phase current is replaced by rated current, I_r, and the absolute value of the derivative is re-written in terms of limits. Both the change in reactance and the change in neutral current are expressed in perunit values. Left section reactance is selected as the base for reactance change and the rated phase current as a base for the neutral current change.

$$\Delta\,I_N(\text{pu}) = \begin{cases} \Delta X_A^l(\text{pu}) \times \frac{K_x}{(K_x+1)^2} & \text{Left section setting} \\ \\ \Delta X_A^r(\text{pu}) \times \frac{1}{(K_x+1)^2} & \text{Right section setting} \end{cases} \qquad (4.63)$$

where the following relationship exists between left section reactance and right section perphase reactance:

$$X^r = K_x X^l \qquad (4.64)$$

When $\Delta X(\text{pu})$ is calculated for a single element failure, the $\Delta I_N(\text{pu})$ will form a base for detection of number of failed elements that is also used to set a magnitude threshold for triggering the phase comparison.

Details on application settings and how the setting quantities are calculated for a given SCB are provided in Section 4.8.2.

4.6 Enhanced Compensated Neutral Current for Grounded Y-Y SCB

4.6.1 Determining the involved phase and section

Developing a fault location method for grounded double wye banks with neutral unbalance protection would be almost similar to ungrounded ones. As there is a pass to ground in this configuration, the zero sequence current exists in the neutral current. However, even sensitive unbalance protection methods [38] have had to ignore the effect of zero

sequence current. This is because compensating the pre-existing unbalance caused by all three sequences of current, i.e. setting the three k-factors, requires a set of three equations while we always have just a set of two (real and imaginary parts of the neutral current). As a result, the zero sequence current is left uncompensated [2]. Such an assumption does not render loss of reliability for the protection and fault location. The reason is, first, the two sections of these grounded banks are manufactured to be identical in impedance (factory matched). Second, a window CT measuring the vectorial difference between the neutral currents is applied. Furthermore, as it will be seen in this section, manufacturing tolerance in the parallel banks impedance (mismatch) will cause a small aggregated k-factor multiplied by the zero sequence current in the expected neutral current calculation, which makes the effect of zero sequence to be negligible [3]. Figure 4.6 illustrates this configuration with its corresponding measurements for neutral unbalance protection.
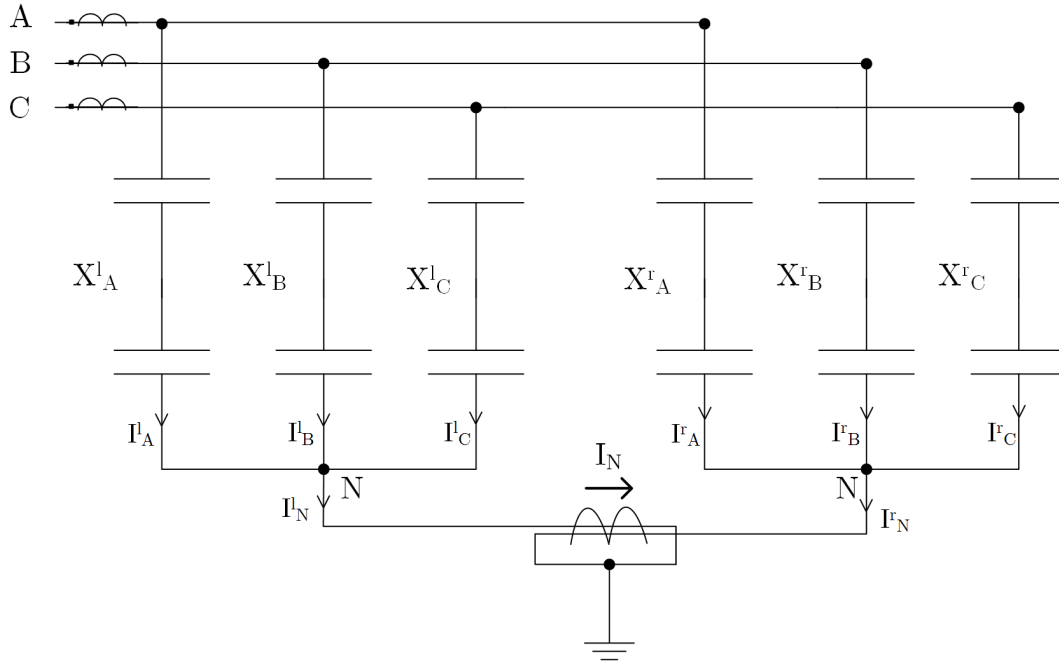
Figure 4.6: Grounded double wye shunt capacitor bank

The pre-failure neutral current can be expressed in an approach similar to (3.15), and (4.45). The current through the window CT in the neutral is referred to as I_N.

$$I_N = I_N^l - I_N^r = (K_A^l - K_A^r)I_A + (K_B^l - K_B^r)I_B + (K_C^l - K_C^r)I_C$$
$$= K_A I_A + K_B I_B + K_C I_C \qquad (4.65)$$

where the k-factors are

$$K_p = \frac{X_p^r - X_p^l}{X_p^l + X_p^r} \qquad p : A, B \ \ or \ \ C \qquad (4.66)$$

If we transform (4.65) from phase coordinates into sequence components [3], it becomes

$$
\begin{aligned}
I_N &= K_A(I_1 + I_2 + I_0) + K_B(a^2 I_1 + a I_2 + I_0) + K_C(a I_1 + a^2 I_2 + I_0) \\
&= I_1(K_A + a^2 K_B + a K_C) + I_2(K_A + a K_B + a^2 K_C) + I_0(K_A + K_B + K_C) \\
&\simeq I_1(K_A + a^2 K_B + a K_C) + I_2(K_A + a K_B + a^2 K_C) \\
&= K_1 I_1 + K_1^* I_2 \qquad (4.67)
\end{aligned}
$$

As stated before, the term corresponding to zero sequence current is neglected to enable auto-set of unbalance k-factors. The coefficient of I_0 itself is likely to get a very small value as the k-factors of different phases defined by (4.66) might be of varying signs. Furthermore, the resultant k-factors will be complex conjugate of each other since K_A is a real value and $a^2 = a^*$.

Since for severe system voltage unbalance the quality of compensation factor would be lower than its actual required value, reference [3] suggests a percent restraint, see Figure 4.7, for a commercial protection operating signal. In the evaluation section it will be shown that restraint supervision is not necessary for supervised monitoring applications such as fault location.
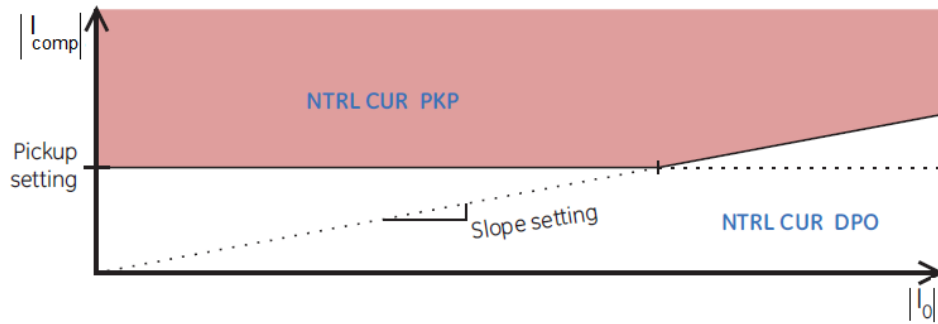
Figure 4.7: Grounded double wye neutral current unbalance protection, restraint supervision [3].

The compensated neutral current for fault location would be the vectorial difference of actual measured neutral current with the expected value of it derived as per (4.67). Therefore, same equations as ungrounded SCBs will be used for fault location and k-factor calculation, see equations (4.57), (4.58), and (4.59).

4.6.2 Estimating the number of failed elements

Similar to ungrounded double wye SCBs, we need to first find out the neutral current derivative with respect to one of the sections of a selected phase (reactance). Then the absolute value of the derivative should be related to a minimum expected change in the reactance, i.e. one element failure. The difference from the ungrounded configuration is the identity which relates the value of the phase coordinate k-factors to the phase reactances as per (4.66). For grounded SCBs the two sections (the two parallel banks)

are factory matched which means the base for number of failed elements would be the same for them. The mentioned derivation could be expressed as

$$\frac{d\,I_N}{dX_A^l} = \frac{d(K_A I_A + K_B I_B + K_C I_C)}{dX_A^l}$$
$$= \frac{dK_A}{dX_A^l}I_A$$
$$= \frac{d(\frac{X_A^r - X_A^l}{X_A^l + X_A^r})}{dX_A^l}I_A$$
$$= \frac{-2X_A^r}{(X_A^l + X_A^r)^2}I_A \qquad (4.68)$$

By taking the same procedure for a failure in the right section we will get similar results, though with opposite effect on the magnitude of the neutral current, see (4.69). This was expected due to the differential property of the measured current through the neutral window CT.

$$\frac{d\,I_N}{dX_A^r} = \frac{2X_A^l}{(X_A^l + X_A^r)^2}I_A \qquad (4.69)$$

Again note that the expected value for X_A^r and X_A^l are the same for this configuration, and in the next equation we will denote both as X. Also to set the function for a particular SCB, the phase current in (4.68) may be taken as its magnitude which will be denoted as the SCBs primary perphase current, I_r. Thus, the final base for detection of number of failed elements would be

$$\frac{\Delta\,I_N}{I_r} = \frac{\Delta X}{2X} \qquad (4.70)$$

in which ΔX denotes the absolute value of the change in one of the locations' reactance, such as phase A left section, as a result of an element failure in that location. X denotes the reactance of that location. The last equation can be interpreted in per unit form as well:

$$\Delta\,I_N(\text{pu}) = \frac{\Delta X}{2}(\text{pu}) \qquad (4.71)$$

4.7 Envision of Additional Unbalance Protection Elements

The suitability of a fault location method depends on capacitor bank's configuration and the available monitoring points. Locating internal failures could be an additional relaying element to be added to a capacitor bank protection and control relay. Thus, it is seldom economic to add voltage or current transducers whose application could be for solely fault location. As a result, this chapter, by discussing two actual SCB configurations, will consider examining utility perspectives that already deploy additional unbalance protection elements.

4.7.1 Additional Voltage Differential Element

Figure 4.8 depicts the provided configuration.
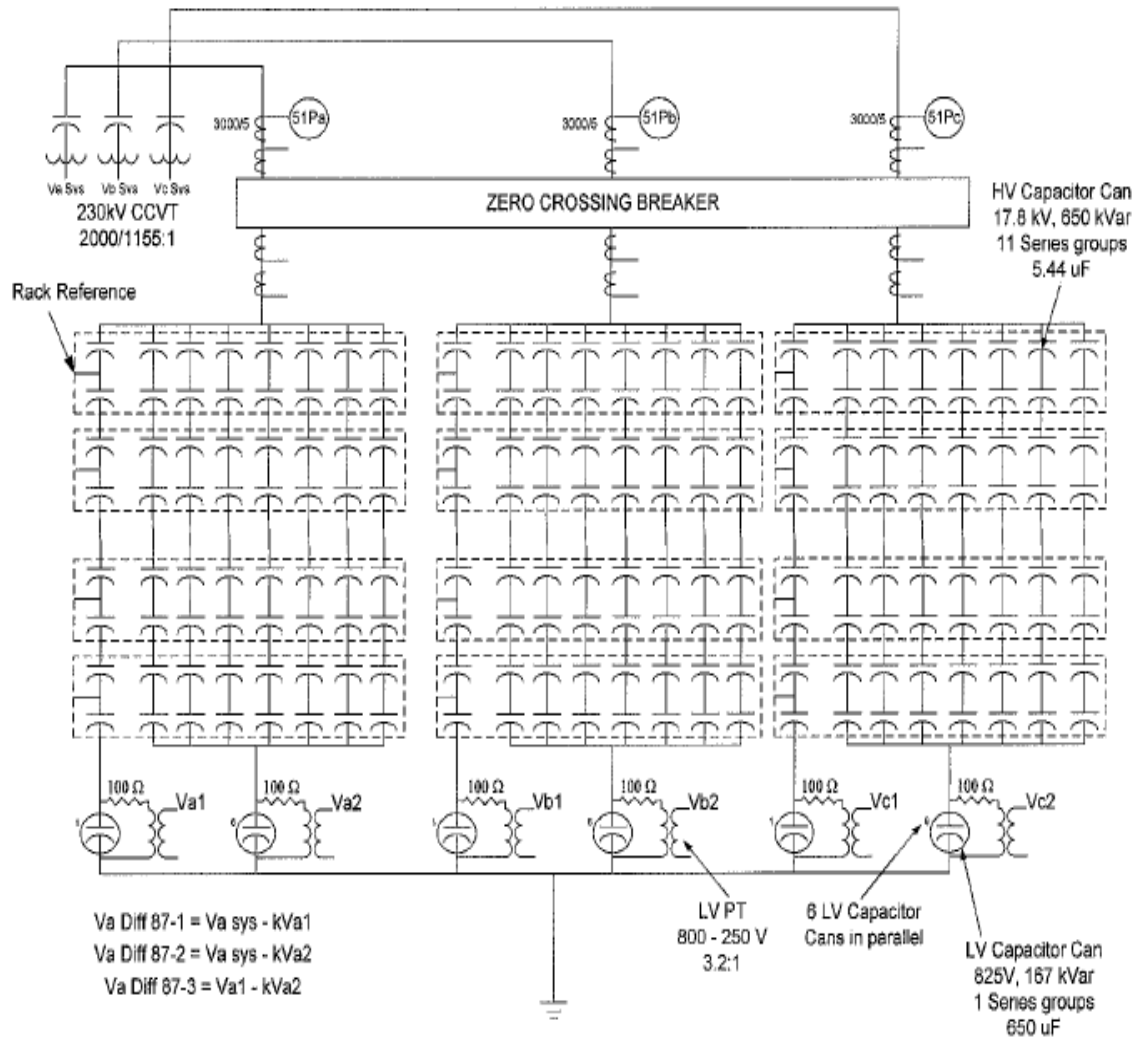
Figure 4.8: 230 kV Grounded Fuseless Bank with Tapped Voltage Measurement in Each Section.

The left string of each phase, depicted along with the rack reference, is in parallel with a group of capacitor units shown on the right side of each phase. Therefore, the configuration is double wye with three differential elements per phase. The aim is to locate the faults on left and right (top of the LV capacitors) of each phase. For each section of the SCB, i.e. right and left, the tap voltage is assessed against the bus voltage with a k-factor that resets the signal.

$$V_{\text{op}} = V_{\text{BUS}} - k_{\text{set}} V_{\text{TAP}} \tag{4.72}$$

The fault location philosophy is as explained in Section 2.2. As can be seen in Figure 4.8, an additional differential function is included in the protection IED of this SCB, namely 87-3, with the following definition:

$$V_{\text{op}} = V_{\text{TAP}}^L - k_{\text{set}} V_{\text{TAP}}^R \tag{4.73}$$

Note that the k_{set} values will take different values for the three differential functions.

Estimating the number of failed elements

Sensitivity analysis of the differential protection function can be used to define a base for the number of failed elements determination. The incremental change in the voltage differential operating quantity can be found by taking the operating signal derivative with respect to the reactance considering a change of reactance in the corresponding part. For the provided fuseless bank design, the top section failures are of concern, thus we assume a failure in one of the sections, suppose left and top, i.e. X_1^L, see Figure 4.9. The lower part of the section is assumed to have constant reactance for this purpose, X_2^L. Bus voltage is also noted as V_p.
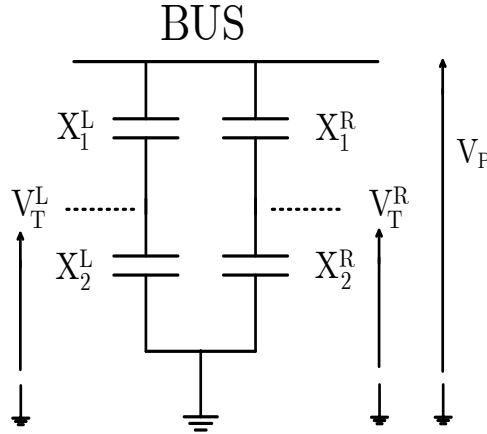
Figure 4.9: A phase of a double wye SCB with voltage differential protection.

$$\frac{dV_{op}}{dX^L} = V_p \frac{d}{dX}(1 - k_{set}\frac{X_2^L}{X^L}) = V_p\, k_{set}\, X_2^L\, (\frac{1}{X^L})^2 \tag{4.74}$$

Replacing the k_{set} with its value as $\frac{X^L}{X_2^L}$ gives

$$dV_{op} = dX^L \times \frac{V_p}{X^L} \tag{4.75}$$

In per-unit form and assuming that the bus voltage is equal to 1 per-unit, we can re-write the last equation in general as

$$\Delta V_{op}(pu) = \Delta X(pu) \tag{4.76}$$

in which the base for per unitizing the reactance is the corresponding section total reactance. We will show in the evaluation results that the third differential function, 87-3,

gives a reliable auxiliary alarm which is helpful in case of bus VT failures. A difference to notice is that the voltages and the k-factor that comprise the operating function of 87-3 have much less magnitude/value than the corresponding ones in 87-1 and 87-2. Moreover, simultaneous failures could be detected successfully, this is due to independence of equations for each phase and section k-factors (87-1 and 87-2 functions), which allows to reset each function without disturbing the detection of failed elements in the rest of the phase and sections.

The 87-3 function is not capable of detecting simultaneous left and right section failures. In this regard, sensitivity analysis can show the effect of the corresponding simultaneous failures for 87-3 operating function.

With reference to Fig. 4.9, the derivative of 87-3 function in Fig. 4.8 can be expressed as follows: First with respect to left section, top of the tap failures

$$\frac{dV_{op}}{dX_1^L} = \frac{d(V_p \frac{X_2^L}{X_1^L + X_2^L})}{dX_1^L} = V_p \frac{-X_2^L}{(X^L)^2} \tag{4.77}$$

in per unit and assuming that the bus voltage is equal to 1 per unit, we can re-write the last equation in a general form as

$$\Delta V_{op}(pu) = \frac{-X_2^L}{X^L} \Delta X_1^L(pu) \tag{4.78}$$

in which the base for per-unitizing the reactance is the corresponding section total reactance.

Same procedure with respect to the right section, top of the tap failures gives

$$\frac{dV_{op}}{dX_1^R} = \frac{d(-k_{set} V_p \frac{X_2^R}{X_1^R + X_2^R})}{dX_1^R} = -k_{set} V_p \frac{-X_2^R}{(X^R)^2} \tag{4.79}$$

again in per-unit and assuming that the bus voltage is equal to 1 pu, we can re-write the last equation in a general form as

$$\Delta V_{op}(pu) = \frac{X_2^L}{X^L} \Delta X_1^R(pu) \tag{4.80}$$

From (4.78) and (4.80), plus the fact that the right and left sections of the SCB of Fig. 4.8 have different reactances, we conclude that upon simultaneous failures in left and right sections, the magnitude of the operating function of 87-3 will get changed less than the expected jump for a single left section element failure. An illustrative scenario will be provided in Section 5.

4.7.2   Additional Neutral Unbalance Element

Based on IEEE Std C37.99 [2], for large and HV capacitor banks, failure of a single element results in a very small operating signal. This implies the need for ultra sensitive unbalance protection. A backup (redundant) neutral voltage unbalance protection is generally provided, this will also help to reduce the chance of missing canceling failures.

Neutral voltage is sensitive enough for protection purposes in case of mirrored failures in both sections (simultaneous masking) while neutral current is not. Similarly, provisions might be made to back up voltage transformer based protections with current based ones or with back up VTs.

Figure 4.10 depicts a configuration in which both neutral current and neutral voltage are measured.
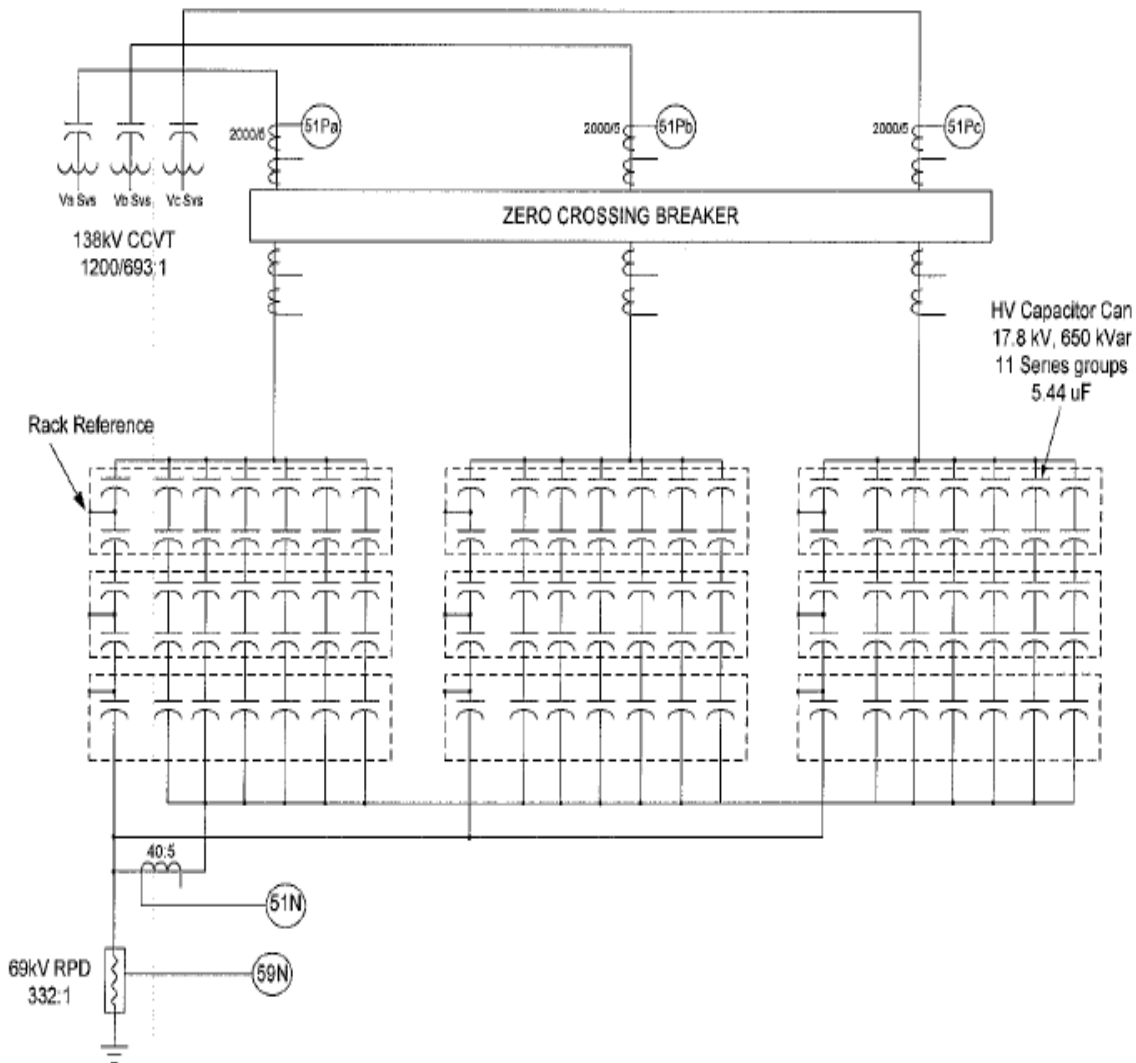
Figure 4.10: 138 kV Ungrounded Fuseless Bank.

A single string on the left side of the illustration represents one wye section which is in parallel with a group of units forming the right wye section. Thus, the configuration is generally the same as what we discussed for double wye ungrounded banks.

As it was mentioned, the additional neutral PT could be an asset for protection, however in terms of fault location the answer is different. Since with neutral unbalance protection

a complete and successful fault location was demonstrated, the only point that might be of concern is for simultaneous failures. Which again for both neutral voltage unbalance and neutral current unbalance it was shown that fault location is not applicable. Since the added neutral measurement does not bring any per-phase measured quantity even applying both of the neutral current based and neutral voltage based fault locations in parallel will not introduce any benefit.

In the next subsection we will discuss "estimation" of the neutral voltage without using the actual measurement to envisage any prospective application for fault location.

Estimation of the Neutral Voltage

IEEE C37.99 [2] introduces formulas for deriving the perunit magnitude of unbalance quantities for protection purposes. A voltage based perunit value can be converted to the primary quantity using system line to neutral voltage as a base and as reported by [26] the formulas give an error of less than 1% when compared to simulations.

A detailed explanation and a perceived new application of the formula presented in [2] for the neutral voltage calculation is discussed here. By assuming a failure in each section of a Y-Y SCB, the perunit capacitance of the phase can be calculated either using the formulas of [2] or by taking the perunit value of the alternative one presented in Section 4.8.2. Suppose the perunit capacitance is C_p for the affected phase, then using the suggested instant of time analysis in IEEE Std C37.99, the neutral voltage can be derived as follows: For the instant of time that the affected phase bus voltage is at its positive peak and considering 120° phase angle shift between the bus voltages, the two other phases are at their half of negative peak value. Therefore, we can make them parallel with a resultant phase capacitance of 2 pu. Fig. 4.11 presents the equivalent circuit for that instant of time.
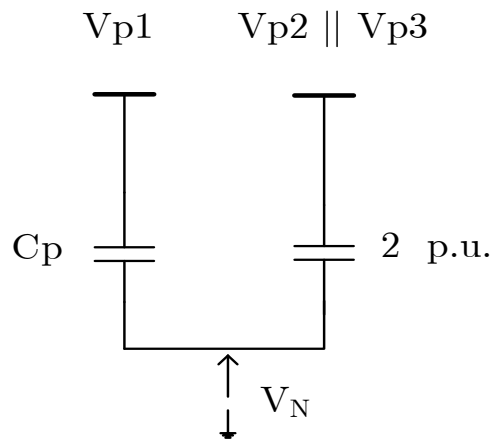
Figure 4.11: Derivation of neutral voltage based on perunit phase capacitance after failure.

where $Vp1$ is the phase with the failed element(s) and the two other phases are signified with $Vp2$ and $Vp3$. A voltage division helps to express the neutral voltage in perunit.

$$(1 - V_N)C_p = (V_N + 0.5) \times 2 \qquad (4.81)$$

or:

$$V_N = \frac{C_P - 1}{C_P + 2} = 1 - \frac{3}{2 + C_P} \text{ pu} \tag{4.82}$$

The last equation is the suggested formula in IEEE C37.99.

Discussion on Neutral Voltage Estimation for Y-Y Banks

Although at first an estimation for the neutral voltage seems to be a useful quantity; however, as it will be discussed, it cannot be relied on for faulted section identification in double wye banks [39].

Fig. 4.12 shows the circuit diagram for cut-set analysis of two single element failure scenarios in the left and the right section of an asymmetrical Y-Y SCB, respectively. Suppose the reactance of the involved phase, say phase A, changes (noted by prime
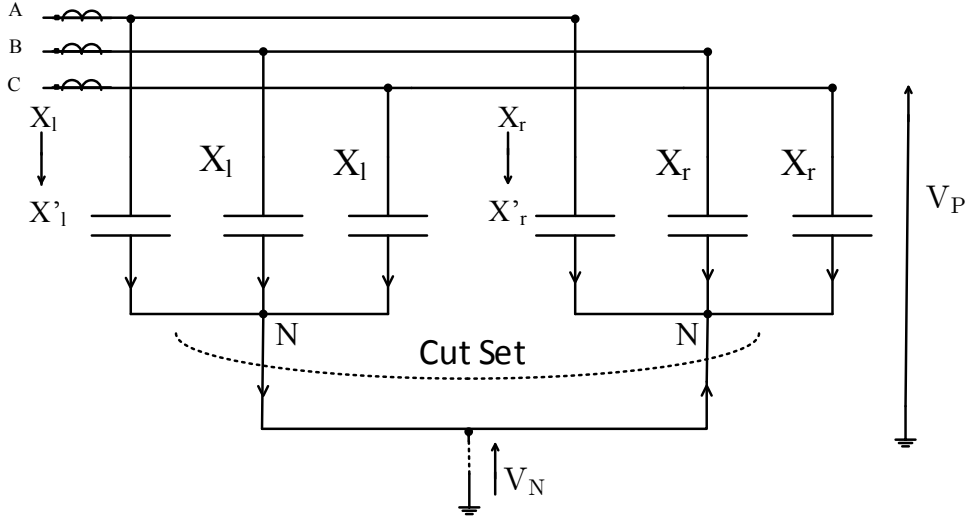
Figure 4.12: Neutral voltage estimate for asymmetrical Y-Y SCBs.

symbol in Fig. 4.12). Then for the described two scenarios, the following equation set holds true.

$$\begin{cases} \frac{V_A - V_{N_l}}{X'_l} + \frac{V_B - V_N}{X_l} + \frac{V_C - V_N}{X_l} + \frac{V_A - V_N}{X_r} + \frac{V_B - V_N}{X_r} + \frac{V_C - V_N}{X_r} = 0 \\[4mm] \frac{V_A - V_{N_l}}{X_l} + \frac{V_B - V_N}{X_l} + \frac{V_C - V_N}{X_l} + \frac{V_A - V_N}{X'_r} + \frac{V_B - V_N}{X_r} + \frac{V_C - V_N}{X_r} = 0 \end{cases} \tag{4.83}$$

Adding and subtracting the underlined terms to the corresponding equation gives

$$\begin{cases} \frac{V_A - V_N}{X'_l} - \underline{\frac{V_A - V_N}{X_l}} + \underline{\frac{V_A - V_N}{X_l}} + \frac{V_B - V_N}{X_l} + \frac{V_C - V_N}{X_l} + \frac{V_A - V_N}{X_r} + \frac{V_B - V_N}{X_r} + \frac{V_C - V_N}{X_r} = 0 \\[4mm] \frac{V_A - V_N}{X_l} + \frac{V_B - V_N}{X_l} + \frac{V_C - V_N}{X_l} + \frac{V_A - V_N}{X'_r} - \underline{\frac{V_A - V_N}{X_r}} + \underline{\frac{V_A - V_N}{X_r}} + \frac{V_B - V_N}{X_r} + \frac{V_C - V_N}{X_r} = 0 \end{cases} \tag{4.84}$$

Naming the neutral voltage of the first scenario V_{N_1}, and second scenario as V_{N_2} helps to

re-write the equation set as

$$\begin{cases} 3V_{N_1}(\frac{1}{X_l} + \frac{1}{X_r}) = (V_A - V_{N_1})(\frac{1}{X'_l} - \frac{1}{X_l}) \\ \\ 3V_{N_2}(\frac{1}{X_l} + \frac{1}{X_r}) = (V_A - V_{N_2})(\frac{1}{X'_r} - \frac{1}{X_r}) \end{cases} \qquad (4.85)$$

This implies that the resultant neutral voltage from same level of failures in the left and the right sections are the same if and only if the change in the two sections capacitance (reciprocal of reactances) are equal, or equivalently:

$$V_{N_1} = V_{N_2} \iff C'_l - C_l = C'_r - C_r \qquad (4.86)$$

Referring to the configurations in Fig. B.4 and Fig. 4.10, it is recognized that the common design for the asymmetrical SCB configurations implies slight differences in the two sections design, such as difference in the per phase parallel strings number for a fuseless bank. Therefore, the change in the phase capacitance after a failure would be the same for the two sections, and that gives equal neutral voltage magnitude, which can not help in determining the faulted section.

4.7.3 Conclusion for applicability of additional protection elements to fault location

The successful determination of simultaneous failures was verified for the additional tapped voltage differential element. This has been due to fault location indicating quantities independence for each phase and section. This allows to reset each function without disturbing the detection of failed elements in the rest of the phase and sections. It was also concluded that the auxiliary alarms of the tap to tap differential element will be useful in case of loss of bus VTs. Sensitivity analysis proved the possible malfunction of this auxiliary alarm for simultaneous left and right section failures.

Neutral voltage estimation applicability to involved section identification in capacitor element failures was discussed and mathematical reason behind the unhelpfulness of this quantity was also provided.

4.8 Provisions for Algorithms Security and Applications

In this section the provisions made to increase the proposed algorithms security and also considerations for deploying the methods in actual relays are presented. These include immunity to gradual reactance changes, applying security counting scheme, and information on the required data for relay settings, plus displaying the fault location results for the bank repair crew and operators. Flowcharts of the proposed methods are also shown, which include these provisions.

4.8.1   Compensation for Gradual Changes in the Reactance

Similar to the difference in the perceived temperature in the sun and the shade for humans, there could be a considerable temperature variance for substation equipments to be in the shade or under direct sunlight. Solar radiation can greatly change the temperature of an equipment, heating it above the air temperature. Although temperature difference of around 10°C is the usual expected value, but extreme examples of possible 30°C difference have also been reported [40]. In power capacitors, solar heating can change the capacitance for three different reasons [19]:

- Changing the dielectric film, usually polypropylene

- Changing the dielectric fluid, mineral oil or other fluid

- Heating of the dielectric fluid causes expansion, better permeating the film

Some of the unbalance protection methods like voltage/current differential can reduce unequal solar heating effect [2] as the affected part of the quantities cancel out each other. This is of higher importance for fuseless banks with lots of series elements. By considering a regular updating for the k-factors and hence making the algorithm immune to gradual changes in the capacitance, actual failures within the SCB can be distinguished reliably. In order to detect sudden changes due to capacitor failures, the k-factor updating is blocked with the very first considerable increase in the magnitude of the fault location principle. Upon detection of the failure the regular update process will be triggered again to ensure detection of subsequent failures. The regular updating of k-factors is also called "self-tuning", and the initial setting of them which is also applied upon failure detection in our proposed methods is referred to as "auto-setting" [38].

In order to find out the rate of this update so that the element failures do not get missed or "learned" by the algorithm, we evaluate a worst case scenario for a partial shading. We refer to IEEE standard for shunt power capacitors [41], the maximum ambient temperature defined in this standard for operation of SCBs is 55°C. Considering the aforementioned 30°C difference between one phase under direct sunlight and the other resting in the shade, and using Figure 4.13, a gradually reached superimposed reactance, defined by equation (4.18), of 1.5% can be anticipated for the worst case scenario. Considering the fact that it takes hours for the 30°C temperature difference to be reached, this anticipated amount is not comparable with even one single element failure effect. References [38] and [42] have reported the fact that capacitor failures can be distinguished from changes due to ambient temperature because of thermal inertia of capacitor cans. For example, for single element failures in single wye SCBs, the magnitude of the superimposed reactance will change 0.3%, or even less, in around 10 ms. On the other hand, it will take thousands of seconds for the worst case scenario of a shading effect to be able to mimic such a change. Simulation results in the next chapters confirm these calculated values. See Table 5.1 and Figure 5.23 in Section 5.

As a conclusion, to enhance the dependability of the proposed methods, the k-factors must be updated after detection of each failure or after repair of the SCBs, and to enhance the security of the proposed methods, k-factors have to be updated at regular intervals of say, once or twice an hour. To avoid interference with the fault location, this

regular updating should be blocked for a short while, once an internal failure is suspected, i.e. when the phase angle comparison is triggered.
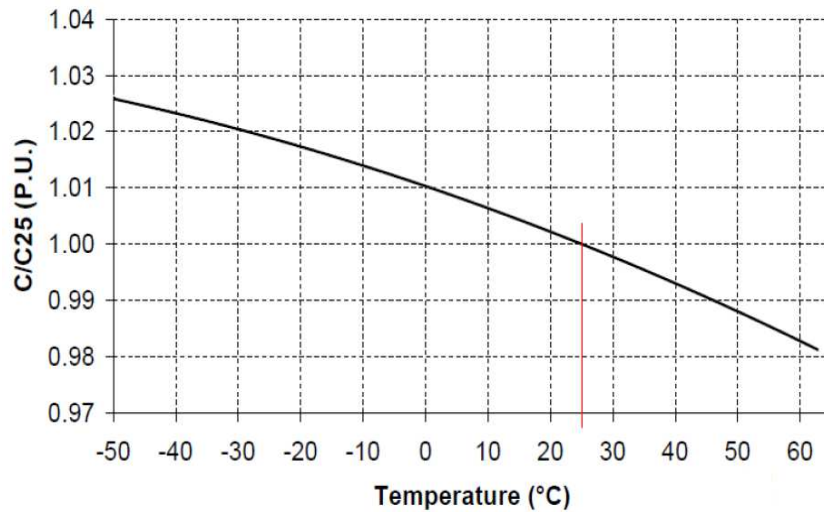
Figure 4.13: Per unit capacitance of the 25°C rating vs. temperature for capacitors impregnated with Faradol 810 insulating fluid [4].

4.8.2 Required Data for the Application Setting

The required data to set up the proposed fault location methods [43, 44] is summarized in this section. We will also present that how the bank and capacitor unit construction information could be used for setting calculations. The following nomenclature shows the required information from a user/customer to set the application:

Su Series groups in the unit

N Parallel elements in a group

P Parallel units in a group

Pst Parallel strings per phase

S Series groups, line to neutral (or to neutral capacitor)

Qu Rated kVAR of each unit

Vu Rated voltage (kV) of each unit

Q Rated MVAR of the SCB (three phase)

V Rated line to line voltage of the SCB (kV)

f Rated operating frequency

Where the element capacitance is not provided directly, capacitance of each element can be calculated using the ratings and construction information of each capacitor unit, see (4.87).

$$C_e = Cu \times \frac{Su}{N} = \frac{Su \times Qu}{N \times Vu^2 \times \omega} \times 10^3 \tag{4.87}$$

where ω denotes the angular frequency in rad/s and Ce, and Cu denote element capacitance and unit capacitance in μF, respectively. Based on the provided construction information for both the bank and its units, the after failure and before failure capacitance are calculated by the fault location algorithm considering a single element failure. For double wye banks the ratio of the nominal section reactances, and the rated primary per phase current of the SCB are also calculated as follows:

$$K_x = \frac{X_r}{X_l} \tag{4.88}$$

$$I_{rated} = \frac{Q}{\sqrt{3}V} \times 10^{-3} \quad (A) \tag{4.89}$$

The before failure per phase capacitance is

$$C = Cu \times \frac{P \times Pst}{S} \tag{4.90}$$

For fuseless banks, according to definition [3], P equals unity. The after failure per phase capacitance for each section would be

$$\frac{Cu \times P}{S}(Pst - 1) + \frac{Cu \times P}{S - 1} \parallel (Cu_f + (P - 1) \times Cu) \tag{4.91}$$

where Cu_f denotes the after single element failure unit capacitance. Depending on the fusing method, this capacitance will get one of the following values:

$$Cu_f = \frac{Ce \times N}{Su - 1} \qquad \text{Fuseless Bank} \tag{4.92}$$

$$Cu_f = (\frac{Ce \times N}{Su - 1}) \parallel (Ce \times (N - 1)) \qquad \text{Fused Bank} \tag{4.93}$$

Note that, the operator $\parallel$, implies the following identity:

$$C_1 \parallel C_2 = (\frac{1}{C_1} + \frac{1}{C_2})^{-1} \tag{4.94}$$

Same equations apply for each section of the double wye bank. The corresponding capacitive reactances are also calculated where needed as $X = \frac{1}{C\omega}$. To ensure method reliability and for the purpose of threshold setting, a safety factor of 0.9 is applied to the calculated change in the fault location principle magnitude for single element failures. The resultant threshold would be the measure for phase comparison activation in the proposed fault location methods and also a base for the number of failed elements determination.

4.8.3   The Proposed Algorithms Flowchart

A characteristic plane relative to the proposed fault location methods is presented in Figure 4.14. For voltage based fault locations the magnitude threshold is set for the percent superimposed reactance. For current based fault locations the magnitude threshold is set for the compensated neutral current in percent of the rated current. If the magnitude goes beyond a specified minimum value then the angle comparison will be activated. It should be noted that for double wye SCBs the angles evaluated by this characteristic are compensated neutral current angle *referenced* to each phase current angle. As a result, the angle boundaries are set around zero phase angle. Figures 4.15 and 4.16 show
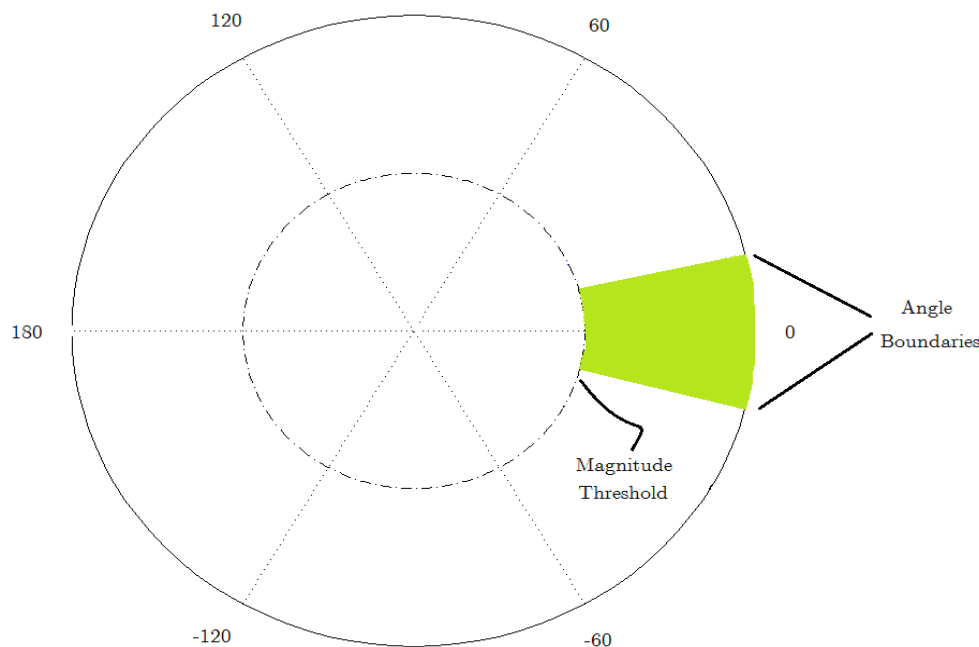
Figure 4.14: General characteristic plane of the proposed fault location methods.

more detailed algorithm steps by flowchart for the proposed SR based methods and the enhanced current based methods, respectively.

4.8.4   Blinder, Counting Schemes, and Blocking the Algorithm

Depending on how close the decision principle is to the security margins, the blinders can be defined. Blinders are the tolerance from the zero degree angle zone proposed for angle comparison for fault location purpose. With 15 degrees safety margin for the proposed methods, an acceptable and reliable operation has been observed for the simulated scenarios.

With regard to the deployed counting scheme, dependent on the counter limit that changes the status of the fault location (a.k.a. pick-up delay), the minimum required time between detectable consecutive faults can be investigated. The counter is set on 30, which requires about 2 cycles of the fundamental frequency in order to change the status of
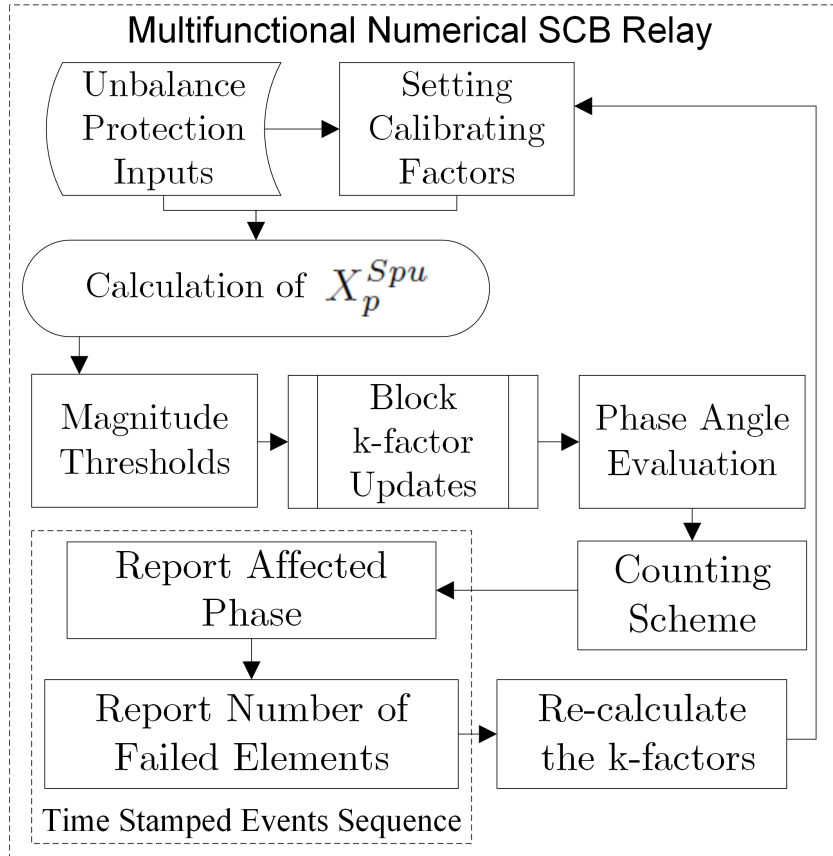
Figure 4.15: Flowchart of the proposed SR based fault location methods.
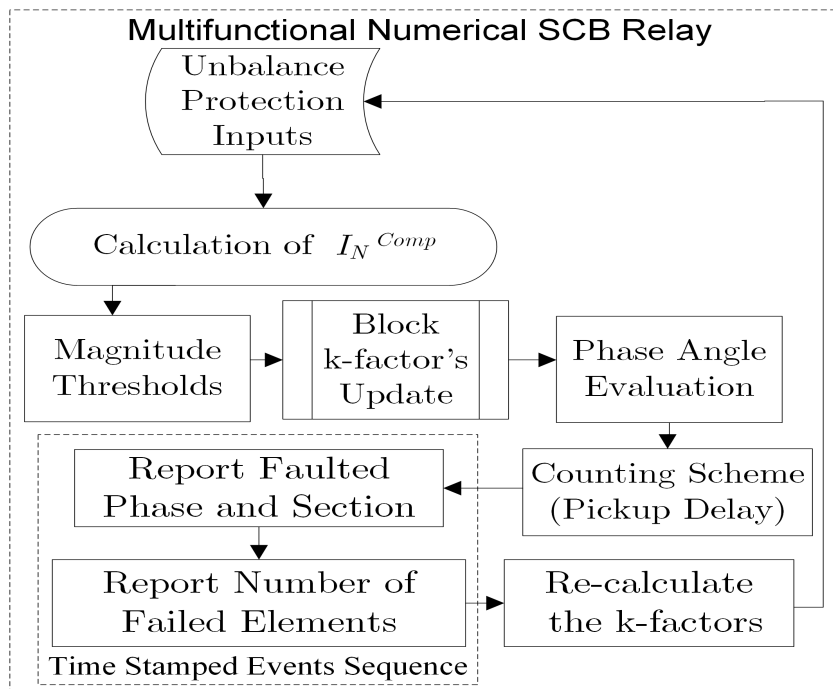
Figure 4.16: Flowchart of the proposed enhanced current based fault location methods.

the fault location report. This setting is also intentional to make the principle variations and the k-factor reset action visible in the evaluation figures. Using this presumed secure setting we performed our investigation on minimum required time between two detectable failures. Simulations show that for a detection time of 30 ms, the proposed methods would be able to determine fault location of a semi-simultaneous consecutive failure as close as 40 ms to the previous failure. However, in practice, low pick up delays are not preferred. Because the role of magnitude criteria becomes very decisive and thus during transients it may result in loss of the algorithm security. For this compromise, reducing the counter setting is not suggested as fault location determination is not time critical, it is for postmortem actions (repair time reduction), and also it is unlikely for two failures to happen exactly at the same time in different locations. In practice, the counting threshold, pick up delay, can be set to say 100 ms and would able to detect consecutive failures that are as close as say 200 ms to each other. Nevertheless, the proposed methods are superior in terms of detection time, as we also note that the more the number of the failures, the more the chances for cascading failures and thus the less time between them. Consequently, the detection time in locating the failures before tripping the SCB could improve the repair time for the capacitor bank and more availability of it in service.

Fig. 4.17 demonstrates the pickup and operation of the fault location based on the counting scheme. Because the voltage stress on the healthy elements in the SCB depends
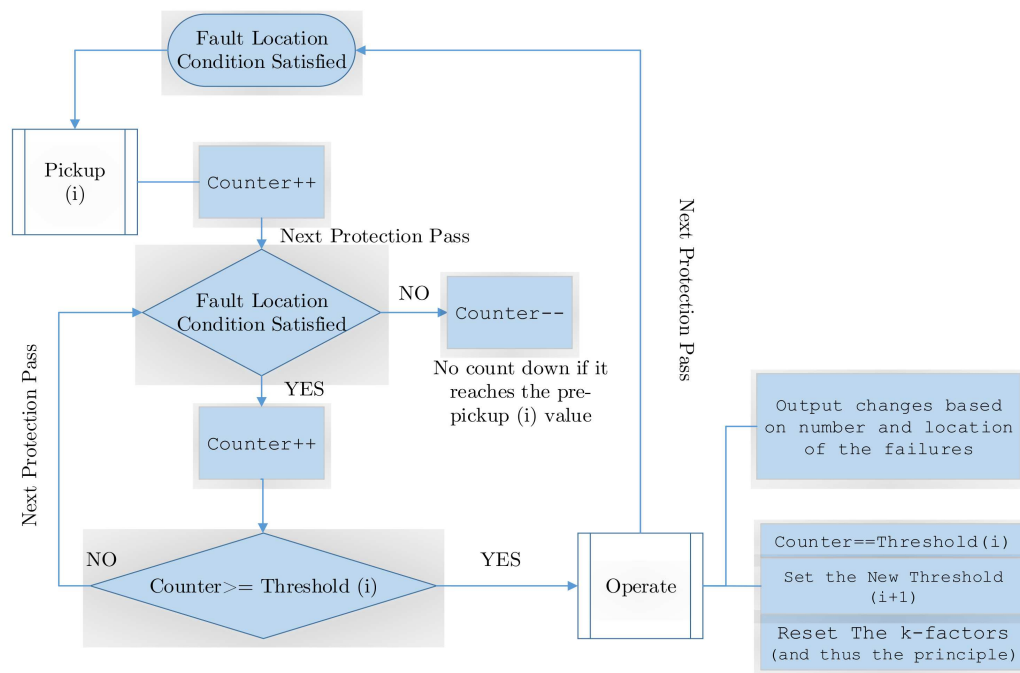

Figure 4.17: Pickup and counting scheme.

on the previous failed elements, an adaptive pick up and pick up delay can be selected. This way tripping the bank can also be initiated from the fault location when the number of failed elements reaches a predefined limit for each phase.

As it will be shown in the next chapter, there are cases for some configurations where it is suggested for security reason to block the fault location function in a protective relay. In case during this short time that the fault location is blocked, failures occur in *other* locations, the algorithm will not be able to detect any subsequent failure unless it gets reset upon unblocking. This is because without resetting the principle it will retain variations due to a missed failure. Thus the trade off would be between missing failures in the same location during the blocking time, due to resetting the k-factors upon unblocking, and not resetting the k-factors by relying on the fact that such a failure scenario is pretty unlikely [21]. Therefore, we have not suggested resetting the k-factors after the blocking interval. A safer approach could be resetting them once no failure is detected for a while after the unblocking moment.

4.8.5   Usage and Information Display for Bank Operators/Service Crews

The fault location algorithm is intended to be integrated into the unbalance relaying of SCB protection relays to provide advance alarms that often reduce the search space (by determining failure location) for planned maintenance. Commercial numerical relays for SCB protection and control [3,45] report the sequence of event records. They can capture and time tag state changes of relaying elements. For every fault event, the following items can be captured: affected phase/section location, number of failed elements, and time stamp of the fault/event. Numerical relays can communicate fault information to HMI/SCADA relay setup tools using communication protocols. Users can latch the front panel display of target messages i.e. faulty phase, number of elements, etc. Moreover, designated LEDs of microprocessor-based annunciators [46] can be configured to indicate the phase with failed capacitor elements to technicians that arrive at the substation.

4.9   Summary

This chapter introduced the theories of the proposed methods and applications for fault location in HV-SCBs. First the Superimposed Reactance (SR) concept was presented as part of the fault location for single wye SCBs with neutral voltage unbalance protection, second the SR was adapted for applying fault location to two other grounding arrangements. Then the neutral current unbalance protection was adapted to suit fault location methods for double wye grounded and ungrounded SCBs. A discussion on applicability of additional protection elements was also provided. Algorithms' characteristics, such as compensation for gradual changes in capacitance, settings calculations, and the flowchart of the proposed methods were also explained. In the next chapter simulation study of these proposed methods will be presented.

Chapter 5

Evaluation of the Proposed and the Investigated Methods

5.1 Introduction

This chapter covers evaluation of the proposed methods, also, where applicable, the SEL method [45] is simulated for comparison. Transient time-domain simulation studies are conducted to demonstrate the effectiveness of the proposed fault location schemes using PSCAD/EMTDC software package. The required voltage and current waveforms are recorded in COMTRADE [1] format which is an standard file format for transient waveform and event data of electrical power systems. Anti-aliasing filters are applied to the outputs of the transducer models. Then the records are played back for a relay model developed in MATLAB. Accordingly, waveforms are resampled at 64 samples per the power frequency cycle. Depending on the signal type, the relay model applies decaying DC removal filter or CVT transient filter and then uses full cycle Discrete Fourier Transform (DFT) for phasor estimation. Phase angle compensation for the delays introduced by the filters have also been considered. Phasor estimation and fault location algorithm are executed every 4 samples. See Appendix A for more details.

Because we deal with internal failures of the SCB, the test power system is selected to be a three phase source connected to the SCB via a transmission line. SCBs are simulated according to their configurations and designs. See Appendix B for details of the SCB designs under study.

In regard to simulation of the pre-existing unbalance in the SCB, based on [4, 21], capacitance of the units has a maximum acceptable tolerance of 10% from the average value. In practice, this is rarely more than 7%. In addition, having this deviation mentioned on the unit nameplate, the capacitor units are arranged in a way that the SCBs have equalized capacitance in strings and thus in the total phase. Thus, an inherent unbalance of around 0.5 % or less is the final tolerance achieved in the capacitor bank *strings*. Regarding the *phase* unbalances, this requirement is reported to be around

---

[1]Common Format for Transient Data Exchange

1% [21]. To validate algorithm performance, the maximum allowable inherent unbalance of 1% is simulated.

Harmonic currents have been injected according to the limits set by the IEEE standard 519 [47].
Signal to Noise Ratio (SNR) of the output of current/potential transformers are assumed to be 50 dB based on their rated secondary current/voltage. For the SCBs grounded through a capacitor, the 50 dB SNR is simulated based on the nominal voltage across the neutral capacitor.

For evaluation under unbalanced voltages, the balanced load is replaced with an unbalanced one. Voltage unbalance of around 2% is considered, which is the maximum acceptable value for the transmission level [48]. The definition of voltage unbalance is as percentage Voltage Unbalance Factor (%VUF) defined in [49]:

$$\%VUF = \frac{V_2}{V_1} \times 100 \tag{5.1}$$

All of the voltage and current figures reported in this thesis are in primary values. To facilitate interpretation of the fault location principle variations, a demonstrative guide is provided in Fig. 5.1. For the voltage based fault locations the plotted quantity would
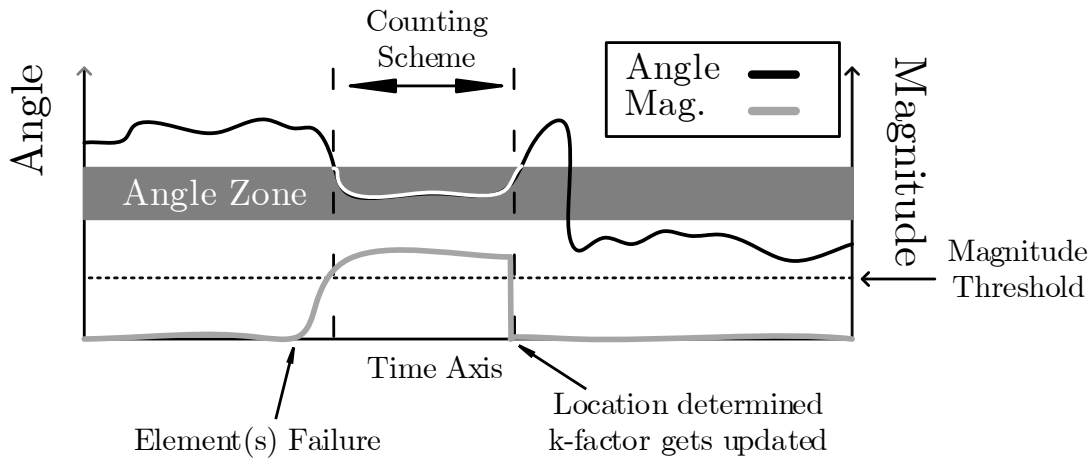

Figure 5.1: Interpretation guide for fault location principle variations.

be the SR, and for the current based fault location it would be the compensated neutral current. Magnitude of the compensated neutral current will be plotted in percentage of the rated current of the SCB, and angle of it is referenced to the corresponding phase current. Note that the magnitude threshold might not be shown on the principle variation figures, instead the tick marks on the magnitude axis are selected based on the threshold. The intervals that have led to internal failure reports are also pointed in the figures. The simulated internal failures include the following cases:

- Single element failure

- Multiple element failure (simultaneous failures at one location)

- Consecutive failure (failure in the same location of a previous failure but with more time interval in between compared to multiple element failures)

In the rest of the chapter, first, the angle zone margin and the counter setting are verified using simulations and then the simulation case studies are presented according to various SCB configurations.

Blinder and Counter Settings

The angle zone in Fig. 5.1 implies a tolerance band around zero for dependability, to consider current/voltage transducer errors, and security, to exclude unbalances that do not originate from capacitor failures. With 15 degrees safety margin, an acceptable and reliable operation has been observed for the simulated scenarios. Fig. 5.2 demonstrates the fault location principle variation for a single wye SCB with an element failure in phase B. Harmonics, voltage unbalance and arbitrary pre-existing inherent unbalance in the SCB were simulated for this case. As it can be seen, in the absence of noise, the
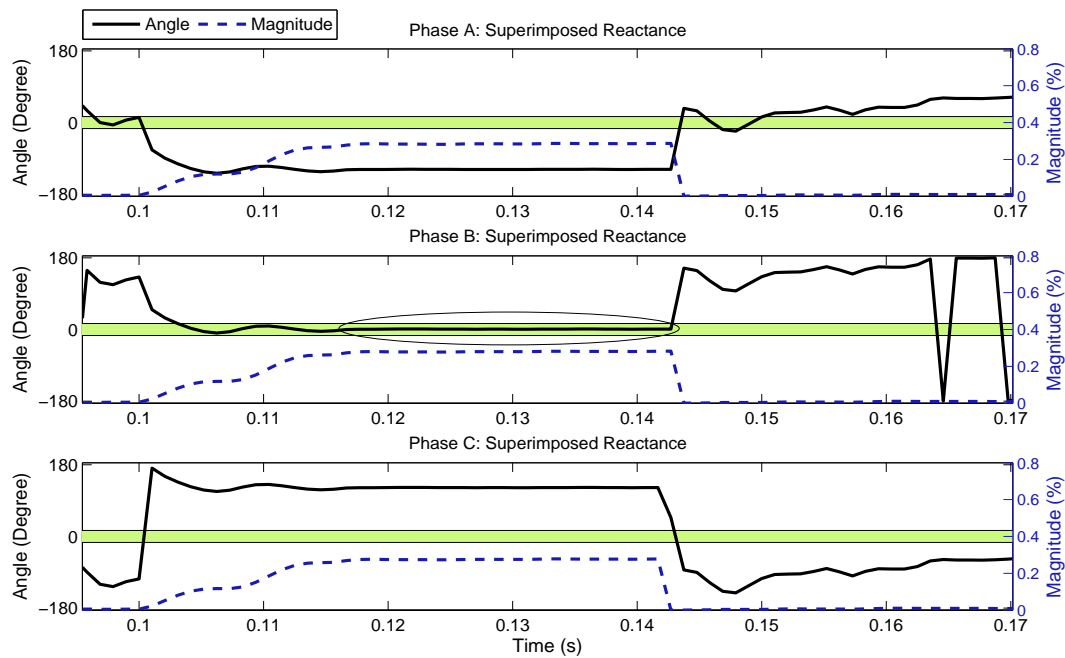

Figure 5.2: Margin evaluation without measurement noise (fuseless wye SCB).

principle is securely far from the boundary and is right at the middle of the angle zone.

The measurement SNR of 50 dB with respect to the *rated secondary voltage* of 115 volts for the neutral PT of an ungrounded SCB, implies noise magnitude of 2.88 times greater than even a 30 dB SNR with respect to the *actual voltage* at the secondary of the neutral PT. The actual voltage at the secondary of the neutral PT has been found to be in the range of 4 volts for internal failures. This ensures that in practice the assumed

15 degrees margin will be more than satisfying in terms of reliability of the margin. See Fig. 5.19 for comparison with the same case study with 50 dB measurement noise.

Same performance has been validated for a double wye SCB. Fig. 5.3 demonstrates the fault location principle for a fused double wye SCB that has been simulated for a failure in the left section of phase C. Depending on the inherent pre-existing unbalance inside the bank (which should be limited to 1% per phase as reported in [21]), the neutral current is simulated to be less than 0.5 Amps. Thus, as the proposed algorithm shows satisfying performance for 50 dB SNR based on the *5 Amps rated* current of the neutral CT secondary, it will have the same successful operation for *signal to noise ratios* of even less than 30 dB, based on the *actual neutral current* in the neutral CT secondary.
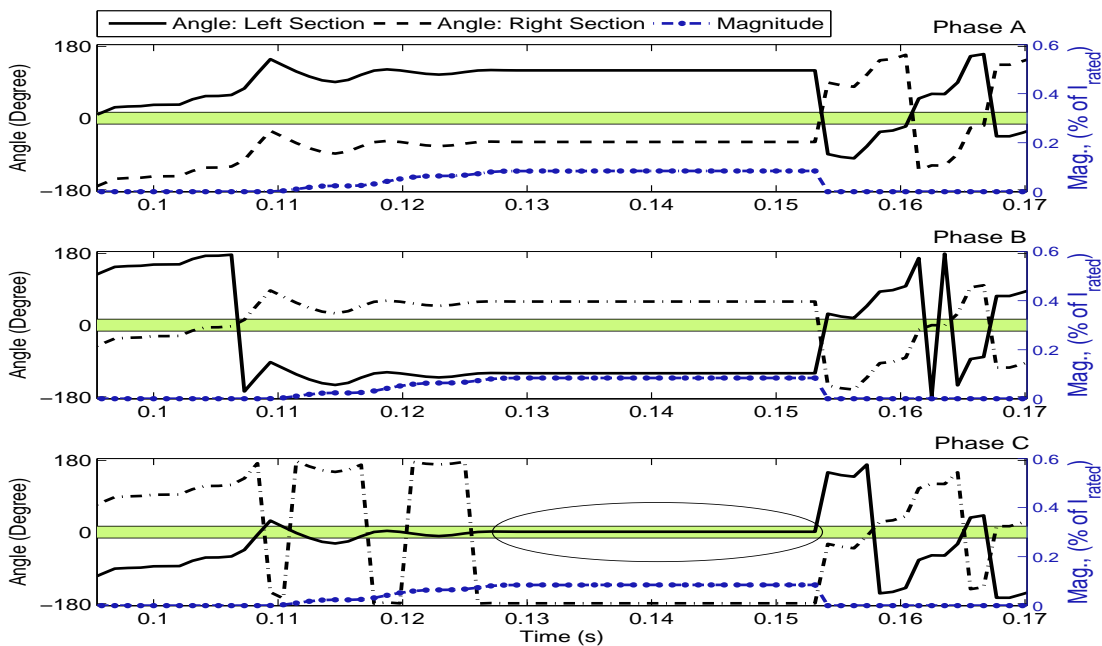

Figure 5.3: Margin evaluation without measurement noise (fused double wye SCB).

To demonstrate what we explained in Section 4.8.4 regarding the counter setting, the following simulations were performed. The point is to clarify that although the fault location might be successful but the security could become a concern if we reduce the counter limit. Figs. 5.4, and 5.5 illustrate simulation for single wye fused SCB. Failure in phase A happens at 0.2 s, and the failure in phase B happens on 0.22 s. Figs. 5.6, and 5.7 illustrate the same issue for a fuseless double wye SCB. Failure in phase A happens at 0.15 s, and the failure in phase B happens on 0.17 s. To further demonstrate the consecutive failures concept, an illustrative simulation scenario is performed. Six consecutive element failures are simulated, the counter threshold is set on 30, and the time between failures is 50 ms. The failed elements location is A, B, C, C, B, A, chronologically. The SCB is fuseless single wye grounded through a capacitor. Figs. 5.8, and 5.9 show successful detection of the failures with the counter setting of 30. Fig. 5.10, illustrates the fact
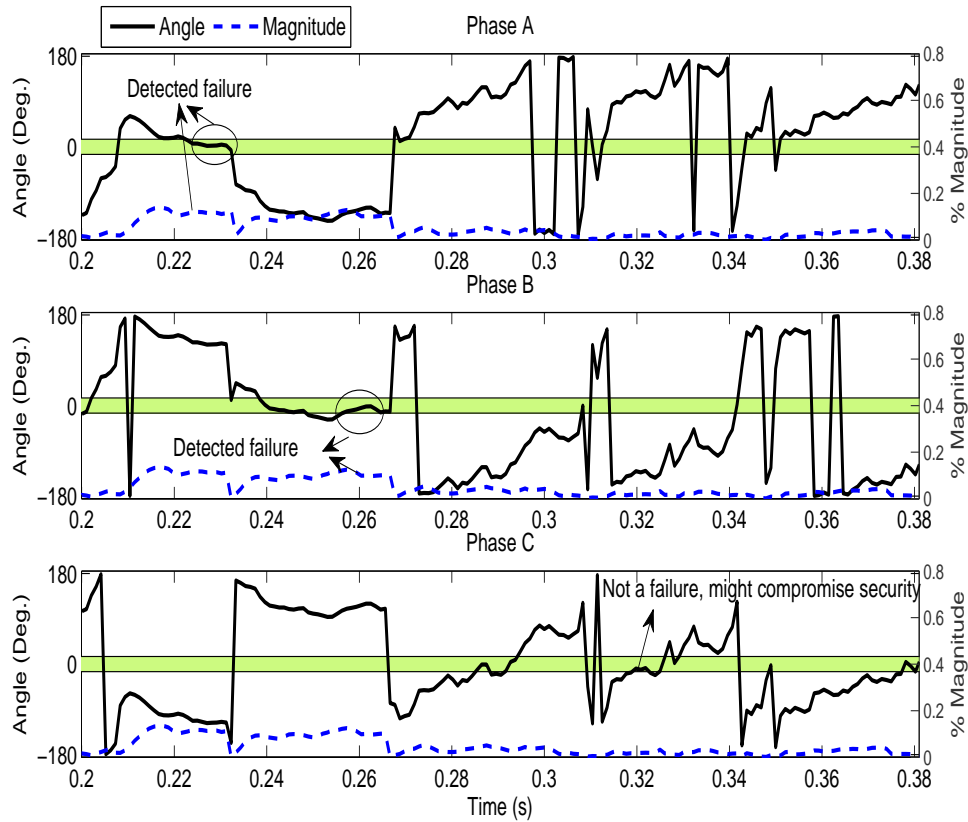
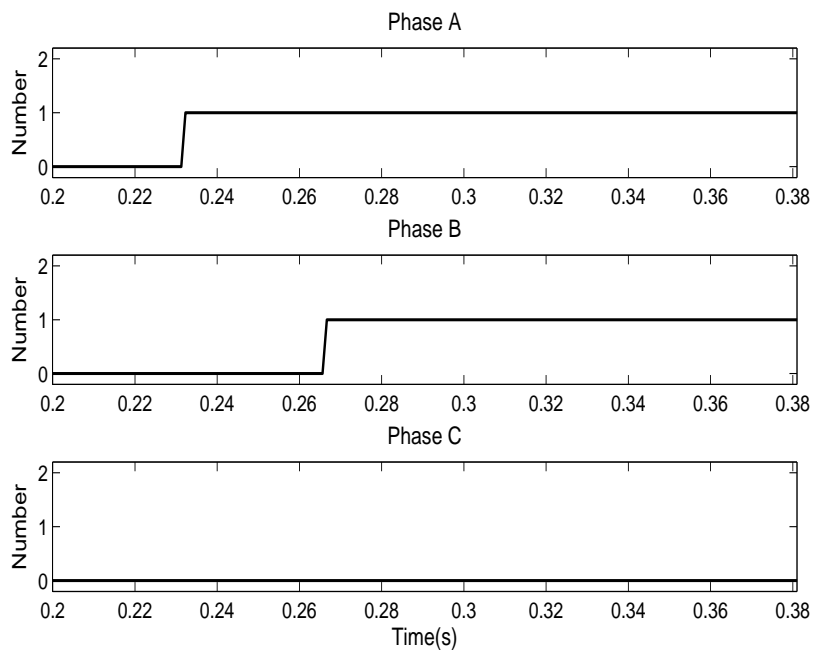Figure 5.4: Fault location principle: smaller counter settings for a single wye SCB.

Figure 5.5: Successful detection of close internal failure [counter set on 10], single wye SCB.
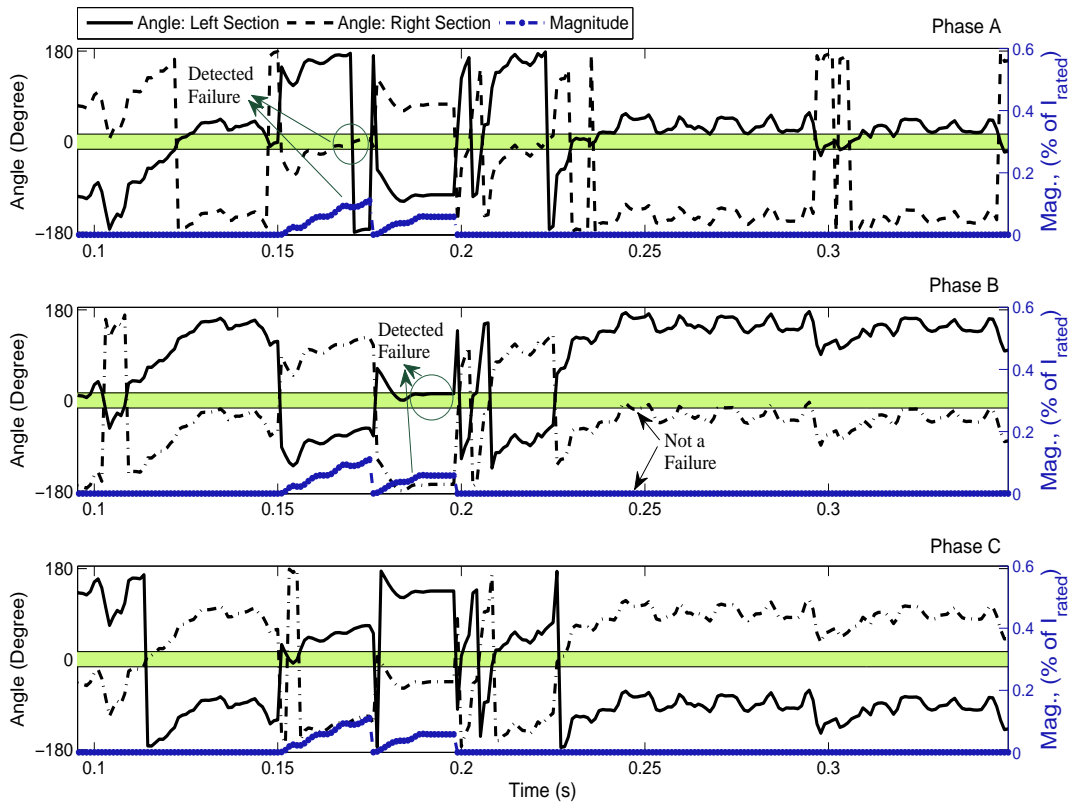
Figure 5.6: Fault location principle: smaller counter settings for a double wye SCB.
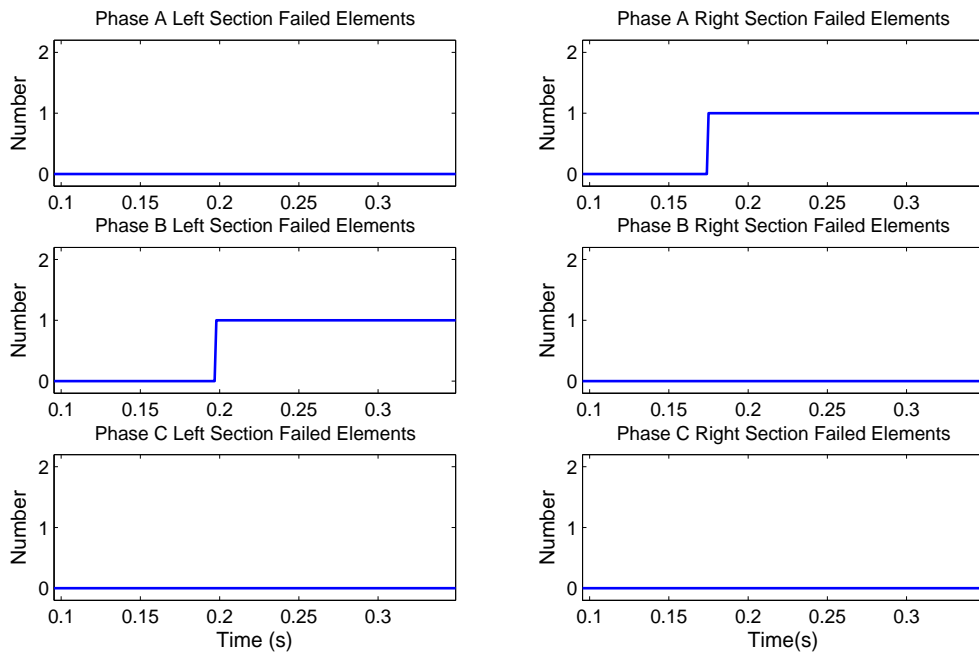

Figure 5.7: Successful detection of close internal failure [counter set on 10], double wye SCB.
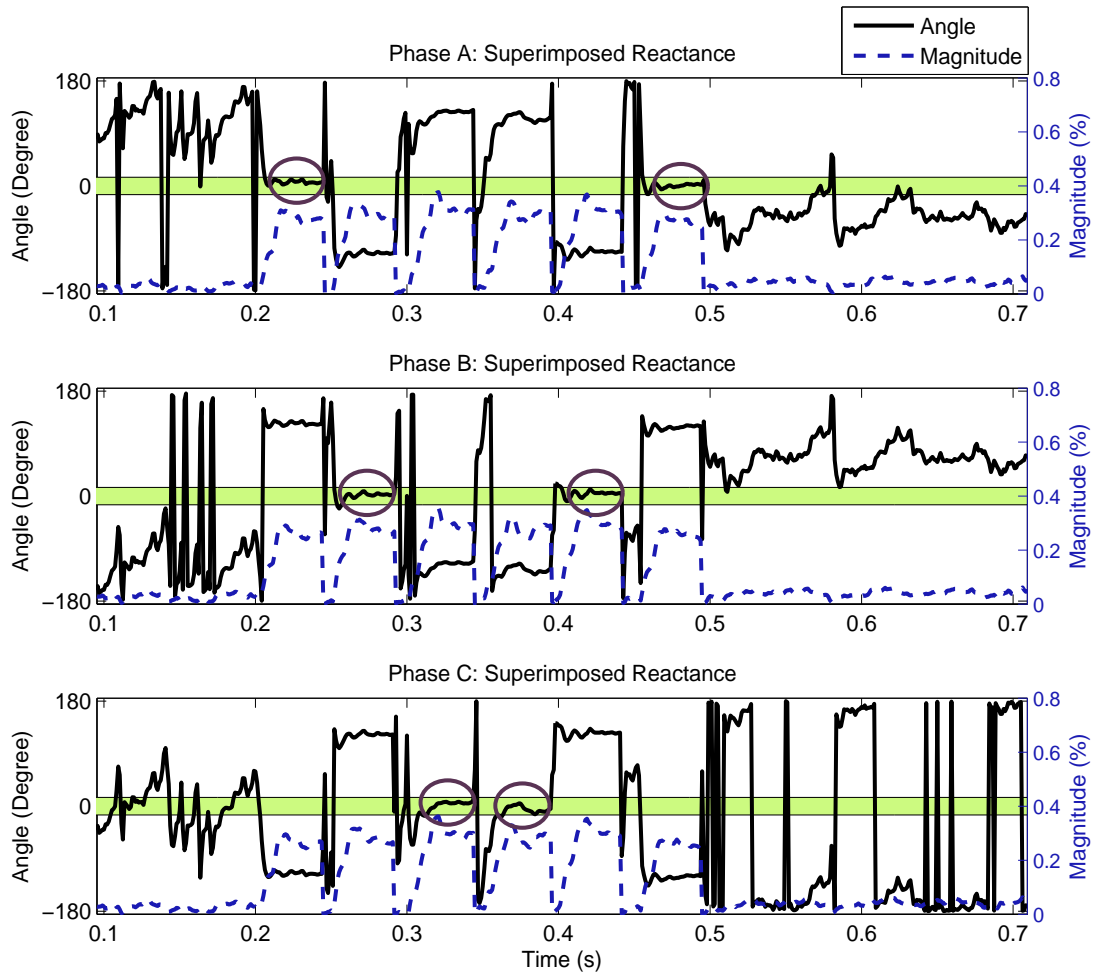
Figure 5.8: Counter setting and detection of close consecutive failures.
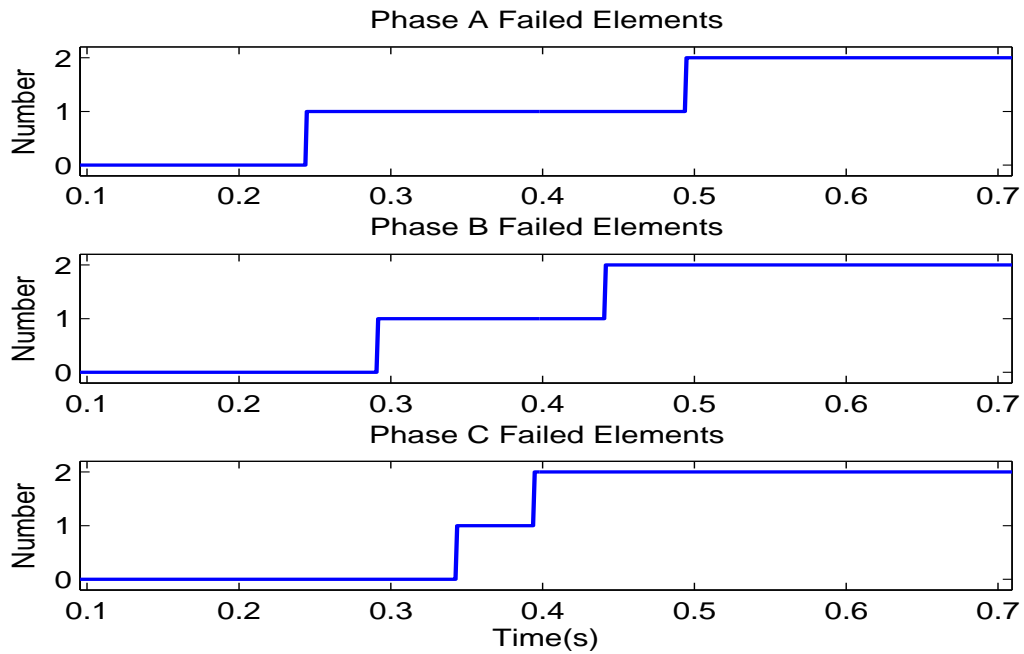

Figure 5.9: Fault location output for close consecutive failures.

that for close failures to be distinguishable, the consecutive failure has to happen after the reset of the principle, i.e. after detection of the previous failure. This is completely dependent on the counter threshold setting.
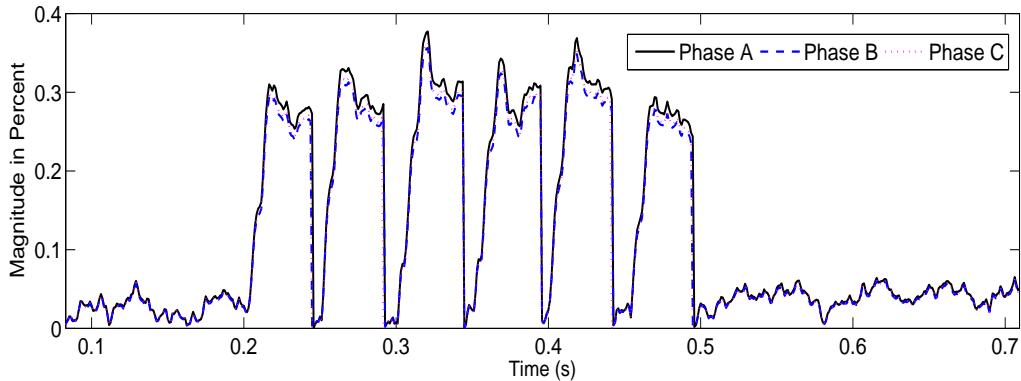

Figure 5.10: SR magnitude jump and reset for close consecutive failures.

5.2   Single Wye Ungrounded

Simulation scenarios along with their corresponding fault location principle variations (track of change) and the fault location output are presented.

Case 1-1 The very first scenario evaluates the case for balanced voltages and balanced SCB. Measurement channel noise and harmonic distortion are considered. An element fails at 0.1 s in a fused SCB. The increased magnitude of the superimposed reactance and the angle for phase A which enters and remains in the angle boundary will result in failure detection in phase A, at about 0.15 s in Fig. 5.12.

Reset of the principle can be seen in Fig. 5.11 as time passes the detection moment (0.15 s), and the principle pattern changes as if no failure has took place. The SEL method, explained in Section 3.3.1, is also simulated for the same case. This method's detection angle variations is shown in Fig. 5.13, in which each colored margin belongs to one phase. Fig. 5.14 shows that this method is also successful for this case.

 Case 1-2 Next case considers unbalanced load in the system and the resultant voltage unbalance. The rest of the scenario is the same as case 1-1.

The proposed method fault location principle (SR), its output, the SEL method detection angle, and its output are plotted in the Figs. 5.15, 5.16, 5.17, 5.18, respectively.   Jumps from 180 to -180 degree in Fig. 5.17 are because it is the angle range defined in the SEL method, refer to Fig. 3.2. As apparent from the results, both the proposed method and the SEL method have an acceptable performance under the introduced voltage unbalance.

Case 1-3 As another consideration for single element failures, pre-existing unbalance in phase capacitances is added to case 1-2, to evaluate the performance of the fault location methods. The proposed method's fault location principle (SR), its output, the SEL method detection angle, and its output are plotted in the Figs. 5.19, 5.20, 5.21, 5.22, respectively.

Again, the compensation terms in detection principles make both methods successful in dealing with cases with inherent unbalances.
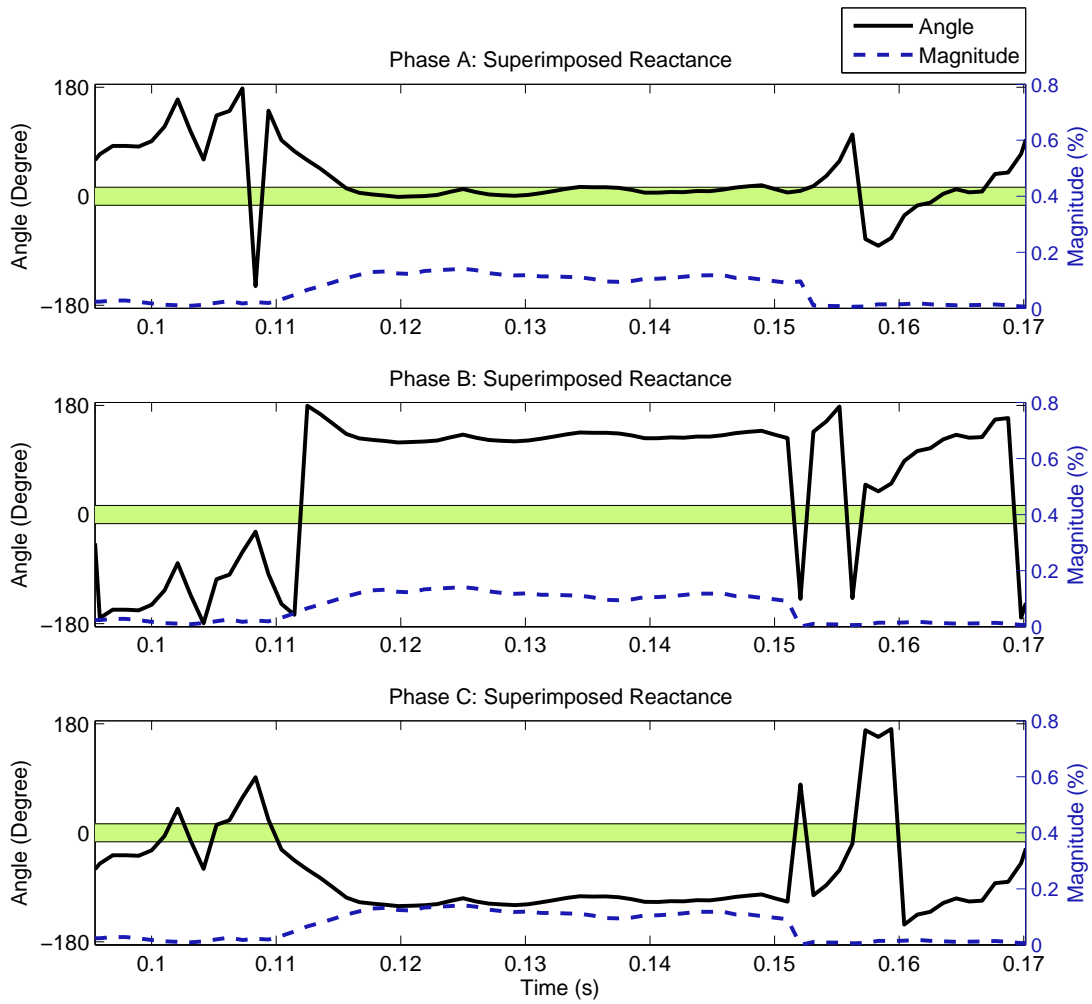
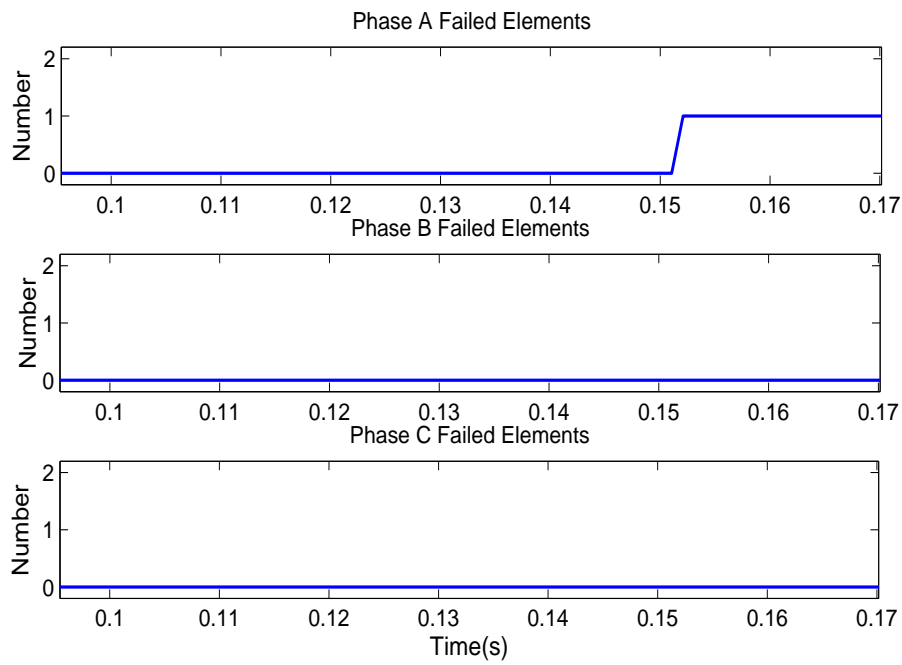Figure 5.11: SR variations, single failure in phase A, Case 1-1.

Figure 5.12: Fault location output, single failure in phase A, Case 1-1.
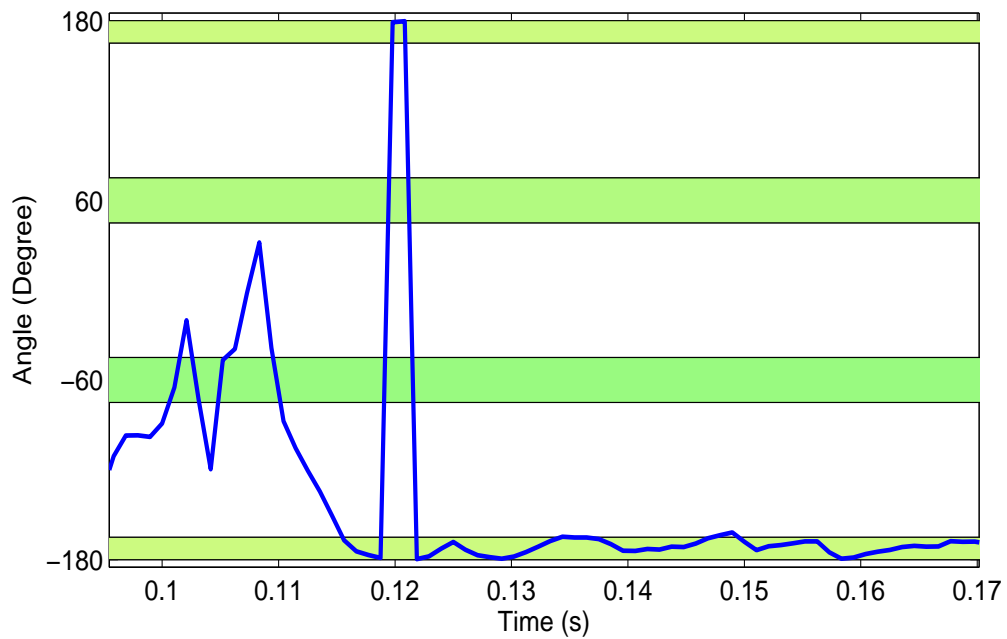

Figure 5.13: The SEL method detection angle, single failure in phase A, Case 1-1.

Figure 5.14: The SEL method fault location output, single failure in phase A, Case 1-1.
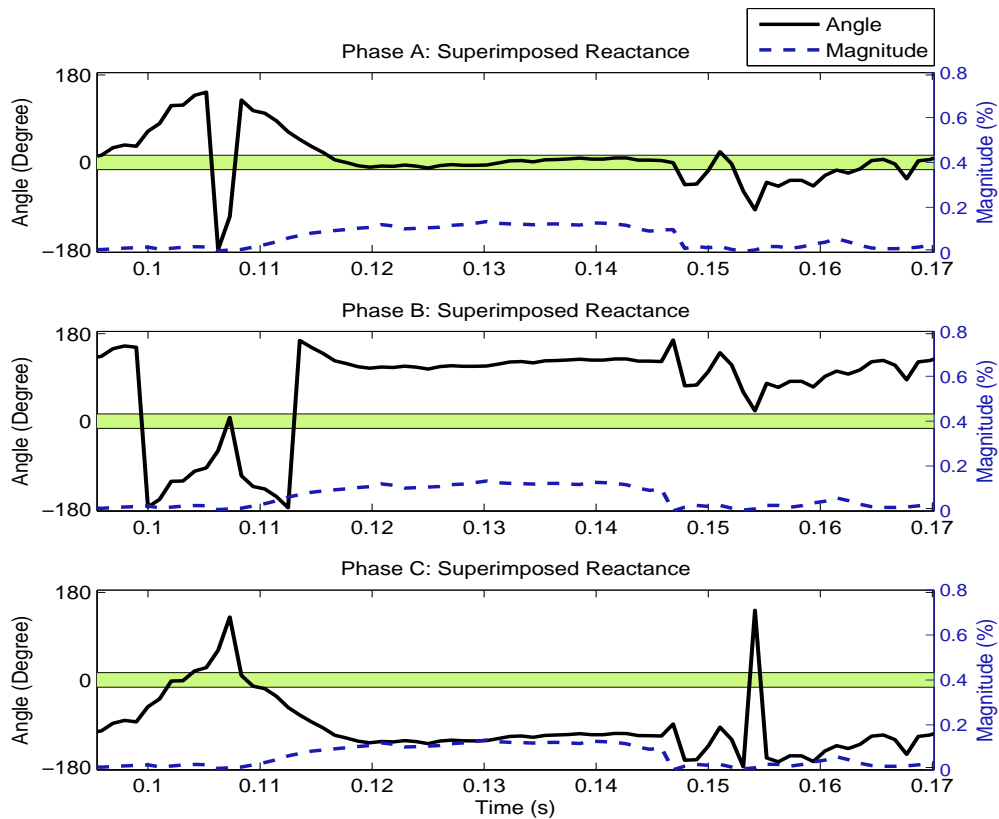
Figure 5.15: SR variations, single failure in phase A, Case 1-2.

Figure 5.16: Fault location output, single failure in phase A, Case 1-2.

Figure 5.17: The SEL method detection angle, single failure in phase A, Case 1-2.
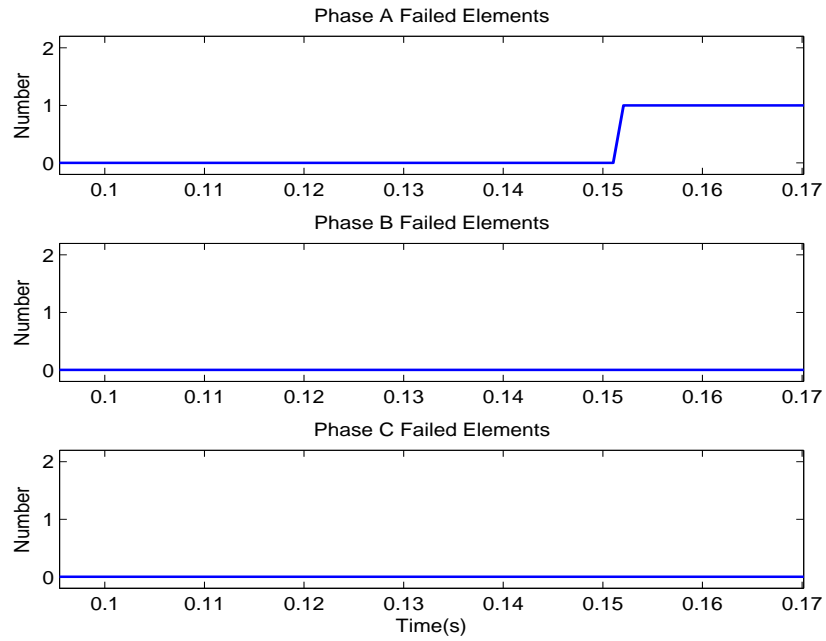
Figure 5.18: The SEL method fault location output, single failure in phase A, Case 1-2.

Figure 5.19: SR variations, single failure in phase A, Case 1-3.

Figure 5.20: The proposed fault location output, single failure in phase A, Case 1-3.

Figure 5.21: The SEL method detection angle, single failure in phase A, Case 1-3.

Figure 5.22: The SEL method fault location output, single failure in phase A, Case 1-3.
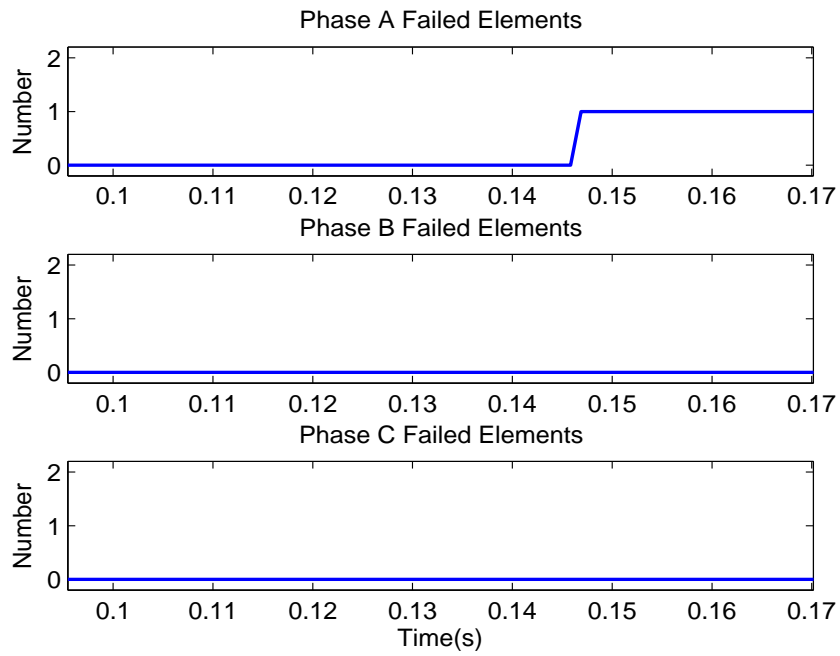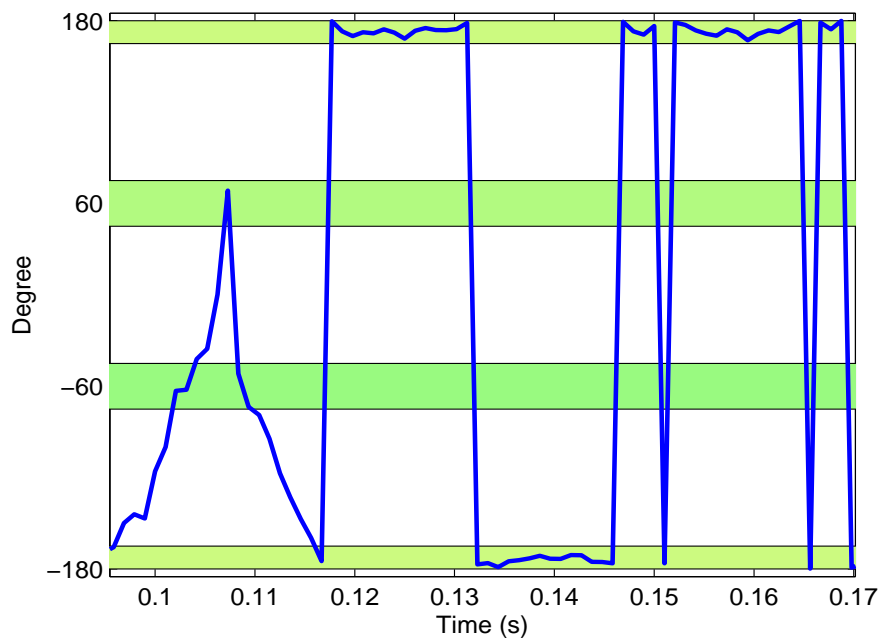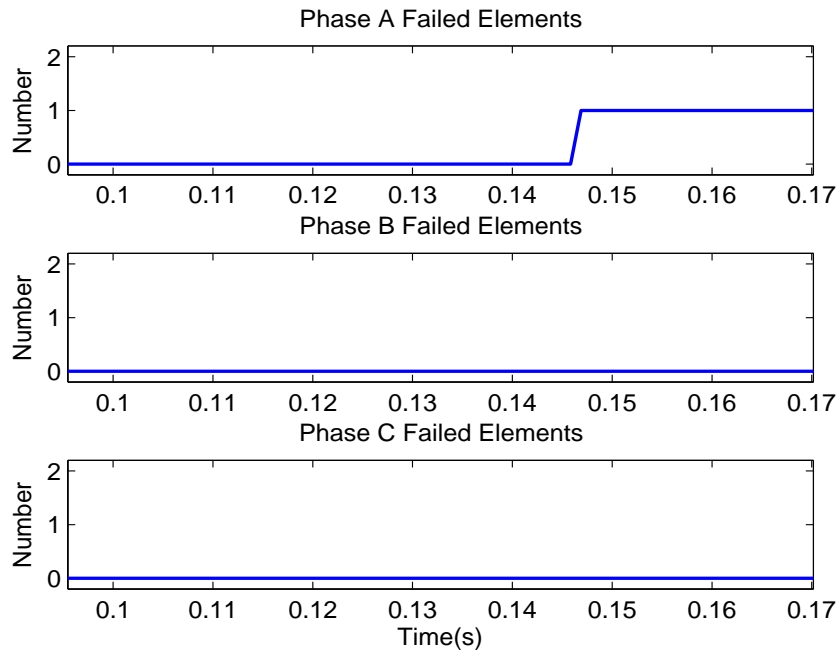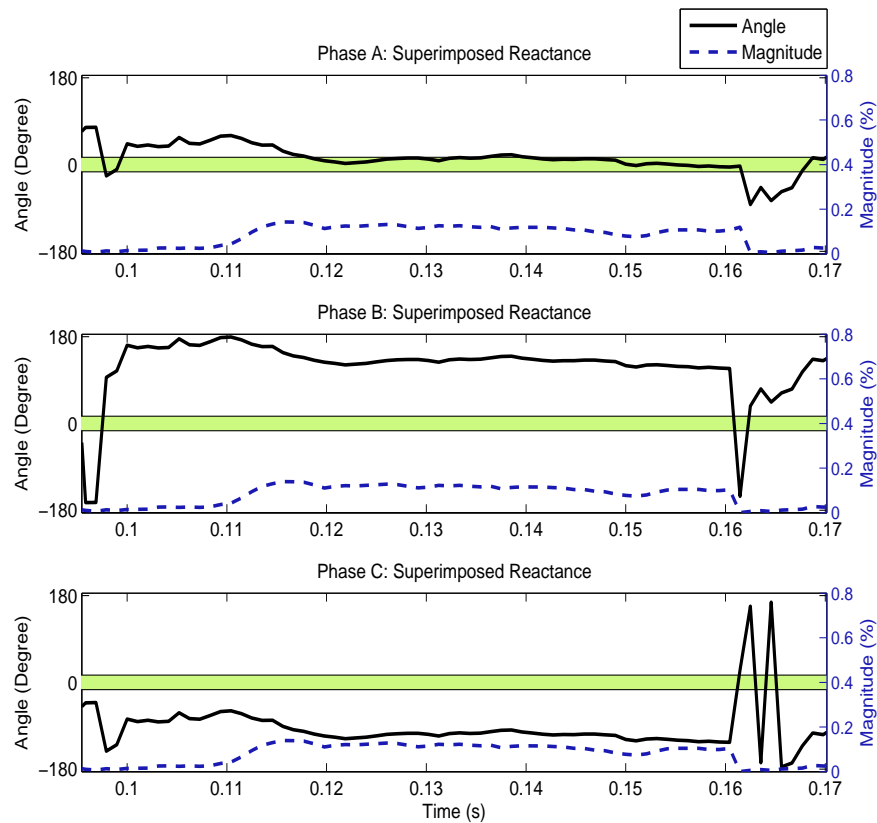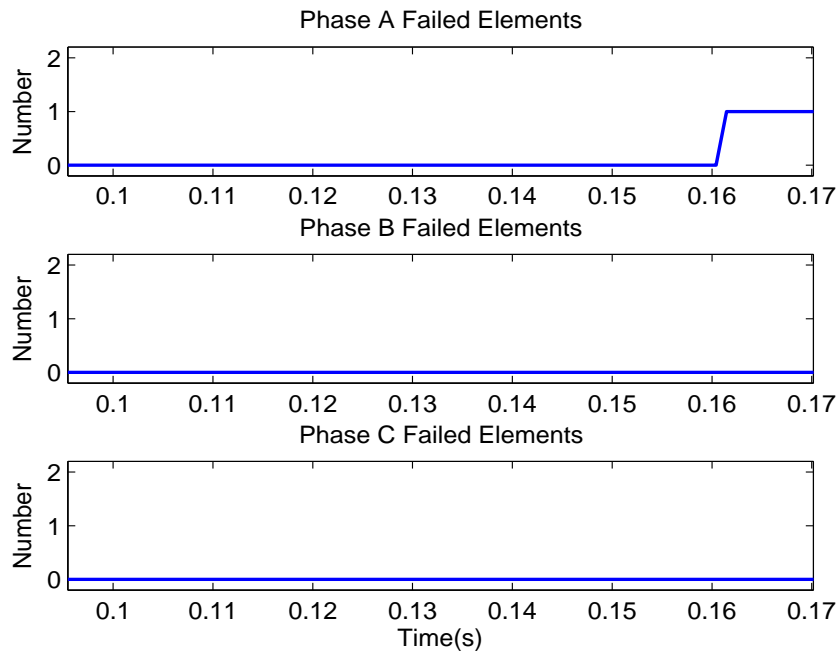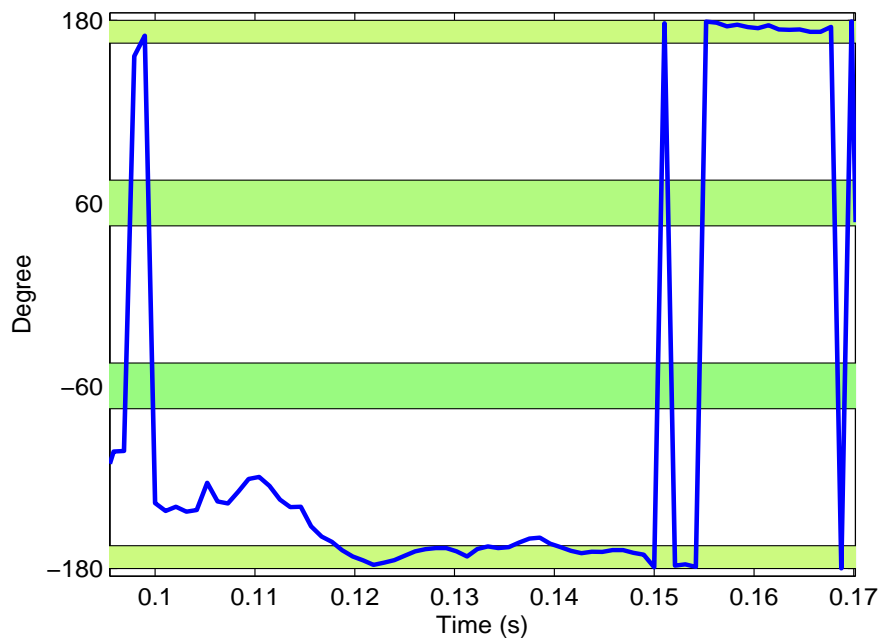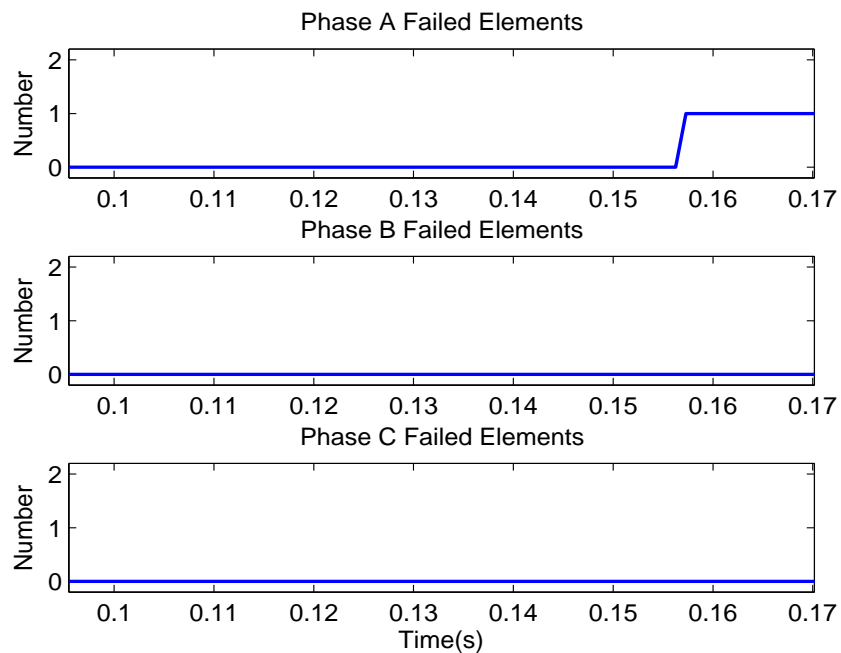
Case 1-4 Until now the case studies were introducing different sources of unbalance step by step. From this point we will perform our evaluations for scenarios which include all of the unbalance sources.

Figs. 5.23 and 5.24 demonstrate variations in the SR and the fault location output for an internally fused SCB, respectively. The following illustrative scenario includes events that are successfully detected as reported in Fig. 5.24. The satisfying performance of the proposed algorithm is validated under pre-existing unbalance, voltage unbalance, harmonics and measurement noise.

- Single element failure in phase A at 0.2 s

- Multiple element failure in phase B at 0.25 s

- Consecutive failure in phase A at 0.3 s

- Multiple element failure in phase C at 0.35 s

As it can be seen, with the latching option and auto-update of the k-factors no masking or unbalance cancellation (a.k.a ambiguous failure) can affect the outputs of the proposed method. The principle gets reset in order for the past failures not to impact detection of subsequent failures, and each failure is detected and reported separately while the health state of the SCB is recorded. In Fig. 5.24 all of the phases have two failed elements after 0.4 s, which would have canceled each others' effect and result in ambiguous or missed failure if the fault location haven't had the calibrating factors updating property.

The number of failures has been detected successfully according to the initial magnitude
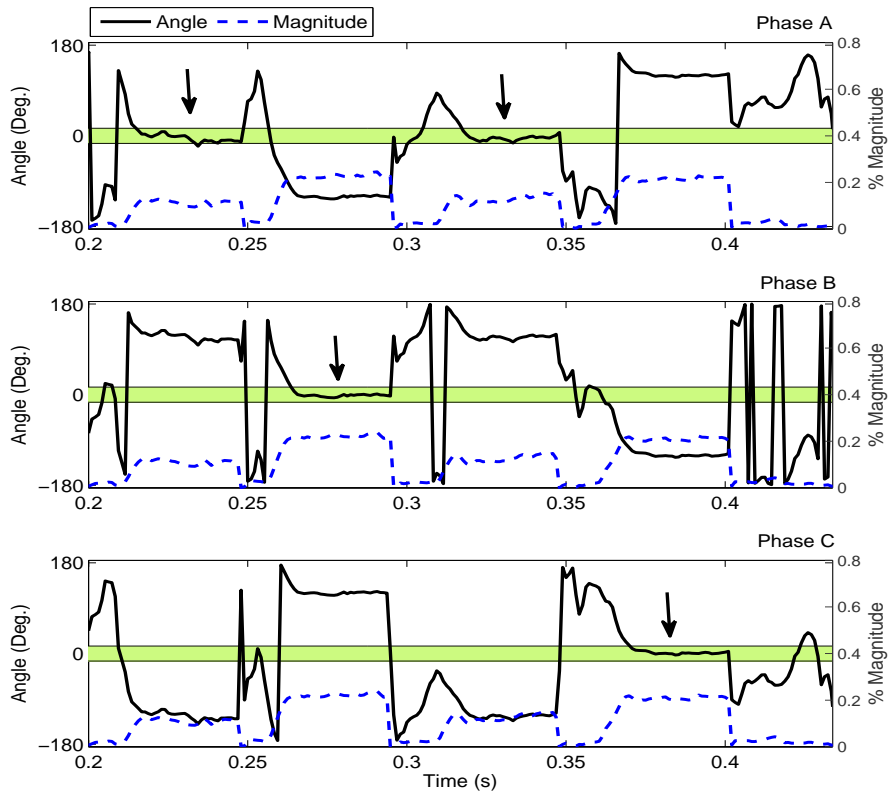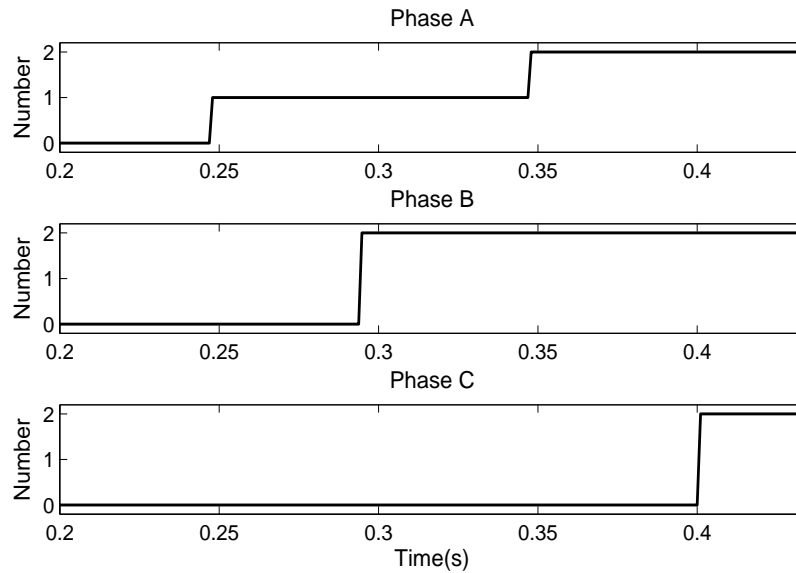
Figure 5.23: SR variations, Case 1-4.

Figure 5.24: Fault location output, Case 1-4.

setting determined for the superimposed reactance, see Table 5.1 for magnitude incre-
ments.

Table 5.2 shows the recorded k-factor values, initial set, and their first updated value
after each of the failures in case 1-4. It is worthwhile noting that the initial values would
have been set to 1.00 if the simulated SCB haven't included the inherent unbalance. Note
that as per (4.21) and (4.22), k-factors of phase B, and C are either reciprocal or ratio
of the two phase A k-factors. Thus, they are not added to Table 5.2.

Table 5.1: Increment in the magnitude of the superimposed reactance: case 1-4.

	Single Failure	Double Failure
Magnitude (%)	0.115	0.228

Table 5.2: k-factor values for phase A, case 1-4.

	Initial	1st Failure	2nd Failure	3rd Failure	4th Failure
k-factors	1.0060|0.9946	1.0070|0.9958	1.0047|0.9957	1.00598 |0.9968	1.0058 |0.9947

5.3 Single Wye Grounded Through a Capacitor

The proposed SR based fault location method is also validated for this configuration.
Case 2-1 A single element failure in phase A of an internally fused SCB takes place at
0.25 s. This scenario includes all of the unbalance sources as in Case 1-4.

A closer look at the magnitude of the fault location principle is shown in Fig. 5.27.
The figure demonstrates that a reliable magnitude threshold can be set smoothly as it is
the case for this worst case scenario.

Case 2-2 The following illustrative scenario includes events that are successfully de-
tected as reported in Fig. 5.29. The satisfying performance of the proposed algorithm is
validated under pre-existing unbalance, voltage unbalance, harmonics and measurement
noise.

- Multiple element failure in phase A at 0.2 s

- A first element failure in phase C at 0.25 s

- Consecutive element failure in phase C at 0.45 s

The successful determination of fault locations in this illustrative scenario implies how
updating of k-factors addresses masking scenarios issue, because having two phases with
failed elements has not lead to a false detection in the third phase (this is an ambiguous
failure scenario as shown in the first chapter). Fig. 5.30 shows tracking of the change
in counters of the three phases. The counter threshold is 30 and it adds up another 30
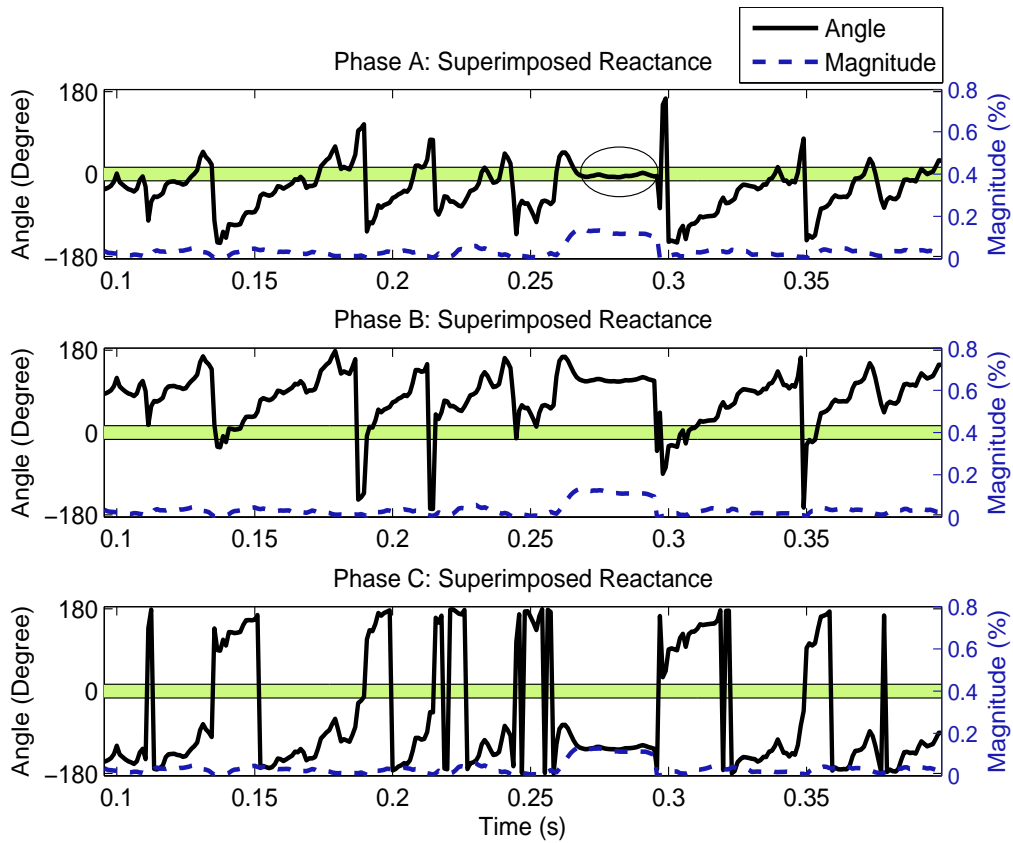counts for a consecutive fault (adjustable setting).

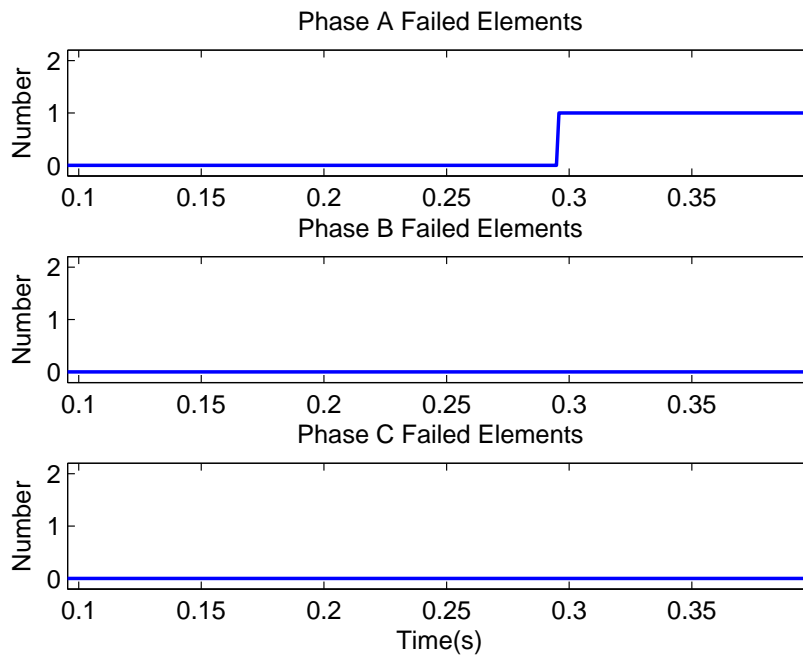Figure 5.25: SR variations for a single element failure in phase A, Case 2-1.

Figure 5.26: Fault location output, single failure in phase A, Case 2-1.
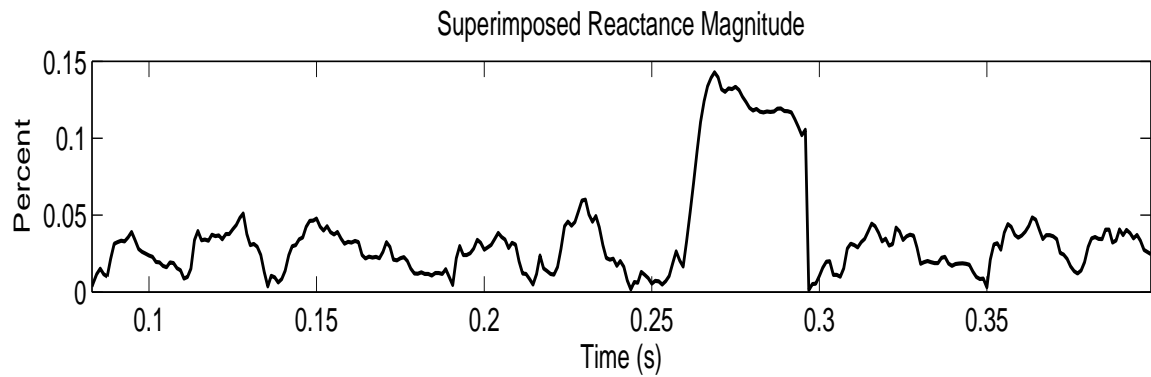
Figure 5.27: Zoomed magnitude of the SR, Case 2-1.
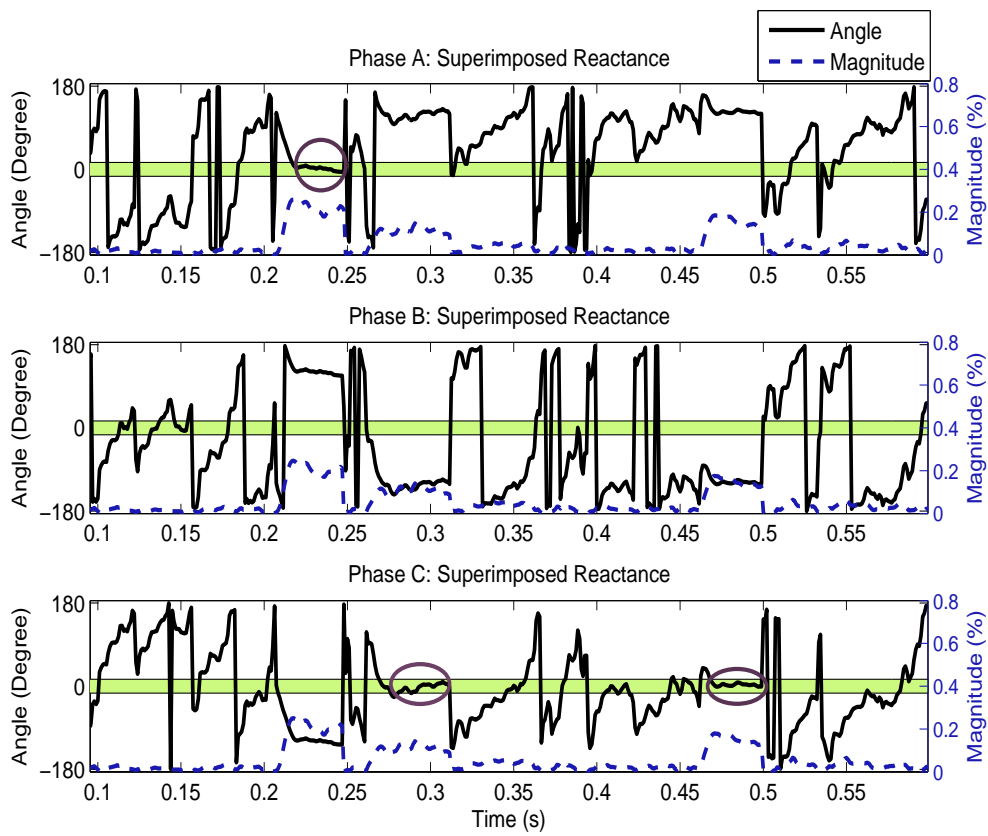
Figure 5.28: SR variations, Case 2-2.
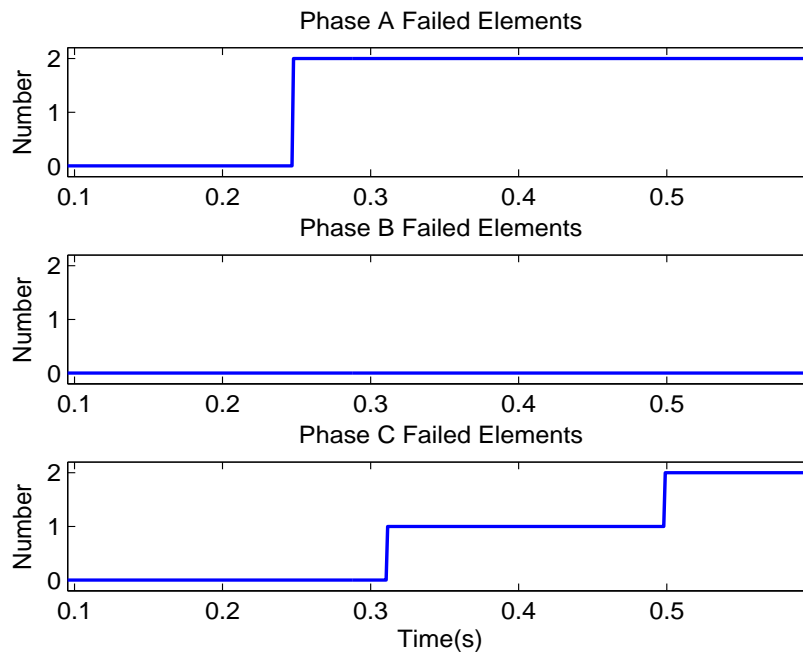
Figure 5.29: Fault location output, Case 2-2.
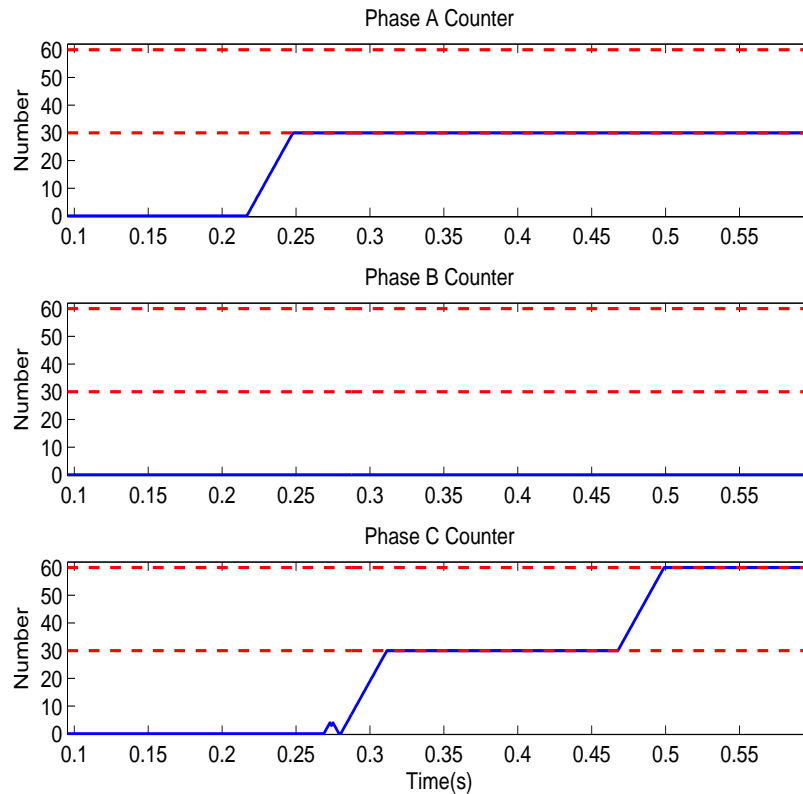
Figure 5.30: Fault location counters, Case 2-2.

5.4 Single Wye Grounded via CT

We will validate the properties and assumptions of the proposed SR based fault location for this configuration.

Case 3-1 The following illustrative scenario includes events that are successfully detected as reported in Fig. 5.33. The SCB is internally fused. Track of the changes in the SR and the counter are plotted in Figs. 5.31 and 5.32, respectively. The satisfying performance of the proposed algorithm is validated under pre-existing unbalance, voltage unbalance, harmonics and measurement noise.

- Single element failure at 0.2 s in phase C

- Multiple element failure in phase A at 0.3 s

- Consecutive failure in phase C at 0.4 s
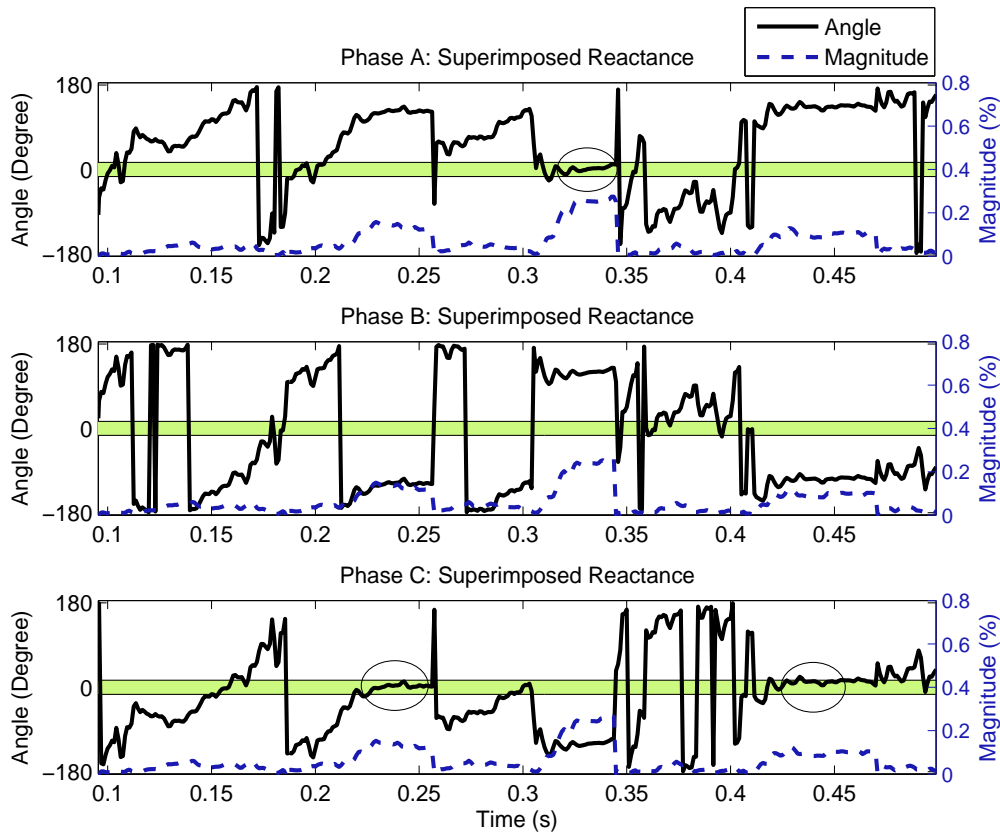
Figure 5.31: SR variations, Case 3-1.

Case 3-2 To check whether keeping the reactance value constant does effect the consecutive failure detection or not, the results for the following scenario is presented here. The SCB is fuseless.

- a unit fails at 0.22 s in phase A

- a consecutive single element failure in phase A at 0.27 s

Figure 5.32: Fault location counters, Case 3-1.

Figure 5.33: Fault location output, Case 3-1.

Figs. 5.34, 5.35, and 5.36, illustrate the successful evaluation. It is worthwhile to note that, as apparent from precision limits, an error in detection of number of failed elements is expected when several elements fail simultaneously (failure of units), since error accumulation will be the consequence. To minimize such an error in detection of number of elements in presence of distracting signals (noise), the base magnitude has been se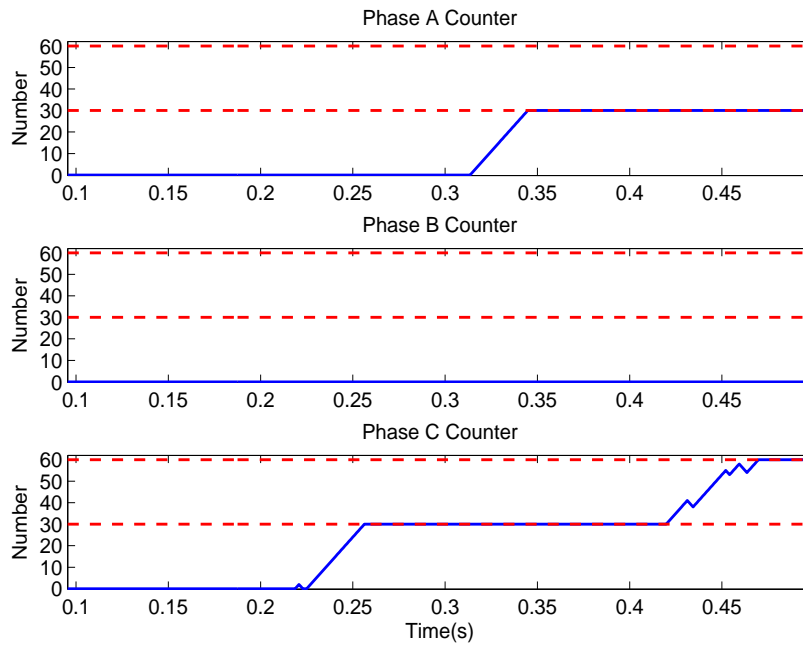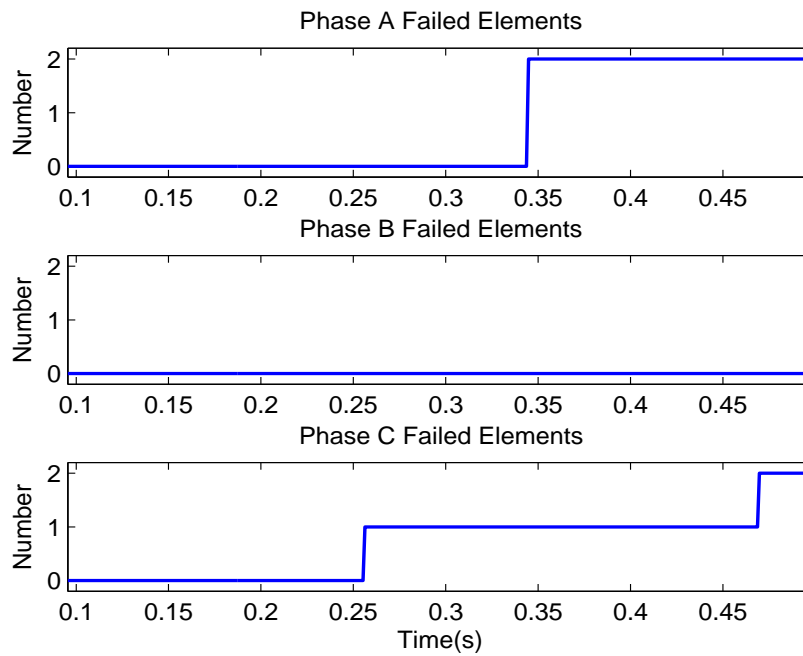t to 0.9 of the expected superimposed reactance magnitude. This makes the base value neither too much large to give less than the actual number of failed elements, nor too much small to give more than the actual number of failed elements. For this illustrative scenario, in the simulated configuration each unit consists of 6 elements, thus the detected number of failed elements matches its actual value, a 6 element failure followed by a single element failure.
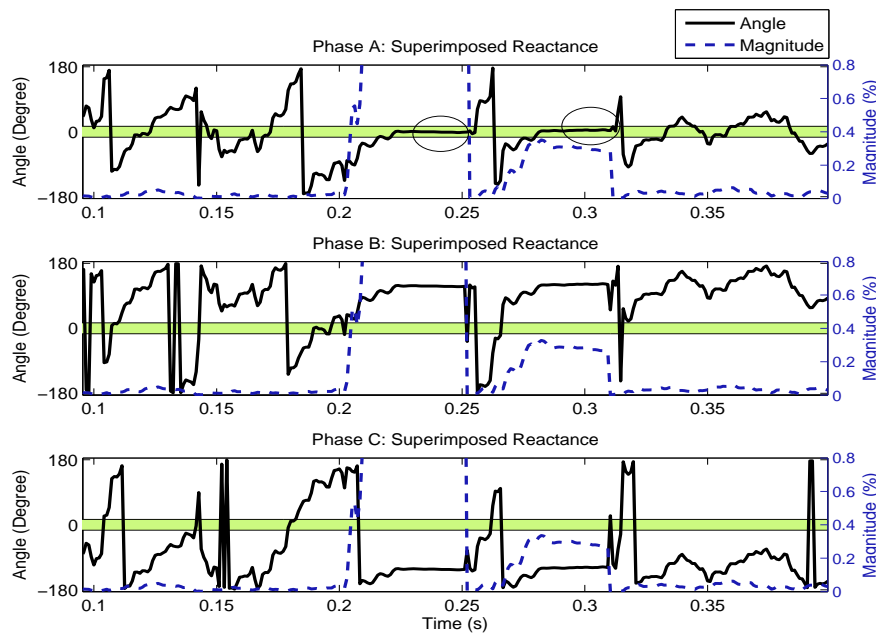
Figure 5.34: SR variations, Case 3-2.

5.5 Y-Y Ungrounded with Neutral Current Unbalance

For double wye SCBs as the fault location is based on another quantity, we again demonstrate the results with scenarios that introduce the unbalance sources step by step, and then we will perform the rest of the cases with all of the unbalance sources involved.
Case 4-1 Measurement noise and harmonic distortion are considered for this case. System voltages and the SCB are balanced. Results are shown for a fuseless SCB. A single element failure takes place in right section of phase B at 0.1 s. The proposed method's fault location principle (compensated neutral current), its output, the SEL method detection angle, and its output are plotted in the Figs. 5.37, 5.12, 5.13, 5.14, respectively. In Fig. 5.13 each colored band corresponds to one of the six possible locations for the failed element.
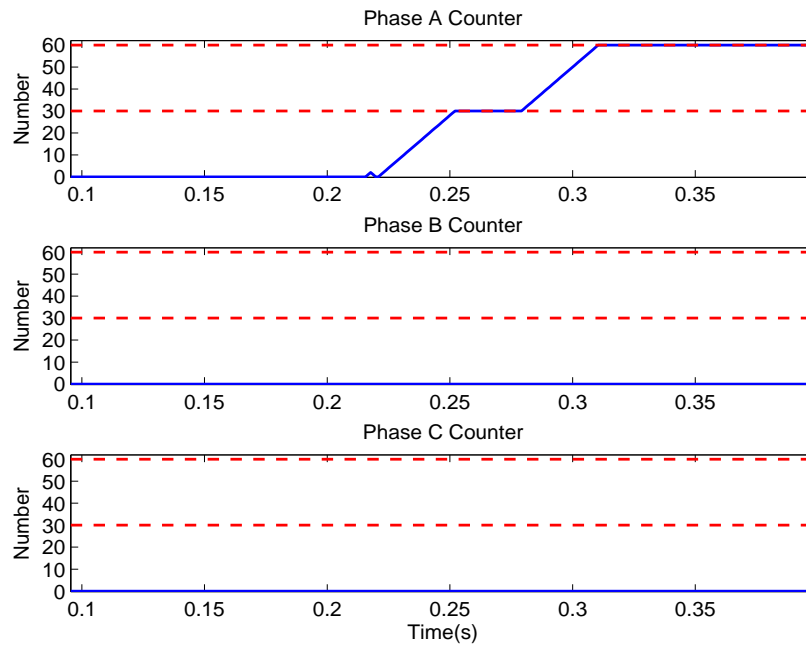
Figure 5.35: Fault location counters, Case 3-2.
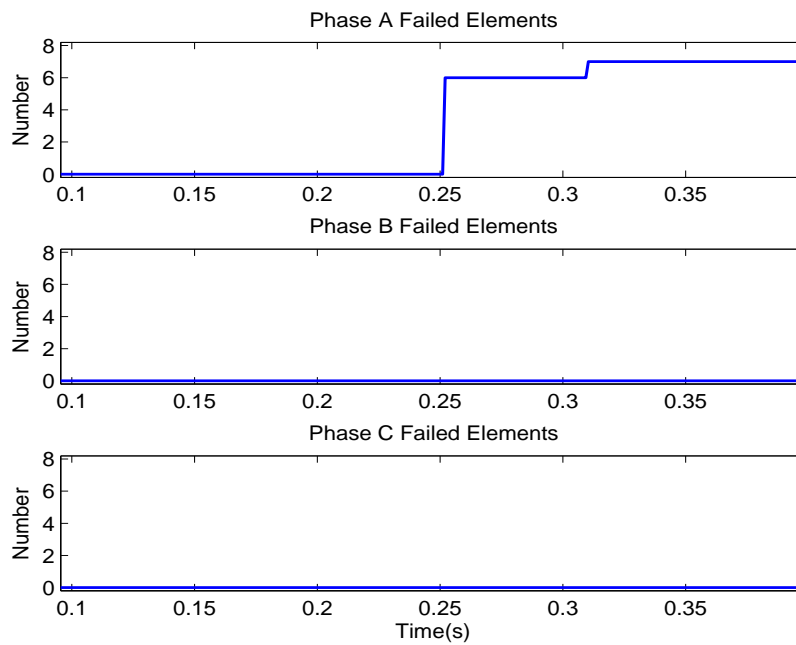
Figure 5.36: Fault location output, Case 3-2.
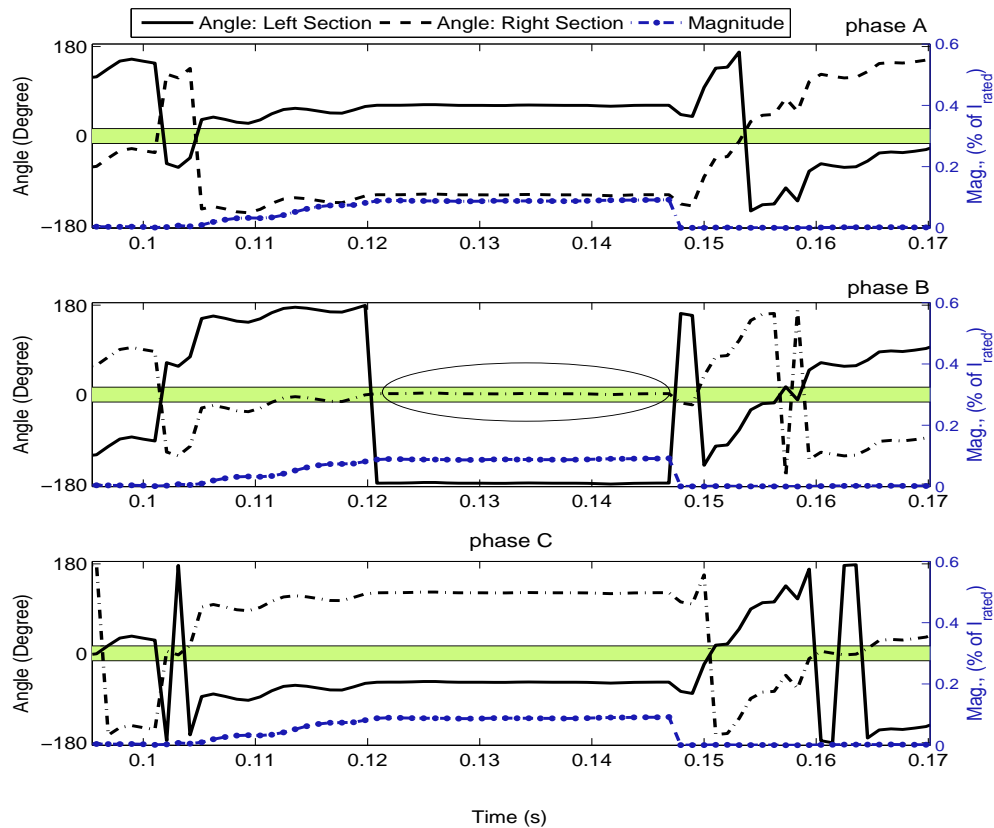
Figure 5.37: Compensated neutral current variations, single failure in phase B right section, Case 4-1.

Case 4-2 After validation of case 4-1, the other sources of unbalance are added to the simulation case. The simulated scenario involves a single element failure at 0.1 s in right section of phase C of a fuseless SCB.

The proposed method's fault location principle (compensated neutral current), its output, the SEL method detection angle, and its output are plotted in the Figs. 5.41, 5.20, 5.21, 5.22, respectively. In Fig. 5.21 each colored band corresponds to one of the six possible locations for the failed element.

As can be seen, both methods demonstrate successful operation and compensation. After validation of the proposed method for the cases that were comparable with the SEL fault location, additional simulation scenarios were carried out to test the unique properties of the proposed method.

Case 4-3 The following illustrative scenario includes events that are successfully detected as reported in Fig. 5.46. The SCB is fuseless. Track of the changes in the compensated neutral current is plotted in Fig. 5.45. The satisfying performance of the proposed algorithm is validated under pre-existing unbalance, voltage unbalance, harmonics and measurement noise.

Figure 5.38: The proposed fault location output, single failure in phase B right section, Case 4-1.

Figure 5.39: The SEL method detection angle, single failure in phase B right section, Case 4-1.

Figure 5.40: The SEL method fault location output, single failure in phase B right section, Case 4-1.

The event sequence for case 4-3 is as follows

- Single element failure at 0.1 s in left section of phase A

- Consecutive failure in left section of phase A at 0.15 s

- Multiple element failure in right section of phase B at 0.22 s

Table 5.3 shows the values calculated and set for detection of the number of failures according to (4.63) for the fuseless SCB presented in Appendix B.

Table 5.3: Increments in the magnitude of the compensated neutral current in percent of the rated current for single element failures.

	Left Section Reference Value	Right Section Reference Value
Magnitude (%)	0.071	0.089

Case 4-4 Regarding the masking issue discussed in Fig. 1.2, a case in which two phases experience left section failures and the other phase undergoes a failure in the right section can lead to incorrect fault location if an algorithm can not reset the constants after each failure. Such a scenario has been simulated as an illustrative example for a fused double wye SCB to demonstrate part of the validation process for the proposed method. See Figs. 5.47, and 5.48. Table 5.4 gives the values for K_1, as per (4.56), initially and right after each failure detection for the described masking scenario.
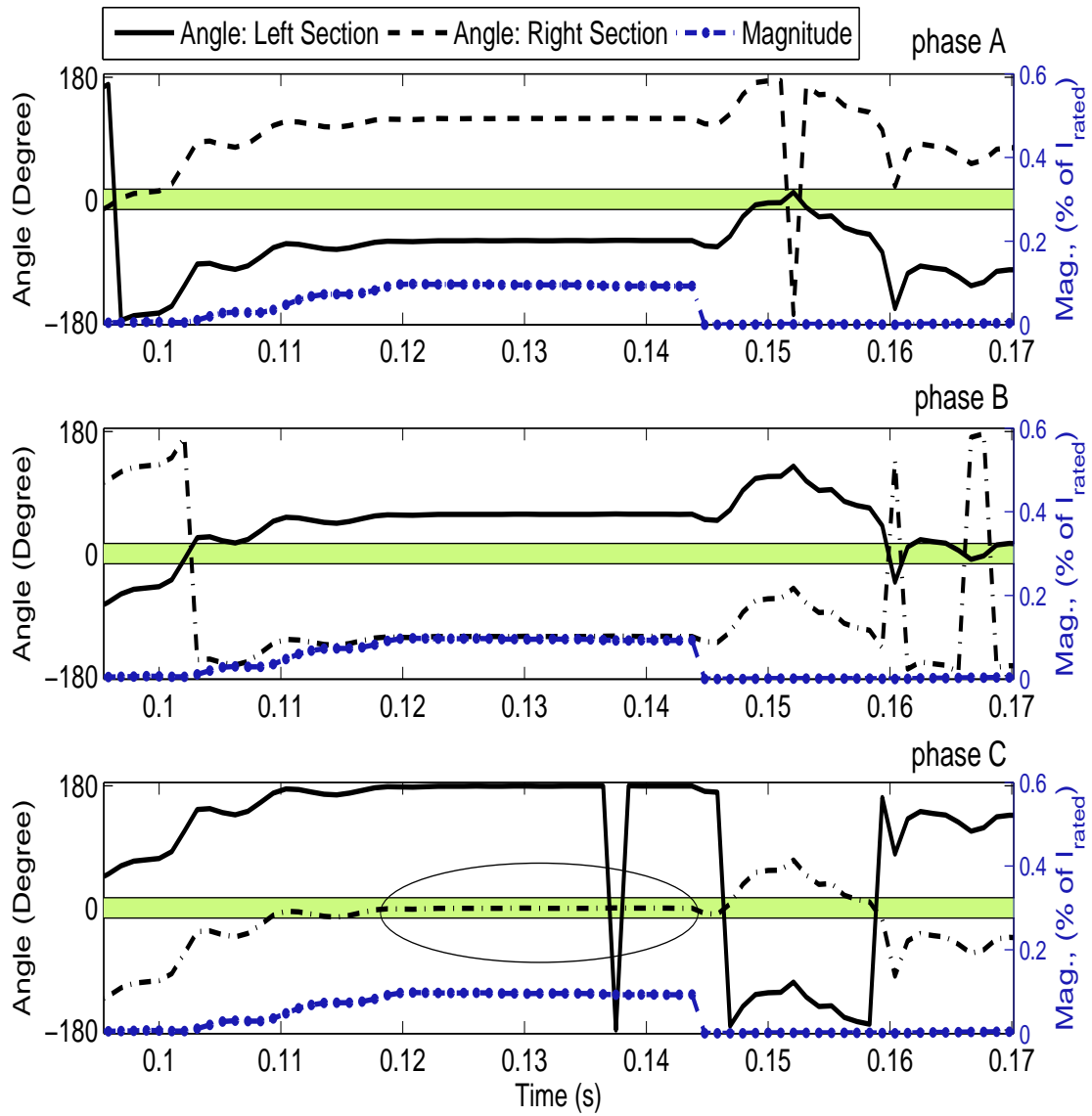
Figure 5.41: Compensated neutral current variations, single failure in phase C right section, Case 4-2.
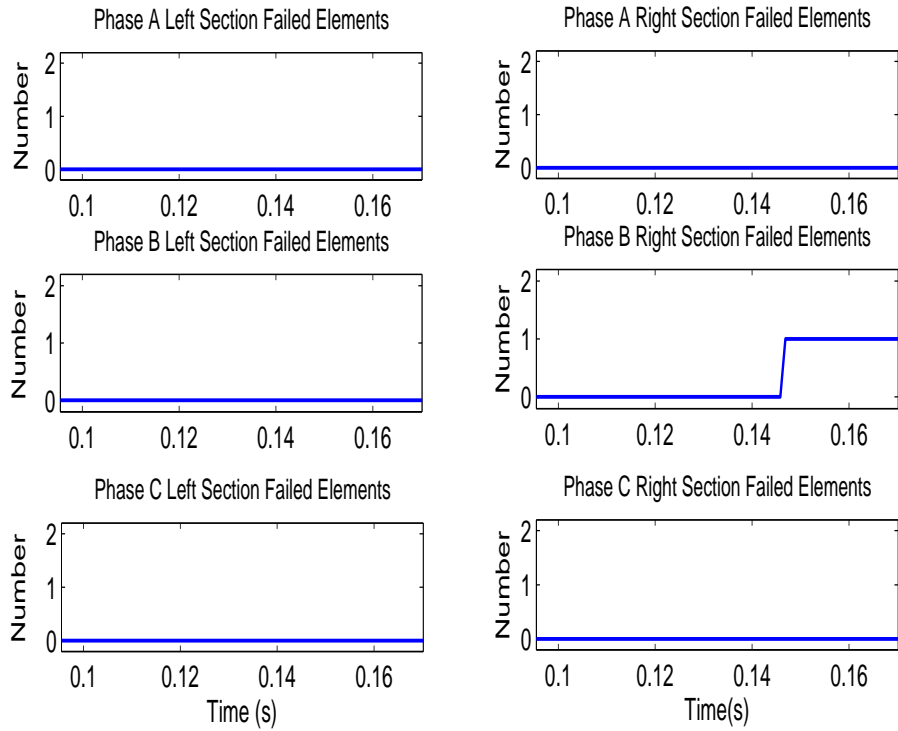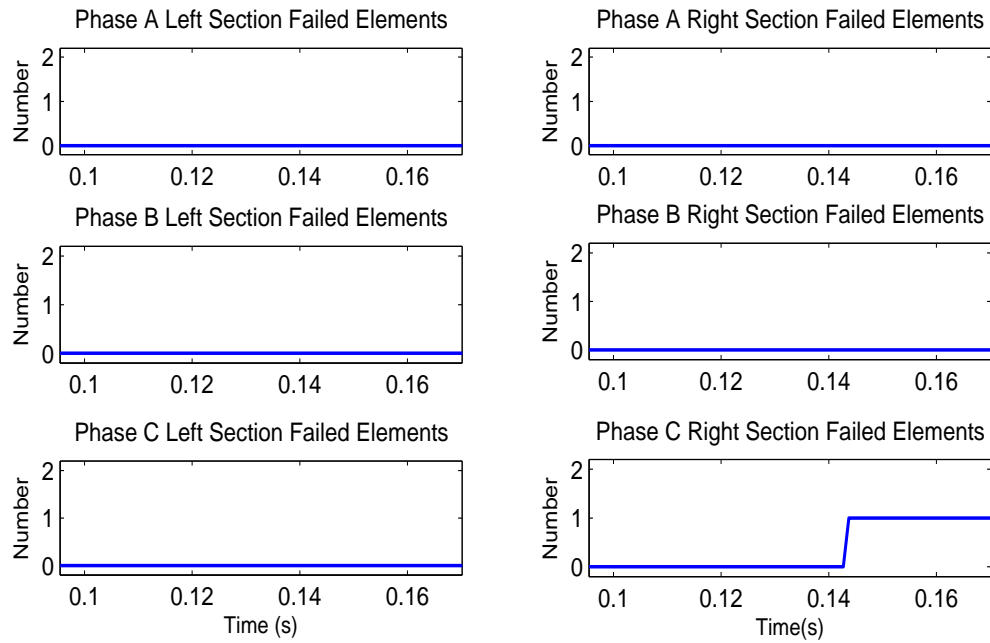
Figure 5.42: The proposed fault location output, single failure in phase C right section, Case 4-2.
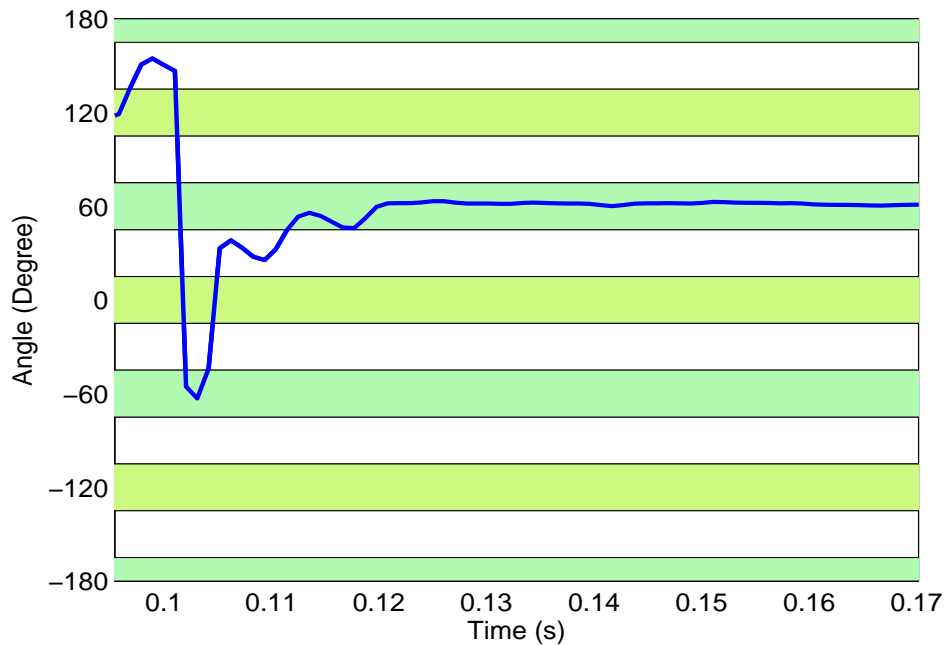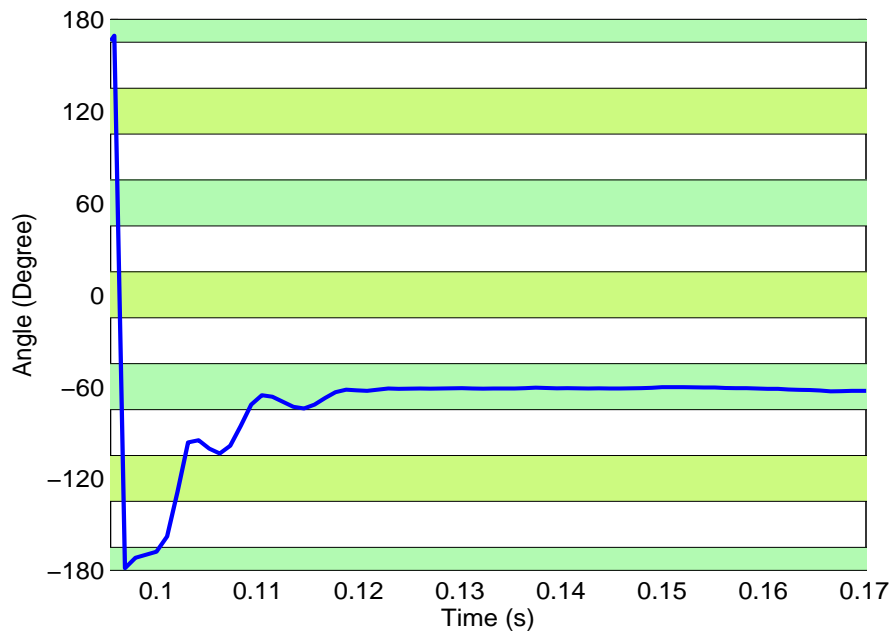

Figure 5.43: The SEL method detection angle, single failure in phase C right section, Case 4-2.
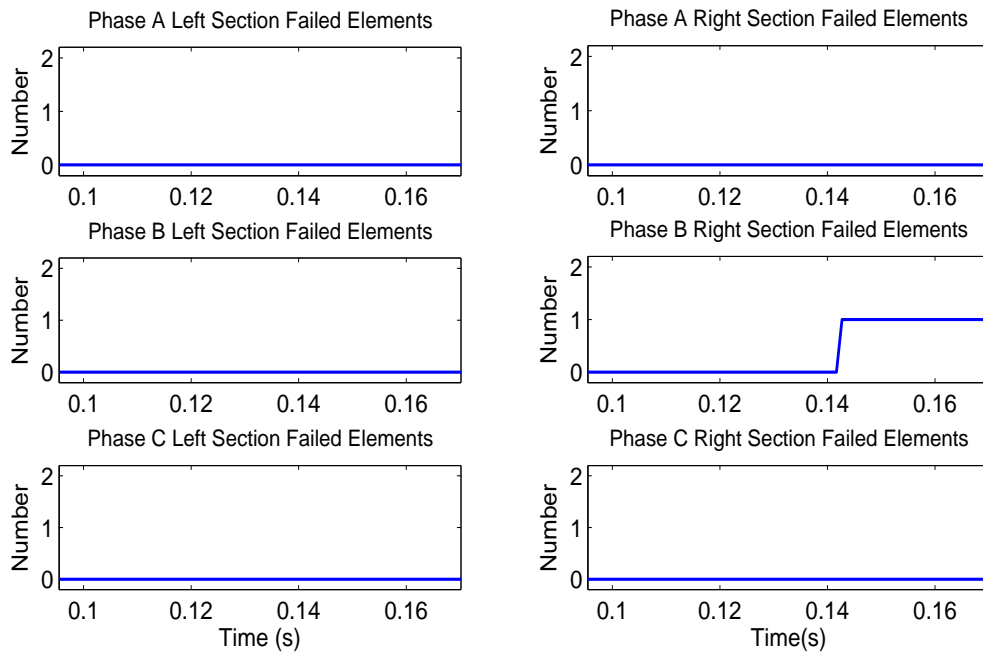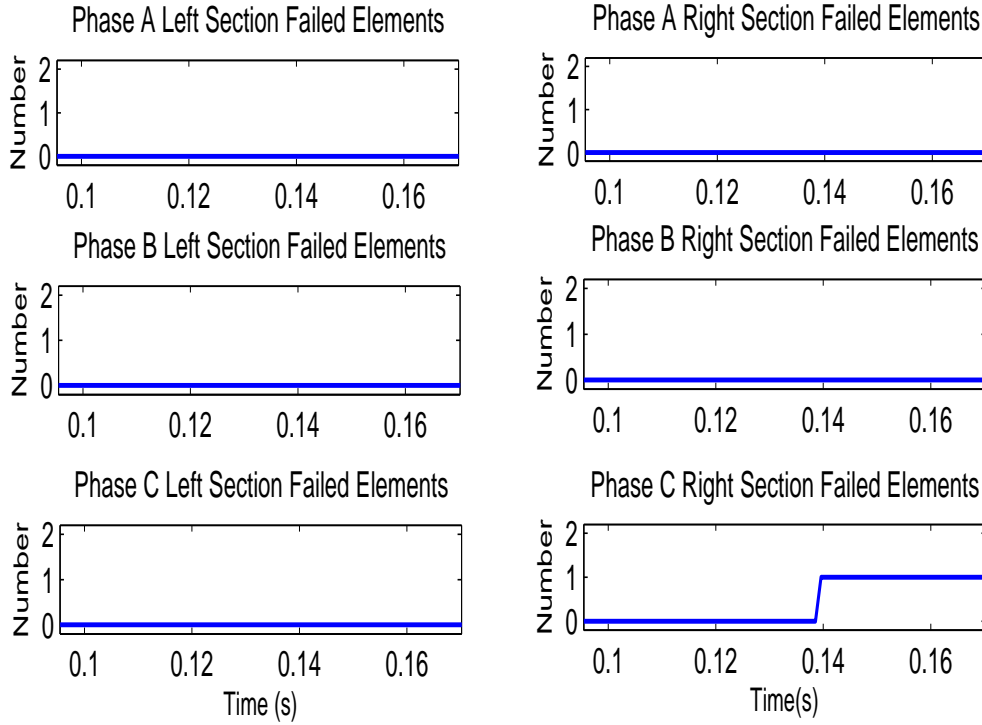
Figure 5.44: The SEL method fault location output, single failure in phase C right section, Case 4-2.

Table 5.4: K_1 magnitude (p.u.) | phase (deg.) sets for case 4-4.

	Initial	**1st failure**	**2nd failure**	**3rd failure**
K_1	0.0017|49.51	0.0025|52.47	0.0023|35.27	0.0037|22.01

It is worth mentioning that the initial magnitude for K_1 approaches zero for a perfectly balanced bank in a system with perfectly balanced voltages. The non-zero set value for the simulated scenario ensures compensation for the part of the neutral current that is not caused by the internal failures (pre-existing unbalance).

5.6   Y-Y Grounded with Neutral Current Unbalance

Determining worst case scenarios is important for the proposed method evaluation. Regarding grounded double wye banks with neutral current unbalance, and with reference to what we discussed for the fault location principle in equation (4.67), the worst case scenario in terms of accumulation of unbalance terms is when the phase k-factors, K_p, have the same sign, or in other words, when left and right section mismatches are in the same direction for all three phases. We have considered this in the comprehensive scenario in case 5-1.

Figure 5.45: Compensated neutral current variations, Case 4-3.
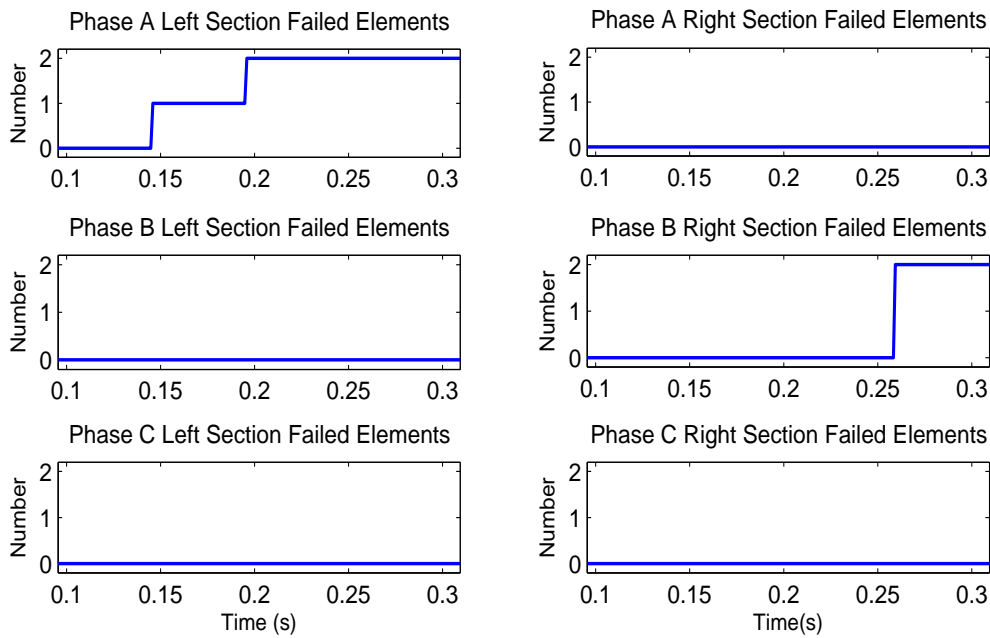
Figure 5.46: The proposed fault location output, Case 4-3.
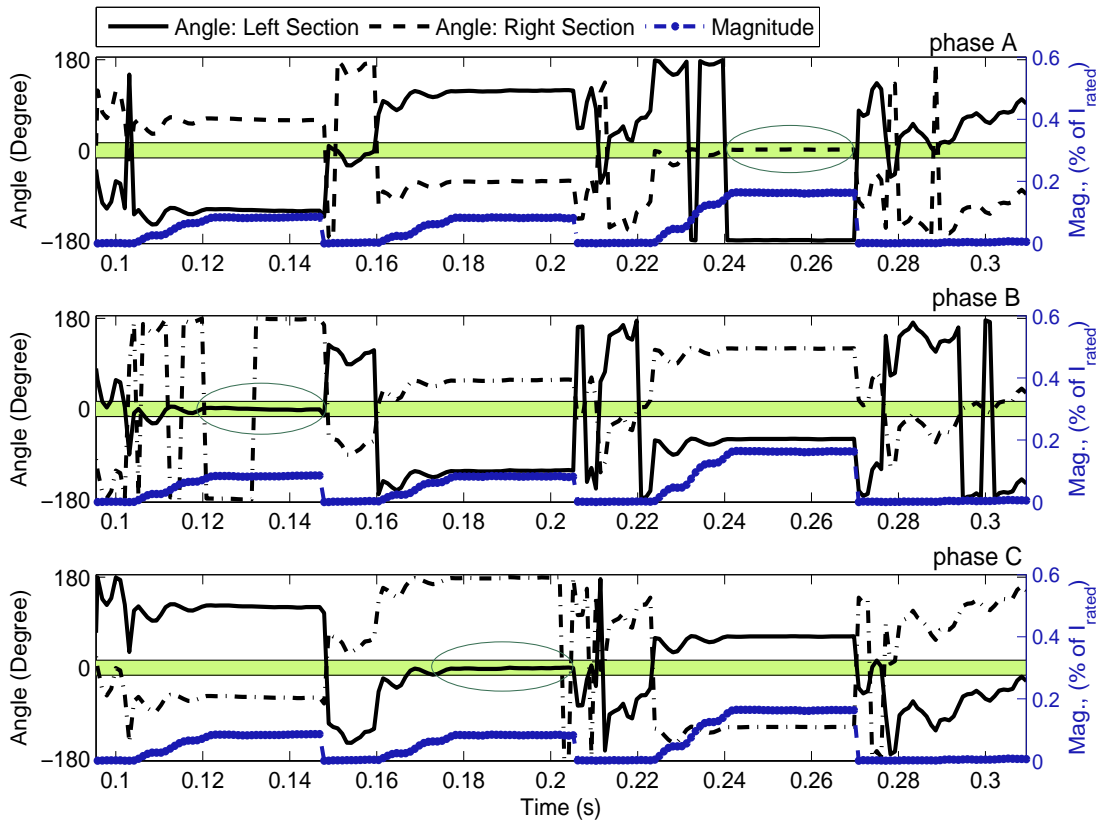
Figure 5.47: Compensated neutral current variations, Case 4-4.
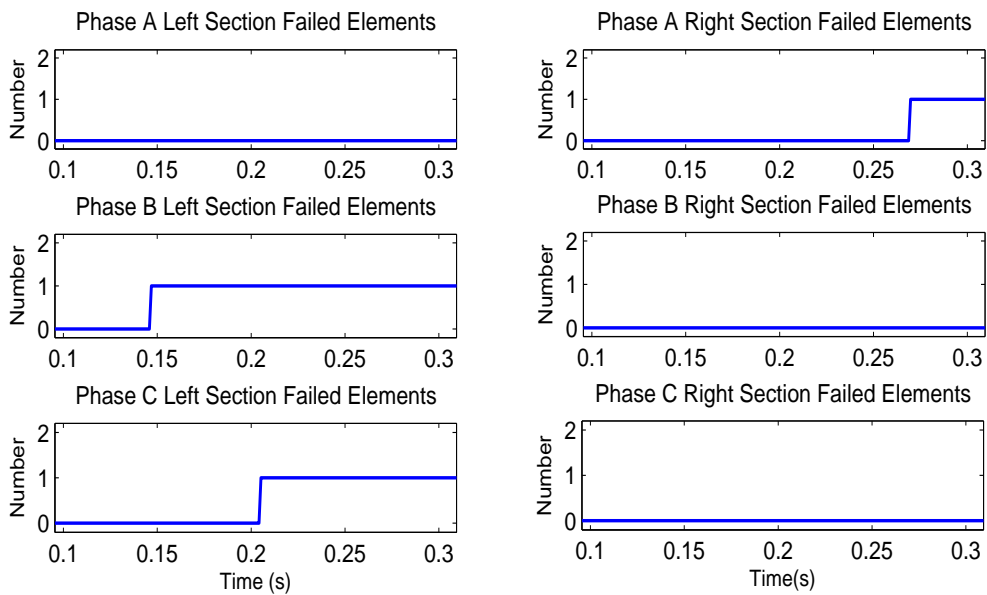
Figure 5.48: The proposed fault location output, Case 4-4.

Case 5-1 The illustrative scenario chosen to present includes the following events for an internally fused SCB:

- Single element failure in left section of phase C at 0.2 s

- Multiple element failure in right section of phase A at 0.3 s

- Consecutive element failure in left section of phase C at 0.4 s

Considering the maximum acceptable voltage unbalance in transmission systems, and pre-existing unbalance in the SCB phase impedances, Fig. 5.49 shows measurements for zero sequence current and the differential neutral current for the described scenario. Cancellation of unbalances that affect both wye sections equally can be seen in the differential quantity. The compensated neutral current is shown in Figure 5.50.

Fault location principle and output are shown in Figs. 5.50 and 5.51, respectively, which

Figure 5.49: Zero sequence current, and uncompensated differential neutral current, Case 5-1

demonstrate successful and reliable determination of the failures. Notice resets in the compensated fault location quantity (Figure 5.50) while uncompensated neutral current is incrementally increasing (Figure 5.49).
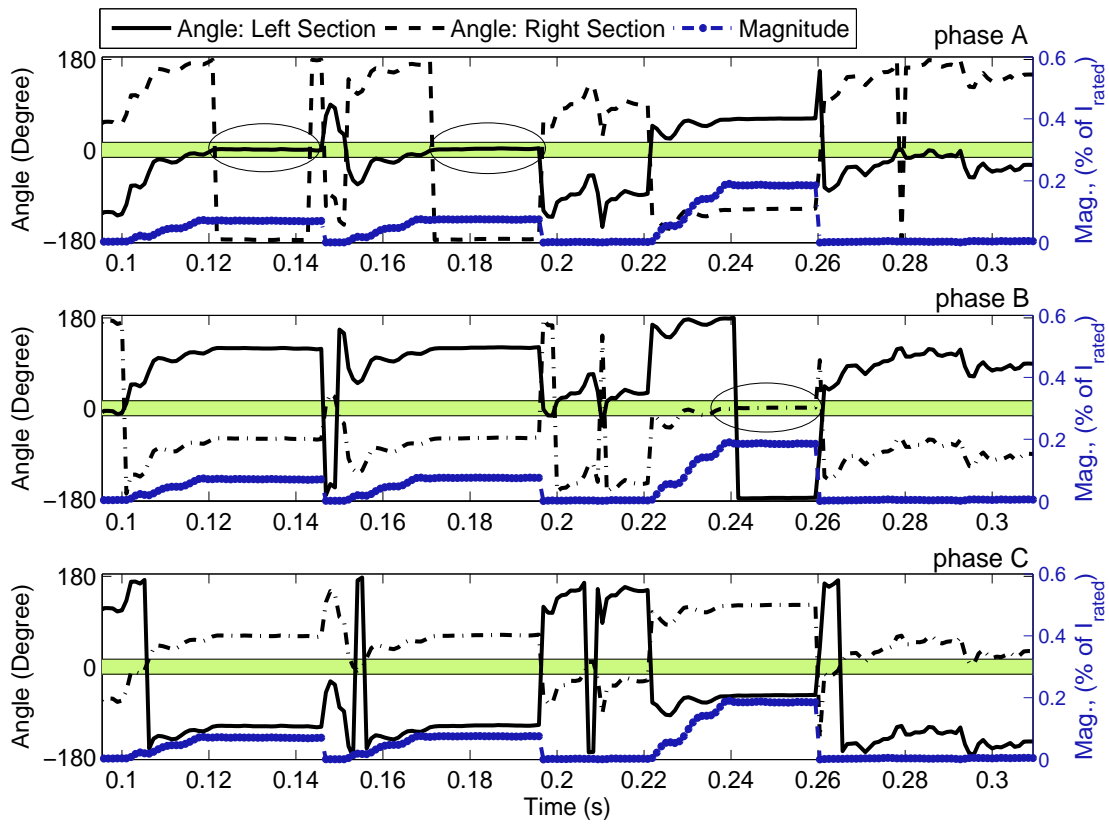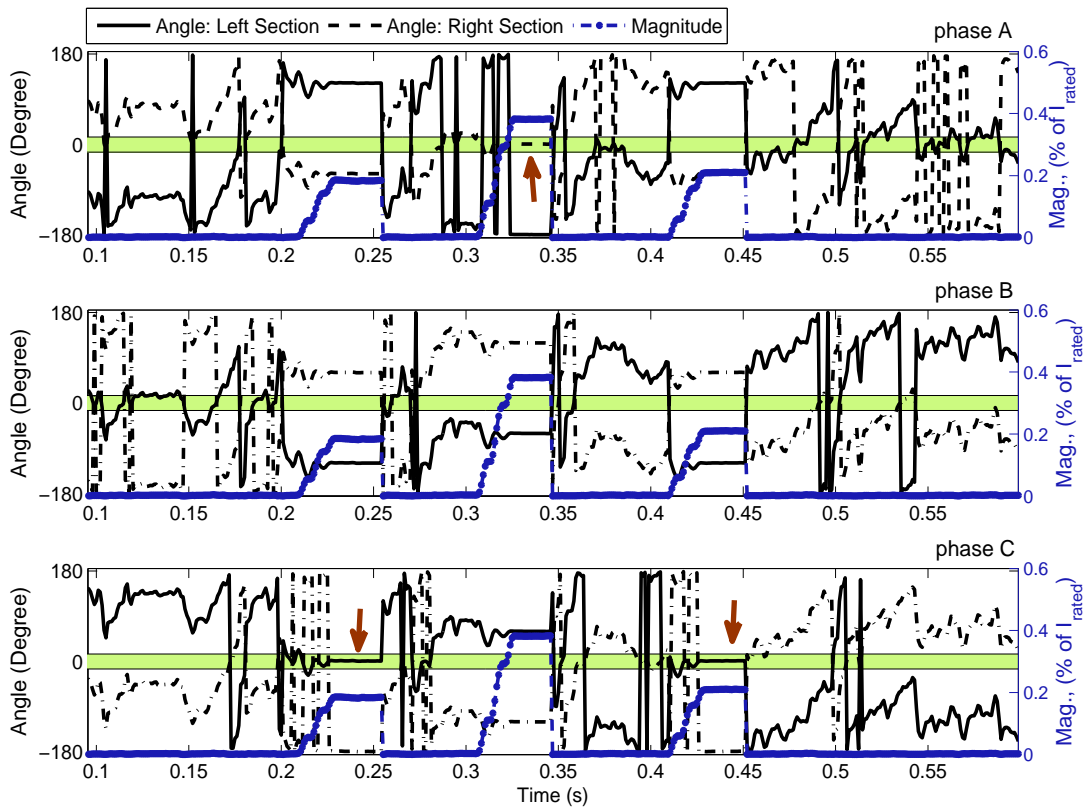
Figure 5.50: Compensated neutral current variations, Case 5-1.
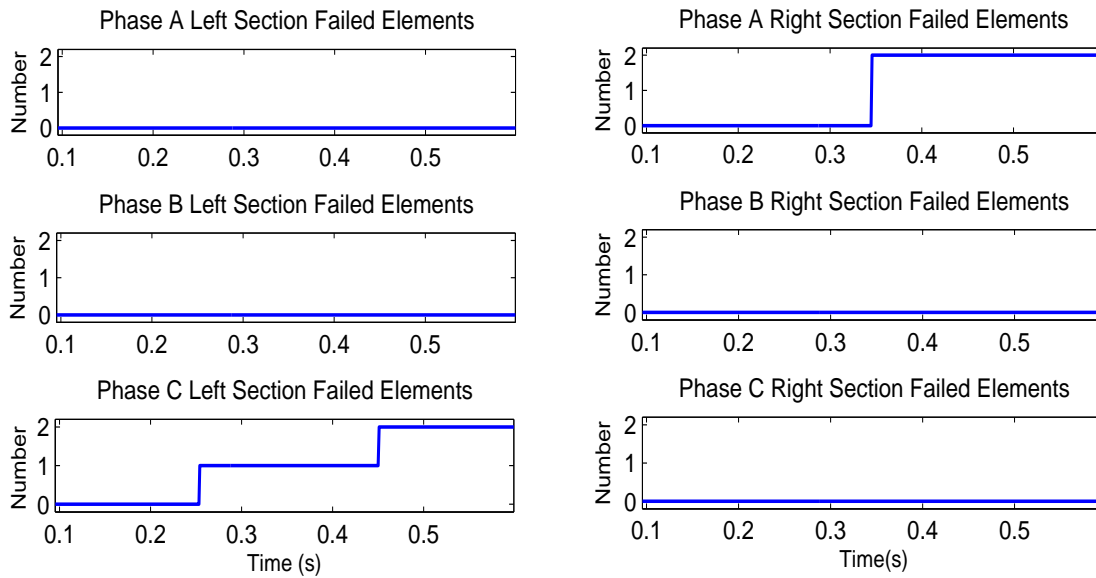
Figure 5.51: The proposed fault location output, Case 5-1.

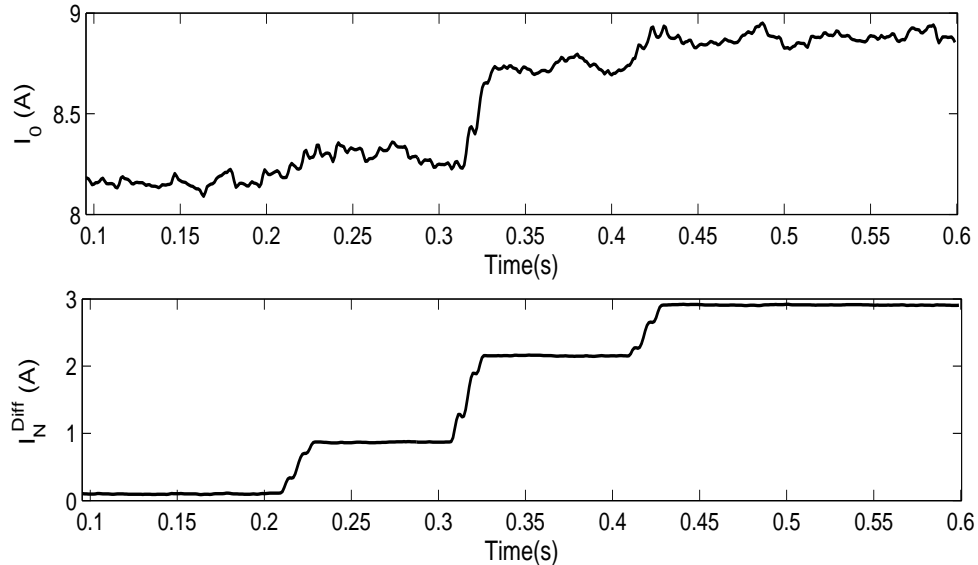## 5.7 Case Studies with Additional Protection Elements

5.7.1 Y-Y Ungrounded with Neutral Voltage Unbalance-Tied Neutrals

In this section first the fact that left and right section failures will result in the same amount of change in capacitance for the typical utility asymmetrical ungrounded double wye bank, Fig. 4.10, is shown to validate the discussion in Section 4.7.2. and then a numerical example is given for the discussed neutral voltage estimation in the same section.

For the SCB of Fig. 4.10 the before failure and after failure phase capacitances, for left section and right section failures are as follows, respectively.

$$\begin{cases} C_l = 1.088 \\ \\ C_l' = 1.108 \end{cases} \tag{5.2}$$

$$\begin{cases} C_r = 6.528 \\ \\ C_r' = 6.548 \end{cases} \tag{5.3}$$

The calculations are done using equations of Section 4.8.2. Values are in μF. As a result, the change in the capacitance for both of the left and right section failure cases is $0.02\mu F$. And thus, the neutral voltage would be the same for the left and the right section failures. This confirms what we concluded in Section 4.7.2.

For the simulated SCB of Figure B.4 the capacitance values are:

$$\begin{cases} C_l = 2.5 \\ \\ C_l' = 2.50704 \end{cases} \tag{5.4}$$

$$\begin{cases} C_r = 2 \\ \\ C_r' = 2.00704 \end{cases} \tag{5.5}$$

which similarly give the same capacitance change of $0.00704\mu F$ and the simulation gives the following neutral voltage for a simplified scenario of balanced voltages and no pre-existing unbalance, with a failure simulated at 0.2 s. Regardless of the section in which the failure takes place, the neutral voltage is the same. The voltage estimation is also evaluated as per (4.82) as follows:

The phase capacitance in per-unit form and using IEEE Std C37.99 is

$$Cp = 1.0015 \text{ pu} \tag{5.6}$$

Using Section 4.8.2 equations, the rated phase capacitance is 5 μF while after the failure the capacitance reaches 5.00704, thus the per-unit value would be 1.00141 which shows
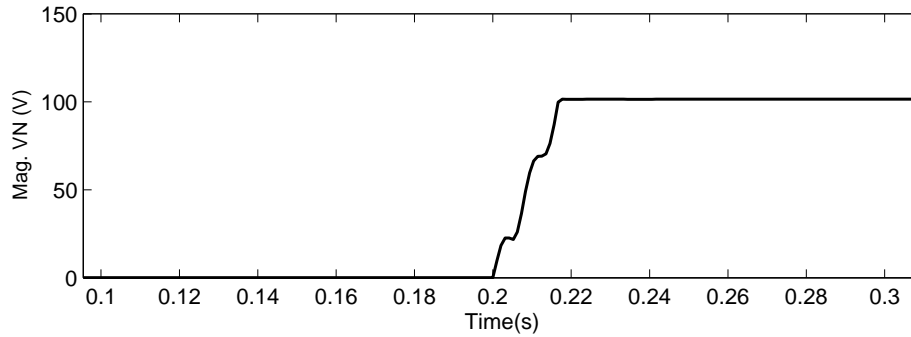
Figure 5.52: The measured neutral voltage for right/left section single element failures.

negligible error in the standard's estimation method.
The resultant neutral voltage would be

$$V_N = \frac{C_P - 1}{C_P + 2} = 5.2193 \times 10^{-4} \text{ pu} \tag{5.7}$$

this corresponds to a peak of $98.015\,V$ for the 230 kV system and matches the simulation result shown in Fig. 5.52.

5.7.2 Additional Voltage Differential Element

Simulation study for the configuration of Fig. 4.8 is presented in this part. The key difference for this configuration is that, due to additional measurements, simultaneous failures in different locations are detectable. It is worthwhile to note that the provided SCB configuration is fuseless and therefore the tap is at the low voltage capacitors. The LV capacitors are formed by parallel connection of fuseless capacitors. As a result, a capacitor failure at the bottom section gives a tap voltage of zero and needs to be tripped as no failures in the top section can be detected without a measurable tap voltage. Therefore, for fault location study we investigate various failures in the top section.
Case 7-1 The following event sequence is simulated:

- First element failure in left section of phase A at 0.2 s

- Consecutive element failure in left section of phase A at 0.25 s

- Single element failure in left section of phase C at 0.35 s

- Multiple element failure in right section of phase B at 0.4 s

The figures for fault location principle (voltage differential) are plotted separately for each phase. Figs. 5.53 to 5.58 demonstrate the successful determination of location and number of the failed elements.
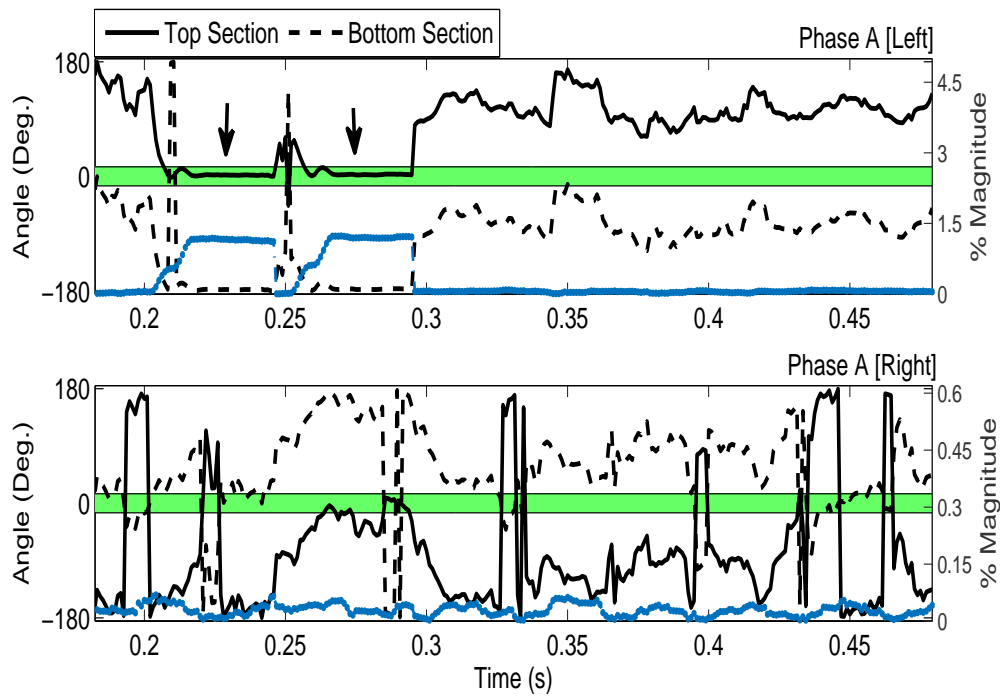
Figure 5.53: Phase A fault location principle, voltage differential protection.
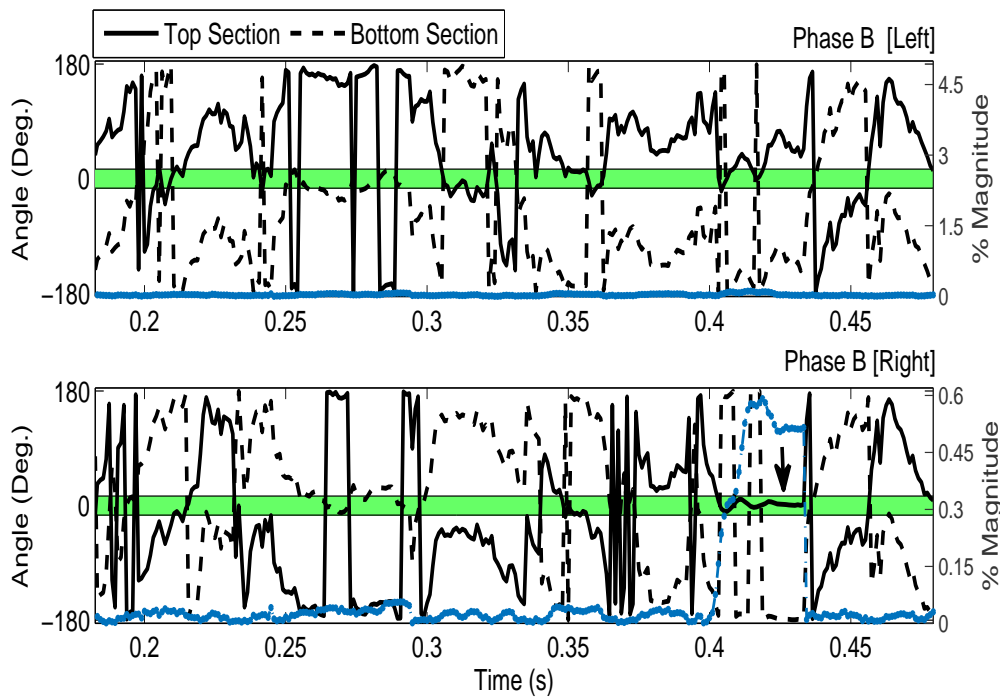
Figure 5.54: Phase B fault location principle, voltage differential protection.
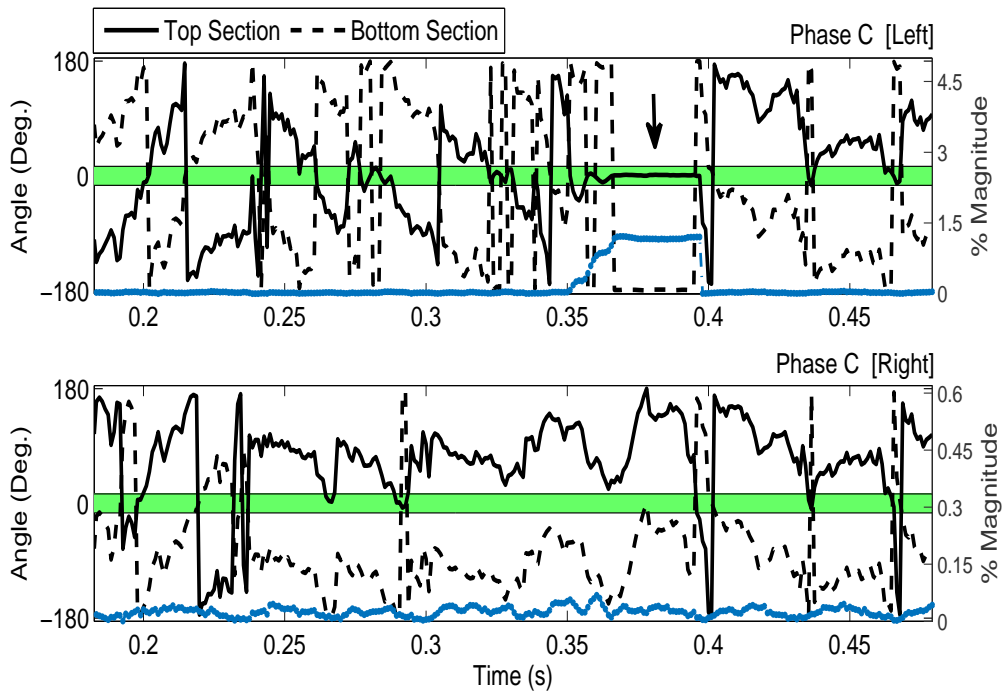
Figure 5.55: Phase C fault location principle, voltage differential protection.
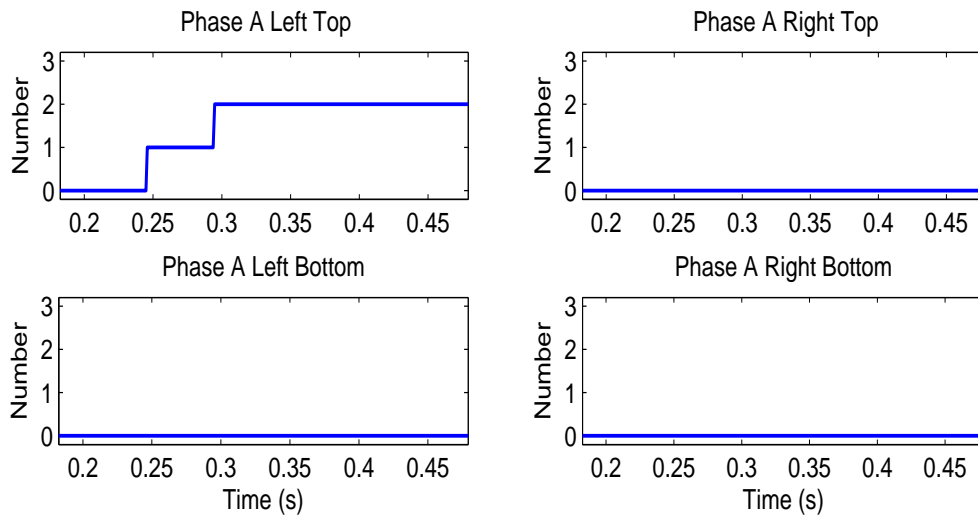
Figure 5.56: Phase A fault location output, voltage differential protection.
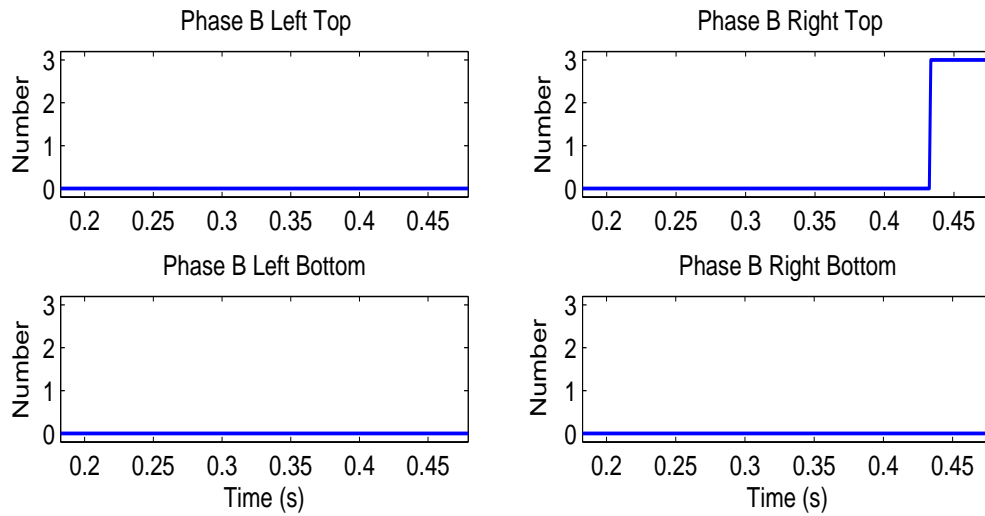
Figure 5.57: Phase B fault location output, voltage differential protection.
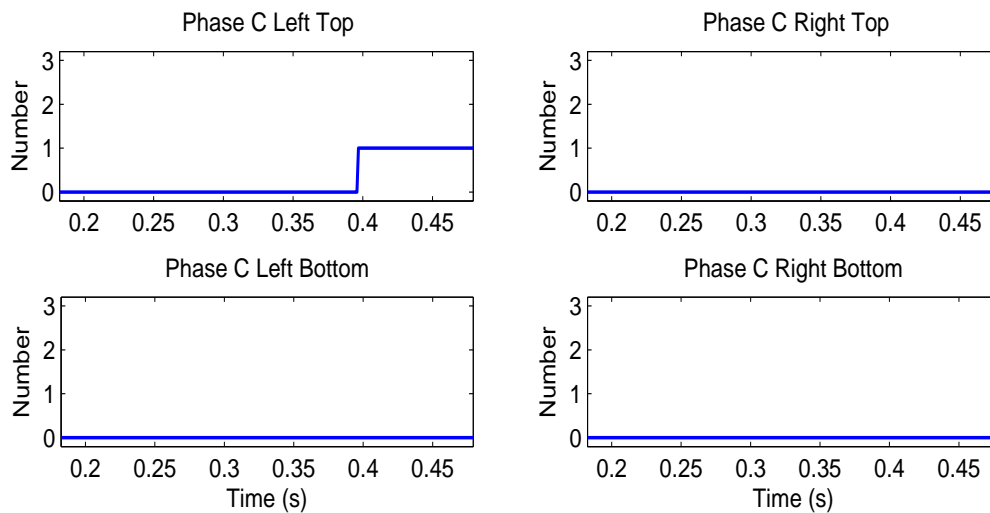
Figure 5.58: Phase C fault location output, voltage differential protection.

Case 7-2 To show the benefits of having separate differential voltage elements (functions) for left and right sections, and also the additional left tap to right tap differential function, a sample simulation scenario is performed. The case includes the following failures

- Single element failure in each phase all at o.2 s

- Simultaneous failures in left and right section of phase A at 0.25 s

Simulation results, Figs. 5.59-5.62, demonstrate the reliable operation of the fault location for the first event, which is an ambiguous (masking) scenario, and the second event, which is a simultaneous left and right failure scenario.

The 87-3 function principle and its resultant alarms are plotted in Figs. 5.63-5.66.
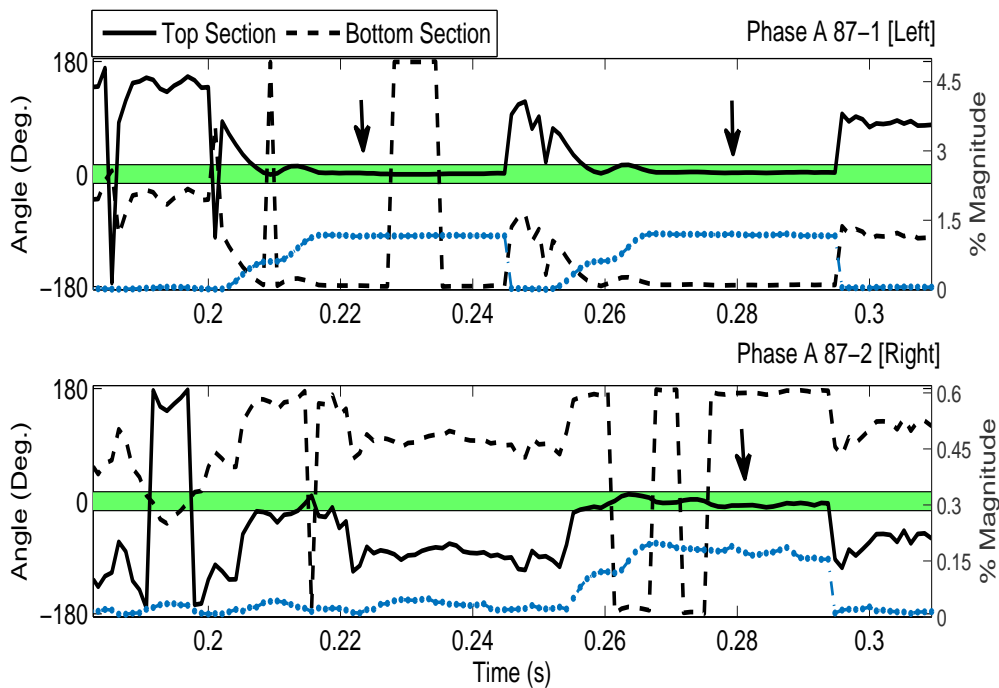
Figure 5.59: Phase A fault location principle, simultaneous failures.

Although the 87-1 and 87-2 functions locate the left and the right section simultaneous capacitor failures, the 87-3 function is only capable of locating one of them. The double arrow deltoid head in Fig. 5.63 points out the discussed fact in Section 4.7.1. Which stated that upon simultaneous failures in left and right sections, the magnitude of the operating function of 87-3 will be changed less than the expected increment for a single left section element failure.
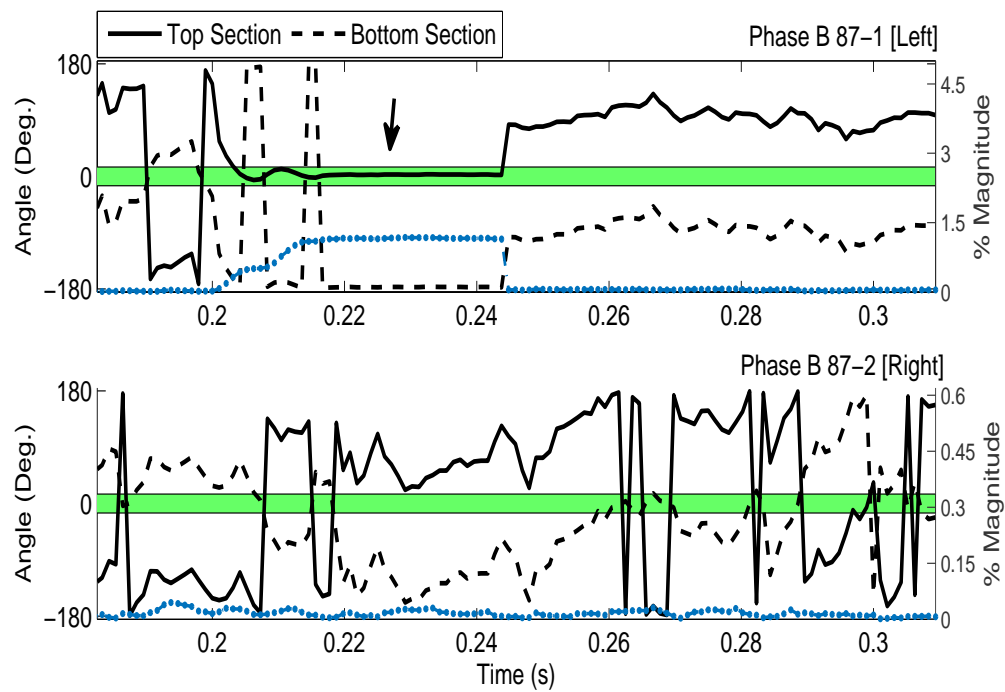
Figure 5.60: Phase B fault location principle, simultaneous failures.
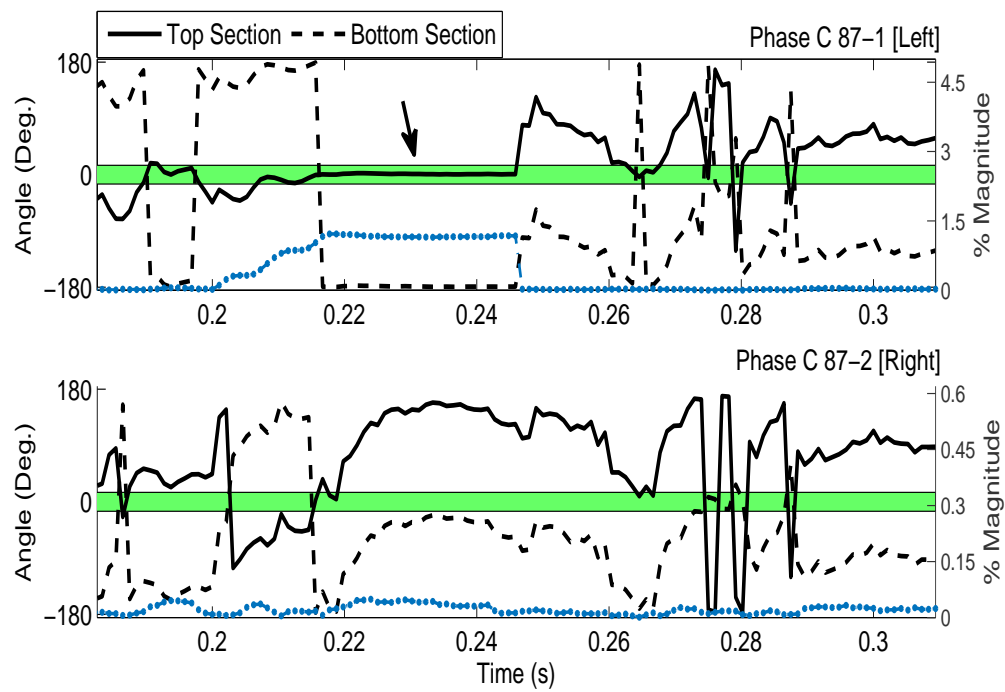
Figure 5.61: Phase C fault location principle, simultaneous failures.
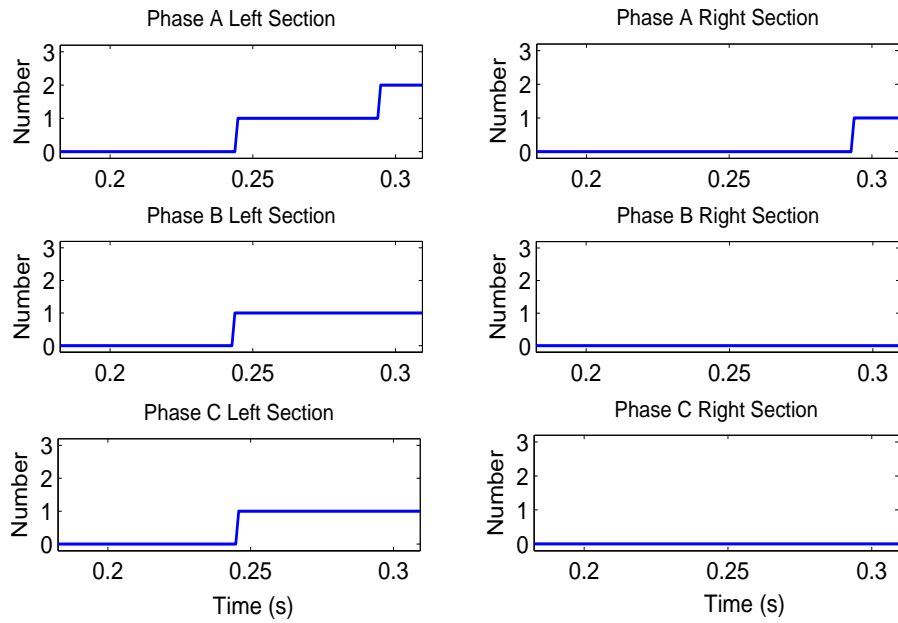
Figure 5.62: Fault location output, simultaneous failures.
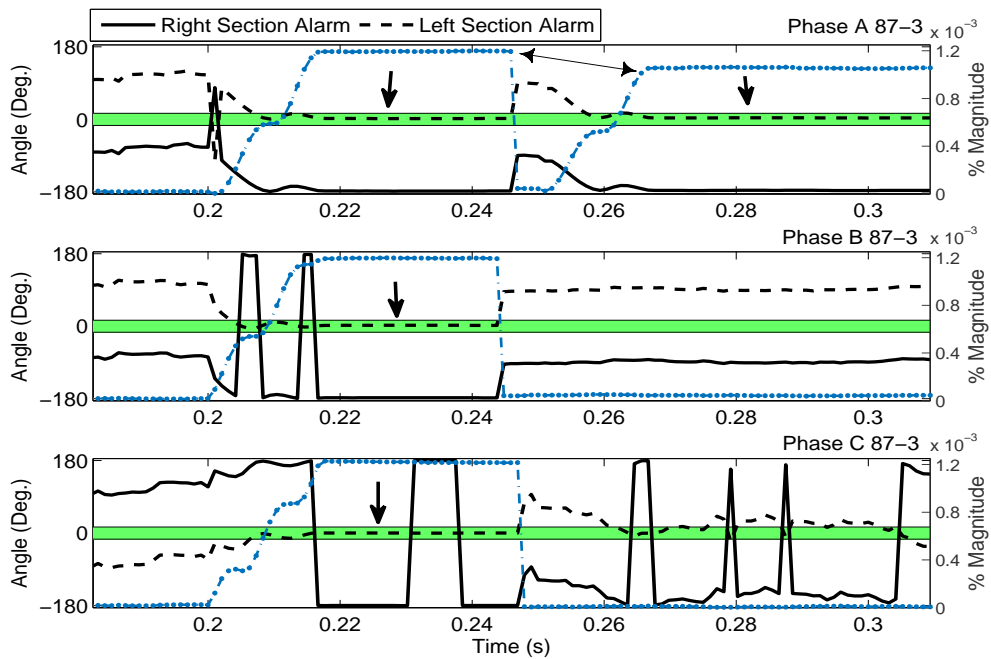
Figure 5.63: 87-3 fault location principle for three phases, simultaneous failures.
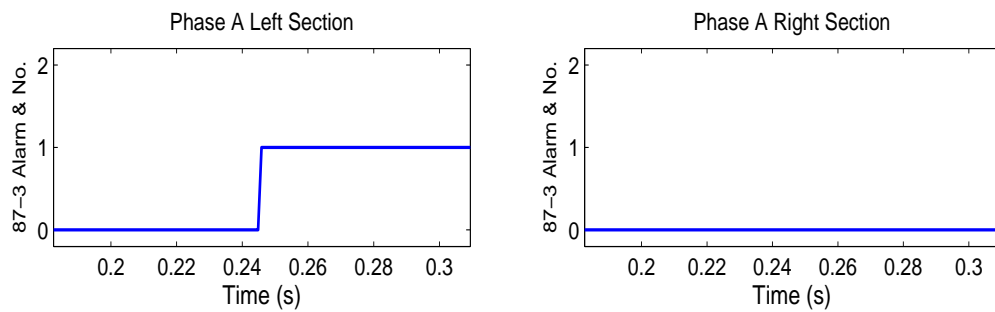
Figure 5.64: Phase A 87-3 fault location alarm, simultaneous failures.
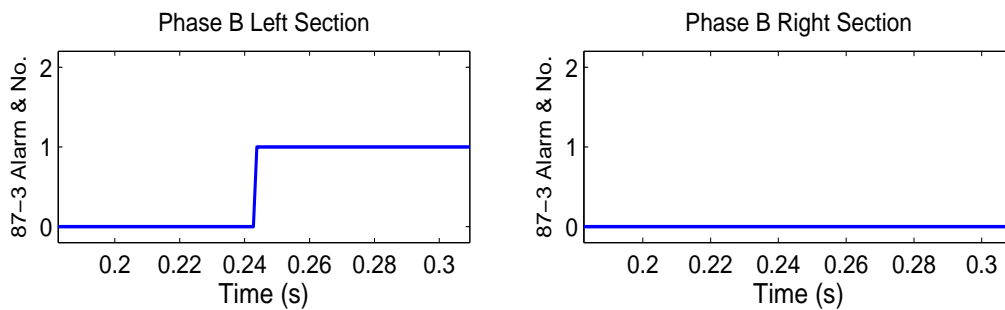
Figure 5.65: Phase B 87-3 fault location alarm, simultaneous failures.
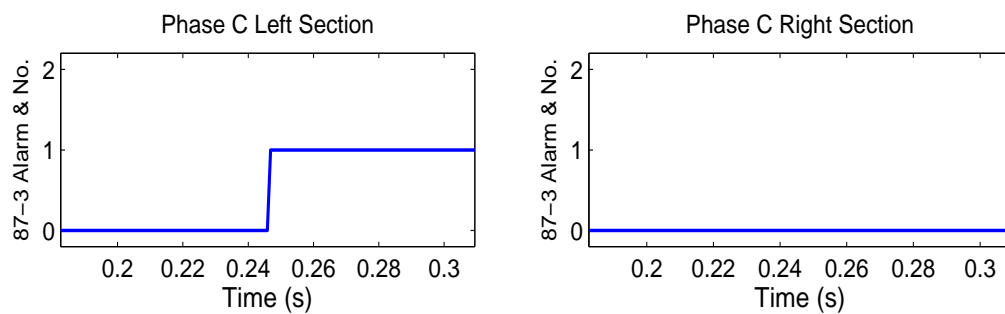
Figure 5.66: Phase C 87-3 fault location alarm, simultaneous failures.

5.7.3 Conclusion on the Results for Additional Protection Elements

Results of a thorough fault location study was demonstrated for an actual double wye SCB with three differential elements. The successful determination of simultaneous failures is due to fault location indicating quantities independence for each phase and section. This allows to reset each function without disturbing the detection of failed elements in the rest of the phase and sections. The auxiliary alarms of the tap to tap differential element were shown to be reliable (for example when needed in case of loss of bus VTs). In addition, sensitivity analysis proved the possible malfunction of this auxiliary alarm for simultaneous left and right section failures. Finally, neutral voltage estimation was evaluated, the mathematical proof and conclusion in the previous chapter regarding failure of this quantity for discriminating between left and right section capacitor faults was verified.

5.8 The SEL Method for Y-Y Ungrounded with Isolated Neutrals

According to the assumptions we investigated for the SEL fault location method for this configuration that deploys neutral-to-neutral voltage unbalance protection, performance analysis of the present method in the literature is required. Therefore, we simulated the method introduced in Section 3.3.3. It is worthwhile to note that the evaluated (SEL) fault location method for this configuration only supports single element failures.

Case 6-1 The single element failure takes place in the right bank of an internally fused SCB at 0.22 s. The affected phase is phase C.

Along with the fault location principle of [27], the function outputs, the differential voltage and the compensated quantity are plotted in Figs. 5.67 5.68 and 5.69. The non-zero value for $V_{N_l N_r}$ in Fig. 5.69 which exists before the internal failure occurrence, confirms the need for the differential voltage quantity compensation. Further illustrative scenarios would be presented in the external unbalance case evaluations.
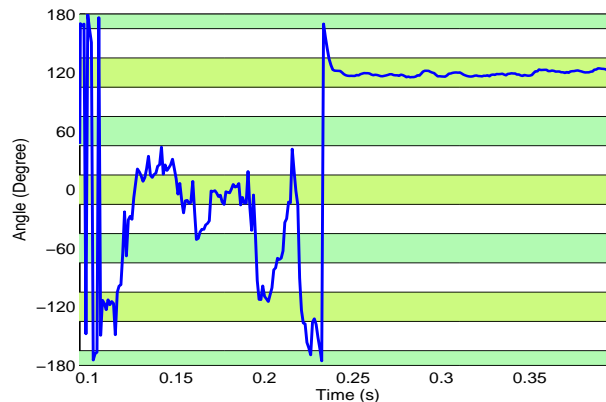
Figure 5.67: The SEL method detection angle, single failure in phase C right section, Case 6-1.
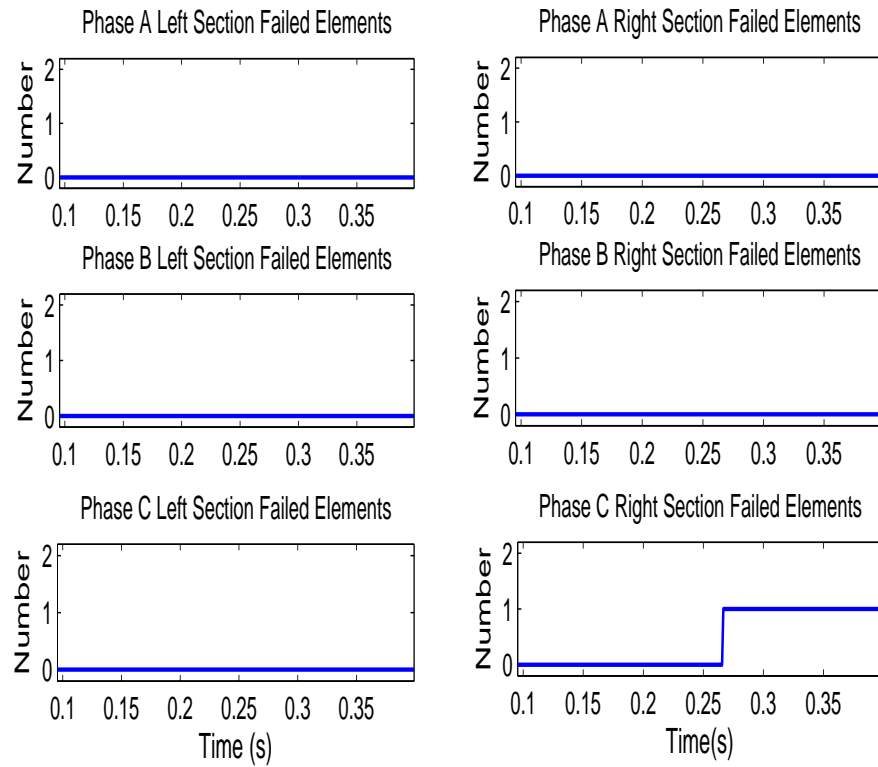
Figure 5.68: The SEL method fault location output, Case 6-1.
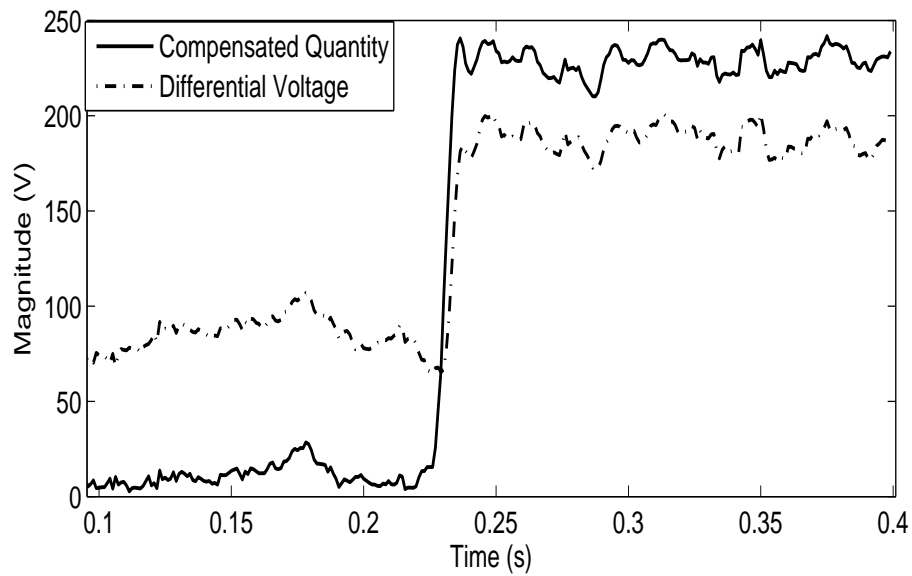
Figure 5.69: Measured and compensated differential voltage, Split wye bank with isolated neutrals

5.9   Further Investigation on Algorithms Reliability

5.9.1   Simultaneous Failures

Simultaneous failures with exactly the same occurrence time are unlikely, compared to the ones in the previously presented scenarios. Since the proposed fault location methods have single decision boundary for each phase and the superposition property is not applicable to the internal failure impacts on the fault location principle, it is expected that fault location methods fail in case failures become simultaneous or super-close.
Fig. 5.70 presents this case for two elements that fail at the same time, one in the right section of phase C, and one in the left section of phase B in a fused double wye SCB. After failures occurrence, the phase angles reach constant values; however, the margins to include these phase angles in the corresponding zero angle zone have to be so wide which will make the fault location vulnerable in terms of loss of security. For instance, a blinder setting of 41 degrees in the presented scenario of Fig. 5.70 is required to detect a phase B failure. The situation would be worse for the discussed SEL method in Chapter 3.3 as it is not phase segregated, and thus, the phase angle can only be compared with one margin for two simultaneous failures in different phases.
For single wye SCBs, two simultaneous failures in phase A, and B in a fuseless SCB are simulated. As can be seen in Fig. 5.71, the voltage based method of fault location (SR) also fails.

In short, the variable range for the phase angle, and also the number of involved phases make the detection of failure location complex and non-practical in terms of the required characteristic for detection of exactly simultaneous failures in different locations.

5.9.2   Susceptibility to External Disturbances

Even though for a supplementary function like fault location, the safe and straight forward solution for reliable operation would be blocking whenever a shunt or series power system fault is detected; but in order not to miss element failures during this transients, we perform simulations to see if blocking is necessary.
For algorithm performance evaluation, temporary faults (representing transients in a shunt branch with respect to the SCB) on the bus that the SCB is located, and also at the remote sending bus is simulated. The results are included depending on the new points that a scenario had brought up. Furthermore, single phase open pole tripping with subsequent reclosing (representing transients in a series branch with respect to the SCB), is simulated and results are demonstrated here.
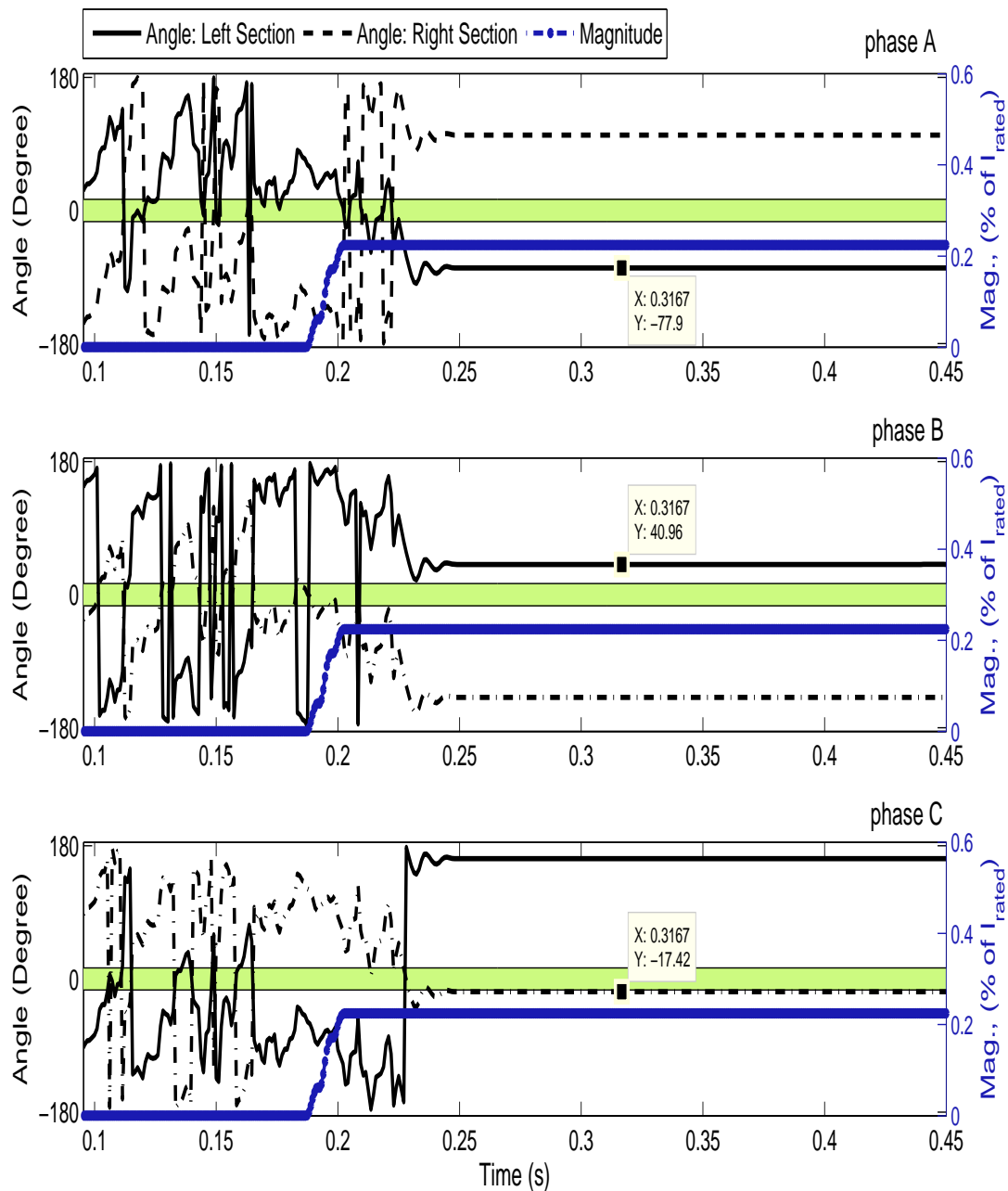
Figure 5.70: Compensated Neutral Current: Fault location malfunction for simultaneous failures.
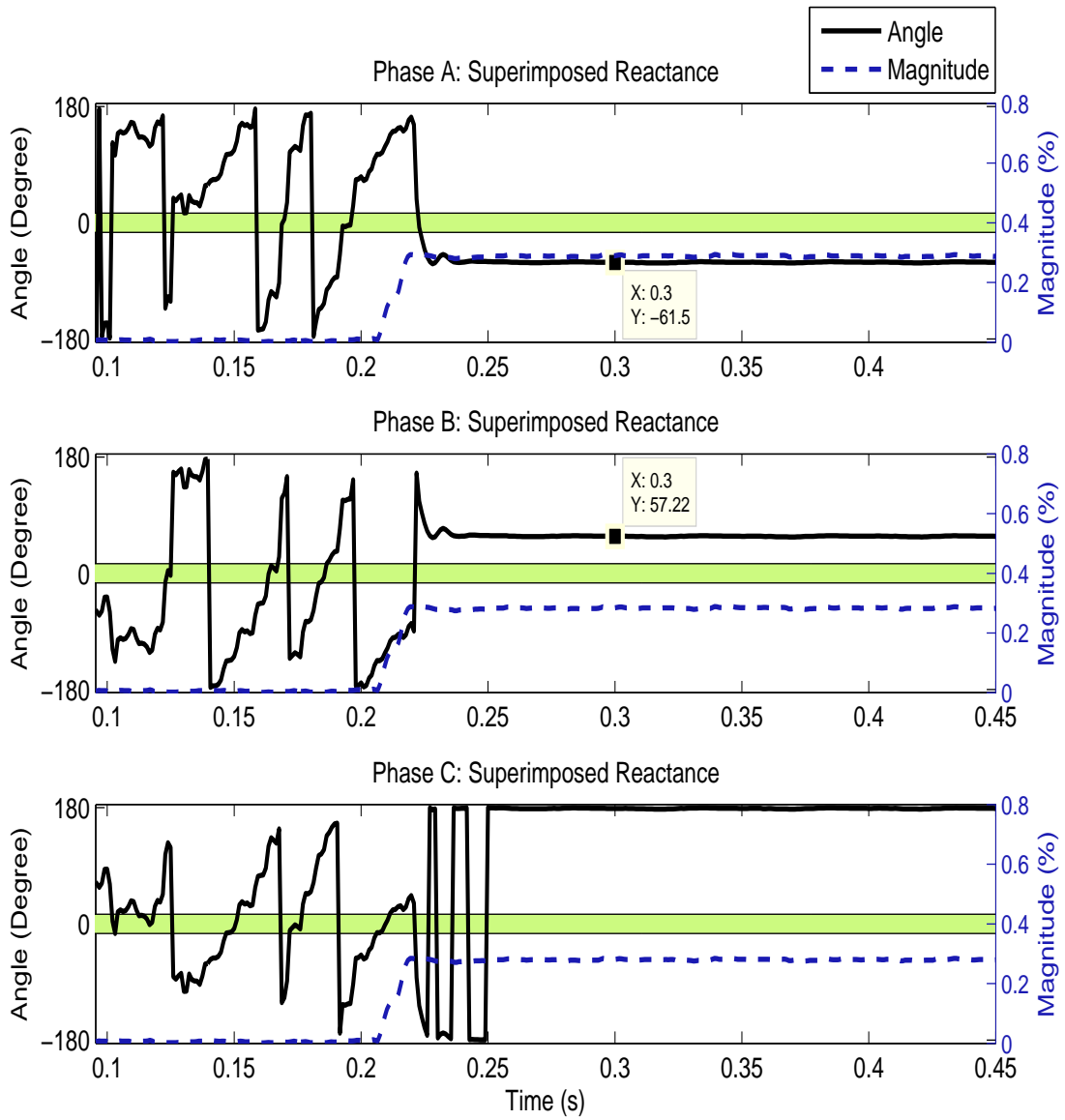
Figure 5.71: Voltage based fault location malfunction for simultaneous failures

Single Wye Ungrounded

Case 8-1 A phase A to ground fault with fault resistance of $0.5\,\Omega$, and duration of 50 ms is simulated. Meanwhile an element fails in phase B of an internally fused SCB. This is an illustrative scenario and simulation of other fault types validated the same performance. Figs. 5.72 demonstrates the SR variations for this case. Fig. 5.73 illustrates severe jumps in the magnitude of superimposed reactance, note that the magnitude is in per-unit in this figure. Fig.5.74 shows the changes in the SR magnitude for the same scenario as case 8-1, with the difference of fault resistance which was changed to $100\,\Omega$. This was intentionally simulated to demonstrate that even high impedance faults change the SR much more than internal failures in a way that the magnitude is reliably far from the thresholds. This would help to block the fault location when external disturbance is suspected due to high level of magnitude in the fault location principle. Fig. 5.75 illustrates the fault location output. In both cases the proposed method has been able to locate the failure once the external disturbance is cleared.
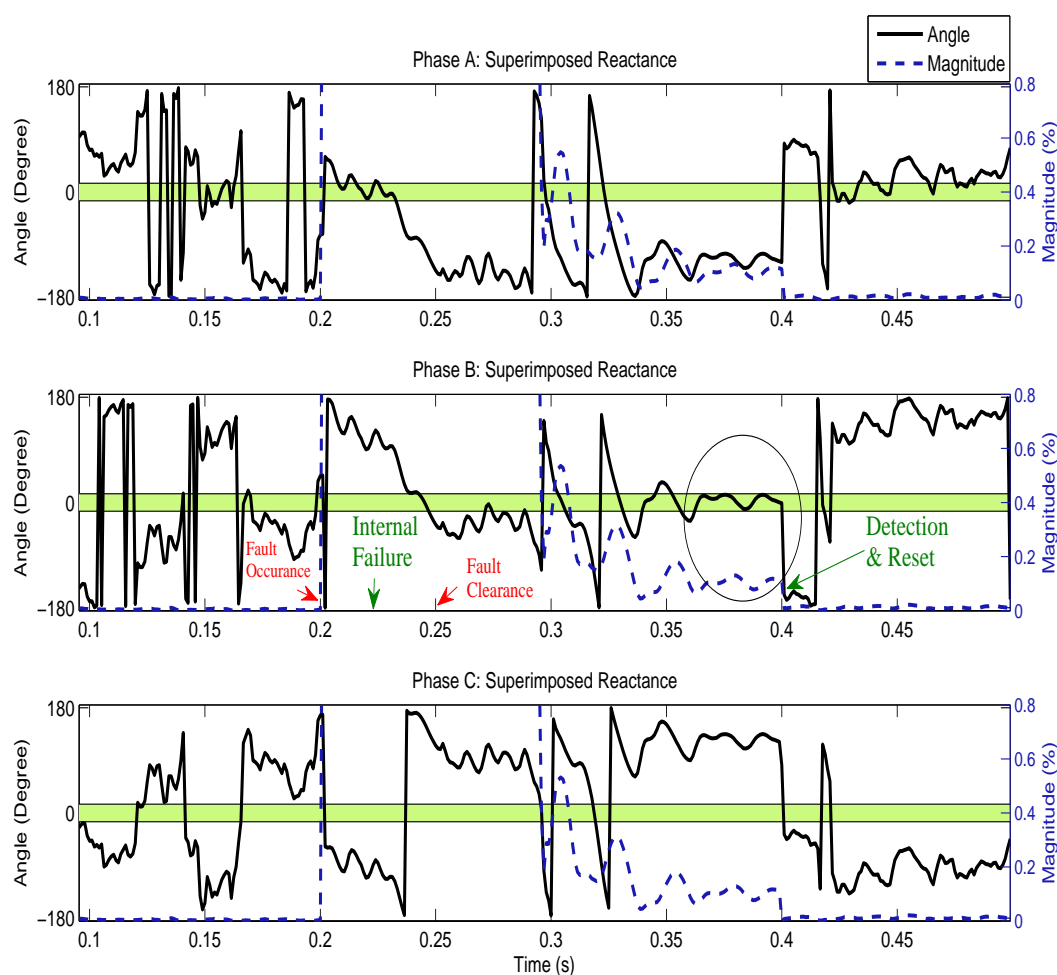
Figure 5.72: Proposed method performance under power system fault, Case 8-1
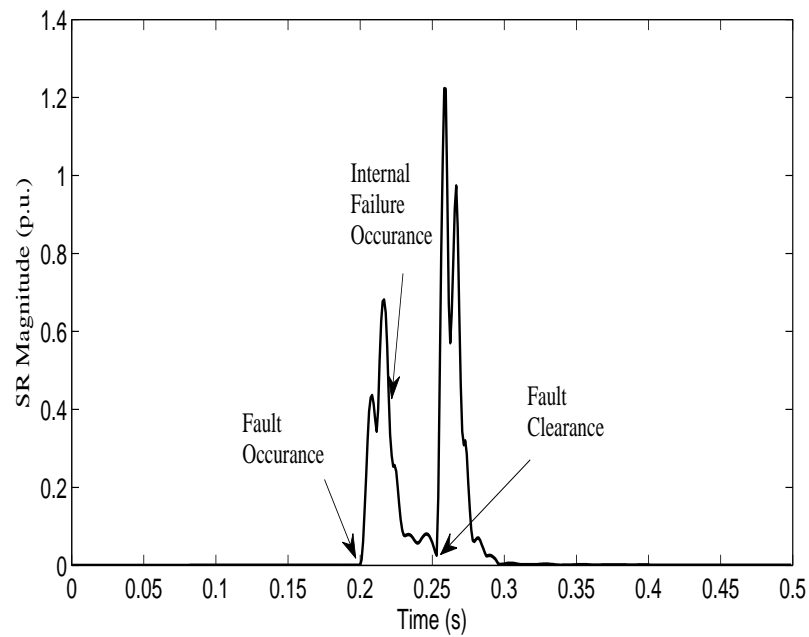
Figure 5.73: Jumps in magnitude of the proposed principle under power system fault, Case 8-1
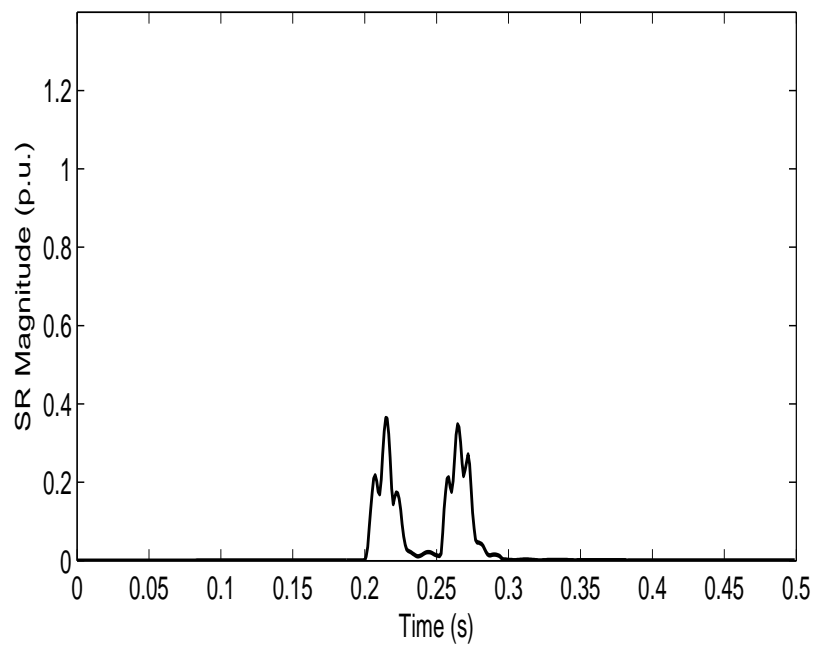
Figure 5.74: Jumps in magnitude of the proposed principle under power system fault, (Case 8-1 with high impedance fault)
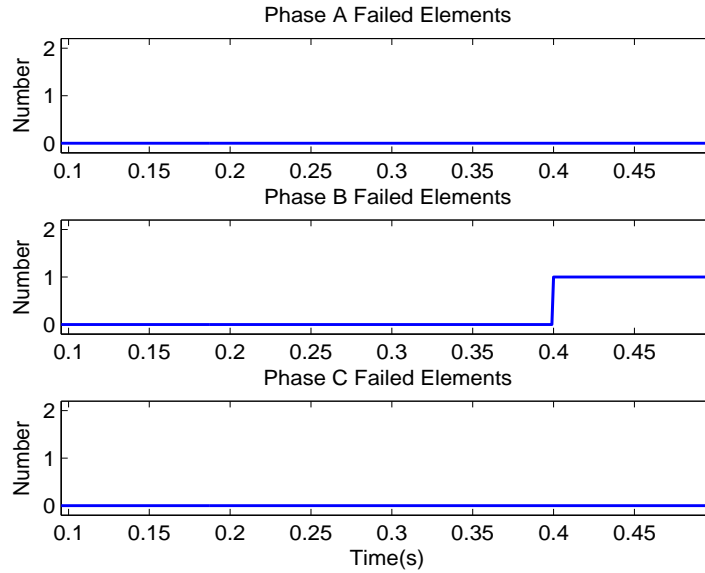
Figure 5.75: Proposed method dependability under power system fault, Case 8-1

Case 8-2 Another illustrative scenario involves a single phase to ground fault in the same phase that will undergo a capacitor failure during this ground fault. Duration of the fault is set to 100 ms, both the power system fault, and the internal failure take place in phase C, at 0.2 s, and 0.22 s, respectively. Fault resistance is 2.5 Ω.
Fig. 5.76 demonstrates that during the ground fault, higher magnitude of the SR, or any other supervisory source, should be used for blocking.
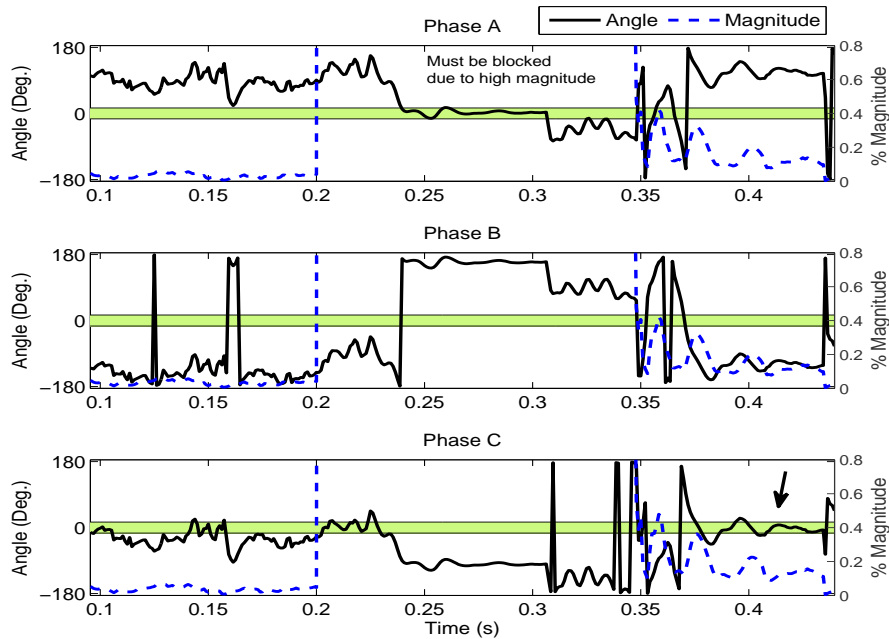
Figure 5.76: The proposed method fault location principle, Case 8-2

Otherwise, as it can be seen from Fig. 5.77, the fault location method would have mistakenly picked up due to momentary angle criteria satisfaction in phase A. As a result of blocking and once the ground fault is cleared the SR method has been able to detect the phase C internal failure, see the arrow pointing to the detection interval in Fig. 5.76 and the counter reaching the threshold in Fig. 5.77.

Case 8-3 A three phase to ground fault is simulated. The SCB is fuseless, and an in-
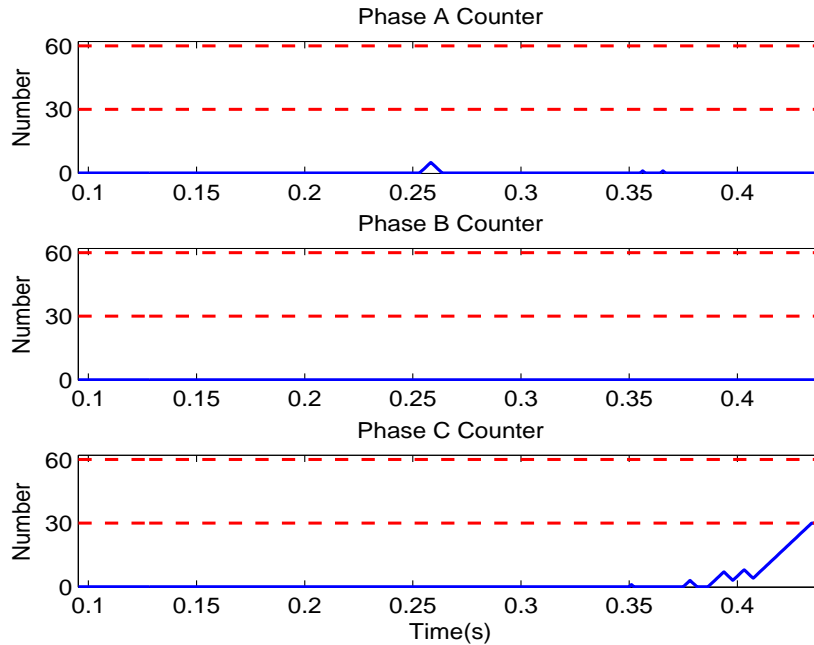
Figure 5.77: The proposed method fault location method counter, Case 8-2

ternal failure takes place exactly at the same time that the power system fault initiates. Results for fault at the SCB bus, in the middle of the connecting transmission line, or at a far bus (with the transmission line in between) were the same. Figs. 5.78 and 5.79 show dependable operation of the proposed method after disturbance clearance.

Case 8-4 Single pole tripping is considered for evaluation, the open pole time duration is selected based on minimum de-ionisation time for fault arc at 230 kV [50]. For an internally fused SCB, in the system shown in Fig. B.5, phase A of the connecting line gets open at 0.2 s and is re-closed at 0.56 s. Meanwhile, at 0.35 s, an internal failure occurs in the same phase. Figs. 5.80-5.82 illustrate the principle variations, changes in the counter, and the fault location principle magnitude (zoomed out) for this scenario, respectively. As can be seen in Fig. 5.80, the fault location needs blocking during the open pole. However, after the reclosure, again the proposed method shows successful detection of the failure location. Notice the suitability of a magnitude based blocking signal as per Figs. 5.81 and 5.82.

Simulation of other open pole scenarios also confirmed this conclusion.
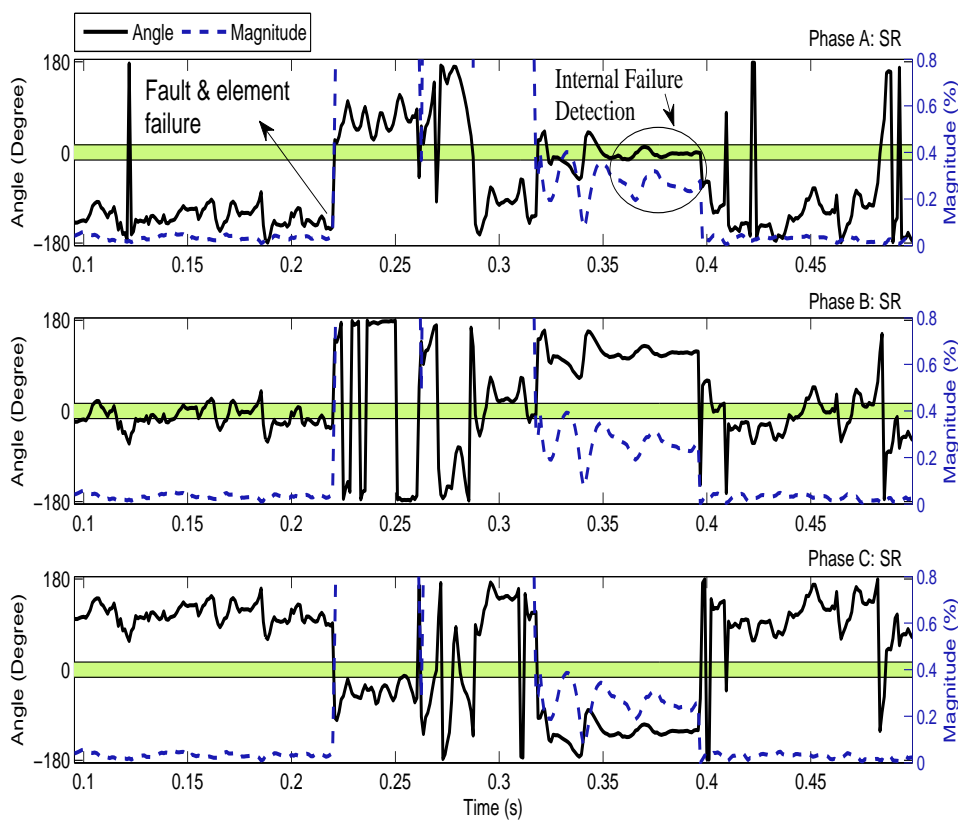
Figure 5.78: Proposed method principle under power system fault, Case 8-3
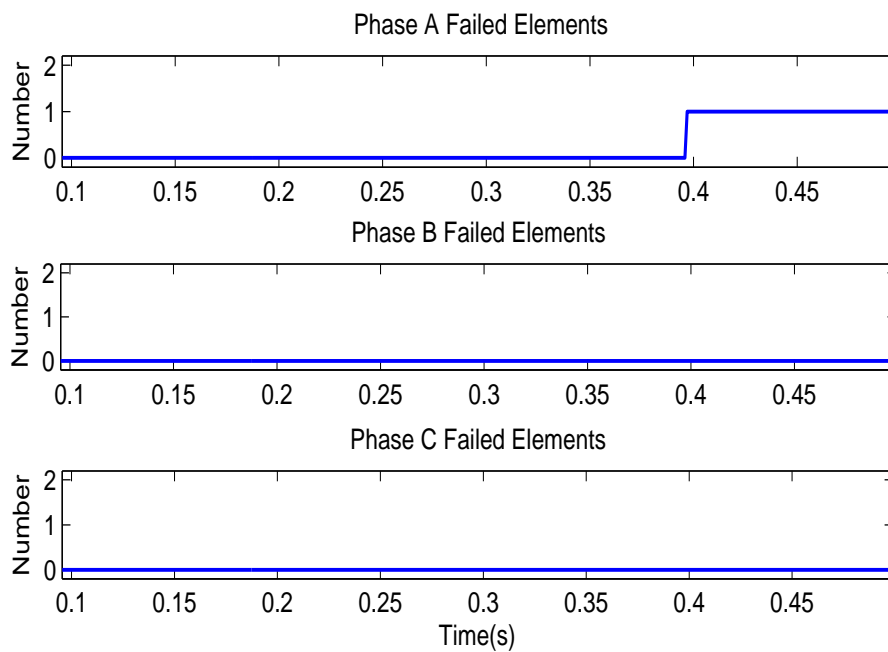
Figure 5.79: Proposed method output under power system fault, Case 8-3
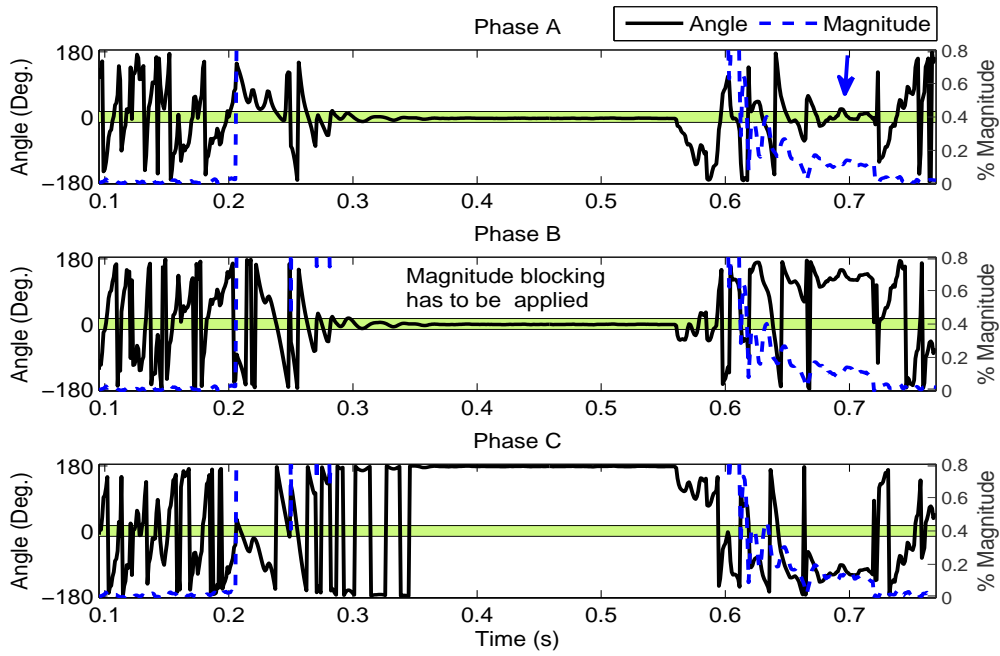
Figure 5.80: Plot of the SR, Case 8-4.
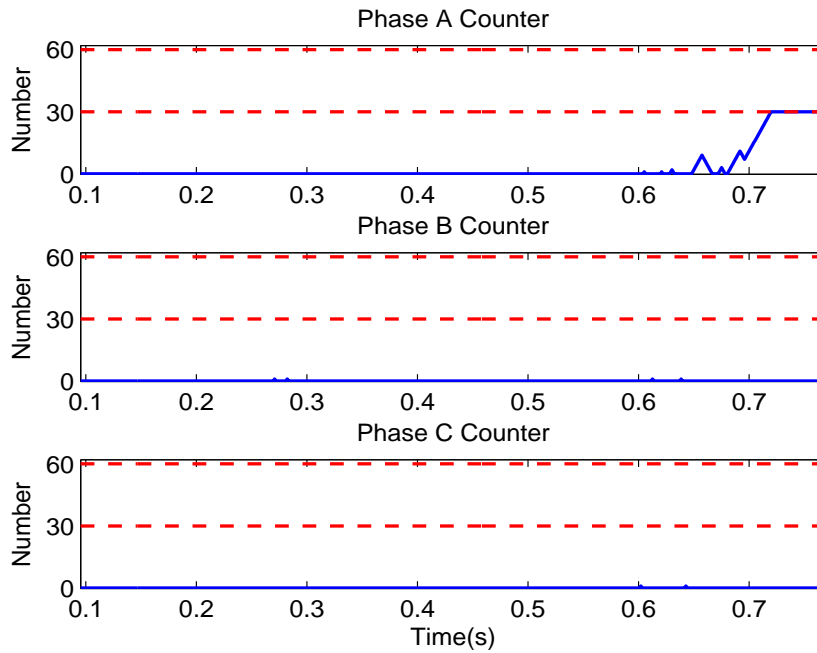
Figure 5.81: The proposed fault location counter during open pole, Case 8-4.
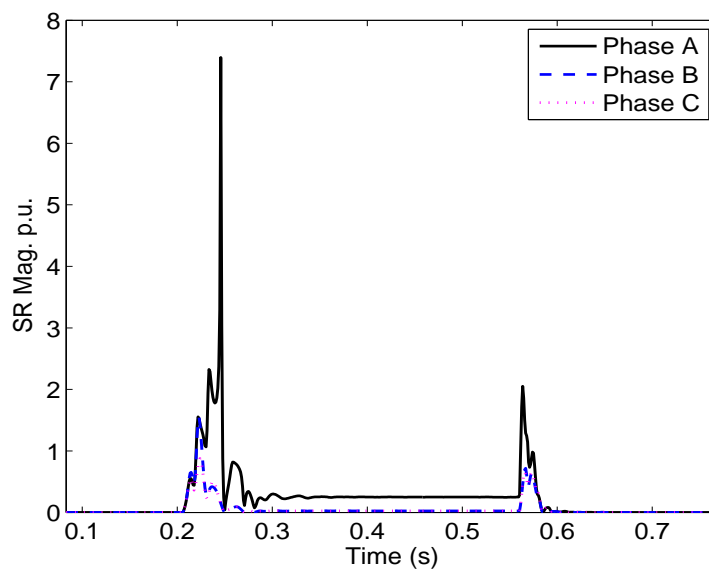
Figure 5.82: SR Magnitude jumps, Case 8-4.

We also simulated the SEL fault location method for the same scenarios to investigate its performance. The SEL fault location principle and its output are shown for case 8-1 in Figs. 5.83 and 5.84. As can be seen, once the system fault is cleared this method also detects the failure correctly. This confirms a delay in fault location, same as our proposed method. Same performance was verified for other scenarios as well.
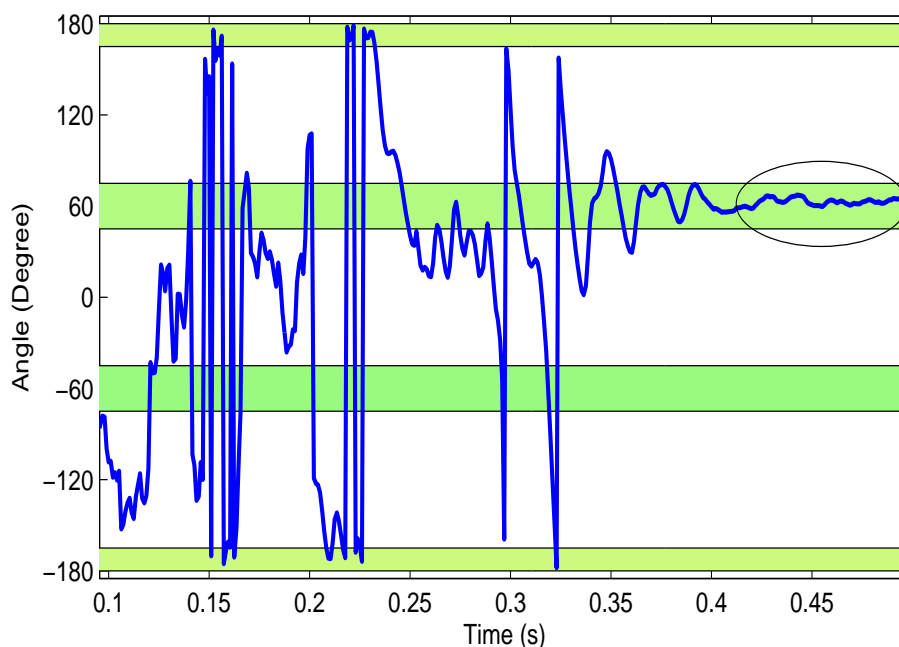
Figure 5.83: The SEL method fault location principle, Case 8-1.
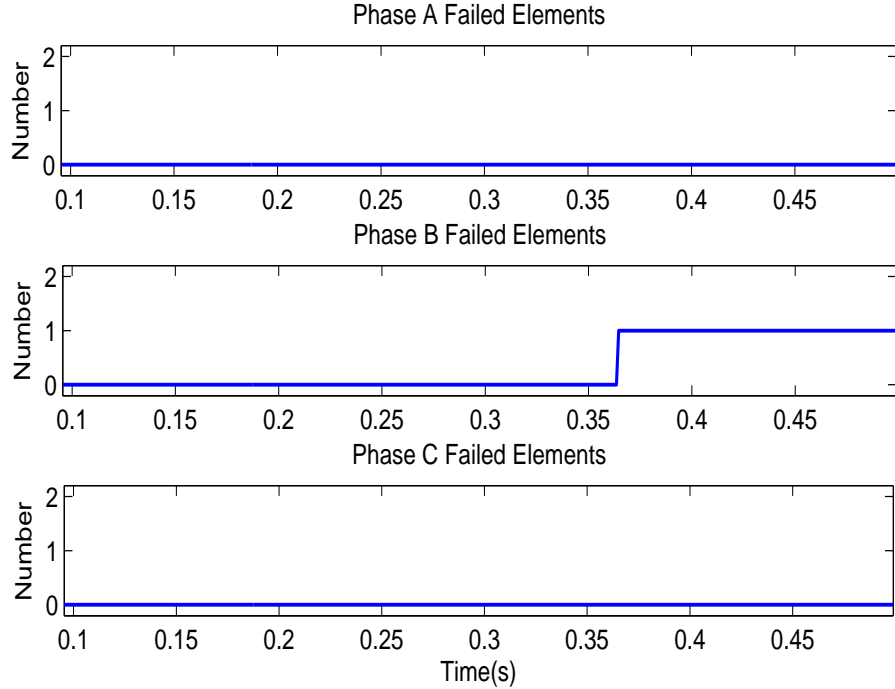
Figure 5.84: The SEL method output, Case 8-1.

Single Wye Grounded Through a Capacitor

Three of the simulated scenarios are brought here for validation purpose.

Case 9-1 For a fuseless bank, at 0.2 s, an element fails in phase B. At 0.22 s a shunt power system fault occurs at a remote bus on the same phase. The fault is cleared at 0.32 s. Figs. 5.85, and 5.86 illustrate the results.   From Fig.5.86 it is concluded that the power system fault makes the picked up counter get reset, however with clearance of the fault, the corresponding counter picks up again, and the right location is determined by the proposed method.

Case 9-2 The simulation case number 8-2, for which the fault location algorithm for ungrounded wye bank was evaluated, was simulated again for the configuration of wye grounded through a capacitor. Simulations illustrate reliable determination of the failure location without the need for blocking. The bank is internally fused for the simulated case of Figs. 5.87 and 5.88.   As it can be seen, although the counter picks up mistakenly first, it resets as the principle does not remain in the boundary. With clearance of the fault, the counter picks up again and determines the right location for the failure. Same results achieved for faults with other resistance, location and duration, both for the fused and fuseless banks.

Case 9-3 A worst case scenario with long duration open pole, 950 ms, in the same phase that the element will fail is selected as an illustrative scenario. Figs. 5.89, 5.90, and 5.91 present the proposed fault location principle, the counter, and the zoomed out per-unit magnitude of the proposed principle.   As the figures present, the proposed method still is reliable for the external unbalance case. Same results were verified for simultaneous failures and open pole tripping.
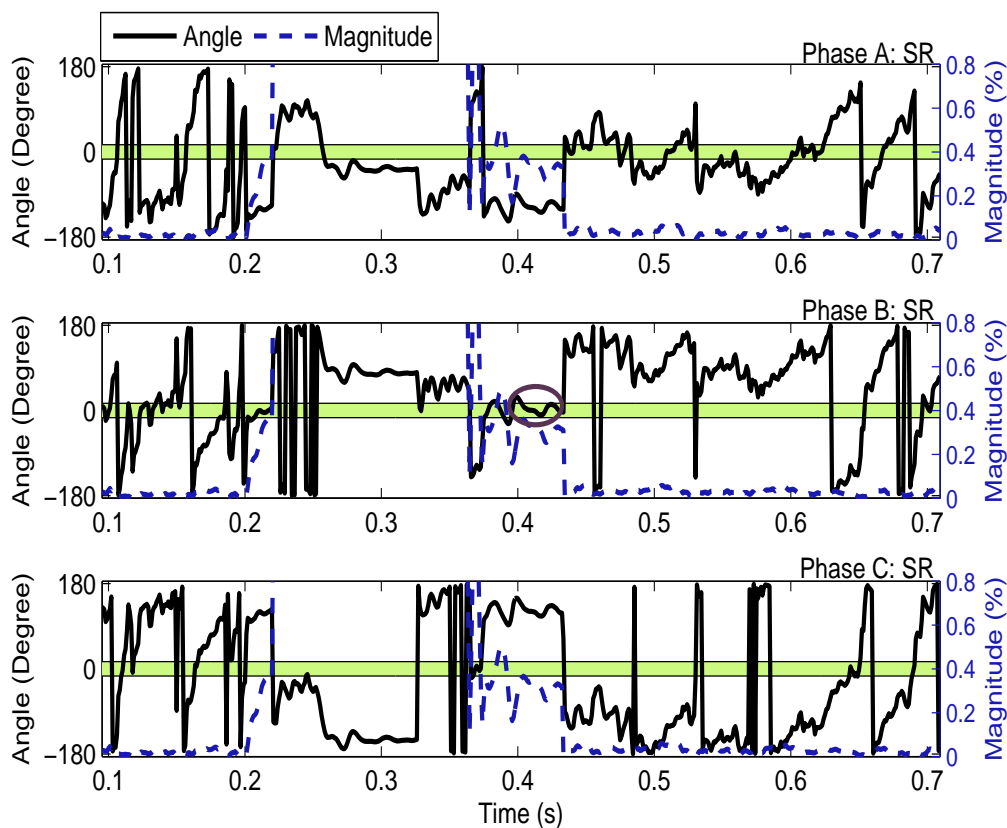
Figure 5.85: The proposed fault location principle for Case 9-1

Figure 5.86: The proposed fault location counter for Case 9-1
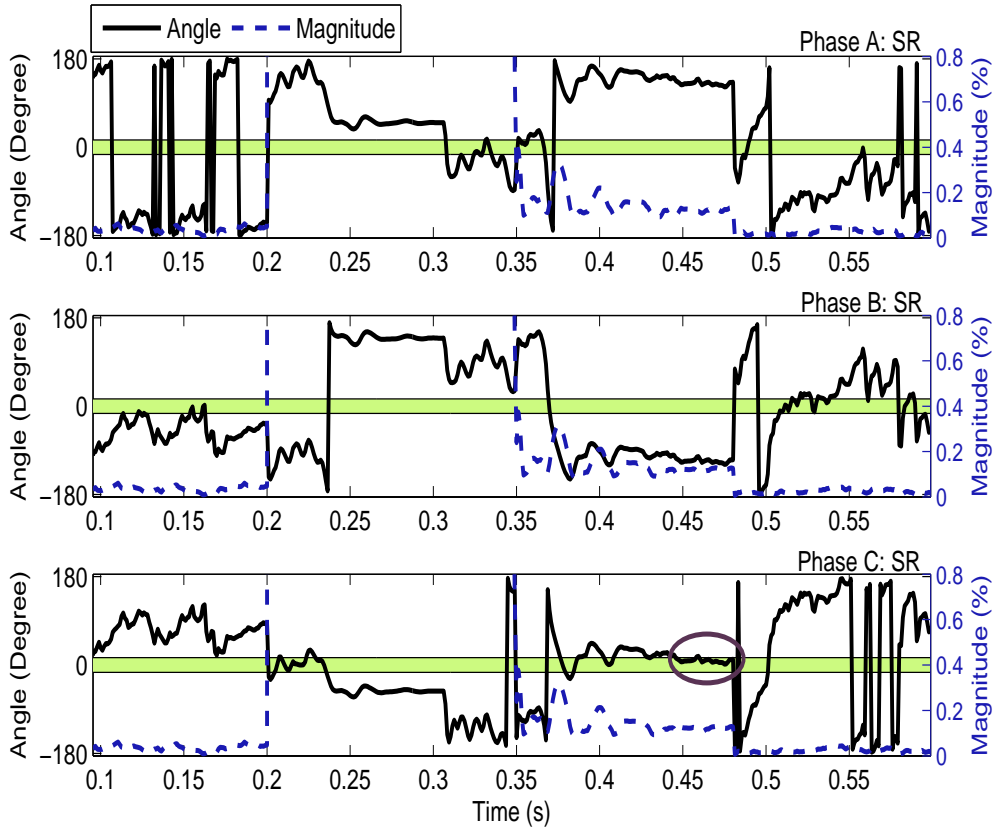
Figure 5.87: The proposed fault location principle for Case 9-2

Figure 5.88: The proposed fault location counter for Case 9-2

Figure 5.89: The proposed fault location principle for Case 9-3
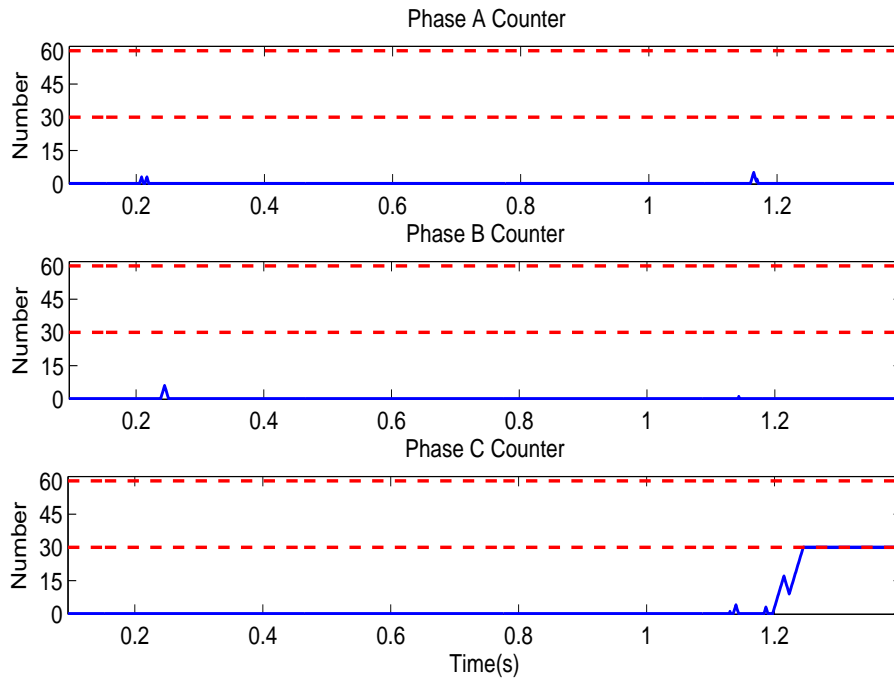
Figure 5.90: The proposed fault location counter for Case 9-3
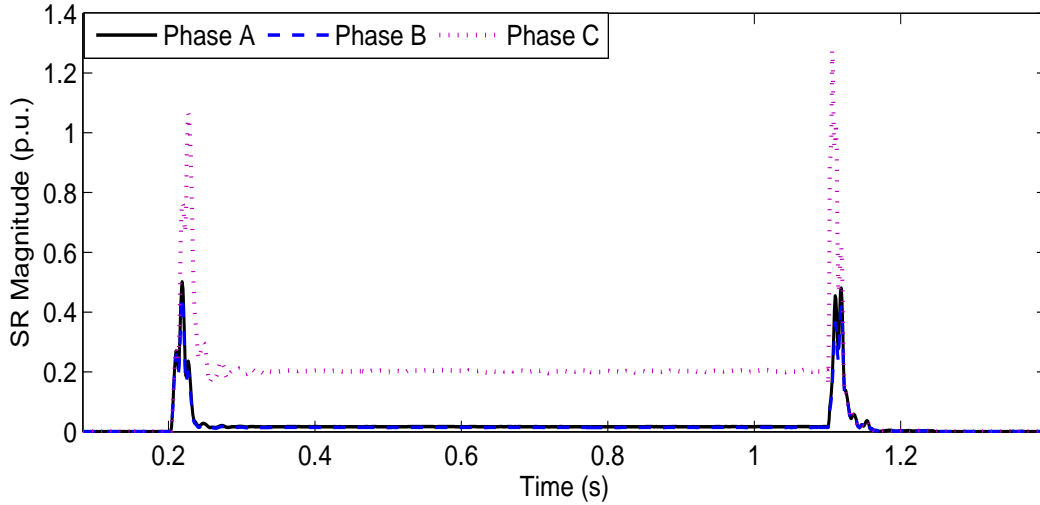
Figure 5.91: The proposed fault location principle magnitude for Case 9-3

Case 9-4 A fuseless bank is chosen to simulate a case in which at 0.22 s an internal failure in Phase A and an open pole in the same phase occur simultaneously. For the sake of clarity of the demonstrations a short dead-time has been considered for this single phase auto-reclosure, i.e. the event lasts 100 ms. Figs. 5.92 and 5.93 show the successful determination of the failure once the external unbalance is cleared. As explained before, applying a magnitude upper limit is not necessary for fault location of this configuration.
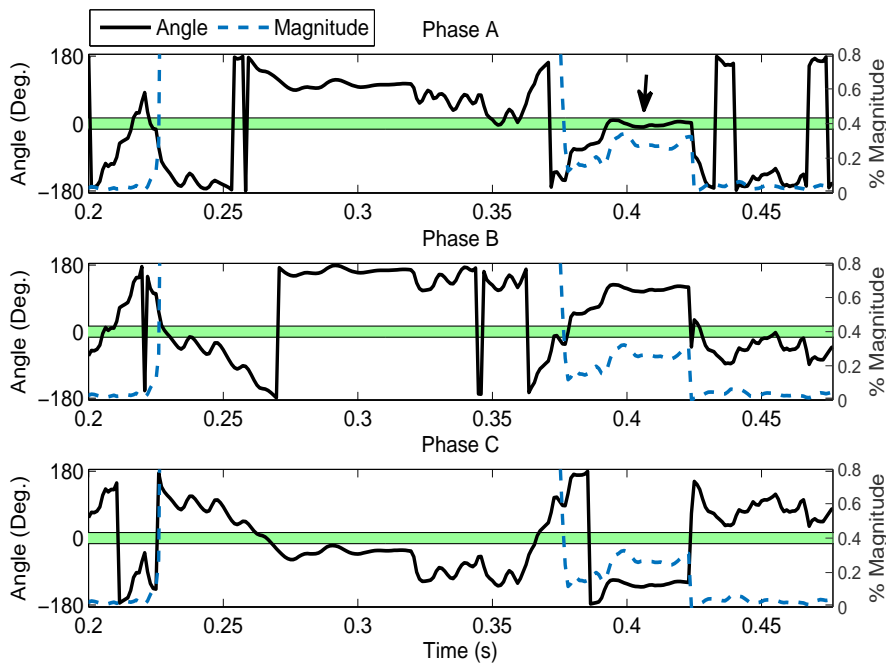
Figure 5.92: The proposed SR variations, Case 9-4 SCB grounded via capacitor.
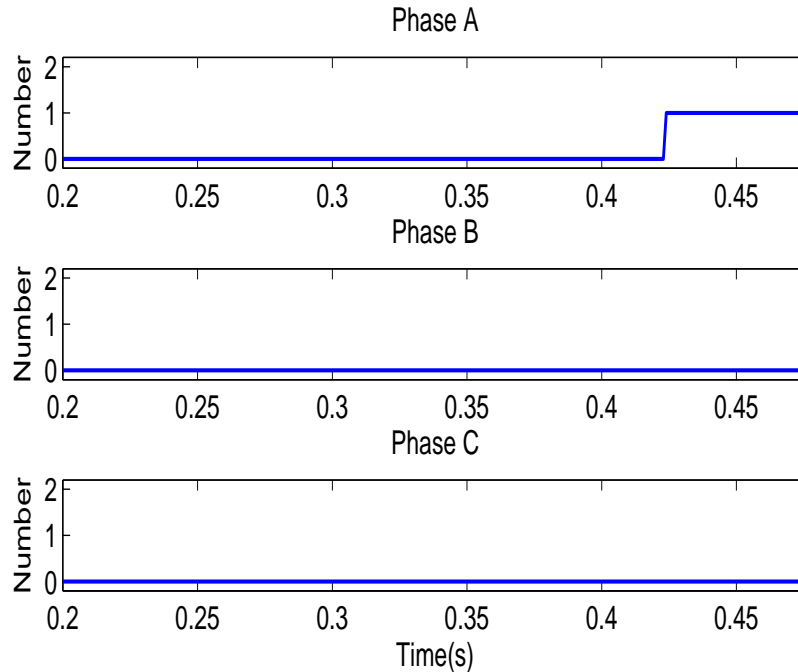
Figure 5.93: The proposed method output, Case 9-4 SCB grounded via capacitor.

Single Wye Grounded via CT

Case 10-1 An internal failure is simulated in phase B at 0.22 s, while a network phase to ground fault exists in the same phase from 0.2 s until 0.3 s. Results are shown for an internally fused SCB. Figs. 5.94-5.96 demonstrate the results. Simulations show the reliability of the proposed method and the fact that a delay dependent on the fault clearance time is introduced in the fault location determination.

Case 10-2 An open pole in phase A takes place at 0.2 s, and lasts till 0.3 s. An element failure in the same phase takes place at 0.22 s in an internally fused SCB. Fig. 5.97 illustrates that during the severe transient caused by the open pole, drastic changes in the SR might render spurious failure detection in another phase, although with phase re-closure, i.e. after 0.3 s, the right location is determinable. Fig. 5.98 demonstrates that the SR magnitude jump is far more than the expected values for element failures. Therefore, blocking by putting limits on the magnitude is included in the code. Figs. 5.99 and 5.100, show the successful results.

Case 10-3 A special scenario is presented for this case. All elements of a unit fail in phase A at 0.2 s then at 0.26 s a phase to phase fault (A-C) with 50 ms duration is simulated. At 0.3 s, another single element failure takes place in phase A. Fig. 5.101 shows the SR variations along with the successful fault location output. This scenario also confirms the discussed assumption in Section 4.4, i.e. larger failures do not compromise detection of future subsequent failures.
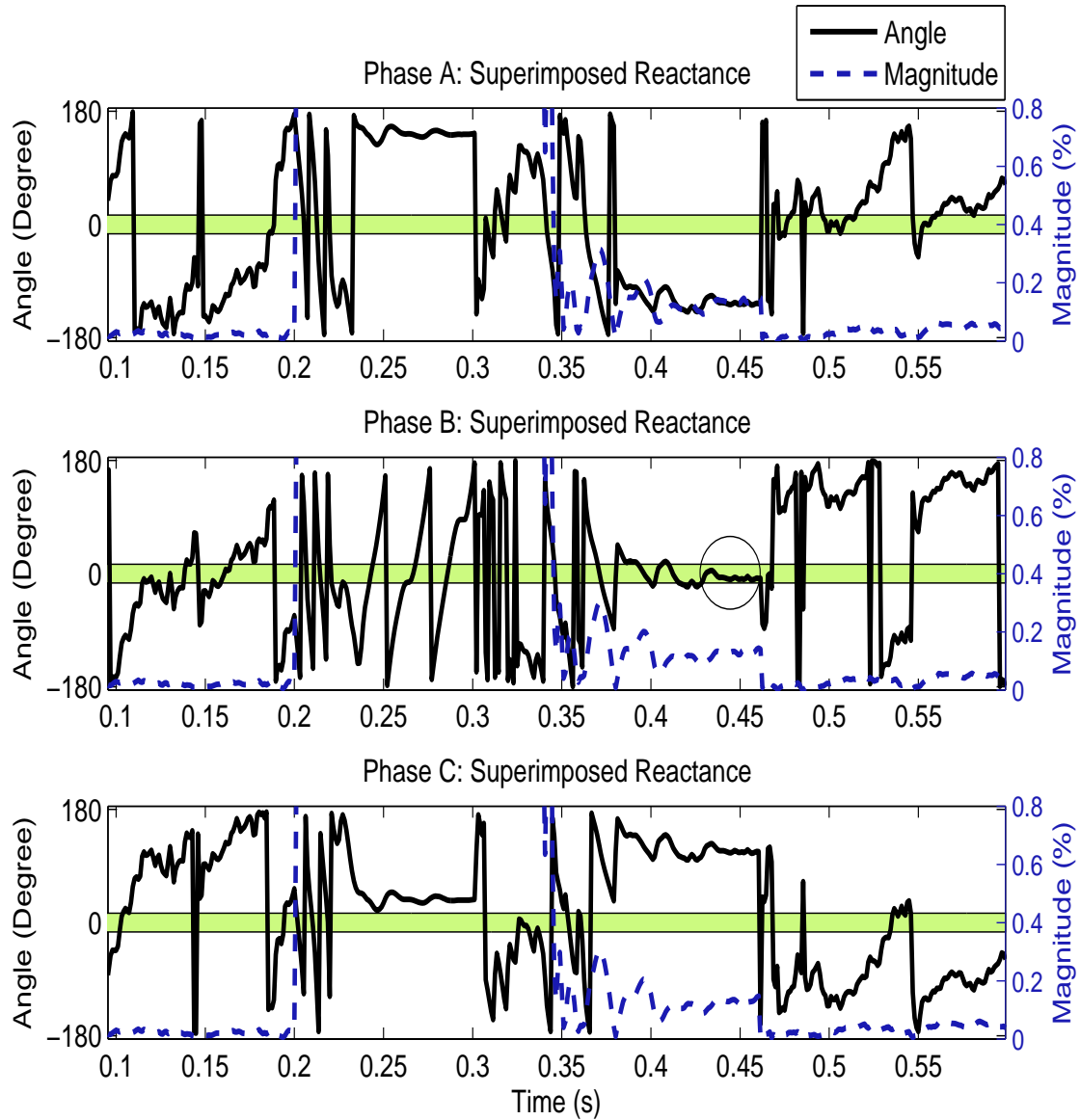
Figure 5.94: The proposed fault location principle for Case 10-1
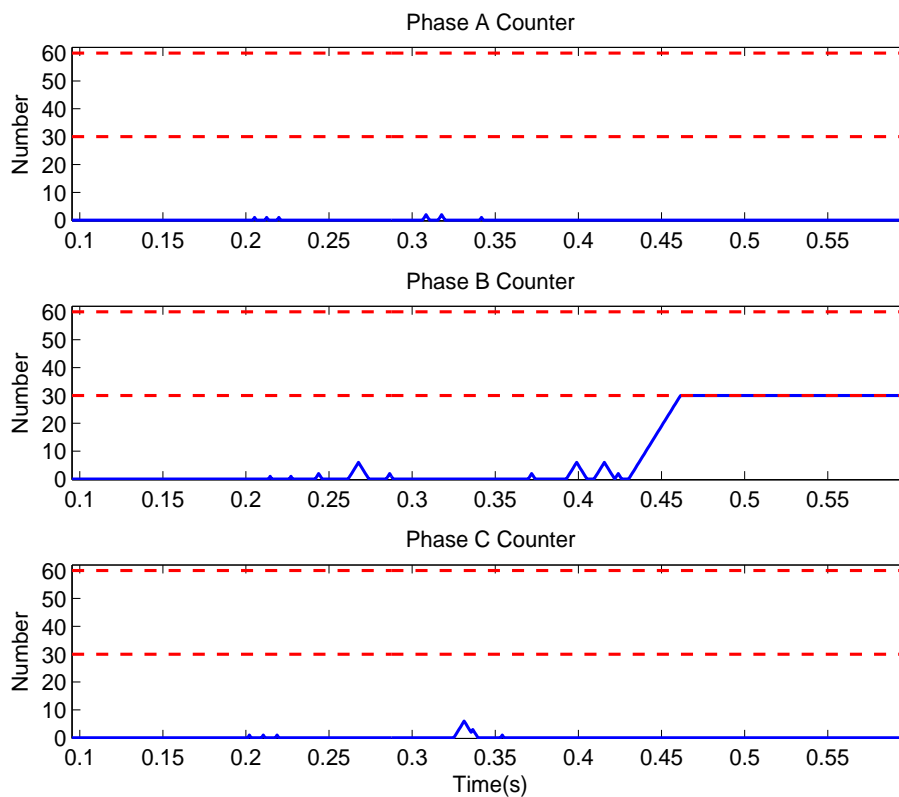
Figure 5.95: The proposed fault location counter for Case 10-1
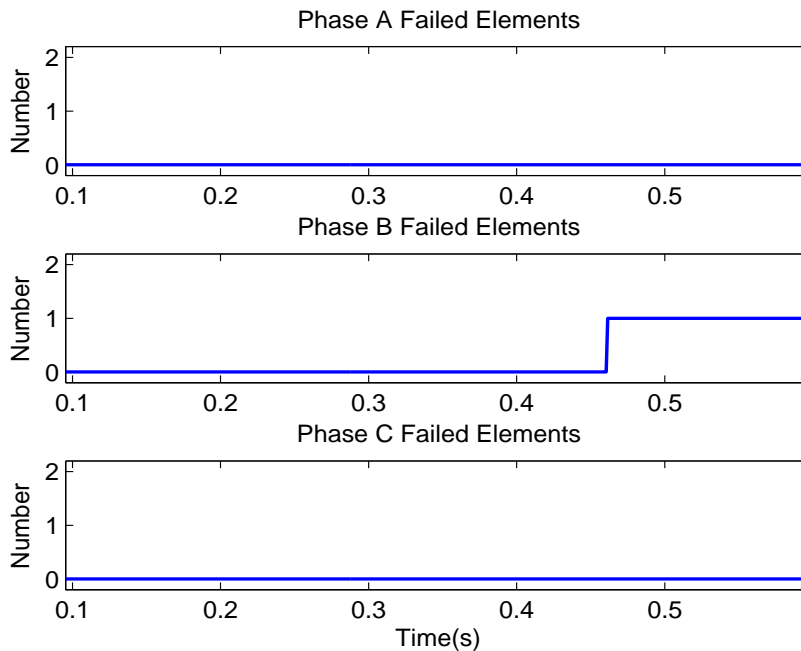
Figure 5.96: The proposed fault location output for Case 10-1
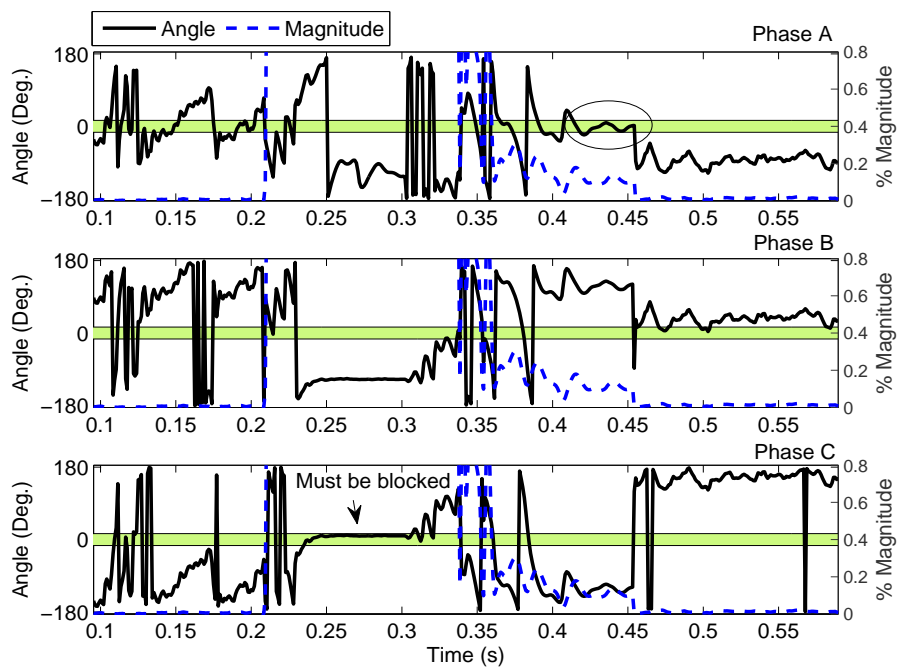
Figure 5.97: The proposed fault location principle for Case 10-2
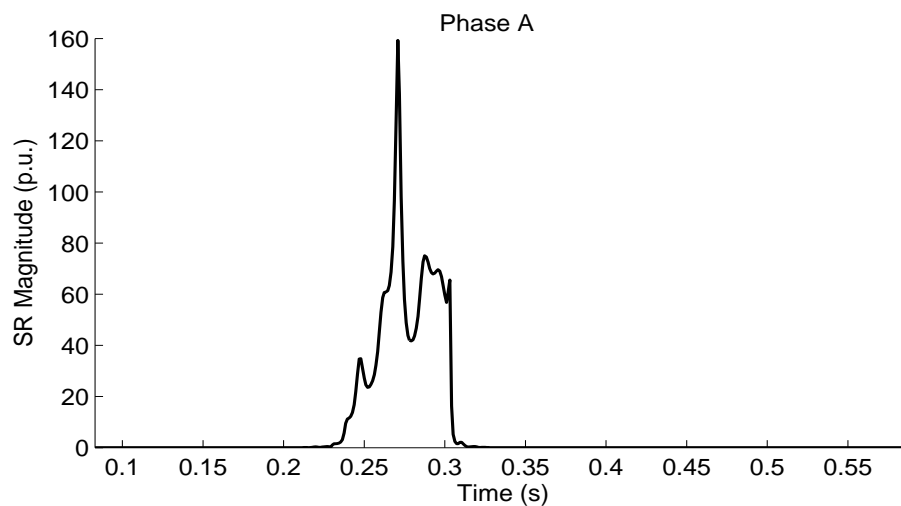
Figure 5.98: The proposed fault location principle magnitude for the opened phase in Case 10-2

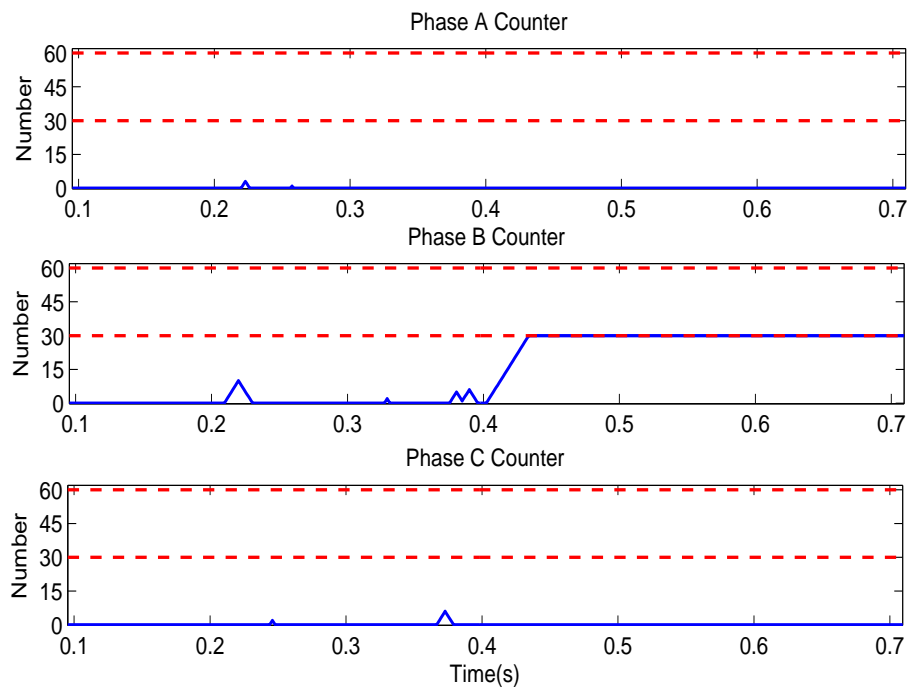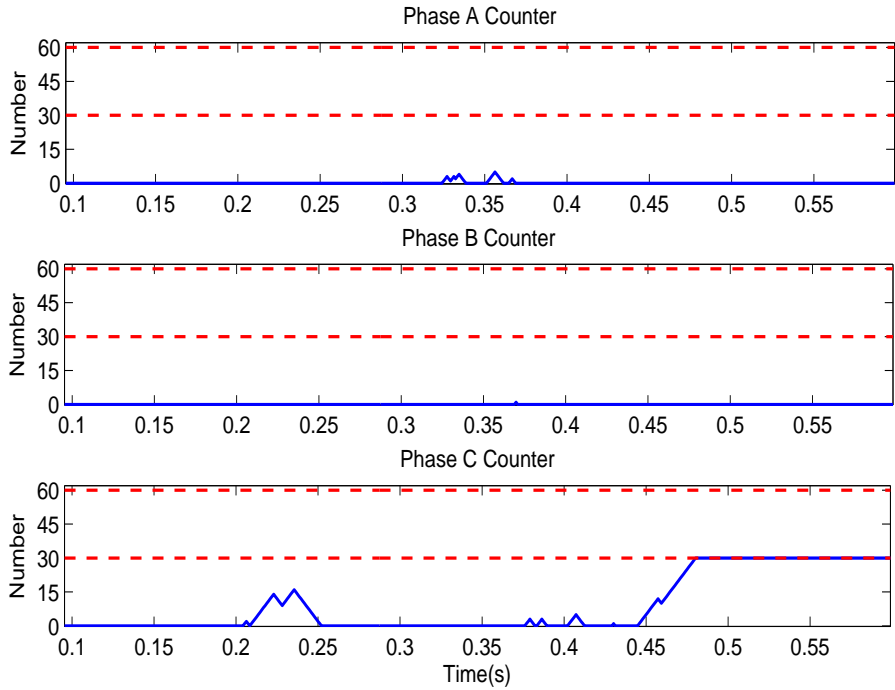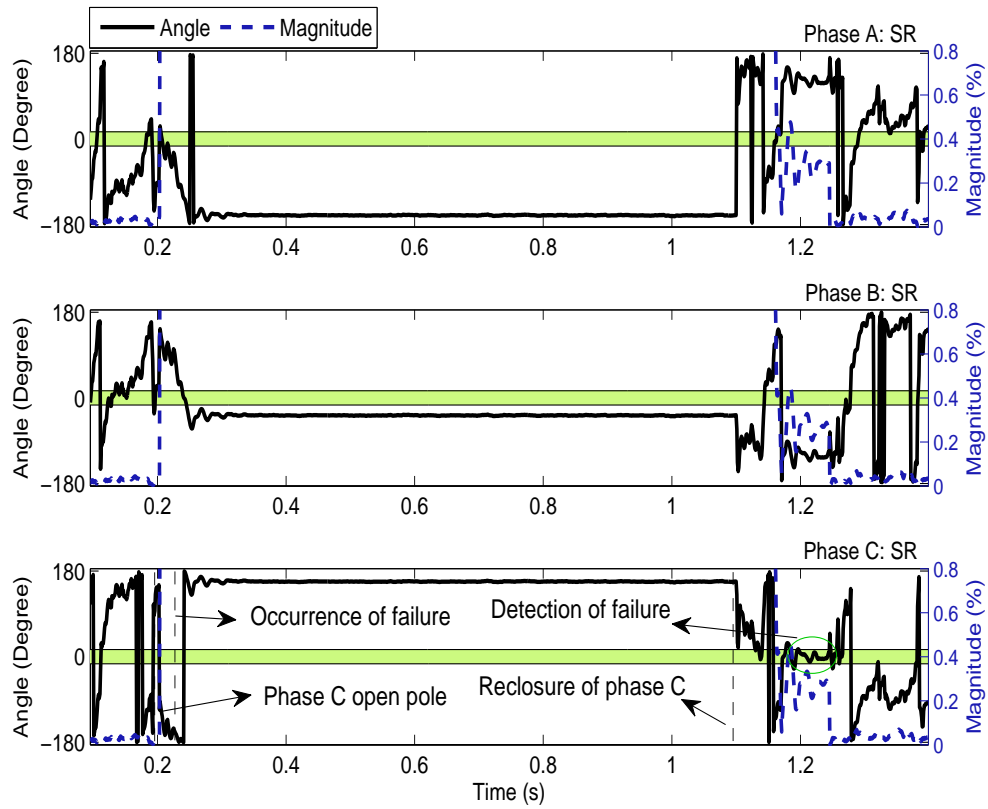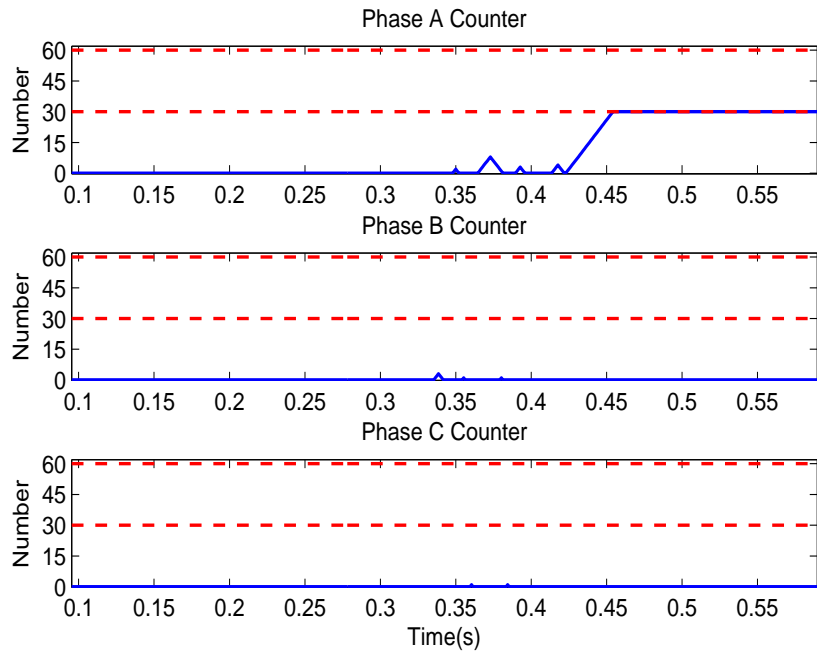Figure 5.99: The proposed fault location counter for Case 10-2
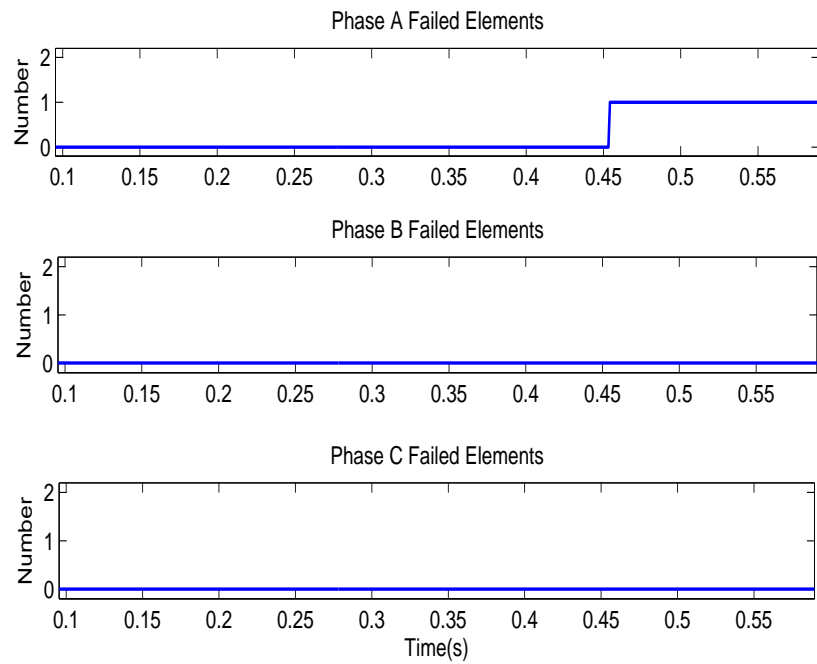
Figure 5.100: The proposed fault location output for Case 10-2
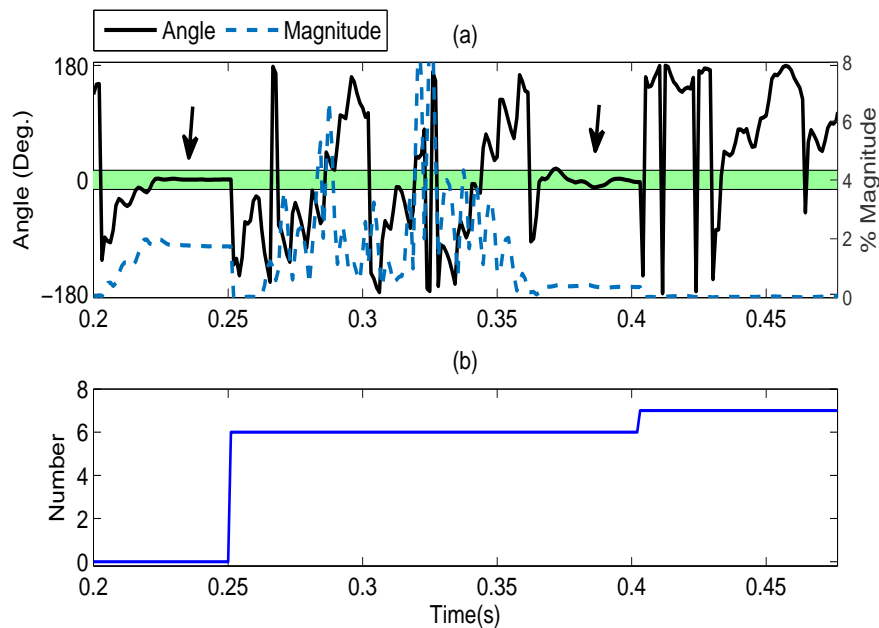
Figure 5.101: Case 10-3, Unit failure and external unbalance case study, SCB grounded via CT (a) the proposed SR variations. (b) output of the fault location.

Conclusion for Single Wye Banks

Several simulations were performed to discover whether failures that occur during power system faults are detectable and countermeasures to maintain the required reliability of the proposed fault location methods were introduced. Simulations show that dependent on the severity of the system faults, the magnitude of the SR can change abruptly to hundred times of its change for a single element failure. Even when the entire unit fails the operating signal would change much less. The exact values depend on number of elements and unit construction, i.e. number of series/parallel connections. The neutral voltage and the ground current change drastically upon occurrence of system disturbances, thus imposing unpredictable variations both in the angle and magnitude of the operating principles. Therefore, fault location of ungrounded SCBs and grounded ones via CT are susceptible to malfunction during the disturbance unless blocking is employed. In the fault location algorithms an upper limit is set for the SR magnitude to ensure that the variations are suspect of element failures and to disable fault location until the power system fault gets cleared. In the actual implementations, blocking this function of capacitor protection relay [21] can be done via communication with a system protective relay or supervision from other protection elements within a multi-functional numerical capacitor bank relay. In another approach, reference [3] uses a restraint signal which is the magnitude of vectorial sum of neutral voltage and zero sequence voltage for its neutral voltage unbalance protection. The susceptibility is much less for banks that are grounded via a low voltage capacitor because the measured neutral point voltage is across the grounding capacitor, and thus in normal operating conditions (no system

faults) it is much greater than the normally close to zero ground current/neutral voltage of the two other configurations.

Some additional results are provided in Appendix C.

Y-Y Ungrounded with Neutral Current Unbalance

Performance of the proposed enhanced neutral current compensated based fault location was tested under various system faults. The following cases are presented as illustrative examples.

Case 11-1 A phase A to phase C fault happens at 0.2 s, meanwhile an internal failure takes place in the right section of phase C at 0.22 s, the power system fault is cleared at 0.25 s. The SCB is internally fused. Figs. 5.102 and 5.103 demonstrate the variations in the proposed fault location principle and the modeled fault location relay output, respectively.
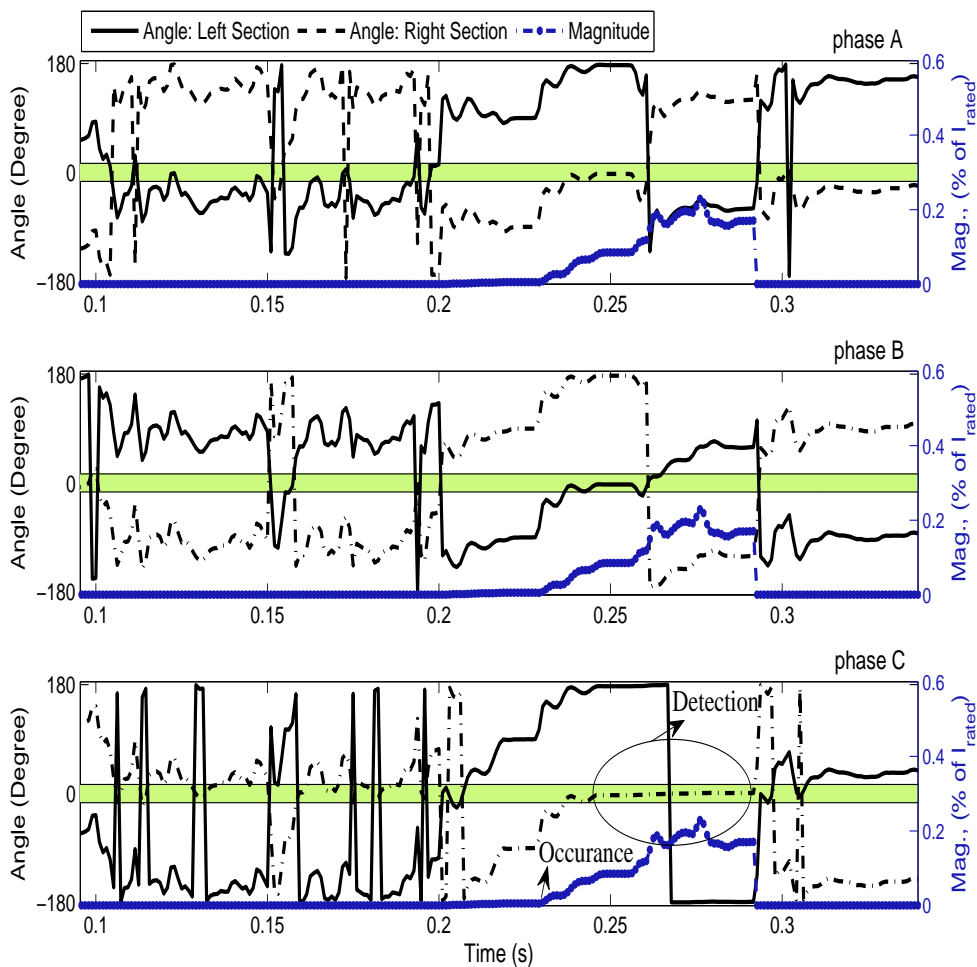
Figure 5.102: Proposed method compensated neutral current, Case 11-1.
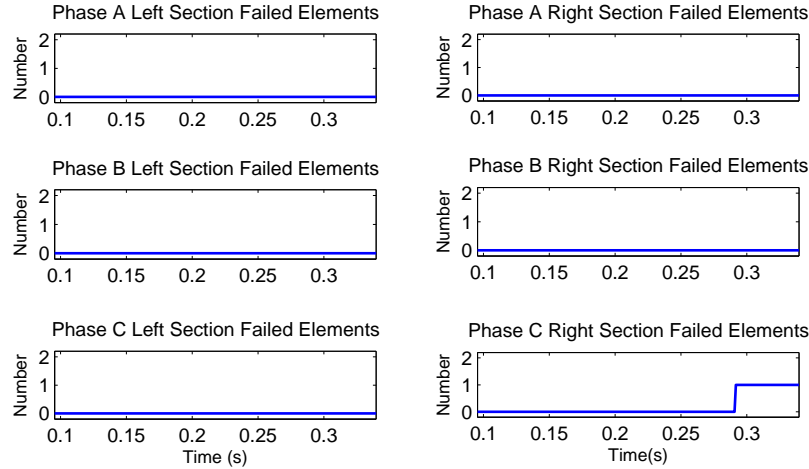
Figure 5.103: Proposed method output, Case 11-1.

To illustrate the counter pickup and latching after reaching a pre-set threshold, Fig. 5.104 is presented here. This Figure shows changes in the fault location counter.

As can be seen in Fig. 5.104, a failure is suspected in the left section of phase B, because the principle has entered the corresponding margin; however, as the principle does not stay inside the margin till the counter reaches a threshold, the counter starts counting down and in fact it gets reset. This is while for phase C in the right section, the counter continues to increase until it reaches the threshold and latches with a correct fault location determination. When interpreting the figures that show principle's angle variations, one should note that the principle will continue to stay inside the detection boundary unless it is reset, i.e. detected by the algorithm, or another consecutive failure takes place. False counter pickups are also not a concern as the counter threshold can be set high enough so that only the correct counters can reach the threshold. Fig. 5.105 illustrates variations in the neutral current, and the compensated neutral current. Furthermore, Fig. 5.106 is provided to compare and observe the way the external unbalance has changed the
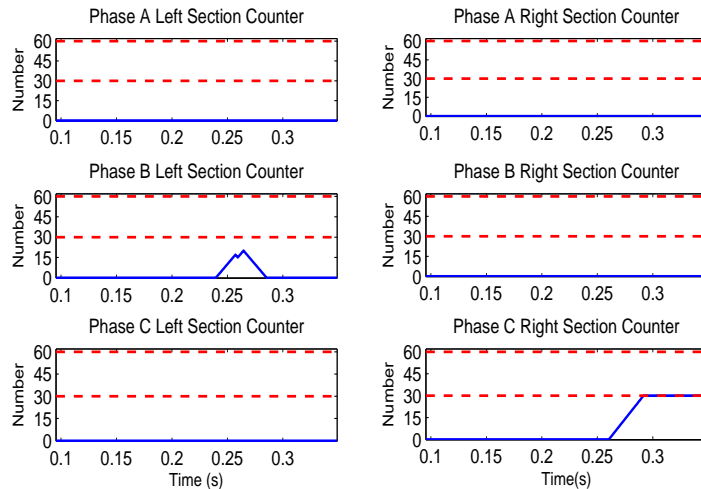
Figure 5.104: Algorithm security considering counter pickup, and count up/down process, Case 11-1

variations in the proposed principle magnitude.
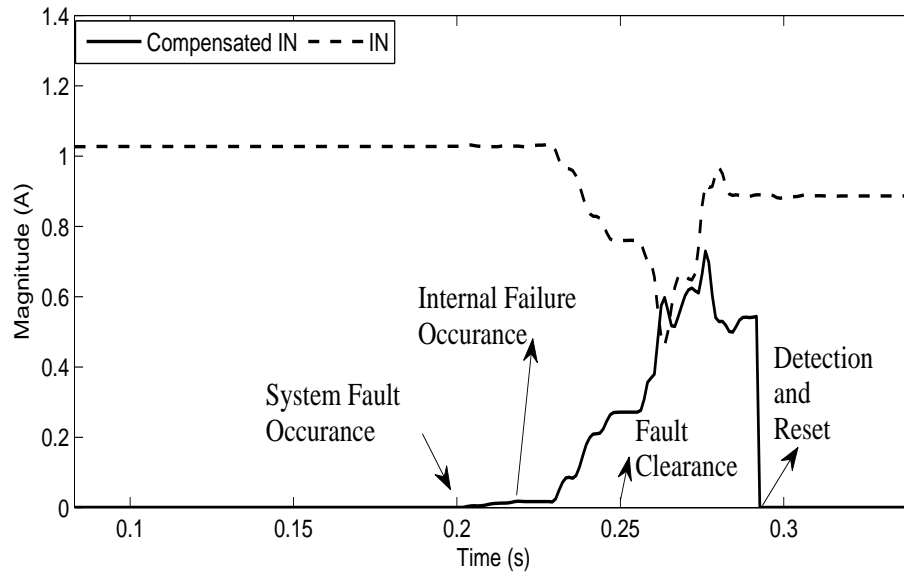
Figure 5.105: Variations in the proposed principle magnitude under power system fault.
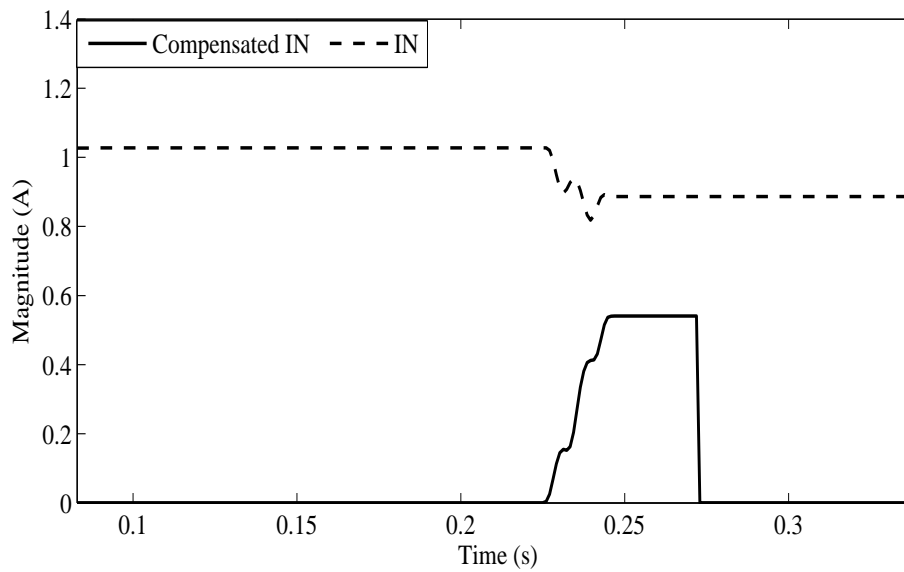
Figure 5.106: Variations in the proposed principle magnitude, without power system fault.

Case 11-2 A phase B to ground fault happens simultaneously with an internal failure in the left section of phase B, both at 0.22 s. The SCB is fuseless. Figs. 5.107 and 5.108 demonstrate the successful fault location results for the proposed method.

Case 11-3 For a 100 ms open pole in phase B, an internal failure in right section of phase C takes place at the middle of the dead-time. The SCB is fuseless. Figs. 5.109- 5.111 demonstrate the proposed fault location method reliable performance. It is worthwhile to note that higher pick up delays further guarantee the discrimination between faulty phase and other phases and the illustrative scenarios provided here assume minimum pick up delays for reliable operation.

Simulations also showed successful performance for the same scenario with the open pole interval, a.k.a dead-time, increased to 360 ms, and also for the scenarios of cases 8-2, and 8-4.

For further evaluation, in the next illustrative scenario, we have increased the dead-time of the open pole. Because it is a common setting that bank undervoltage protection trips the SCB in a second when the bus voltage reaches 0.7 pu [3], an open pole of less than a second is considered for worst case simulations.

Case 11-4 An open pole tripping for phase B is simulated at 0.2 s, internal failure in right section of phase C occurs at the same time in the fuseless SCB, the line reclosure takes place after 950 ms.
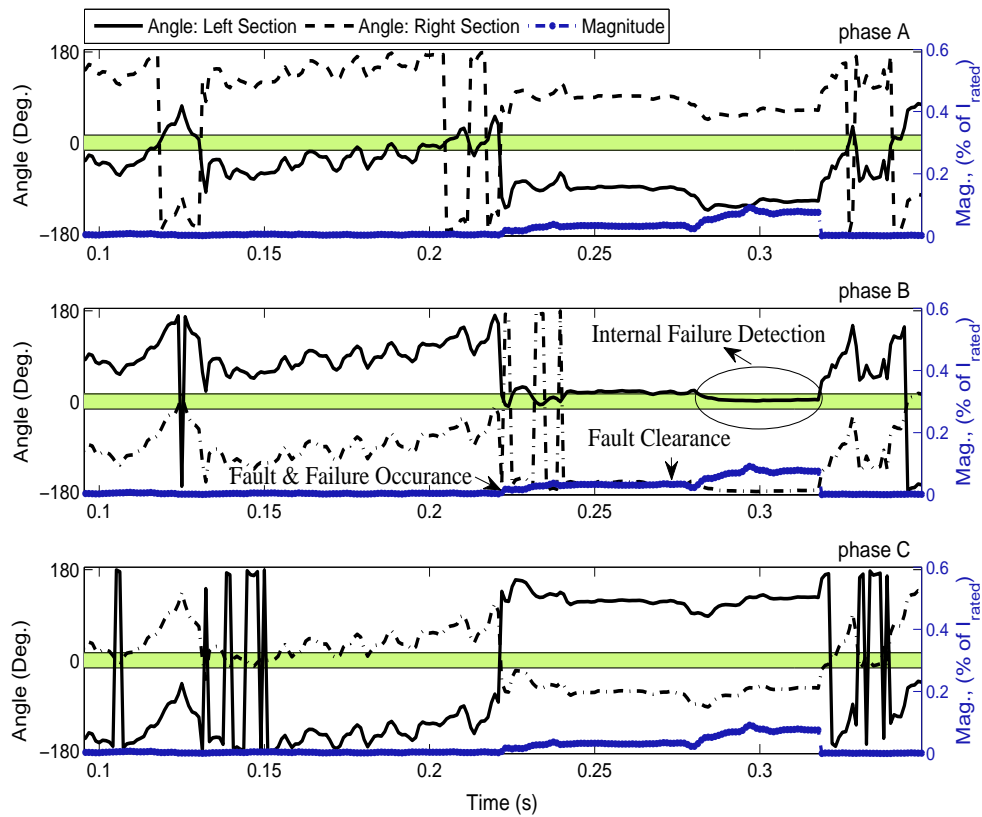
Figure 5.107: Proposed compensated neutral current, Case 11-2.
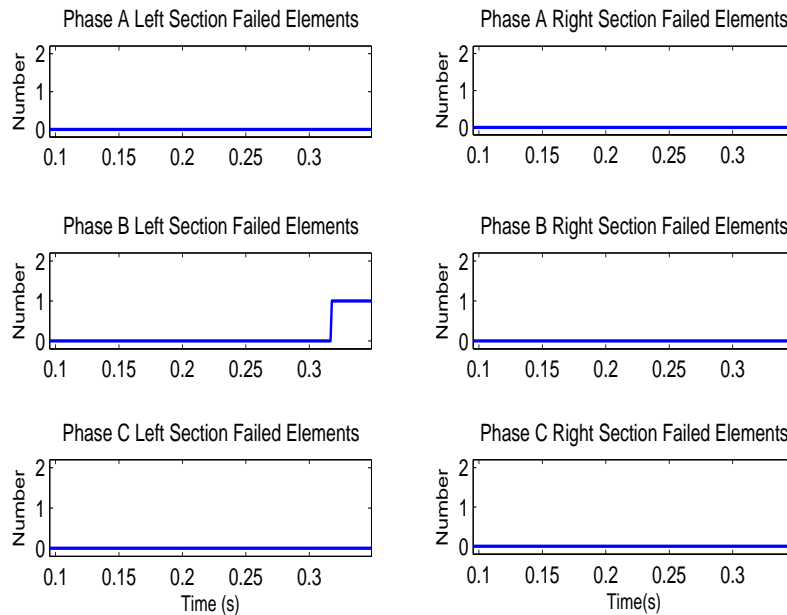
Figure 5.108: Proposed method output, Case 11-2

Fig. 5.112 shows the proposed principle for the first 40 ms of the simulation. It shows the principle reaching the corresponding fault location boundary, and the reset followed by fault location determination without any interference from the open pole of the other phase.

Figs. 5.113, and 5.114 demonstrate the counter and output of the fault location function for Case 11-4, respectively.

Case 11-5 Phase B is opened at 0.2 s and reclosure takes place 950 ms later, meanwhile an internal failure in the same phase happens for the internally fused SCB at 0.5 s in the left bank. Simulations show that the fast detection of the failure depends on whether the open pole is in the same phase as the failure or not. In case that failure is in a different phase, then the proposed method can detect the failure faster. Figs. 5.115, 5.116, and 5.117, illustrate the proposed fault location principle, the counter, and the output, respectively.

As can be seen in Fig, 5.117, the failure is detected within about 600 ms. The reason for this delay is demonstrated in Fig. 5.115. The open pole in the same phase as the internal failure, has made the jump in the principle magnitude to be lower than the expected value. This happens while the angle criteria is within the margin of detection. With the closure of the opened breaker pole, the magnitude also satisfies the detection criteria and the failure location is determined successfully.
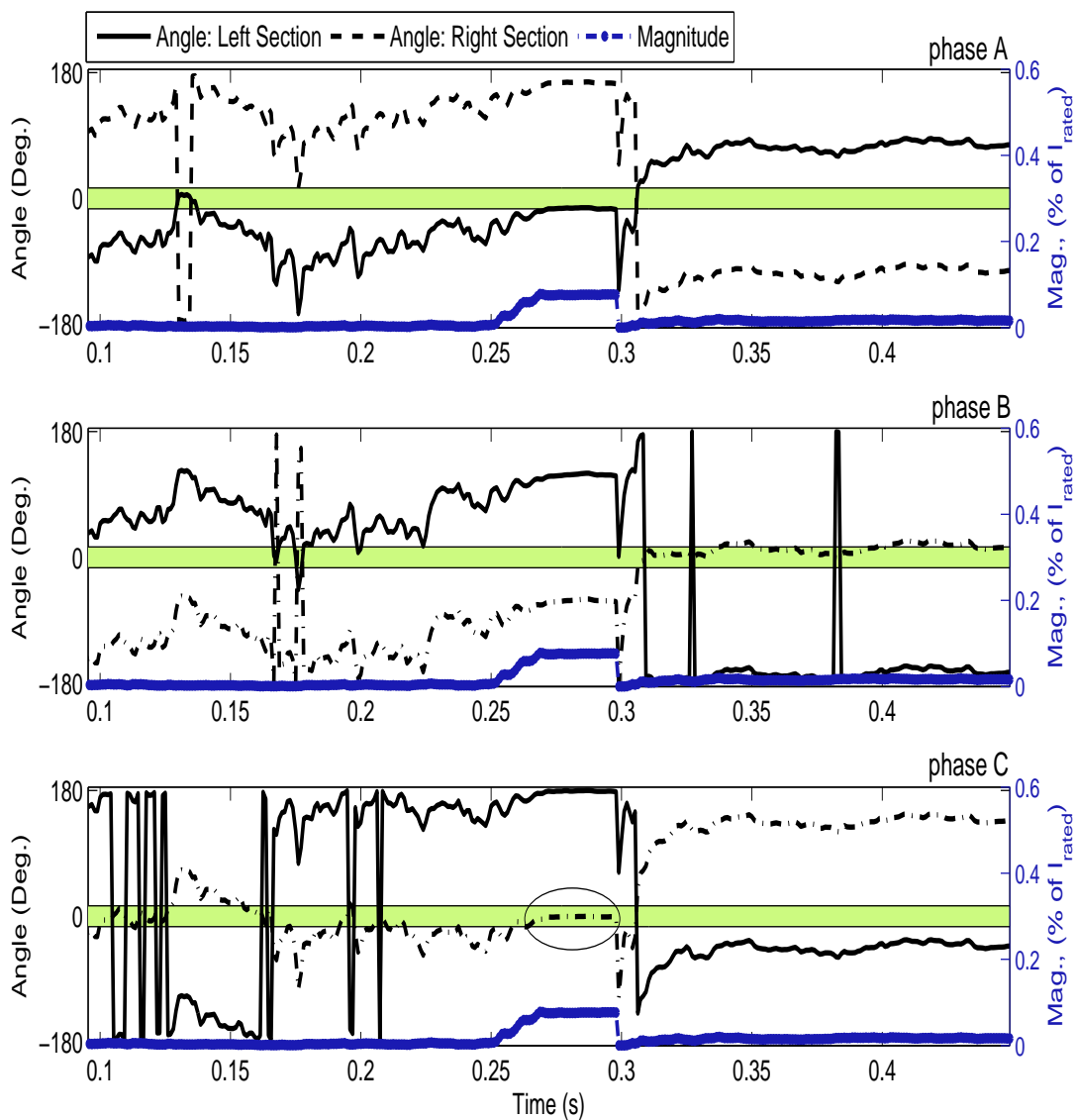
Figure 5.109: The proposed fault location principle, Case 11-3.
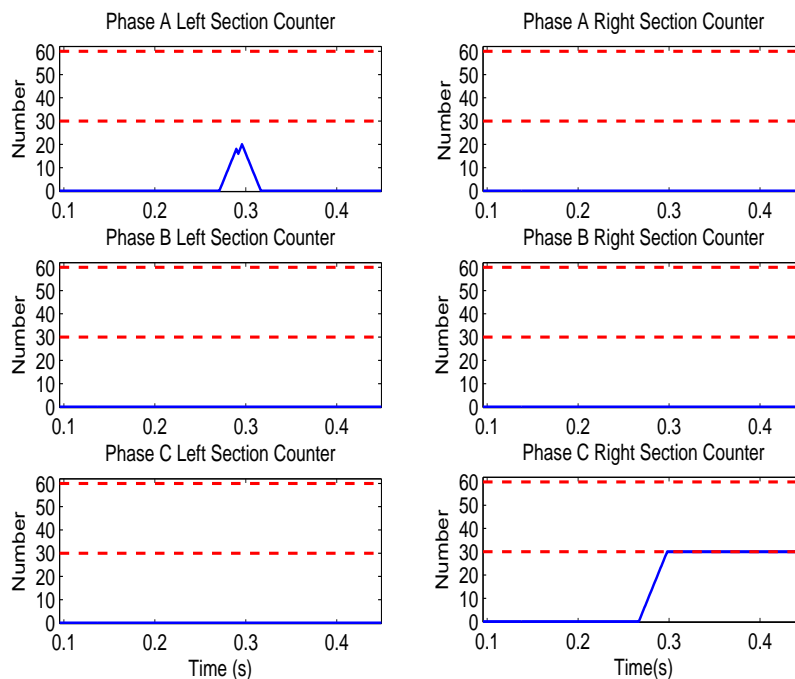
Figure 5.110: Algorithm security considering counter pickup, and count up/down process, Case 11-3
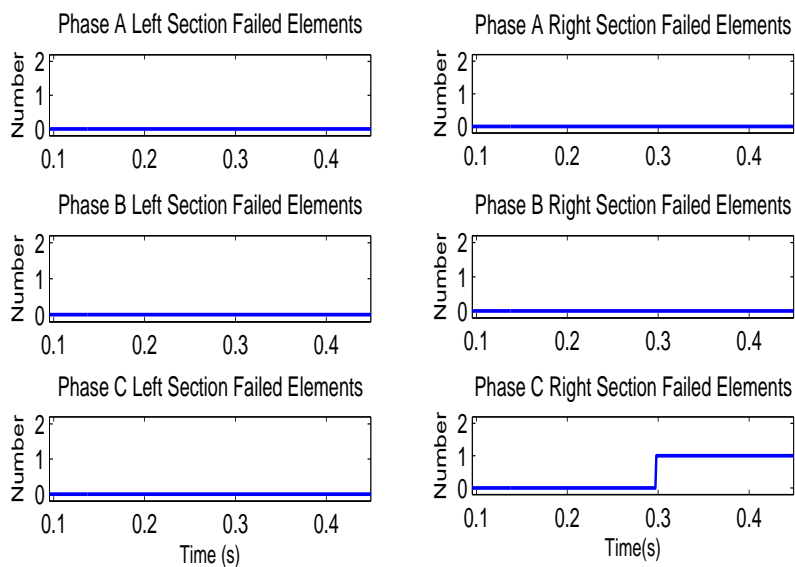
Figure 5.111: The proposed fault location output, Case 11-3.
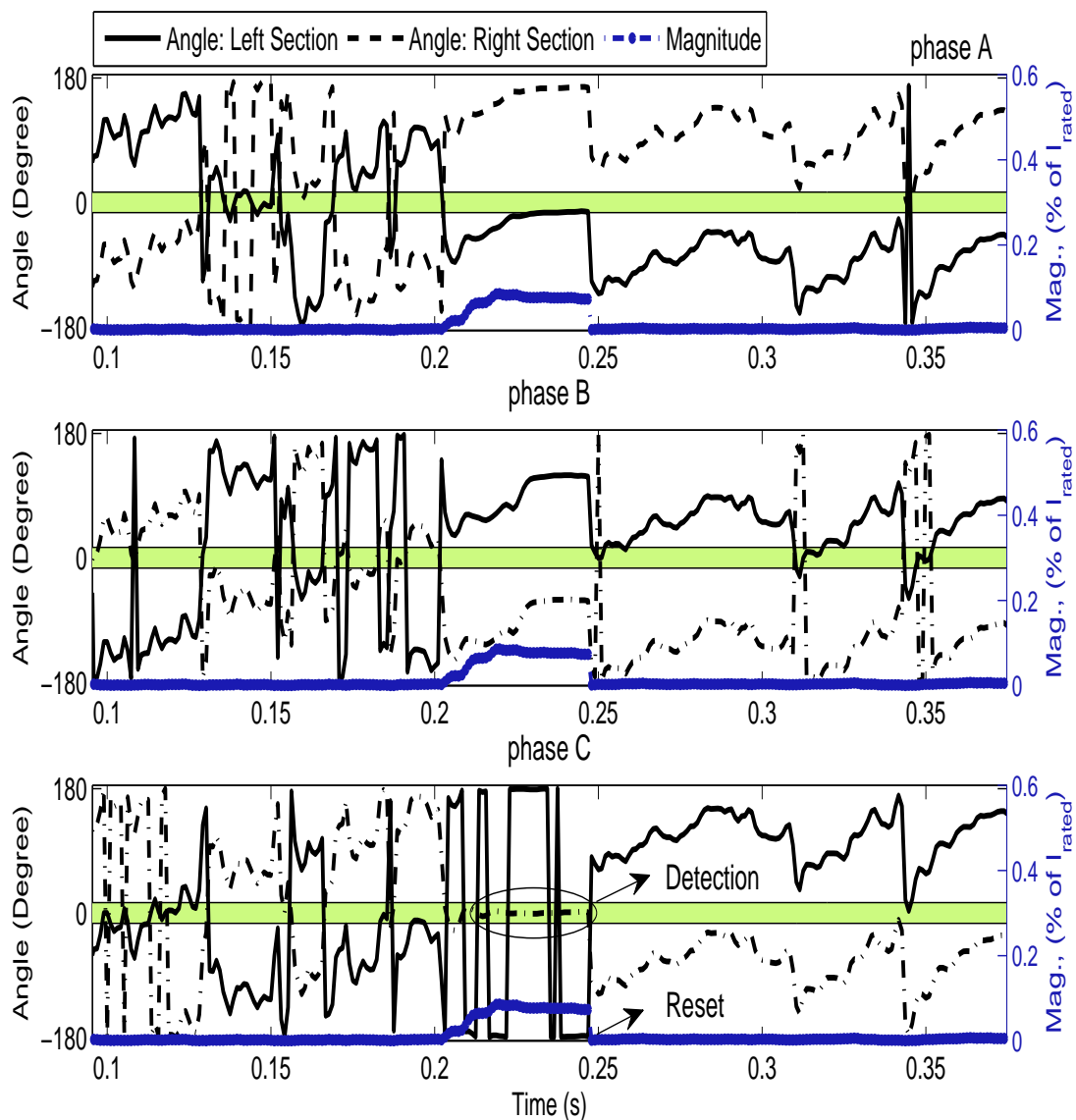
Figure 5.112: The proposed fault location principle, Case 11-4.
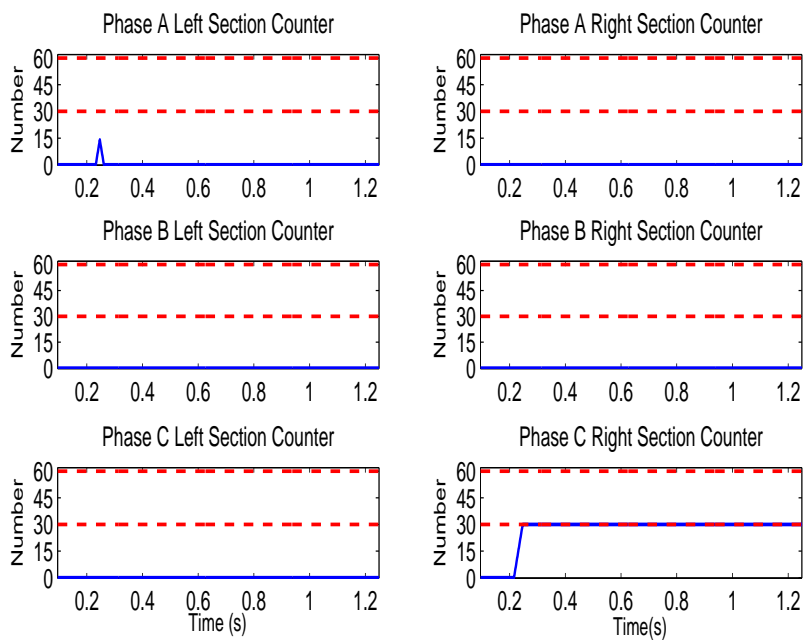
Figure 5.113: Algorithm security considering counter pickup, and count up/down process, Case 11-4.
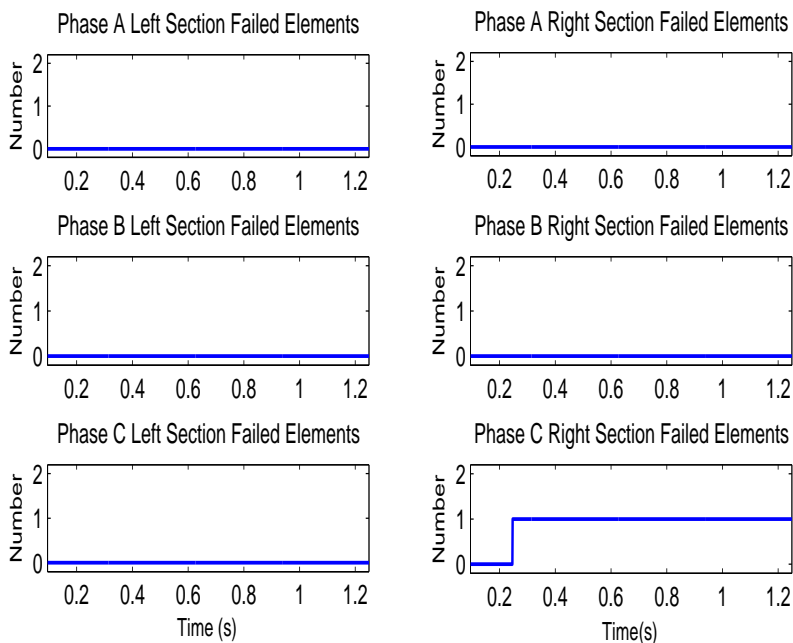
Figure 5.114: The proposed fault location output, Case 11-4.
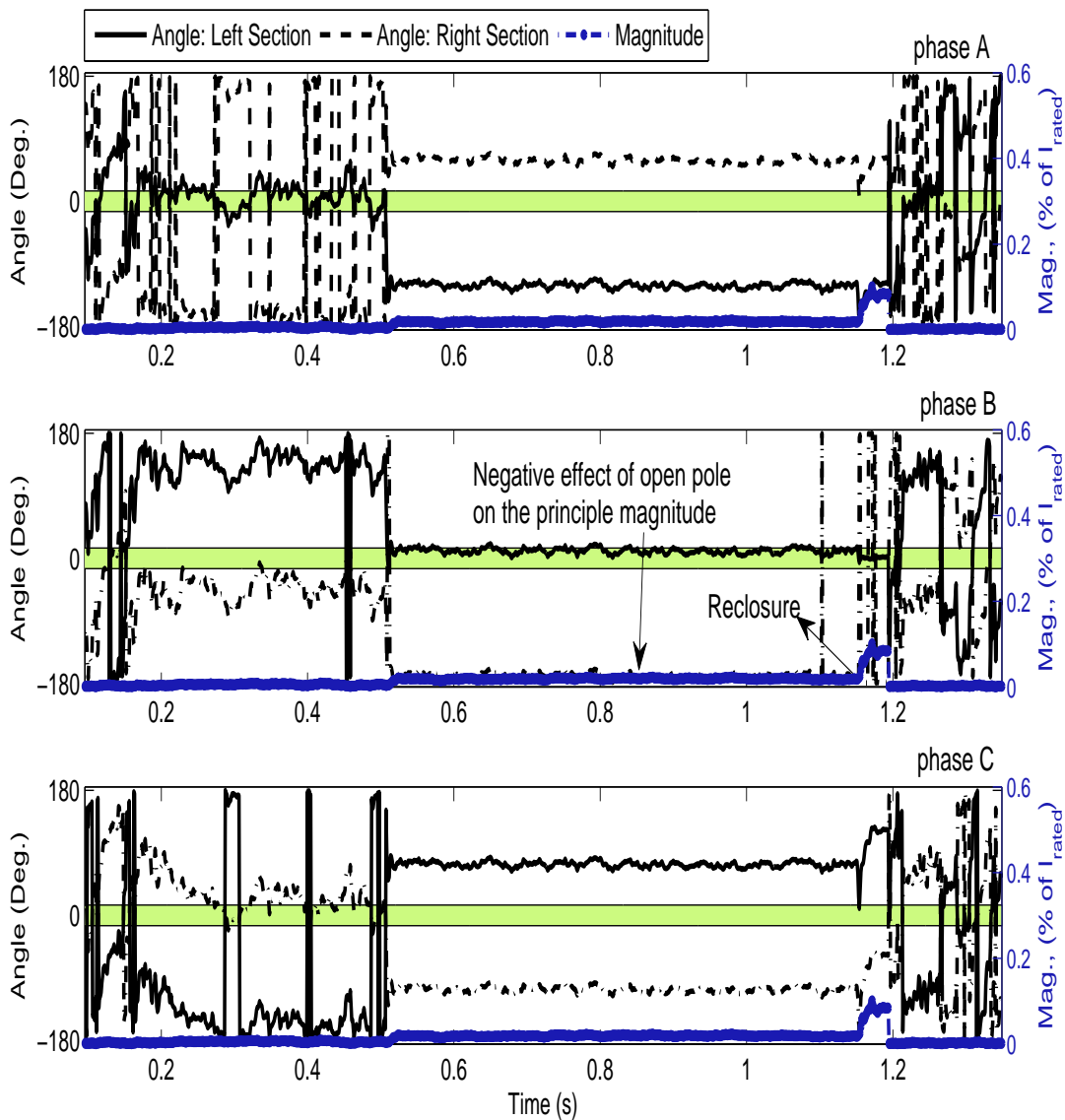
Figure 5.115: The proposed fault location principle, Case 11-5.
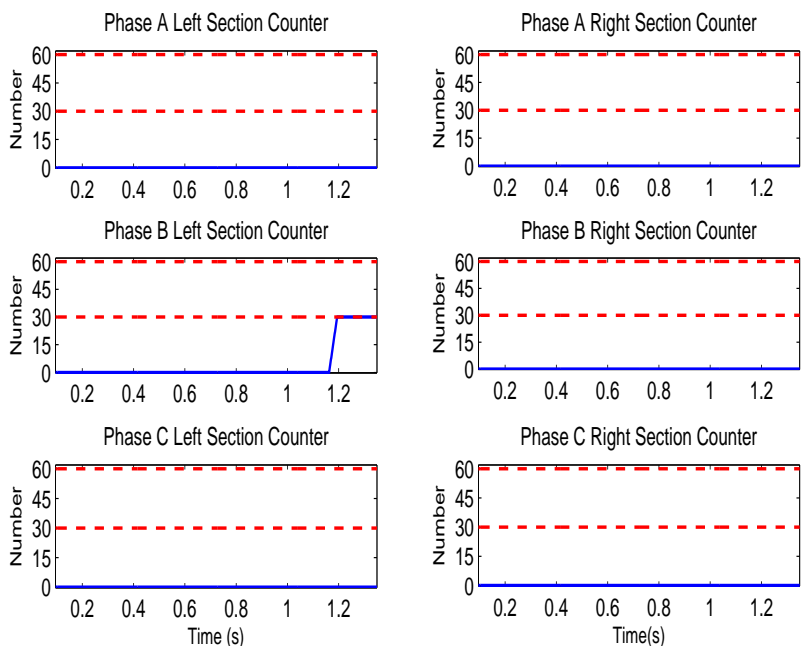
Figure 5.116: Algorithm security considering counter pickup, and count up/down process, Case 11-5.
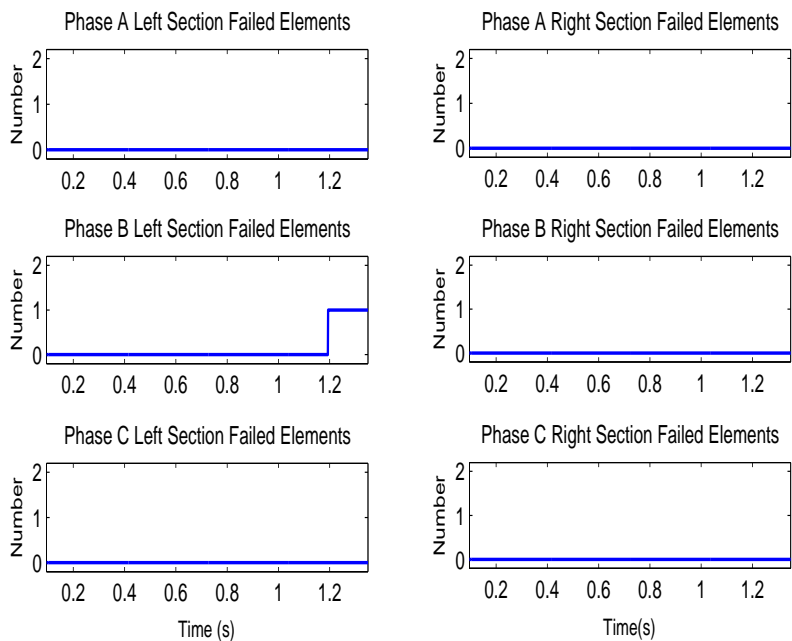
Figure 5.117: The proposed fault location output, Case 11-5.

The SEL method also was tested for reliability under external unbalances. Figs. 5.118, and 5.119 demonstrate the SEL method performance for case 11-1. Each colored zone belongs to one of the six possible locations. As can be seen, the SEL method
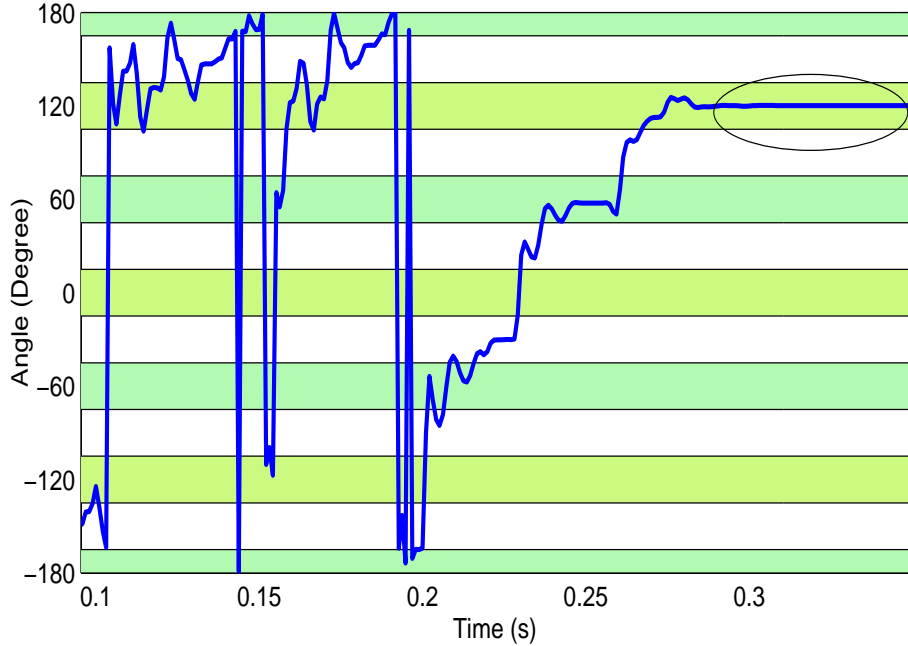
Figure 5.118: The SEL method principle for Case 11-1.
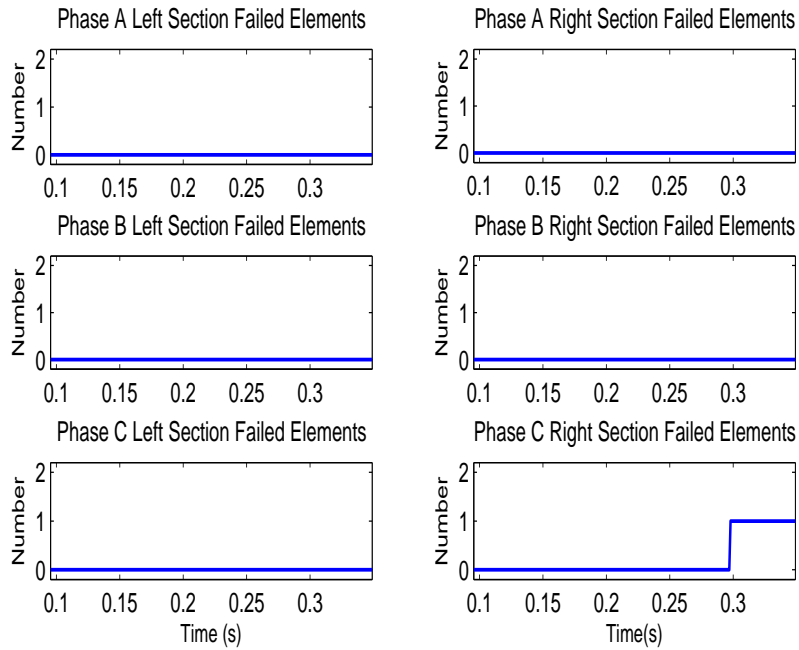
Figure 5.119: The SEL method output for Case 11-1.

also performs well. In addition, for simultaneous shunt fault and internal failures same performance was validated.

For the case 11-3, the SEL method evaluation is presented in Figs. 5.120, and 5.121. As can be seen the SEL method also determines the location of the failure successfully.
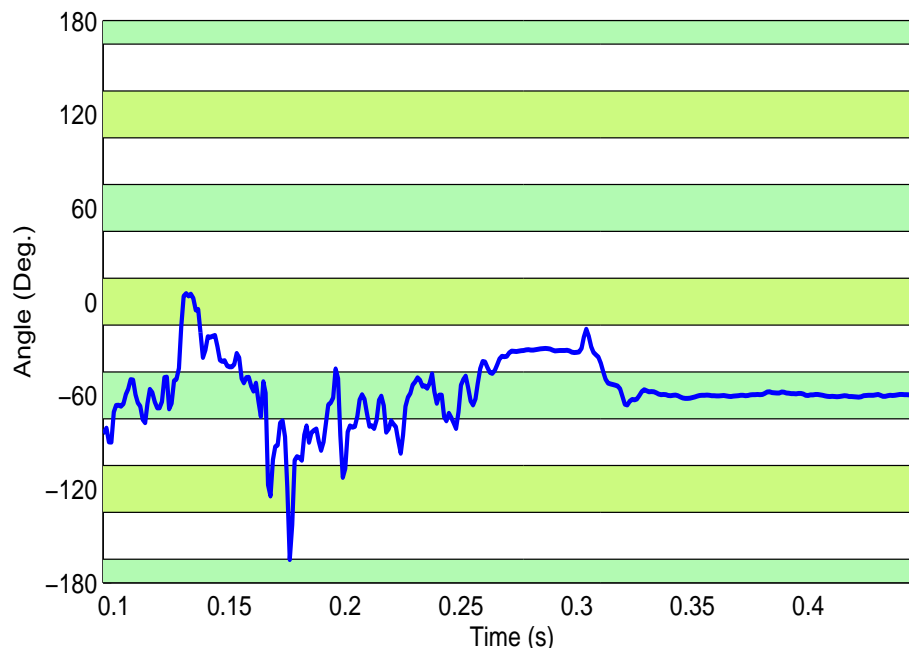
Figure 5.120: The SEL method principle, Case 11-3.

The SEL method assessed performance for case 11-4 is also selected for illustration here. Figs. 5.122, and 5.123 show the fault location criteria, and its output, respectively. As can be seen although the SEL method can detect the failure, however, it seems to take much longer time than our proposed method for fault location determination. The reason is that during the open pole the magnitude of the negative sequence current becomes comparable to the positive sequence current, therefore the assumption that the phase current magnitude is only influenced by the positive sequence current magnitude is no longer valid unless the negative sequence current magnitude reduces, i.e. the line reclosure takes place (at 1.15 s). This fact is presented in Fig. 5.124. Note that the longer it takes for a failure location to be determined the more the chances of occurrence of consecutive events, thus the subsequent failures will be missed unless a k-factor auto-set is performed.
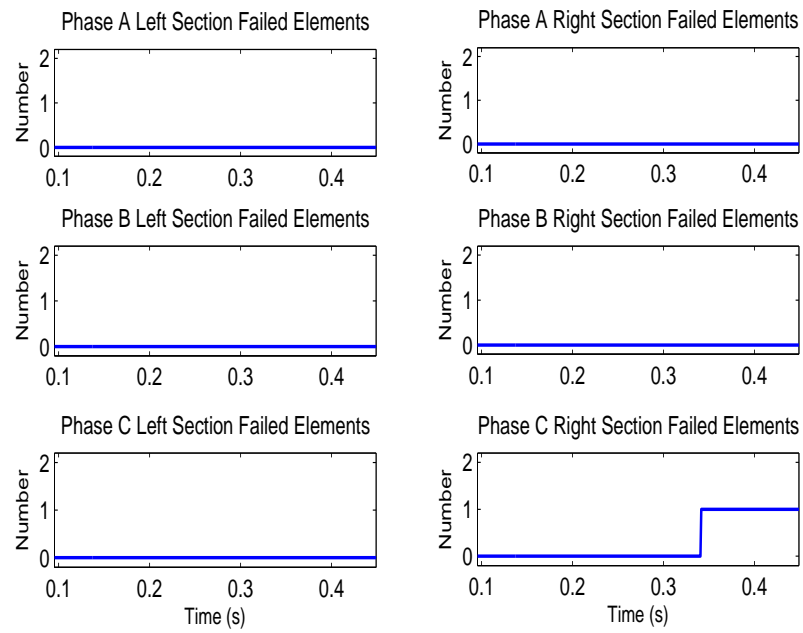
Figure 5.121: The SEL method output, Case 11-3.
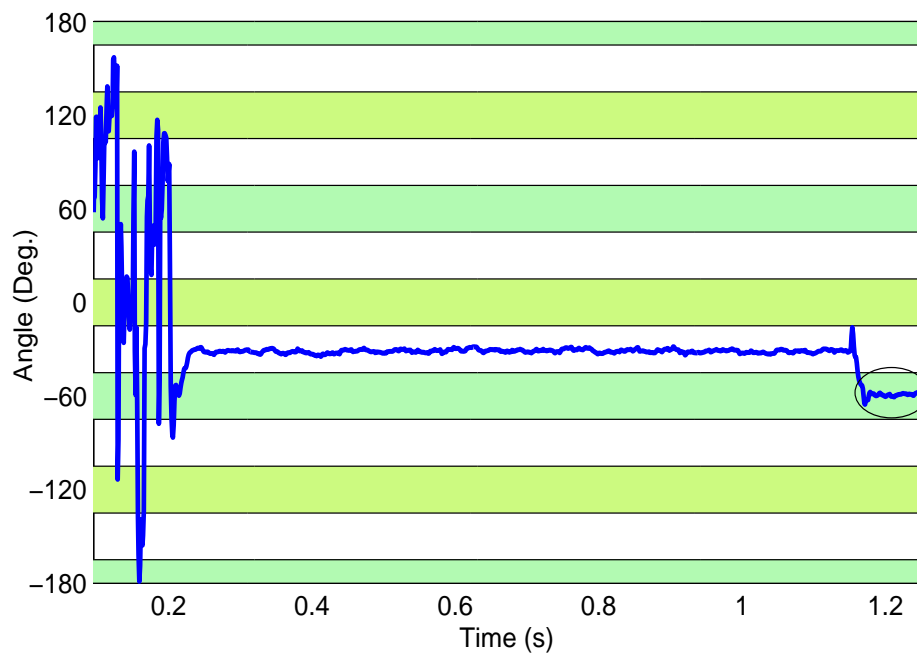
Figure 5.122: The SEL method principle, Case 11-4.
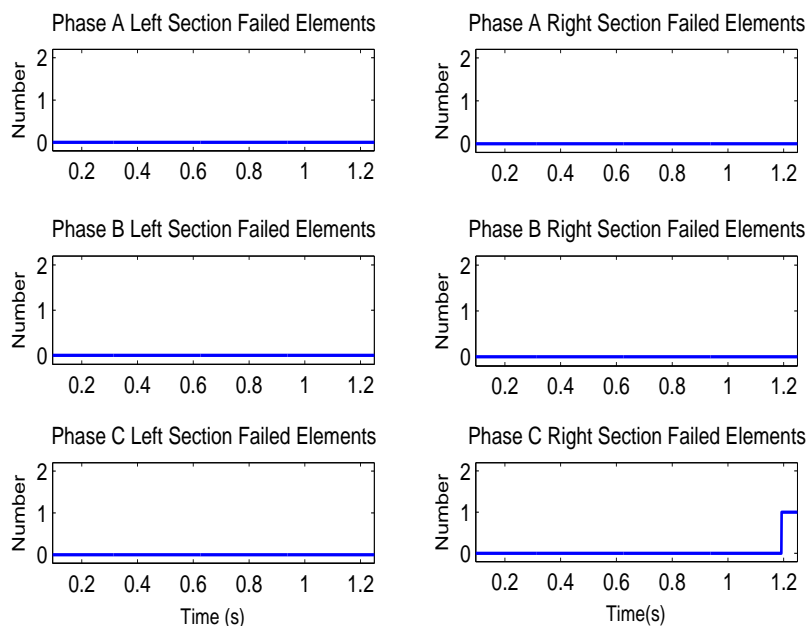
Figure 5.123: The SEL method output, Case 11-4.
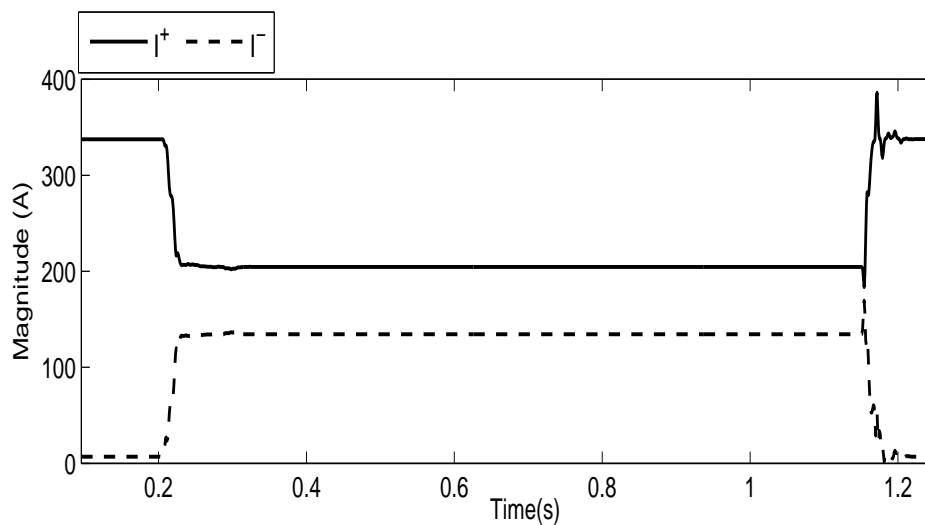
Figure 5.124: Positive sequence and negative sequence line currents, Case 11-4.

Case 11-5 for the SEL method is selected to present here as it demonstrates the important role of magnitude threshold. Figs. 5.125, and 5.126 are plots of the simulation results, and output, respectively. From the fault location output it seems that the SEL method has lost its security because of a failure detection in phase A during the very first moment after the open pole operation. Fig. 5.127 shows the compensated neutral current of this method. In [31] the magnitude threshold is not disclosed in detail, however, having this case study, the importance of this criterion is shown.
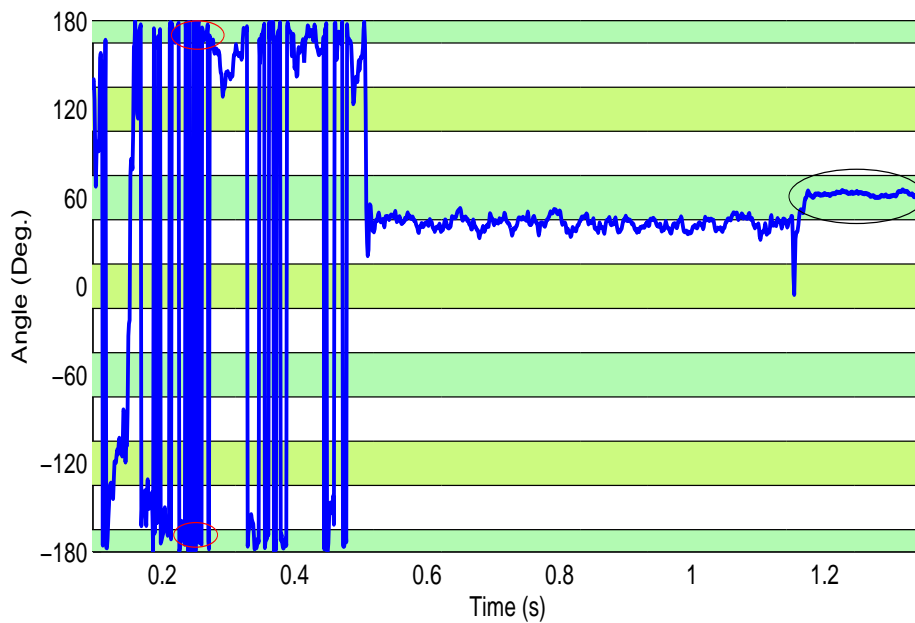
Figure 5.125: The SEL method principle, Case 11-5.
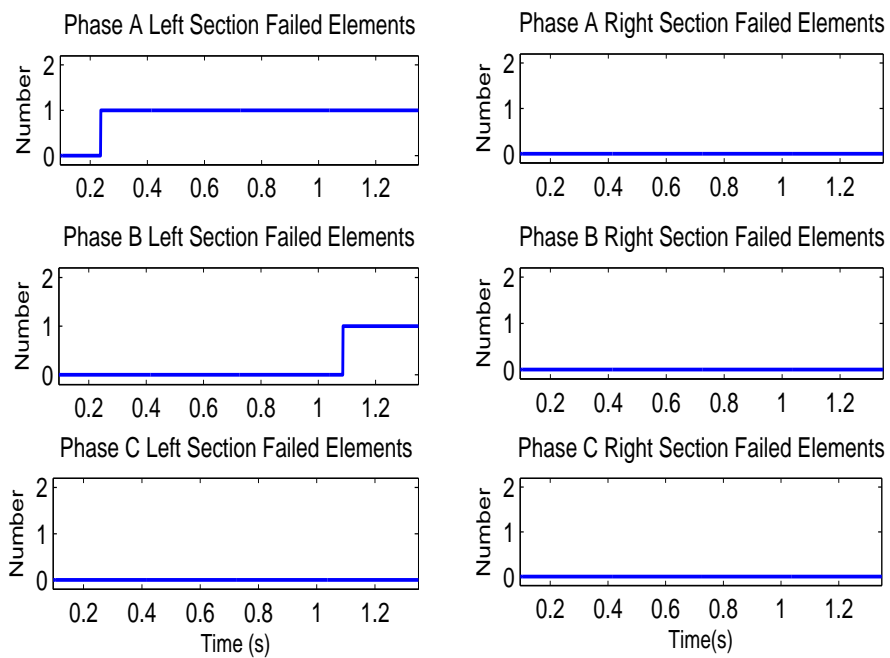
Figure 5.126: The SEL method output, Case 11-5.
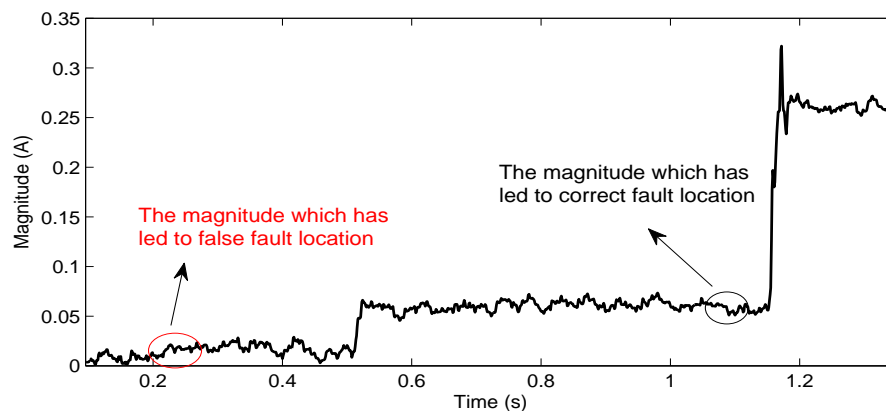
Figure 5.127: The SEL method compensated neutral current magnitude, Case 11-5.

Y-Y Grounded with Neutral Current Unbalance

For double wye grounded banks with neutral current unbalance protection, particularly we should refer to (4.67), and (4.66) where the uncompensated term in the neutral differential current depends on the mismatch between the right and the left section reactances and the level of unbalance that affects I_0. Therefore, solid ground faults (bolted faults) for SCBs with same sign mismatches for all three phases are worst case scenarios for external unbalance susceptibility evaluation.

Case 12-1 Simultaneous shunt ground fault and element failure happen for phase B at 0.2 s. The fault clearance time is 100 ms and the failure is in the right bank of a fuseless SCB. The residual current, and the measured differential current are shown in Fig. 5.128. The fuseless bank rated current peak is 354 A, which signifies the increment in the differential neutral current to be around 1 percent. The proposed fault location principle, compensated neutral current, and the output counter are shown in Figs. 5.129 and 5.130.
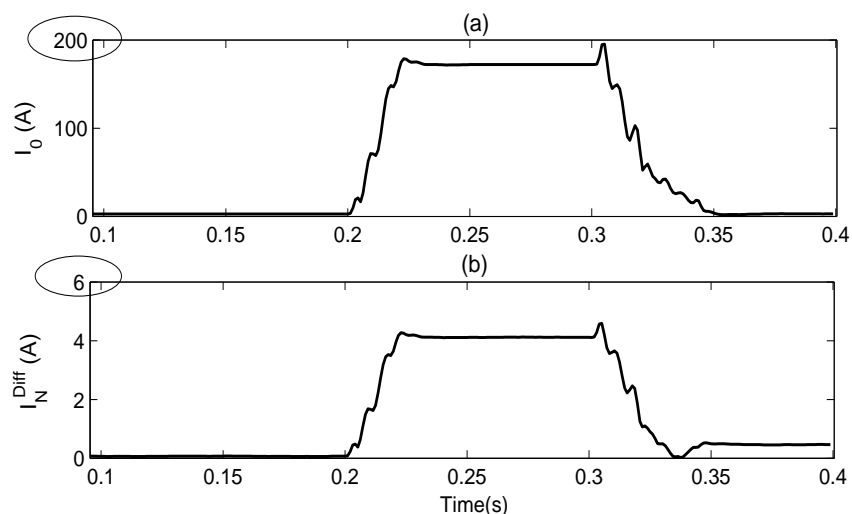
Figure 5.128: Case 12-1, (a) Zero sequence current. (b) uncompensated differential neutral current.
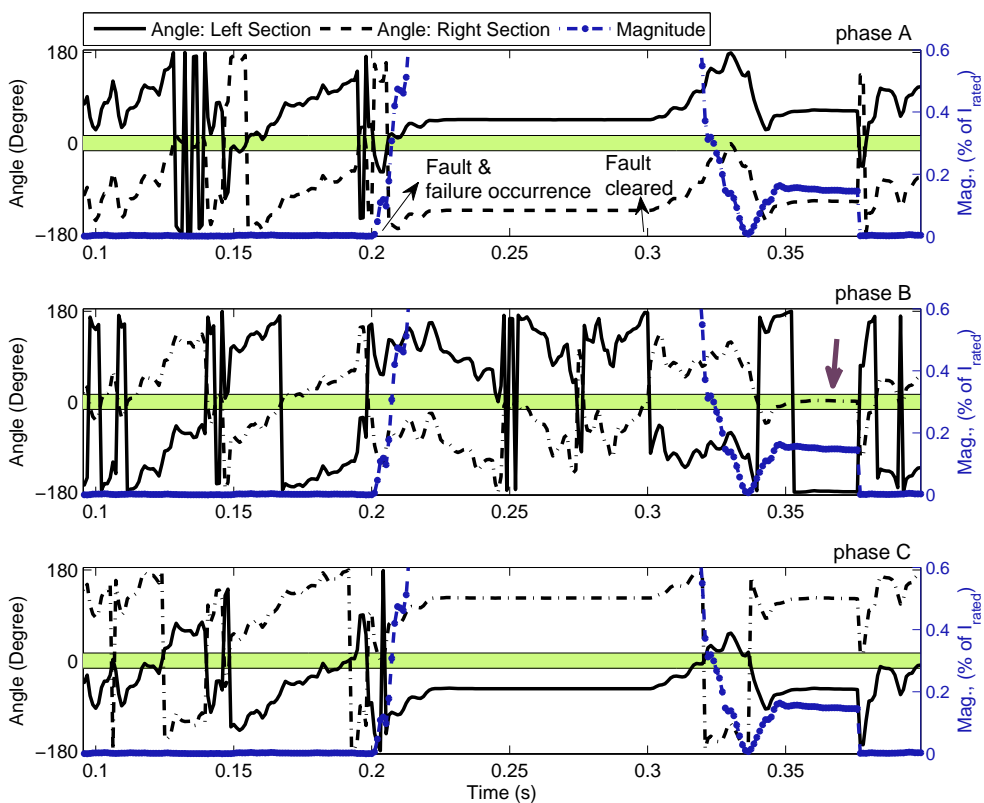
Figure 5.129: The proposed fault location principle, Case 12-1
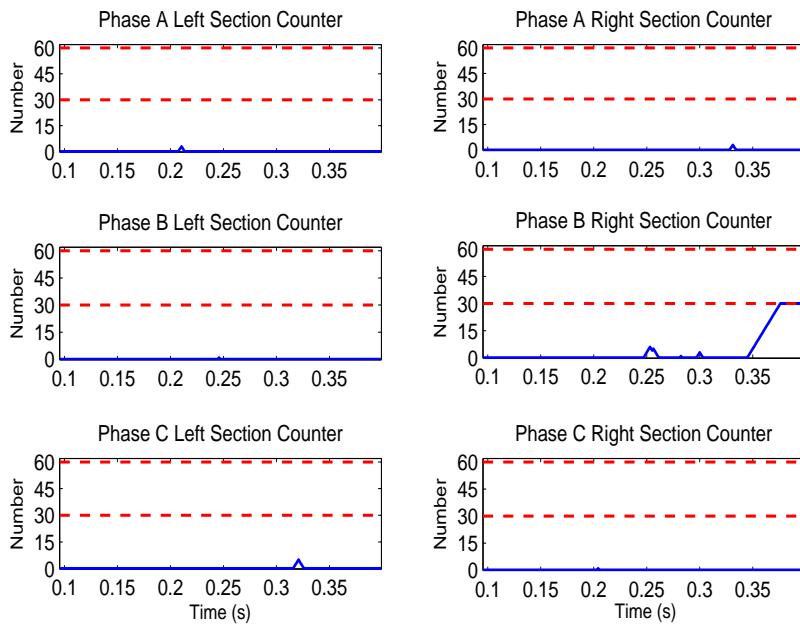
Figure 5.130: Counter of the proposed fault location method, Case 12-1

As can be seen the fault location is determined with a delay that is directly dependent on the fault clearance time. However, more important is that the detected fault location is still reliable, regardless of the severity of the shunt fault. Fig. 5.128 shows that the differential neutral current magnitude is not affected by the zero sequence current level, which is present due to the external unbalance.

Same results were confirmed for single phase to ground fault in the other phase, and also for double phase to ground and three phase to ground faults.

Case 12-2 For the same SCB, same internal failure takes place but this time the external fault, instead of shunt fault, is an open pole in the same phase. The open pole lasts for 360 ms. The residual current, and the measured differential current are shown in Fig. 5.131. The proposed fault location principle, compensated neutral current, and the output counter are shown in Figs. 5.132 and 5.133. Further simulation cases also
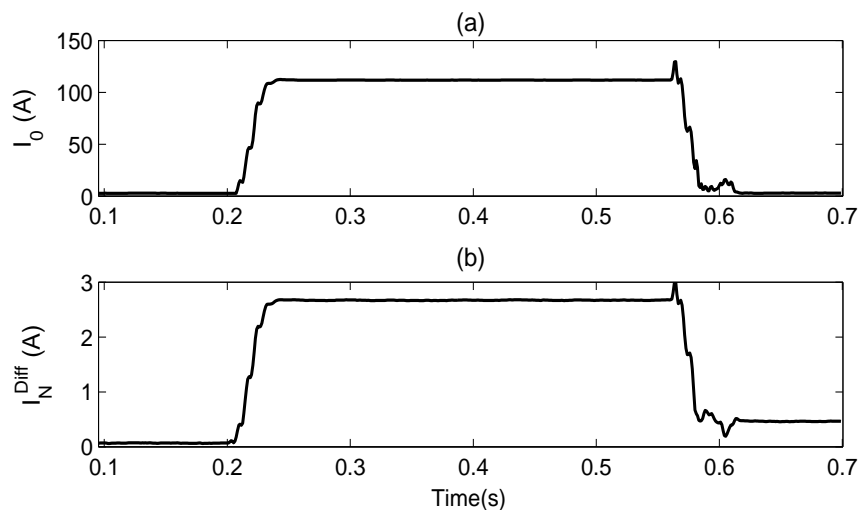
Figure 5.131: Case 12-2, (a) Zero sequence current. (b) uncompensated differential neutral current.

showed that same detection delays do exist even if the open pole does not happen for the same phase as the internal failure.

Case 12-3 The illustrative scenario is as follows for a selected SCB which is fuseless:

- A phase A to ground fault takes place at the SCB bus at 0.2 s, the fault gets cleared at 0.3 s

- An internal failure in right section of phase A is simulated at 0.22 s

- Two elements fail in the left section of phase C at 0.36 s

- A single phase tripping takes place in phase C of the connecting transmission line at 0.38 s and a successful reclosure happens at 0.48 s

The fault location principle is demonstrated in Fig. 5.134. As can be seen in the fault location report, presented in Fig. 5.135, the external failures do not render spurious reports, although they introduce detection delays.
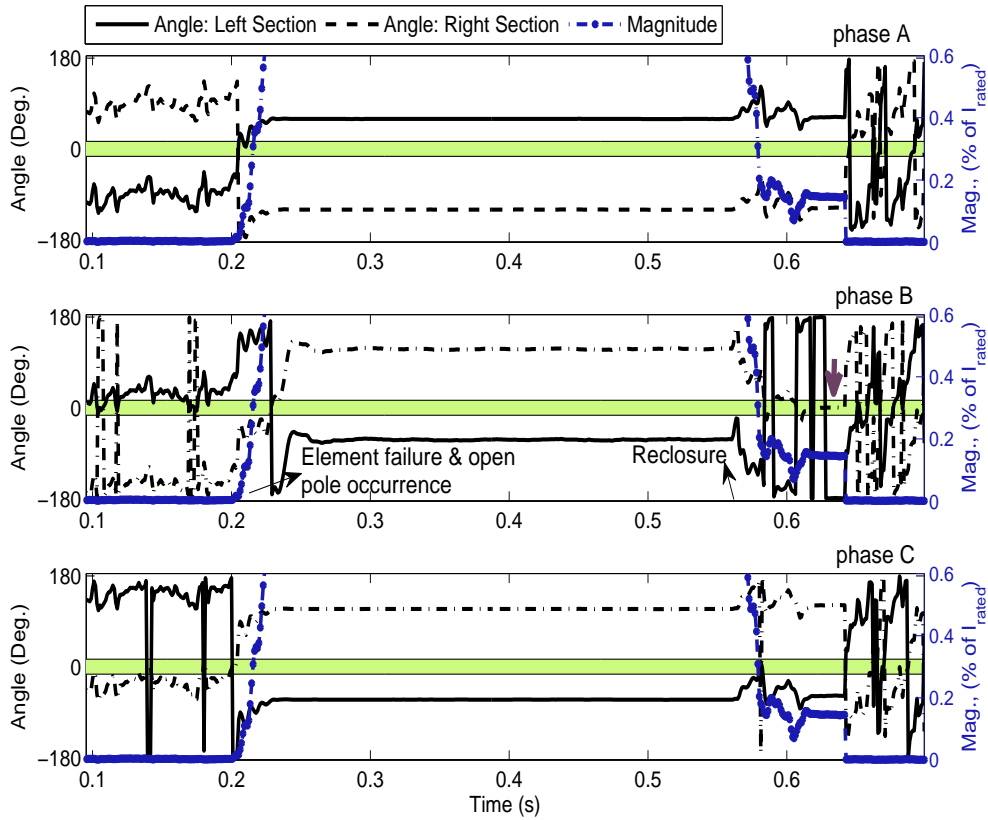
Figure 5.132: The proposed fault location principle, Case 12-2
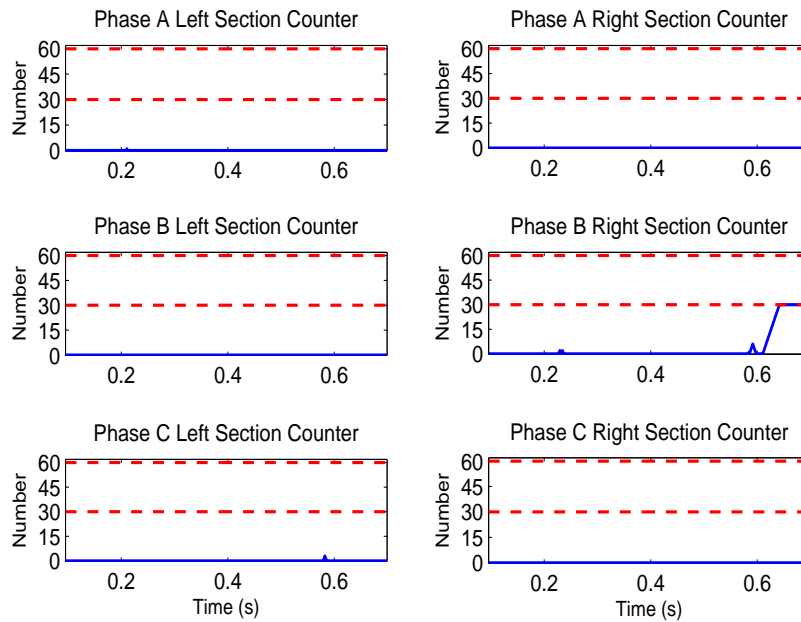
Figure 5.133: Counter of the proposed fault location method, Case 12-2
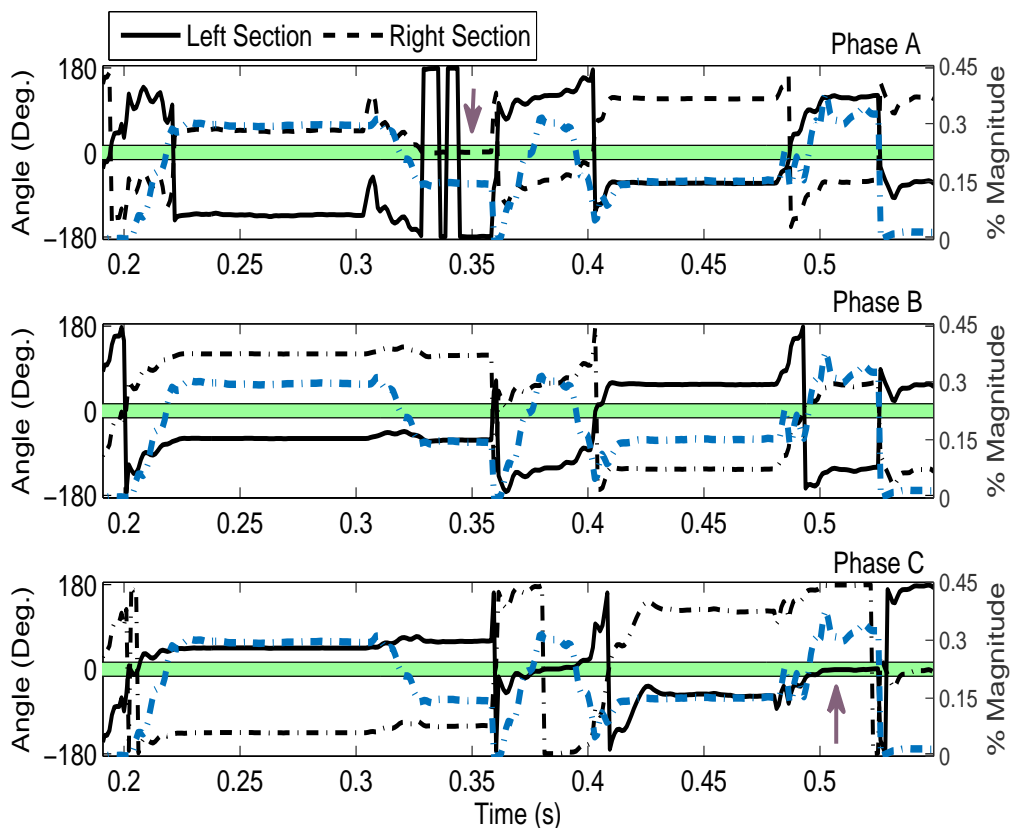
Figure 5.134: The proposed fault location principle, Case 12-3.
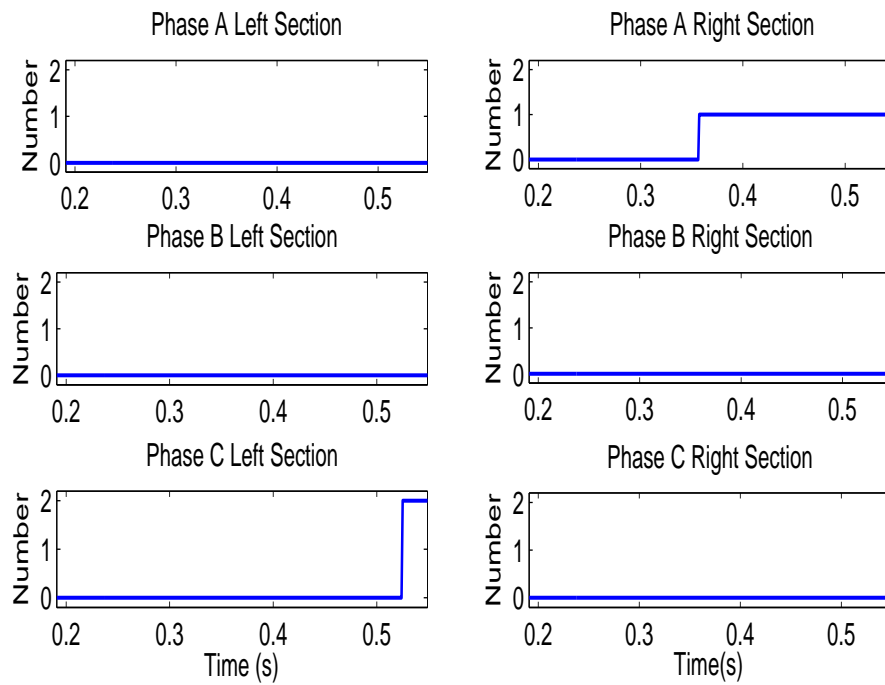
Figure 5.135: The proposed fault location output, Case 12-3.

The SEL Method for Y-Y Ungrounded with Isolated Neutrals

To complete investigation of susceptibility to external unbalances, we performed simulations for this configuration that deploys neutral to neutral voltage unbalance protection. Presented studies are under scenarios that might cause assumption violation, see Section 3.3.3.

Case 13-1 A failure in the left section of phase B of a fuseless SCB takes place at 0.22 s. An external solid fault, phase C to ground, is simulated to disturb the principle from 0.2 s until 0.3 s. Figs. 5.136- 5.138 demonstrate the results.
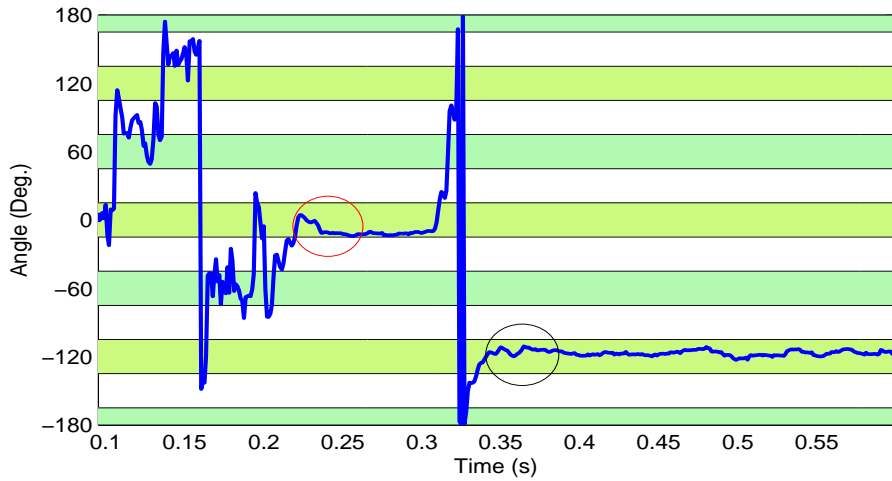
Figure 5.136: The SEL method referenced angle for fault location under external unbalance, Case 13-1
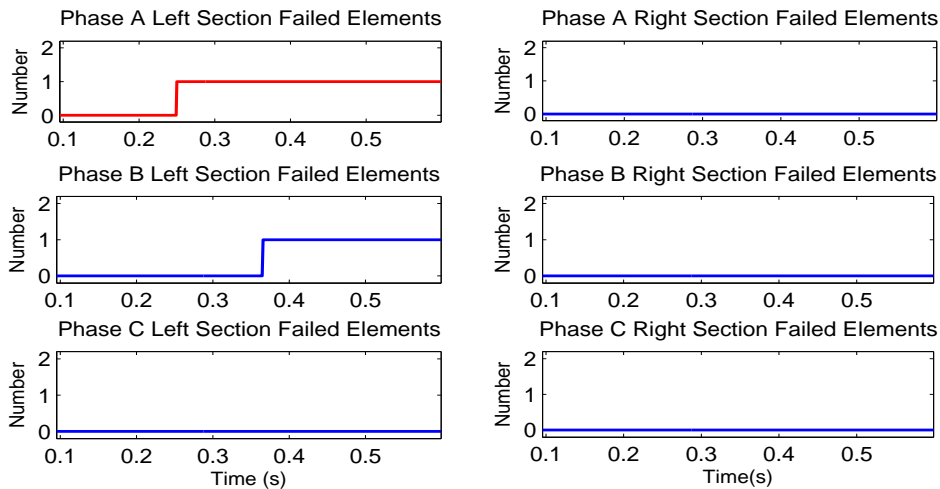
Figure 5.137: The SEL method fault location output, Case 13-1
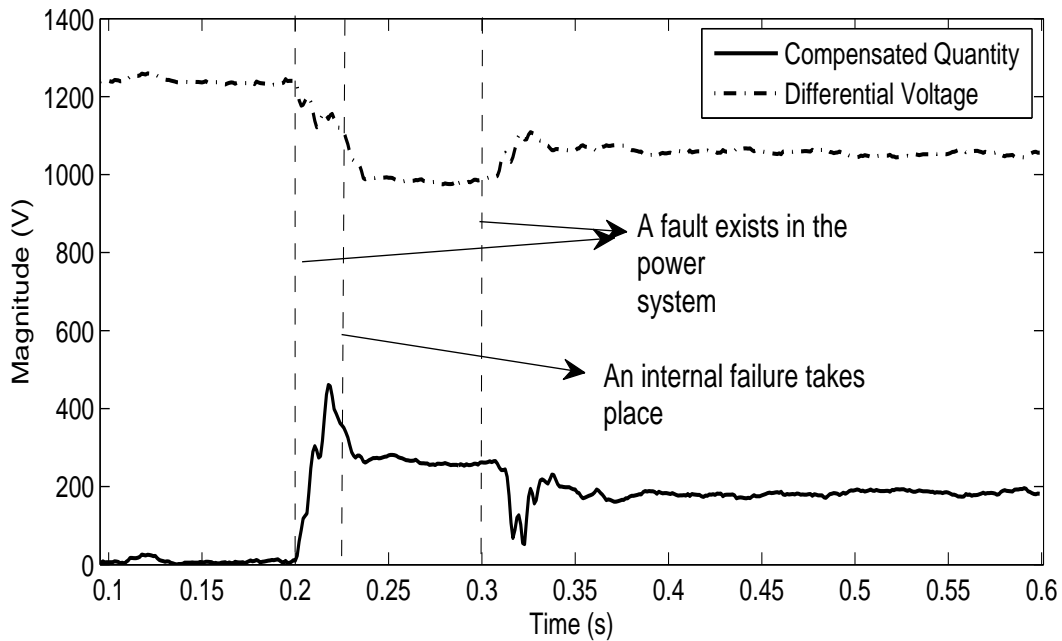
Figure 5.138: Measured and compensated differential voltage under external unbalance, Case 13-1

As it can be interpreted from these figures, the SEL fault location method seem to lose security during the fault presence in the network, shown by red output in Fig. 5.137. However, upon clearance of the fault, the fault location shows dependability and does not miss the past internal failure. A solution could be blocking the fault location with detection of power system faults. The reason behind this loss of reliability is in fact the increase in the voltage unbalance during the fault, see Fig. 5.139. Note that having considerable voltage unbalance violates the assumption of negligibility of the negative and the zero sequence voltages effect on the fault location principle phase angle.

As it was explained in Section 3.3.3, the SEL method seems to have the assumption that $\angle(V_p - V_{N_l}) = \angle V_p^+$, where V_p denotes the phase that has the failed element, thus a case study was developed to demonstrate a scenario in which by occurrence of a phase to ground fault the assumption is violated during the presence of the fault.

Case 13-2 Fig. 5.140 illustrates the simulation results in which an element failure in right section of phase C happens simultaneously with a shunt fault of phase C to ground. The SCB is internally fused with nonidentical section reactances that also include pre-existing unbalance. The fault is cleared after 100 ms. As can be seen in this figure, during the fault the assumption violation keeps the phase angle out of the fault location boundary.
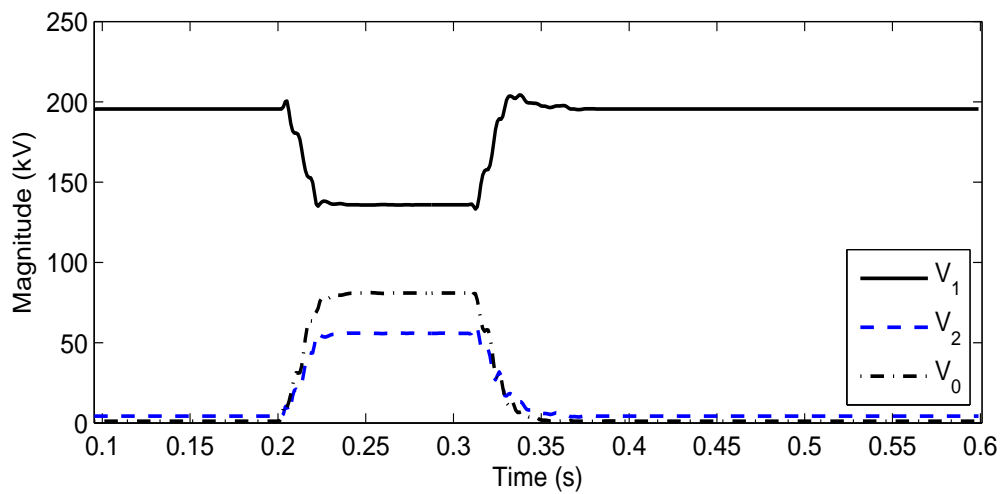
Figure 5.139: Voltage unbalance during power system fault, Case 13-1
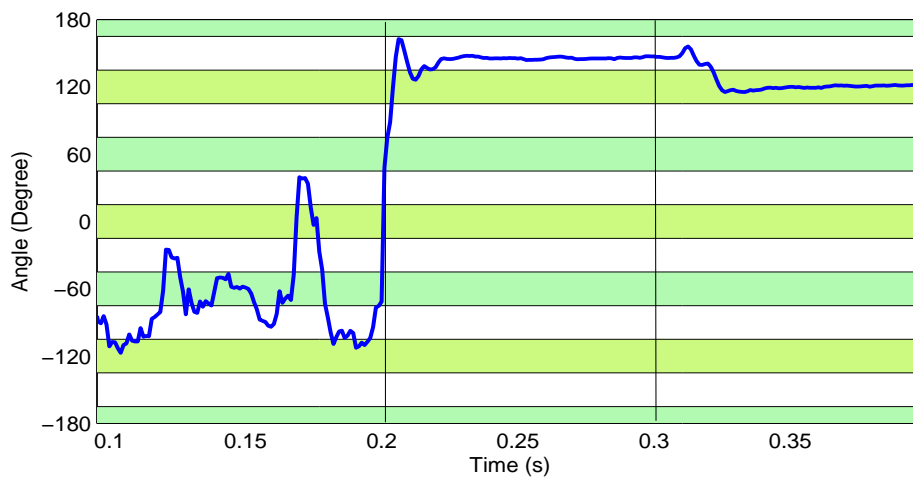
Figure 5.140: Case 13-2, Referenced angle for the SEL method, under ground-fault of the phase with failed elements.

Y-Y with Voltage Differential

For the utility configuration of Fig. 4.8, both series and shunt external unbalances were simulated. An illustrative scenario is provided here to demonstrate their impact on the fault location reliability.

Case 14-1 The scenario includes both shunt and series disturbances as follows:

- a phase B to ground fault happens at 0.2 s, which is cleared at 0.3 s

- a capacitor element fails in the left section of phase B at 0.22 s

- at 0.42 s, another element fails, this time in phase C, right section

- at 0.44 s an open pole takes place for phase C which lasts for 100 ms

Simulations show reliable operation of the described fault location in Section 4.7.1. The fault location principle for the first failure involved phase, based on the differential element, is provided in 5.141, and Fig. 5.142 shows the tap to tap differential element for all of the phases. Same applies to Figs. 5.143, and 5.144 for the second failure. Note the time axis intervals for these eight figures, the simulation time is divided in two parts for the sake of the principle plots clarity.

   The fault location outputs for each phase, and the output alarms of the third differential element are plotted in Figs. 5.145, 5.146, 5.147, and 5.148, respectively.   As it can be seen the third element even detects the failures faster for this special case. This was likely to happen as the sensitivity and magnitude thresholds are different for this element.
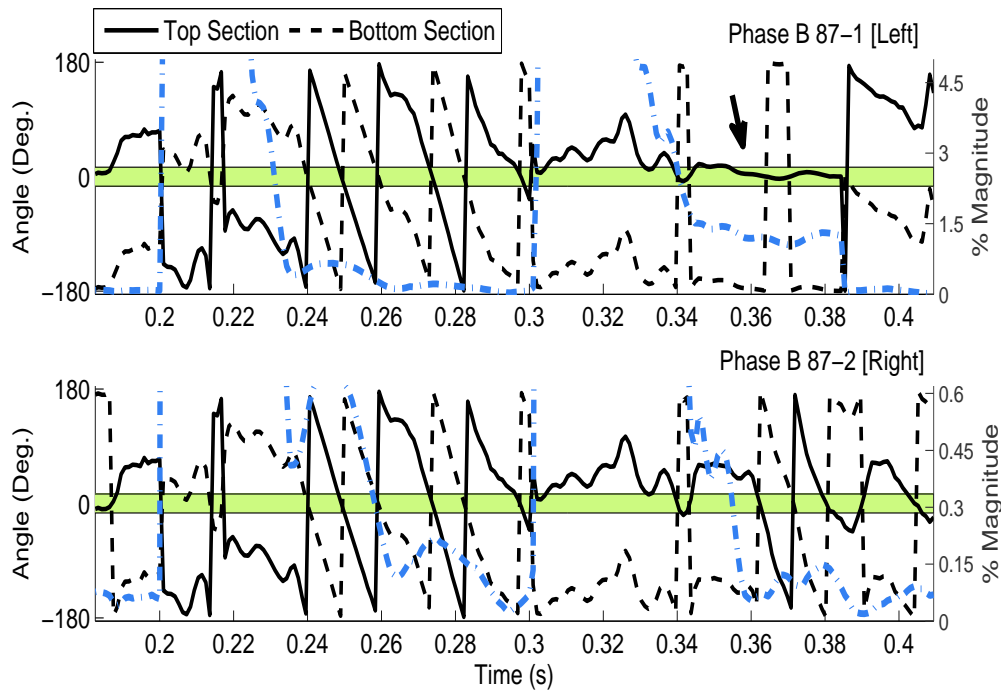
Figure 5.141: Phase B fault location principle, Case 14-1 first failure.
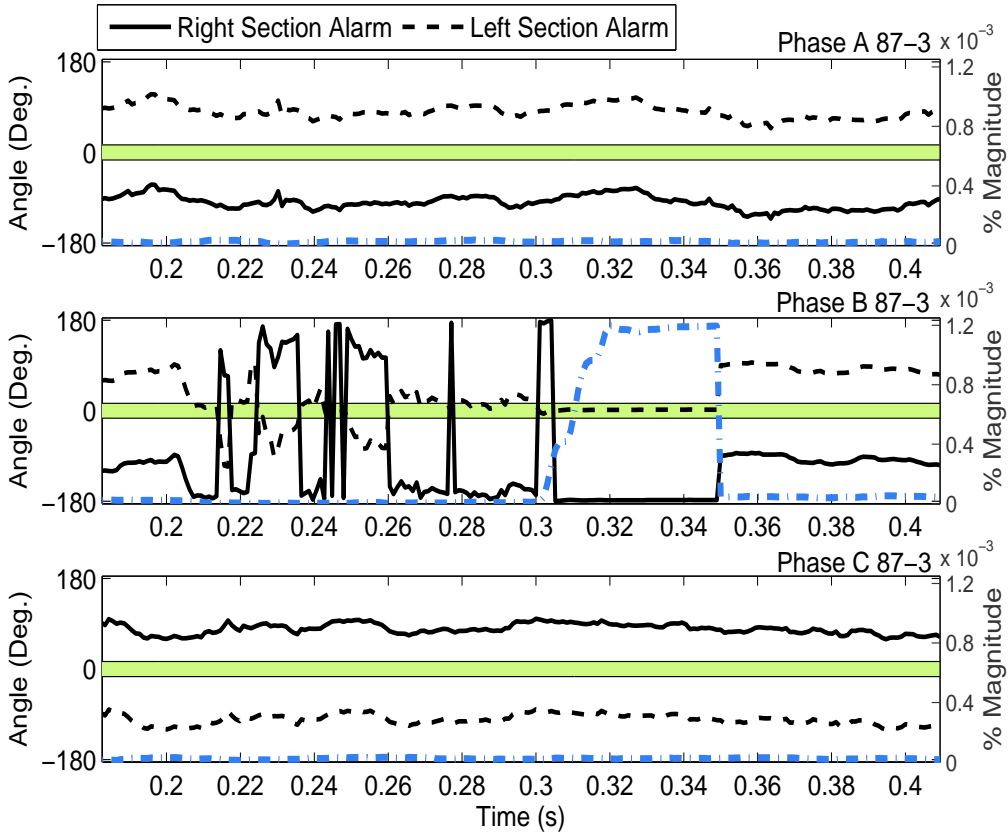
Figure 5.142: 87-3 fault location principle for three phases, Case 14-1 first failure.
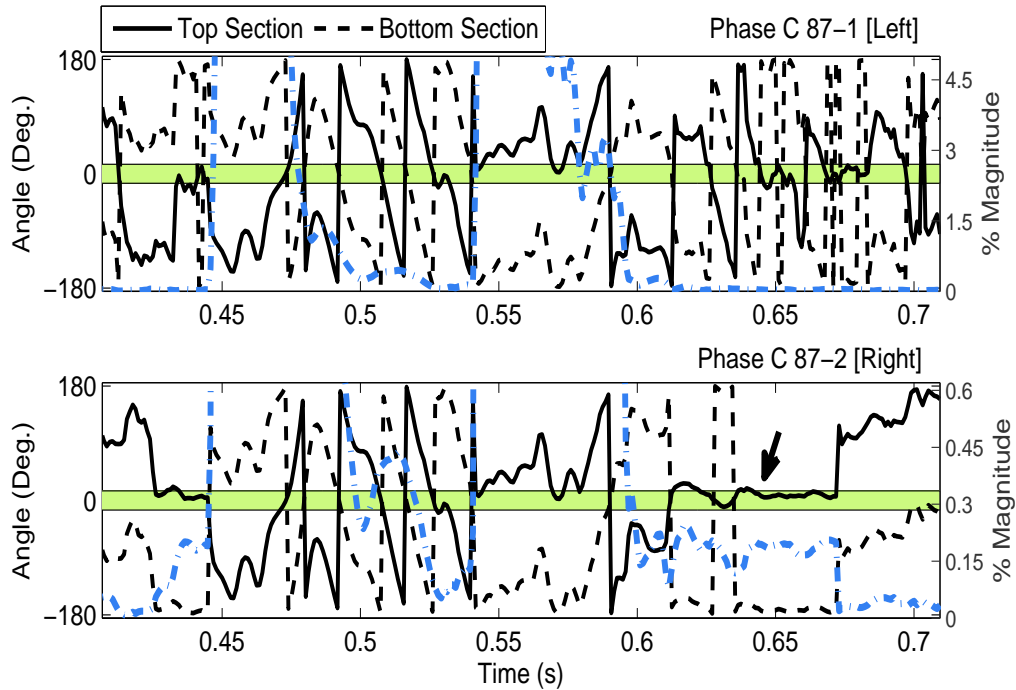
Figure 5.143: Phase C fault location principle, Case 14-1 second failure.
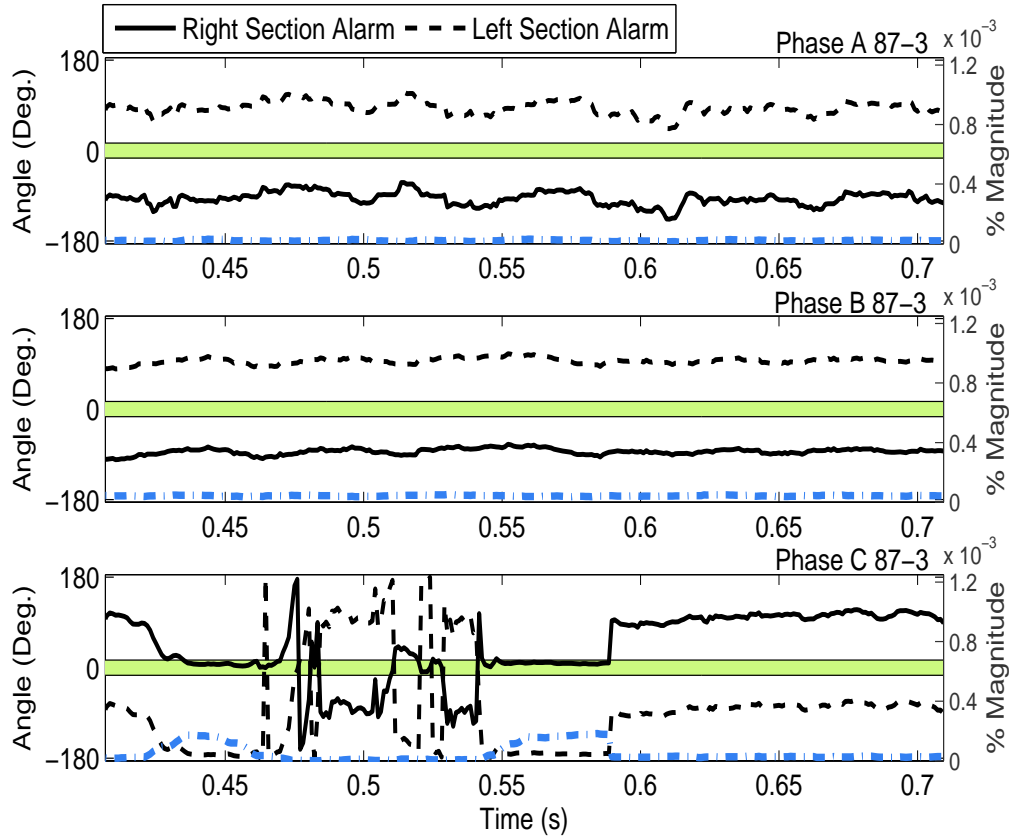
Figure 5.144: 87-3 fault location principle for three phases, Case 14-1 second failure.
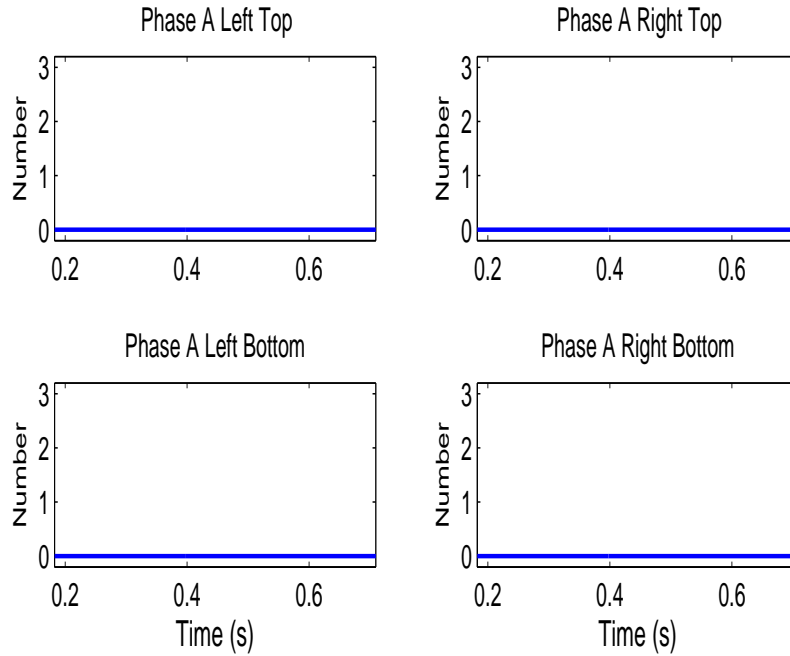
Figure 5.145: Phase A fault location output, Case 14-1.
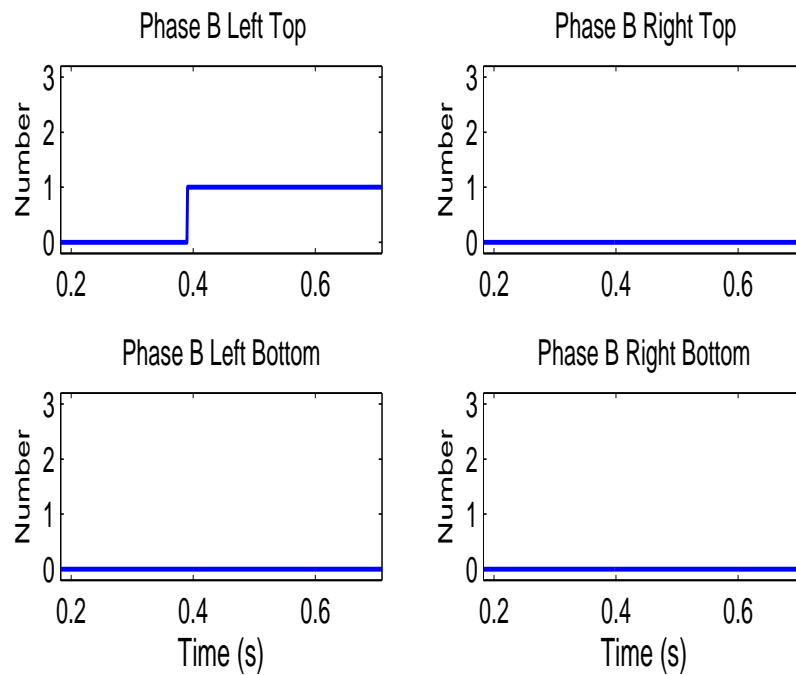
Figure 5.146: Phase B fault location output, Case 14-1.
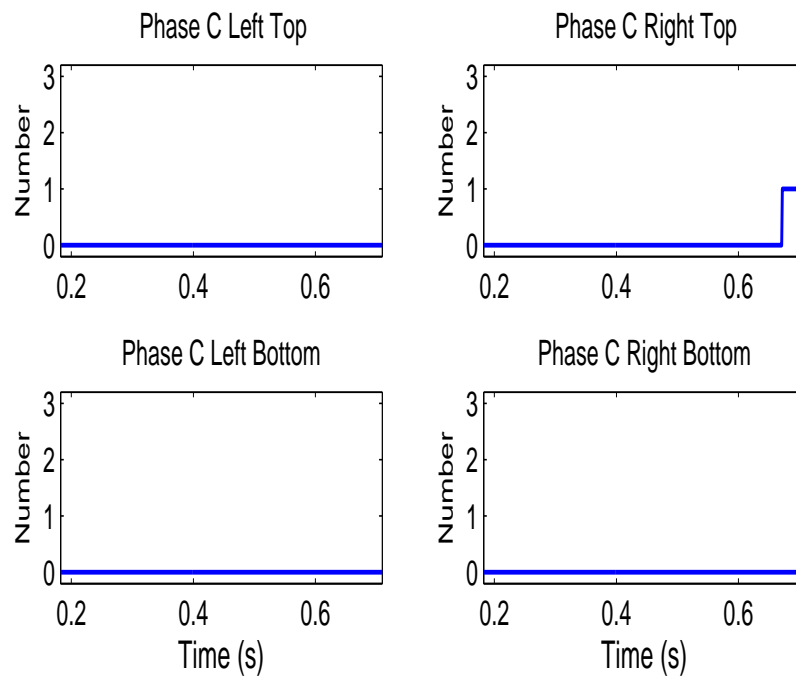
Figure 5.147: Phase C fault location output, Case 14-1.
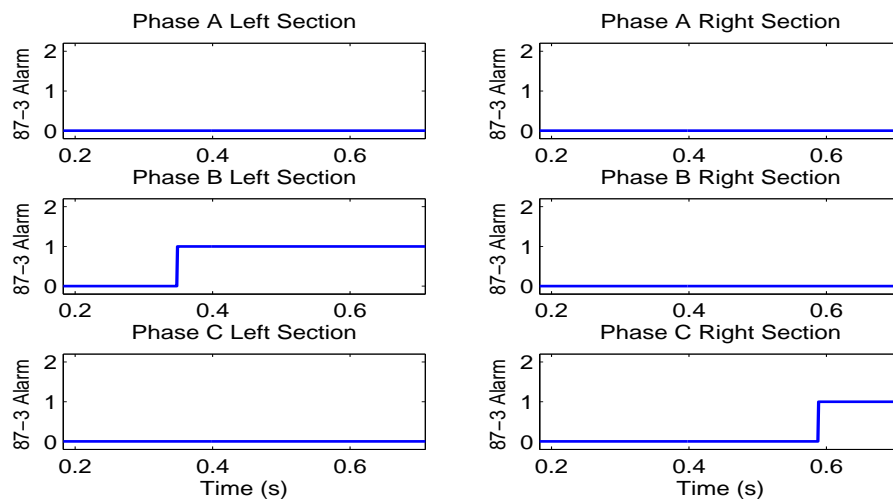
Figure 5.148: Third (87-3) differential element alarms, Case 14-1.

Track of the changes in the counters of this element are shown in Fig. 5.149, see how the open pole occurrence prevents the first counter pickup of phase C from reaching the alarm level. Although with reclosure, the second time that the counter picks up, it reaches the corresponding alarm level successfully.
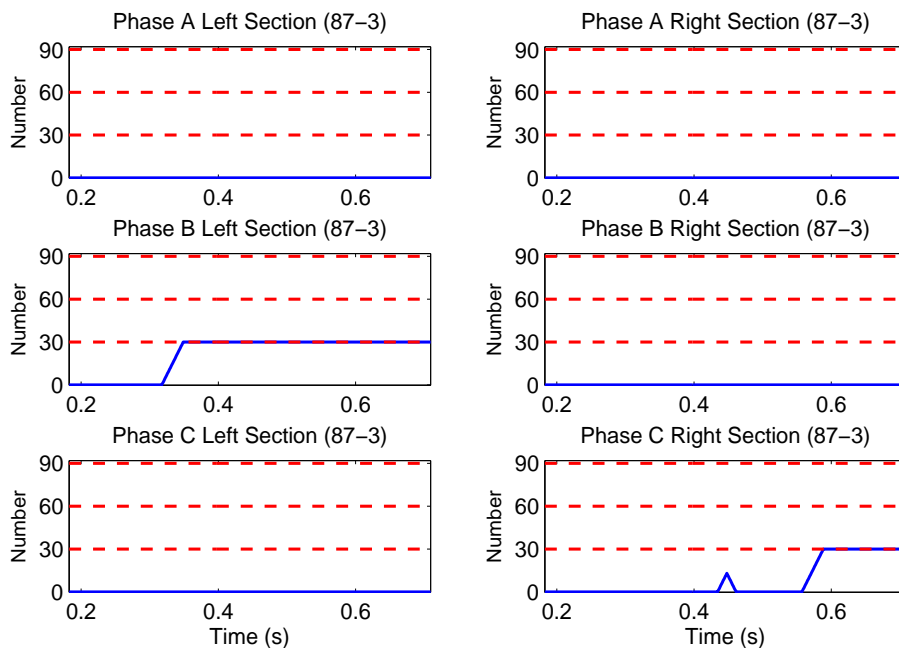
Figure 5.149: Third (87-3) differential element counters, Case 14-1.

Conclusion for Double Wye Banks

A comprehensive investigation on fault location in double wye shunt capacitor banks with different unbalance protections was performed. The investigation covers both ungrounded, and grounded banks with either of the internally fused or fuseless technologies. Both the proposed methods and the investigated methods of the literature were evaluated. Because for double wye shunt capacitor banks, system (external) unbalance affects both wye sections equally, it is not necessary to block the fault location function under such a condition. However, simulations demonstrated that for double wye banks with isolated neutrals (neutral to neutral voltage unbalance protection) the SEL fault location method, present in the literature, seemed to require blocking during external disturbance. Apart from reliable performance of the evaluated methods, simulations showed that delays may be introduced in the detection depending on the type and phase of the external failure, whether it involves the same phase as the capacitor failure or it involves another phase of the system. See Appendix C for some more additional results.

5.9.3   Regular Updating of the k-factors

To demonstrate the k-factors regular updating importance and how it mitigates the gradual changes effect in reactance caused by weather conditions, partial shading or aging, illustrative simulations are performed. A linear change in one of the phase capacitances is assumed. The change starts at 0.2 s and its upward ramp ends after about 50 ms. Algorithm setting for regular updates is set faster than the linear change rate and triggers once every fifteen protection passes (an arbitrary setting for this illustrative example). As a worst case scenario it is assumed that the other phase/sections of the SCB do not experience the linear capacitance change so that the event can mimic an internal failure. Note that for the sake of simplicity and clarity of the plot, the rate of change is much faster than what we explained in Section 4.8.1. Figs. 5.150 and 5.151 present the fault location principle variations. They illustrate the reactance change in the phase B of a fuseless single wye SCB and in the left section of phase A of a fused double wye SCB, respectively. The moments of regular reset are signified by arrows. As it can be seen, without a regular update, such a condition can lead to a false failure report as both magnitude and angle criterion can satisfy the fault location conditions.
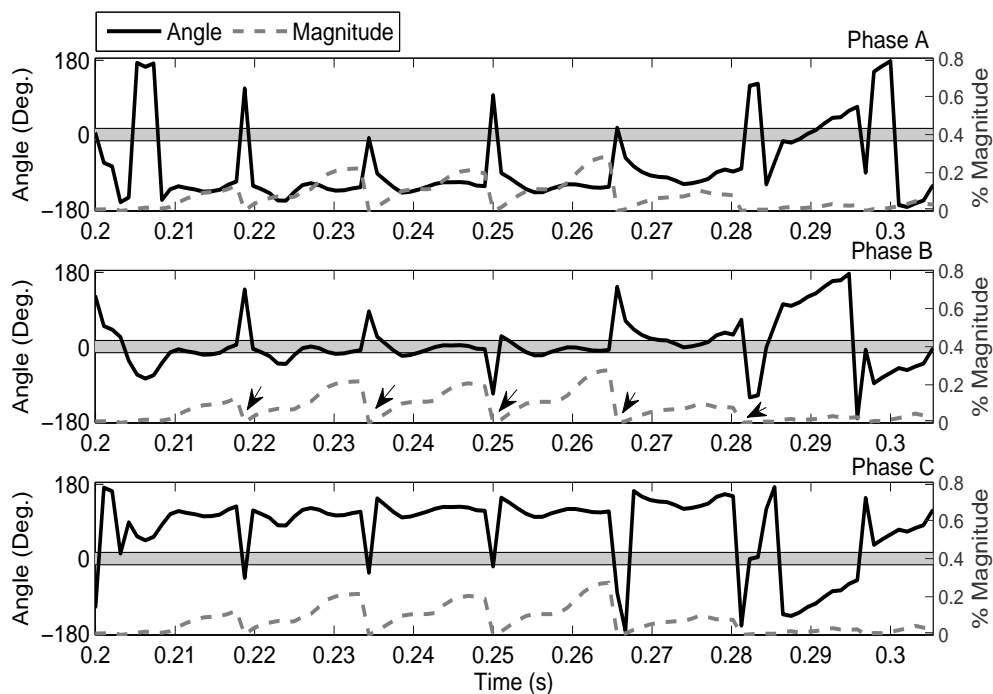
Figure 5.150: K-factors regular updates impact on the security of SR based fault location method.
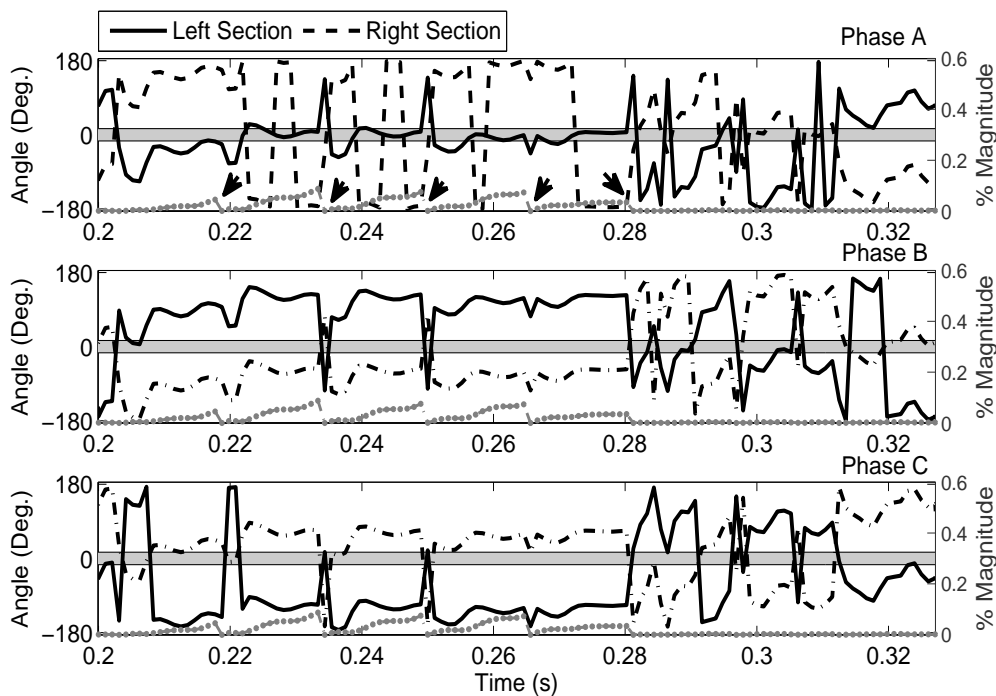
Figure 5.151: K-factor regular updates impact on the security of enhanced neutral current based fault location method.

5.10 Proposed Methods Verification for an Existing Utility System

In the previous subsections of this chapter, the fault location methods were evaluated on either adapted bank constructions from industrial publications/standards or actual banks. To further verify the proposed methods, a power system model representing an actual utility was provided. Fig. B.6, in the Appendix B, shows the single line diagram of the system and Table B.3, in the Appendix B, provides details on the ungrounded fuseless bank connected to this system. Both the proposed methods for ungrounded double wye banks and the ungrounded single wye banks will be verified in this section for fault location determination. It is worth noting that this double wye bank has once assumed to have neutral current unbalance protection and once, as a single wye bank, neutral voltage unbalance protection.

Case 15-1 Simulation includes the following internal failures:

- a capacitor element fails in phase B at 0.2 s

- three capacitor elements fail at 0.3 s, in the same phase

Figs. 5.152-5.154 illustrate the operating principle, the security counters, and the output of the fault location. As can be seen the proposed SR method determines the failures successfully. Simulation of shunt faults at the bus showed successful detection of the failure. If the shunt fault involves the same phase as where the element fails, the detection will be delayed until the fault is cleared.
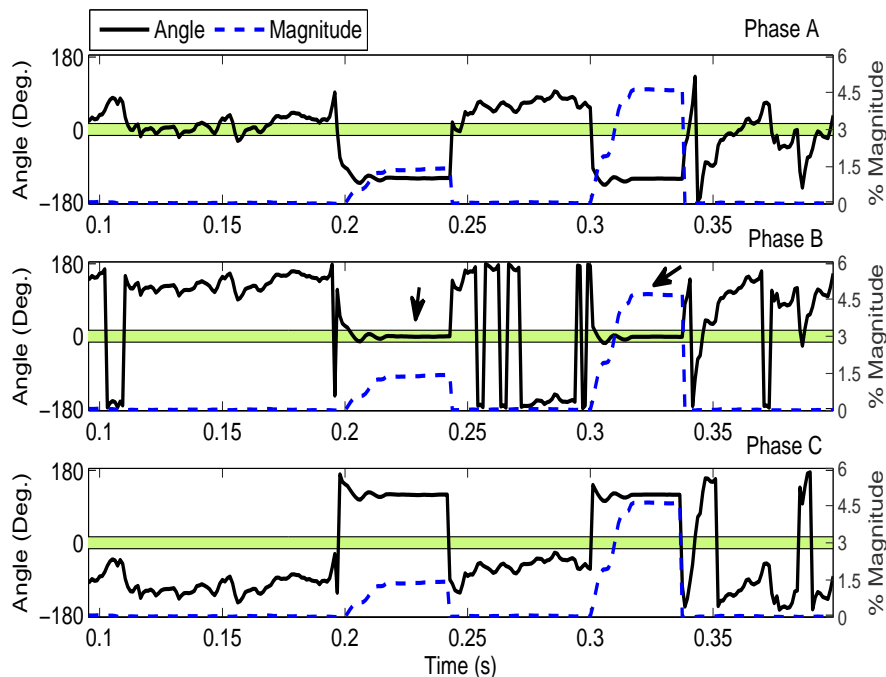
Figure 5.152: The proposed SR fault location principle for Case 15-1.
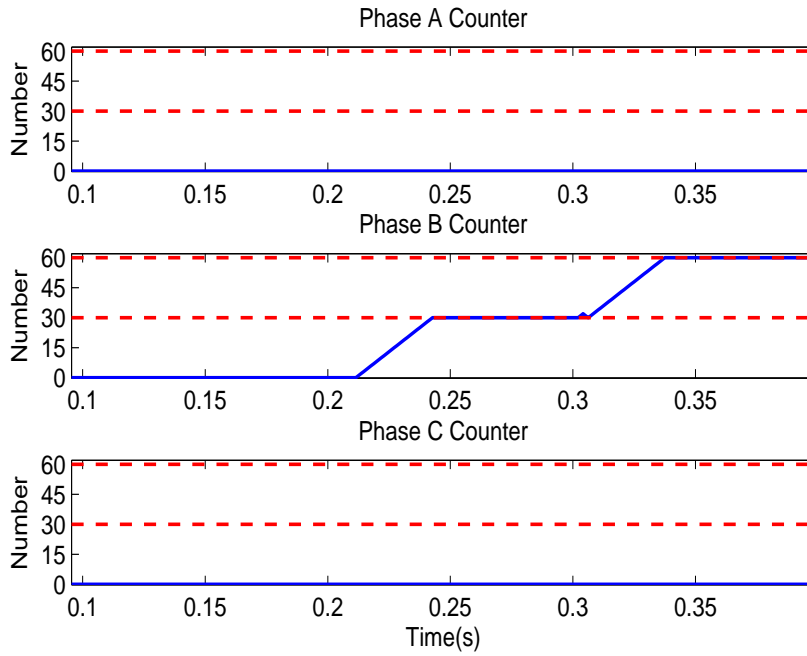
Figure 5.153: The proposed SR fault location counter for Case 15-1.
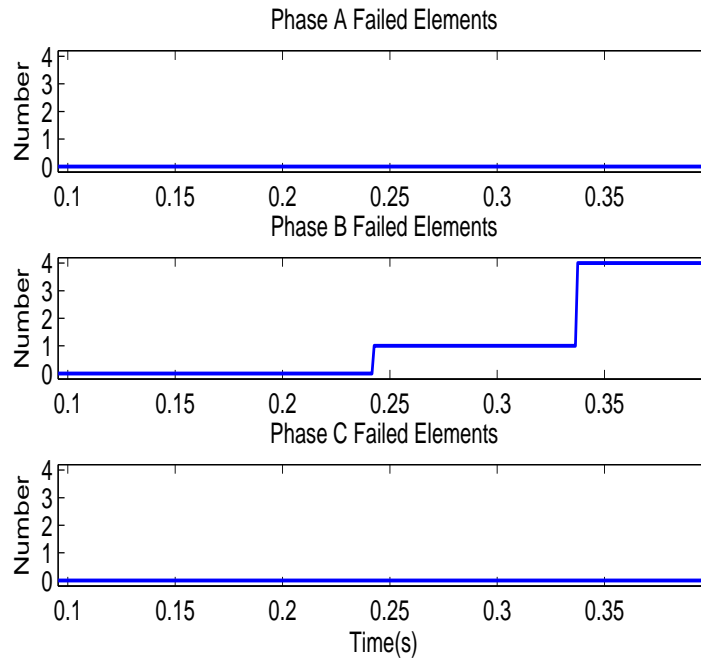
Figure 5.154: The proposed SR fault location output for Case 15-1.

The following scenario is selected for demonstration of the results.

Case 15-2 The scenario includes the following events:

- a phase B to ground fault happens at 0.2 s and is cleared at 0.35 s

- an element fails in the same phase at 0.25 s

Figs. 5.155-5.157 illustrate the operating principle, the security counters, and the output of the fault location. As can be seen the proposed SR method determines the failures successfully, note that this is a result of utilizing angle criterion, magnitude criterion, and pickup counters.
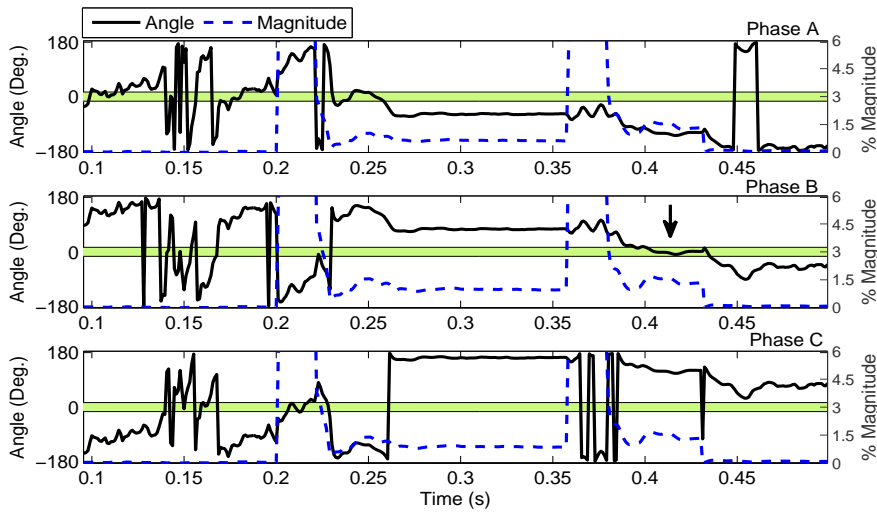
Figure 5.155: The proposed SR fault location principle for Case 15-2.
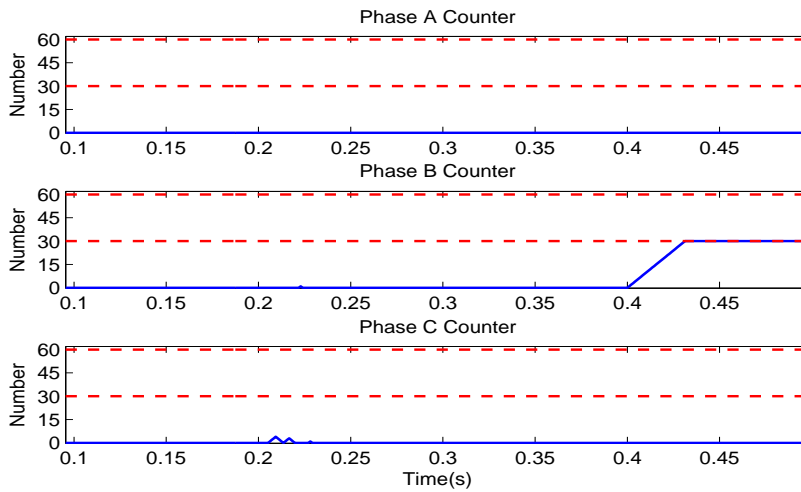
Figure 5.156: The proposed SR fault location counter for Case 15-2.
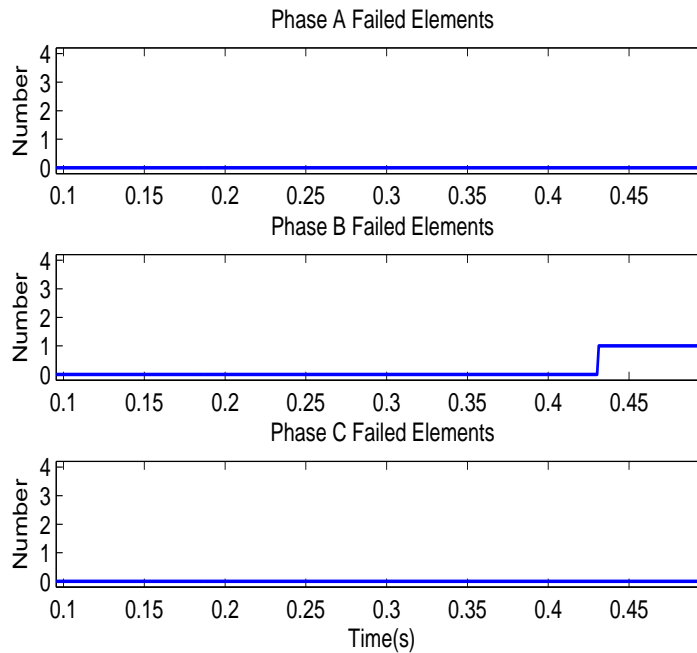
Figure 5.157: The proposed SR fault location output for Case 15-2.

The same power system is simulated for verification of the enhanced fault location method for double wye banks. A complete illustrative scenario is chosen for demonstration of the results.

Case 15-3 The scenario includes the following events:

- an element fails in phase A of the right section at 0.2 s

- a phase A to ground fault happens at the Bus at 0.3 s and is cleared at 0.45 s

- an element fails in phase A of the right section at 0.3 s

- another element fails in phase A of the right section at 0.35 s

- an element fails in the left section of phase C at 0.5 s

Figs. 5.158-5.160 illustrate the operating principle, the security counters, and the output of the fault location. As can be seen the proposed enhanced method determines the failures successfully. It is worthwhile to note that the two consecutive failures happened during the shunt fault are not distinguishable in terms of occurrence time but the method successfully determined that there were two failures. This is because the algorithm is somehow blind during the external faults as it was concluded before.
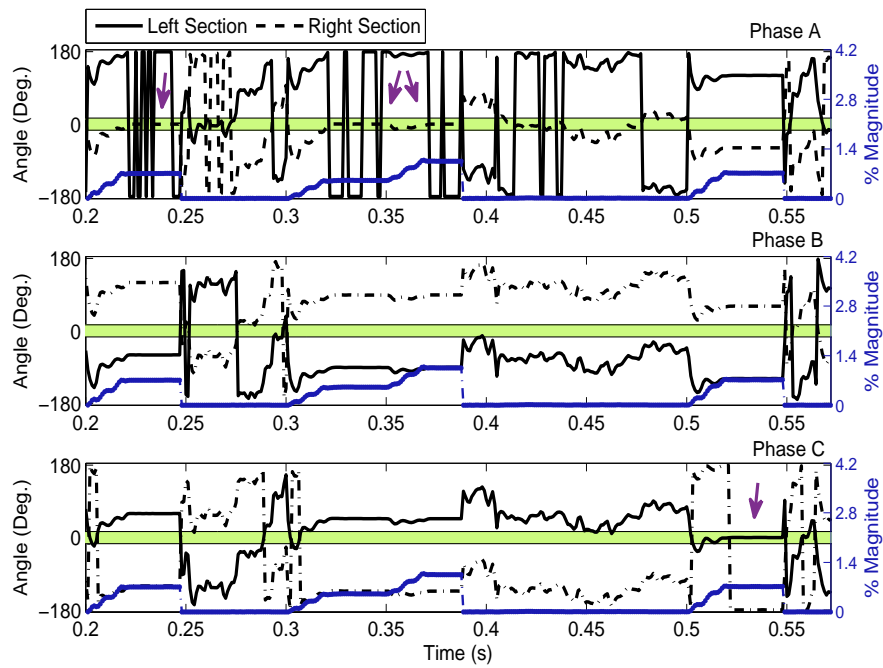
Figure 5.158: The proposed fault location principle for Case 15-3.
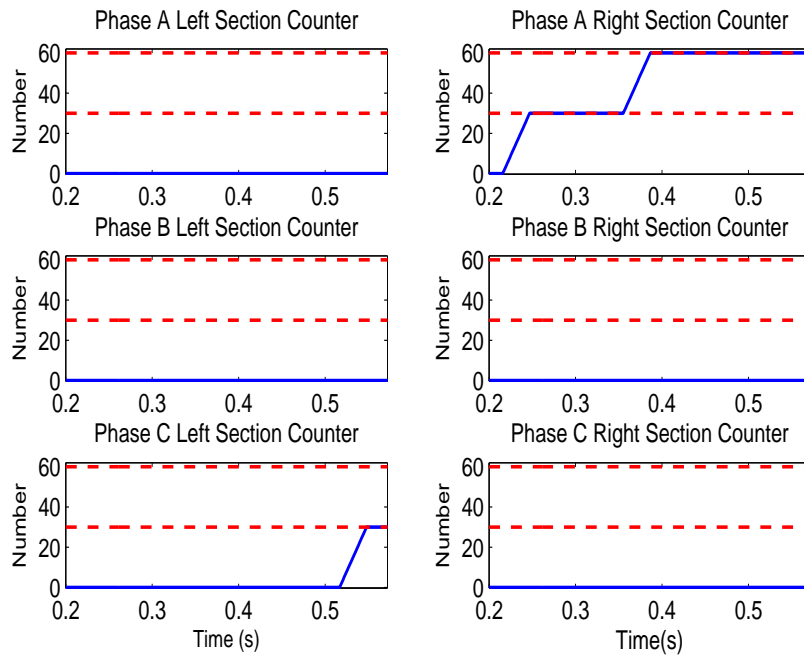
Figure 5.159: The proposed fault location counter for Case 15-3.
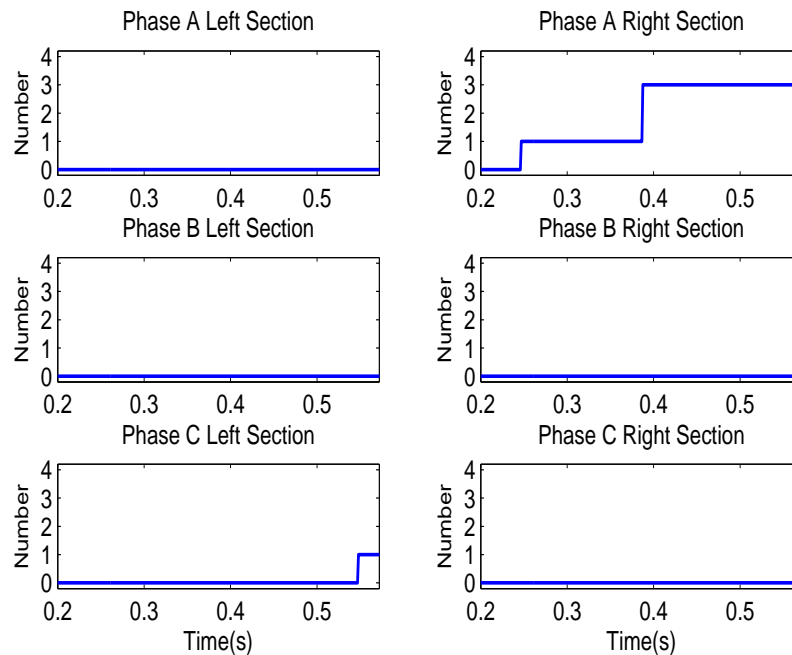
Figure 5.160: The proposed fault location output for Case 15-3.

5.11 Summary

This chapter presented a comprehensive method validation. Both the proposed methods and the literature methods that were investigated in terms of assumptions in the previous chapter, were evaluated. Beside the evaluations under normal system conditions, external unbalances were also deployed in the simulations to check the fault location algorithms reliability. Simulations included measurement noise, harmonics, and steady state voltage unbalances. Results validate reliability of the methods, although in some configurations blocking was applied to prevent from loss of algorithm security.

Chapter 6

Proposed Methods Applications and Online Monitoring

6.1 Introduction

In this chapter, the proposed methods' properties are further compared and discussed to demonstrate their advantages and applications. A commercial shunt capacitor bank relay is tested to present the shortcomings of conventional unbalance relaying. Features of the proposed methods make them online monitoring methods rather than only fault location methods. In this regard, applications such as fuse saving for externally fused SCBs is perceived and verified using an illustrative scenario, also the existing fault location methods are compared with regard to required features for online monitoring application.

6.2 Online Monitoring vs Fault Location

The proposed methods can be viewed as rather online monitoring methods [51] than fault location only methods. This originates from their self-tuning property. Dynamic calibration of the operating quantity enables generating internal failure reports with the following applications:

- Providing time stamped event records for postmortem and root cause analysis

- Quantifying the unbalance level to arrange preventive maintenance during planned outages

- Localizing the fault location problem down to 1/6 (Double Banks) or 1/3 (Single Banks) of the search space for internally fused and fuseless HV-SCBs

- Fuse saving for externally fused SCBs

The proposed methods features are summarized for the sake of comparison in the two next subsections.

6.2.1   Failure's Involved Phase Determination Methods

Table 6.1 summarizes the proposed method online monitoring features vs the existing fault location methods. The following explain each row of Table 6.1.

Table 6.1: Method Comparison for Internal Failures
Online Monitoring (Ungrounded Wye Banks)

Proposed Calibrated SR Method	SEL Method Discussed in [26, 27, 34, 35]	Method of [36]
✓Determining the involved phase	✓	✓
✓Addressing ambiguous failures	✗ Disclaimer 1	✗ Disclaimer 2
✓Determining consecutive failures	Mentions manual re-set [27, 35] (no demonstration)	✗ Disclaimer 2
✓Dynamic report of number of failed capacitors	✗	✗
✓Fuse saving for externally fused SCBs	Mentioned in [35] (no demonstration)	✗
✓Adapted for banks grounded via CT/ Capacitor (Neutral Unbalance Protection)	✗	Disclaimer 3

Disclaimer 1 The method seems to apply a manual reset, therefore it seems to be vulnerable to offsetting failures.

Disclaimer 2 The method compensates for pre-existing imbalance based on when the bank is commissioned (undamaged) only, therefore it seems that it does not consider consecutive failures and their offsetting effect.

Disclaimer 3 The method is not dependent on neutral measurement. Therefore, grounding impedance or measured quantity is not discussed.

The first row shows the common feature of the methods, which is determining the involved phase for a single event of capacitor element failures.

The second row points out to the fact that failures in different phases can offset against each other. When the algorithm does not automatically record the determined failures or is not able to determine subsequent failures or has a high pickup delay, due to algorithm security or safety margin, such failures will result in ambiguous alarms or no alarms.

The third row points out the ability to reset the operating quantity and to forget previous failures in order to determine any consecutive failure. If the algorithm can not forget the past failures it won't be able to determine consecutive failures because pre-existing unbalance has impact on the operating quantity.

The forth row highlights the online monitoring feature of dynamic reporting of number of failures. Although magnitude of operating quantities are proportional to the unbal-

ance; however, quantizing the level and following failures is an online monitoring feature that conventional unbalance protection methods do not provide.

The fifth row shows the application of the monitoring method for fuse saving for externally fused SCBs, which is a direct result of online monitoring. The method in [35] only points out to such an application but does not elaborate on this or provide any demonstration.

The sixth row presents the adapted SR feature that is proposing online monitoring for two other grounding arrangements from IEEE Std C37.99: SCBs grounded via CT and grounded via a low voltage capacitor (at the common neutral point). The method of [36] does not need neutral measurement, instead requires three phase currents in addition to the bus voltages, and therefore is applicable to ungrounded and grounded banks. However, we wish to note that measuring a corresponding neutral quantity is the common practice for unbalance protection of ungrounded banks and for solidly grounded banks the common practice is deploying voltage differential (tap voltages are provided).

Both of the methods' details are not disclosed in readily available literature. However, the SEL method discussed in [26,27,34,35] was simulated based on the available resources. Details such as magnitude criteria, algorithm pick up and drop out conditions were not available. Therefore, except for the rudimentary simulation cases that determine involved phase of single failures, we didn't include particular simulation results of that method in the previous chapter.

The investigated scenario is:

- Single element failure in phase A at 0.2 s

- Multiple element failure in phase B at 0.25 s

- Consecutive failure in phase A at 0.3 s

- Multiple element failure in phase C at 0.35 s

Fig. 6.1 shows successful pick up of a first failure (pointed out by the arrow), but as it can be seen from Fig. 6.3, this method seem not to be able to pick up for the second failure, please refer to Section 3.3 for details of the detection zones marked in gray in this figure. Even with occurrence of the second failure, the first failure's operand will drop out if the pickup delay is not short enough. The offsetting effect is apparent in the magnitude shown in Fig. 6.2.
In comparison, Fig. 6.4 shows the proposed method's successful determination of each of the failures which is a result of calibration and reset of the SR followed by each failure detection and record.

6.2.2 Failure's Involved Phase and Section Determination Methods

Table 6.2 summarizes the proposed method online monitoring features vs the existing fault location methods.
 The SEL method was simulated using the basic information in the literature.
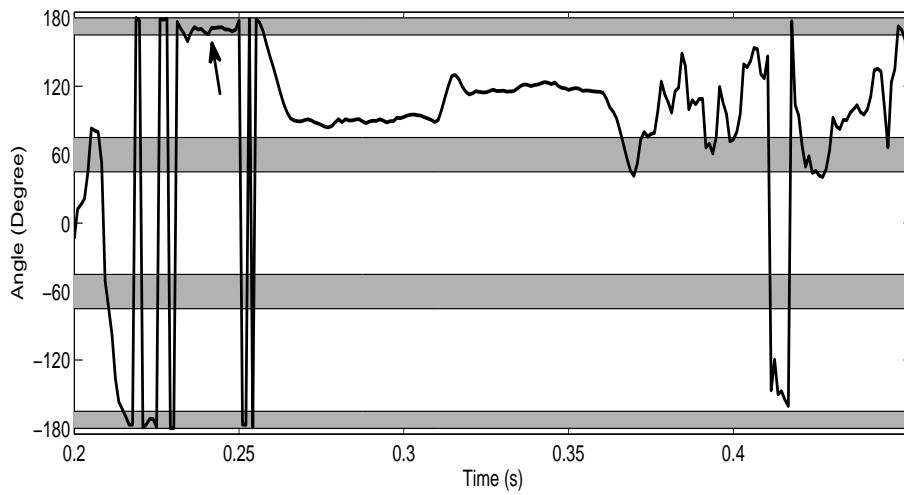
Figure 6.1: Involved phase determination criterion for the SEL method-each colored zone represents one phase
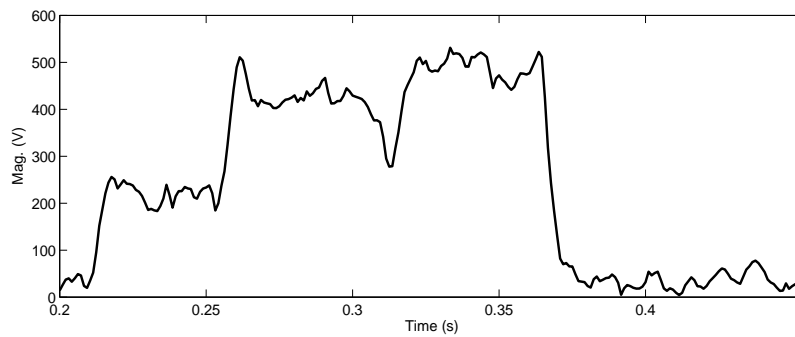
Figure 6.2: Magnitude of the operating function of the SEL method, note the impact of offsetting against the previous failures.
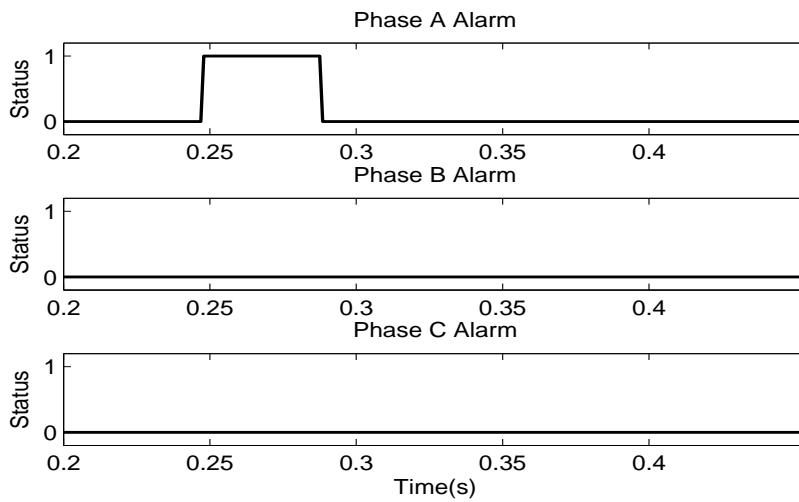
Figure 6.3: Assertion and de-assertion of the output operand for the SEL method

Table 6.2: Method Comparison for Internal Failures Online Monitoring (Ungrounded Y-Y Banks)

Proposed Enhanced Current-based Method	SEL Method Discussed in [26, 27, 34, 35]	Method of [37]
✓Determining the involved phase	✓	✓
✓Addressing ambiguous failures	✗ Disclaimer 1	Disclaimer 2
✓Determining consecutive failures	Mentions manual re-set [27, 35] (no demonstration)	Disclaimer 2
✓Dynamic report of number of failed capacitors	✗	Via lookup table (not calibrated)
✓Fuse saving for externally fused SCBs	Mentioned in [35] (no demonstration)	✗
✓Adapted for grounded banks (Neutral Unbalance Protection)	✗	Disclaimer 3
✓Less detection delay under external disturbance	Disclaimer 4	Disclaimer 3

Disclaimer 1 The method seems to apply a manual reset, therefore it seems to be vulnerable to offsetting failures.

Disclaimer 2 Method works based on angle of step change for a single quantity based on one of the phases (see literature review). Preliminary simulations show that this angle seems to be close to zero for subsequent unbalance current measurements, thus it can not identify consecutive failures or compensate for pre-existing unbalance.

Disclaimer 3 Details of the method is not disclosed in the readily available literature, comparison simulations not available.

Disclaimer 4 According to our simulations this method seems to have more delay in some cases.
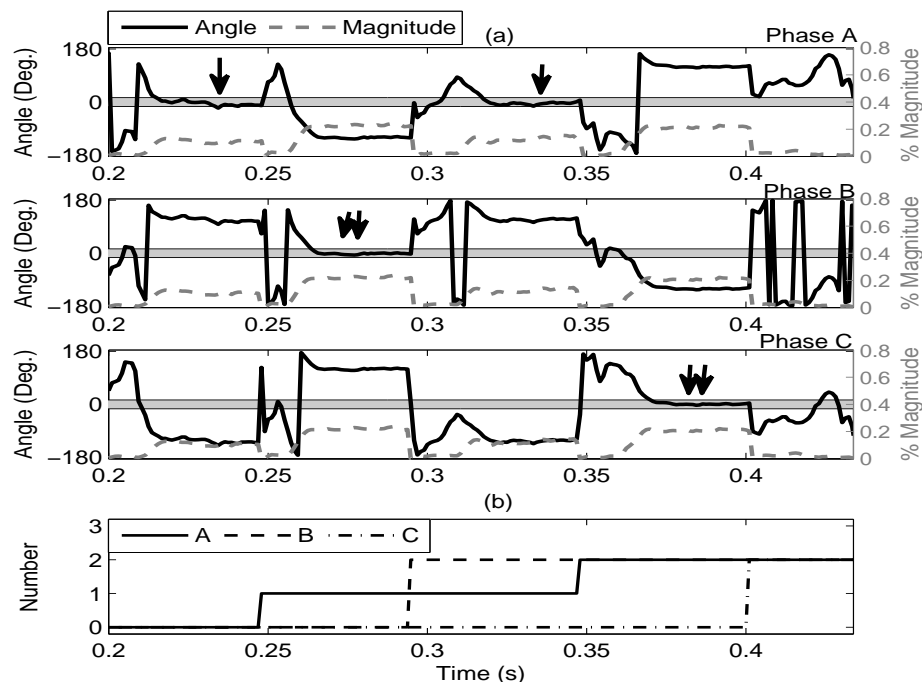
Figure 6.4: Online monitoring Application for Involved Phase Determination.

An offsetting scenario was considered to demonstrate the shortcomings that SEL method seem to have. It is worthwhile to recall that in the previous chapter the delay issue of this method was verified under the external unbalances due to presence of a considerable neglected negative sequence current. The illustrative offsetting scenario to be compared here is:

- Single element failure in phase B left section, at 0.2

- Consecutive failure in phase B right section, at 0.25

- Single element failure in phase C left section, at 0.3

- Consecutive failure in phase C right section, at 0.35

In Figure 6.5 successful determination of the first failure by the SEL method is shown by an arrow, however, as pointed by the circle, the consecutive failure in that phase is missed. The third failure is also determined successfully but its consecutive failure is again missed. Figure 6.6 demonstrates the offsetting effect of the consecutive failures. The magnitude goes back to zero once a subsequent failure balances the previous one. The output operand of the SEL method is shown in Figure 6.7. In comparison with the SEL method, Figure 6.8 shows successful monitoring of all of the four failures by the proposed method. Figure 6.9 depicts the resultant outputs from the proposed online monitoring method.
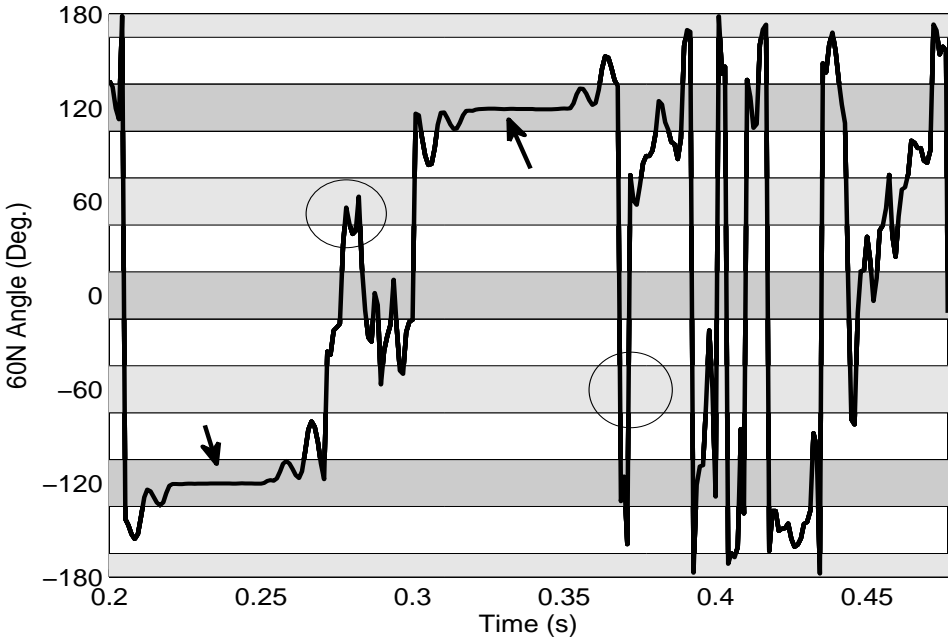
Figure 6.5: Involved phase and section determination criterion for the SEL method-each colored zone represents one phase/section
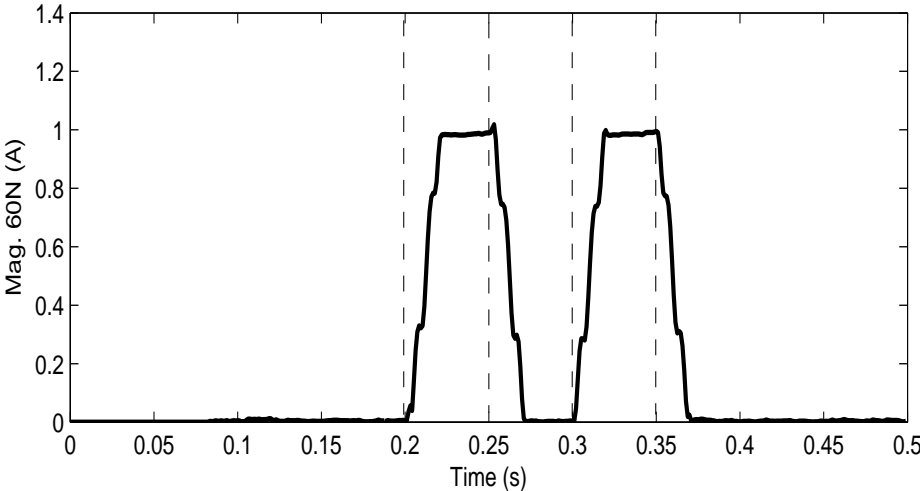
Figure 6.6: Drop out and masking apparent in the SEL operating function magnitude.
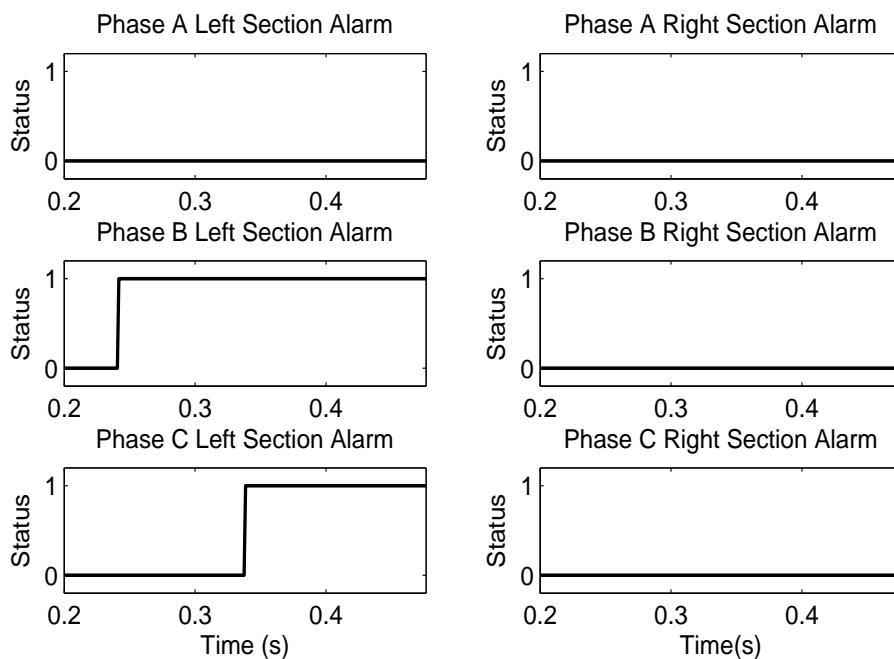
Figure 6.7: Missing consecutive failures for the SEL method
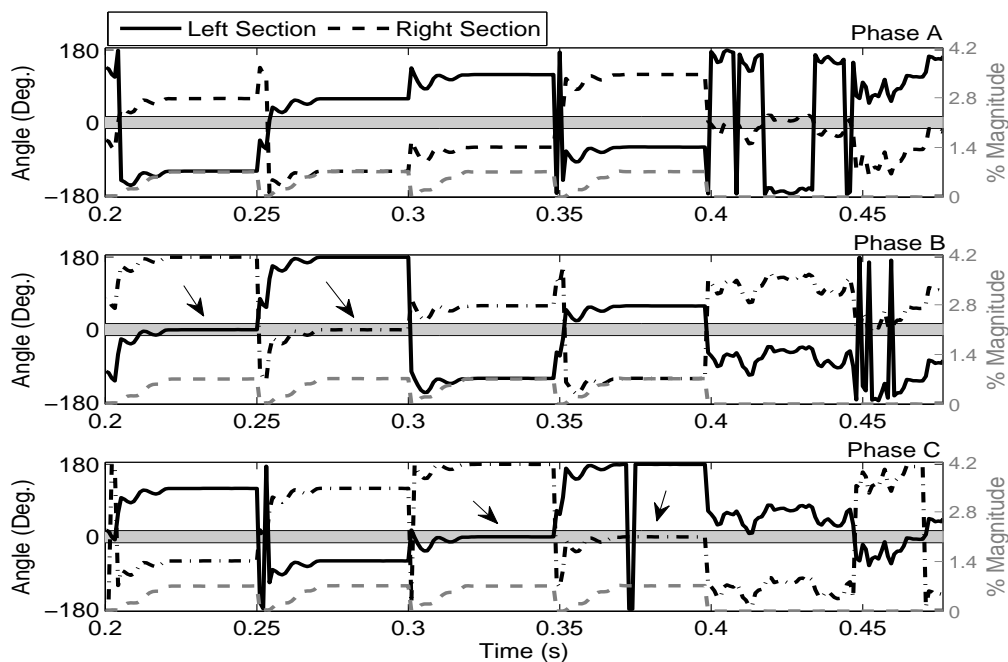
Figure 6.8: Online monitoring Application for Involved Phase and Section Determination, Decision Criteria.
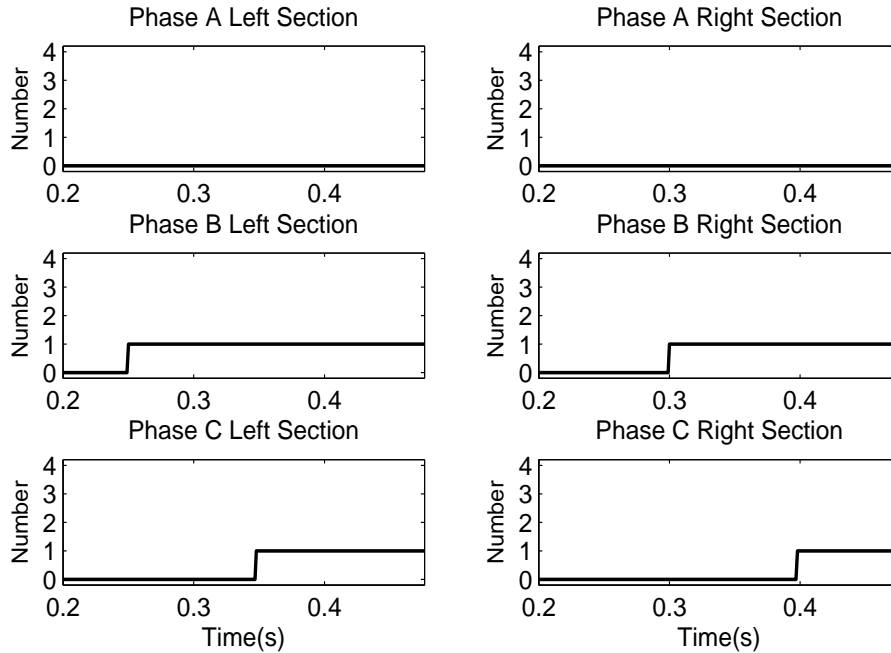
Figure 6.9: Online monitoring Application for Involved Phase and Section Determination, Outputs.

6.3   Demonstrating Fuse Saving for Externally Fused SCBs

Developing fault location methods is not meaningful for externally fused SCBs since they have failed units visual indication. However, because it is more common for them to experience cascading element failures [52], there is a perceived application of internal failure monitoring for fuse saving in this type of capacitor unit design [35]. This means providing advance alarms before the unbalance leads to fuse operation. Similar to fuseless SCBs, the failed elements remain as short circuits, thus verified fault location methods for fuseless SCBs are considered verified for externally fused SCBs as well. This is due to the same PSCAD model and MATLAB algorithm for these two unit design philosophies. As an illustrative case study for an ungrounded externally fused bank the following events were simulated. Details of the bank and the utility system are covered in Appendix B Table B.4 and Fig. B.6, respectively.

- Single element failure in phase A at 0.2 s

- Double element failure in phase C at 0.25 s

- Consecutive element failure in phase C at 0.3 s

- Consecutive element failure in phase A at 0.35 s

The variations in the SR along with the successful outcome of the proposed fault location method are presented in Fig. 6.10.
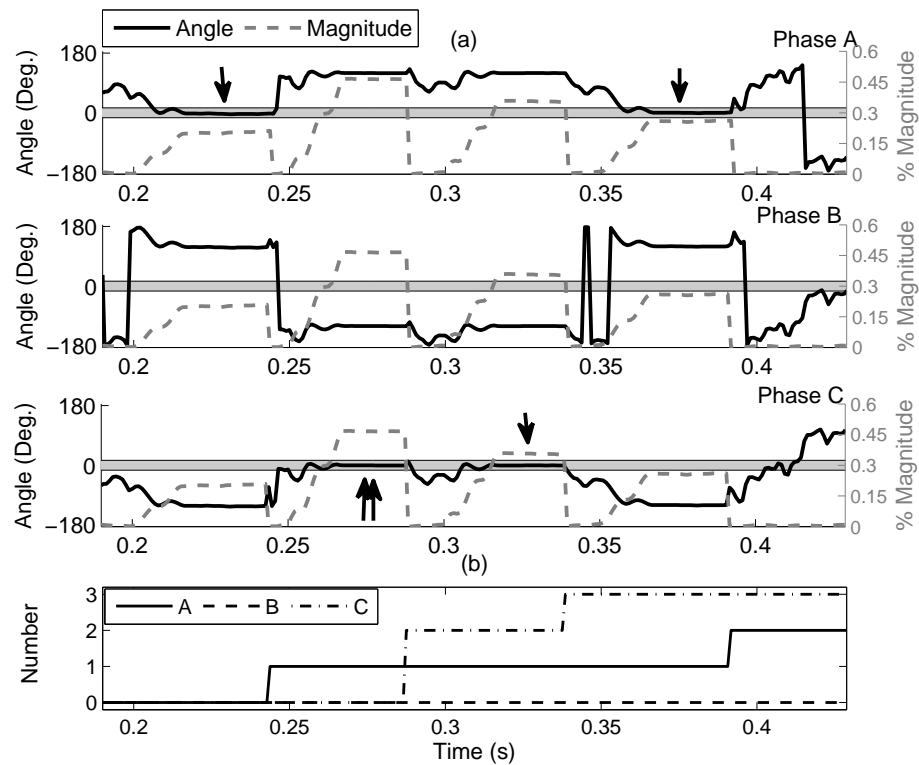
Figure 6.10: Fault location report for externally fused SCBs (a) the proposed SR magnitude and angle variations. (b) involved phase and number of shorted parallel element groups.

6.4 Comparing Conventional Unbalance Relaying of a Commercial Relay

Conventional unbalance relaying is dedicated to internal failures detection and to trip the bank when the unbalance level can cause cascading failure and damage to the bank. Therefore, failure information such as the involved phase or auto re-calibration of the operating quantity are not considered for such a protective function. Here we demonstrate what are the operand states for the mentioned illustrative scenarios and what they lack in terms of online monitoring information.

6.4.1 The open loop test set-up

In order to test a commercial multi-functional capacitor bank relay, LabVIEW software was used for play back of PSCAD COMTRADE records. The hardware platform is NI cDAQ 9178 with NI 9264 analog output module. The commercial relays available in our research laboratory accept low level inputs and the step down ratio is compensated by the relay in order to process the same signals as the PSCAD time domain simulations, by the protective functions. The corresponding step down scales are calculated separately for voltages and currents as follows:

$$\frac{V_{out}}{V_{in}} = \frac{2.5}{2.12 \times \frac{115}{\sqrt{3}} \times \sqrt{2}} \tag{6.1}$$

$$\frac{I_{out}}{I_{in}} = \frac{2.5}{23 \times 5 \times \sqrt{2}} \tag{6.2}$$

In which the outputs are limited to 5 V_{p-p}, and the rms value of the rated secondary of the VTs and CTs are 115 L-L and 5 A, respectively. A safety margin factor in pu of this secondary value is also considered for system transients.

6.4.2 Relay outputs analysis

To further demonstrate the proposed method advantages, a commercial relay was tested using PSCAD COMTRADE records. To test the voltage based unbalance protection, same event sequence as the scenario in Fig. 6.4 was played back for the relay. For the sake of comparison, the relay pickup and dropout delays have been adjusted similar to the proposed method; however, it is common practice to apply a delay of 10-30 s for the most sensitive stage of the conventional unbalance protection, STG1 in Fig 6.11, and a short dropout delay of 0.25 s for all of the stages. The relay oscillography records are depicted in Fig. 6.11, where the arrows show the assumed short pickup delays. In comparison with the demonstrated report of number and location of element failures by the proposed method in Fig. 6.4, the following points can be seen for the tested conventional unbalance protection.

- At instant 1, STG 1 has picked up, however the involved phase is unknown.

- At instant 2, STG 2 has picked up, however there is not enough information regarding the current and the former event (Phase A one failure, Phase B two failures). This is considered as an ambiguous alarm.

- At instant 3, a consecutive failure happens in phase A but no change can be found in the relay operands. This shows missing an event. The operating quantity's magnitude is not proportional to the level of unbalance when consecutive failures happen in *different* phases.

- At instant 4, all of the phases have two failed elements, this is an offsetting scenario and as it can be seen the operating quantity jumps to the pre-existing unbalance value and the picked up functions are reset.

Furthermore, if the pickup delays had been set to their typical value, even the first picked up stage would have been dropped out before it can operate the function output, resulting in missing all of the internal failures. The mentioned points demonstrate the importance of a per-phase indicating quantity with automatic re-calibration upon determining each failure for the purpose of online monitoring.
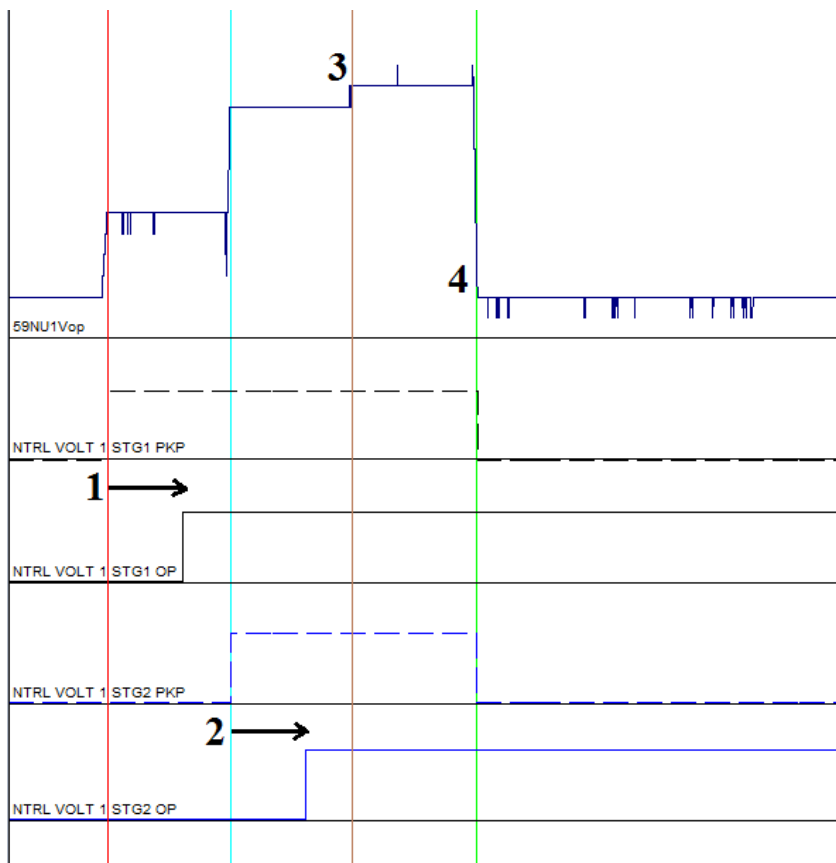
Figure 6.11: Relay oscillography records for voltage based unbalance protection.

To test the current-based unbalance protection methods for comparison with the proposed involved phase and section determination methods, the scenario of Figure 6.9

was played back for the relay. After adjusting each stage's pick up value the following points can be seen in the resultant relay oscillography records, Figure 6.12. The top plot shows the operating quantity which is magnitude of a neutral current based signal.
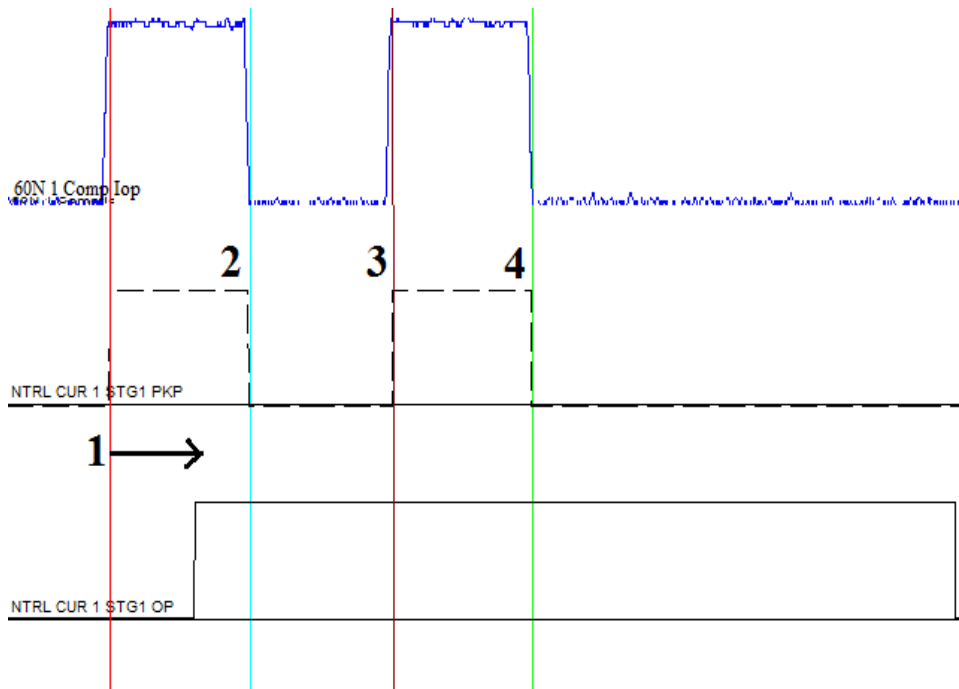
Figure 6.12: Relay oscillography records for current based unbalance protection.

- At instant 1, STG 1 has picked up, however the involved phase/section is unknown.

- At instant 2, the offsetting effect resets the operating quantity, the consecutive failure is missed and even the previous failure is determinable only when the drop out delay is high or operand has a latched setting.

- At instant 3, again STG 1 picks up but without involved phase/section information.

- At instant 4, again offsetting resets the operating quantity resulting in missing the events.

6.5 Summary

In this chapter applications of the proposed fault location methods were demonstrated. Fuse saving for externally fused banks and online monitoring of internal failures can result in preventive maintenance for SCBs. By determining ambiguous failure scenarios, the proposed reliable monitoring methods can reduce the outages due to cascading failures. This property was highlighted by comparison with a commercial relay unbalance protection operands for the simulated illustrative scenarios.

Chapter 7

Summary, Conclusions and Future Works

High Voltage Shunt Capacitor Banks (HV-SCBs) are manufactured with series and parallel connection of capacitor units. Each capacitor unit itself is comprised of tens of capacitor elements. Internal element failure is a common source of unbalance in SCBs as a result of dielectric failure. After certain number of element failures, tripping should take place which prevents from cascading failures or further voltage stress on the remaining elements. As an online monitoring tool which assists decision making and front line crews to spend less time on maintenance service, fault location of HV-SCBs is an asset for a capacitor bank protection and control relay. It helps to determine the location of those failed elements that have led to tripping. Fault location data is also useful for planning maintenance schedules before an unplanned trip takes place.

7.1   Summary and Conclusions

The challenges for fault location determination and the motivation for the project was explained first. One of the challenges for locating internal failures is the number of available measurement points or equivalently the number of transducers that measure voltages/currents of the SCB. This limits the fault location to determining the phase and section in which the element has failed. Because it is seldom economic to add voltage or current transducers for solely fault location, the thesis has aimed to propose methods based on the already available measurements that are practically available from utilities' existing monitoring programs. The other challenge is cascading failures, and failures that become ambiguous because of the impact of subsequent failures. This challenge was addressed in the thesis by determining consecutive failures location and resetting the algorithm principle. The proposed principles also include inherent compensation terms and updating routines, not to operate for other sources of unbalance than internal failures, such as: system unbalance, inherent unbalance due to manufacturing tolerances, gradual changes in capacitance due to weather conditions, partial shading, and aging of the cans.

The theory of unbalance protection methods as the sensitive relaying scheme to internal

failures in SCBs was discussed in a separate introductory chapter. Application of the known relationships among the measured voltages/currents taken around the SCB for deriving unbalance operation functions was presented. The fundamentals of compensating terms in unbalance relaying were explained as the basis for devising fault location methods.

An extensive literature survey was carried out because the subject was covered under various titles in patents and industrial conferences rather than common academic literature. The literature survey was further elaborated by investigating the approaches to deriving the final decision making equations of a relevant fault location method in the literature. The literature survey chapter also gave an idea of different connections in SCBs and the most commonly available measurements.

The main chapter of the thesis describes the proposed methods. The proposed methods are divided into two categories, those based on a new indicating quantity derived by estimation of the change in each phase reactance, namely the "Superimposed Reactance (SR) based" methods, which are actually voltage-based, and the ones that are enhanced versions of current-based unbalance protection. Apart from the main case study of SCBs that were adapted from the literature data, particular existing utility configurations were also discussed for fault location in regard to additional measurements. Beside each method's decision criteria derivation, the dynamic unbalance compensation, detection of number of failed elements and other detailed settings of the methods, such as blinders, and counting schemes were presented.

Similar to many other protection applications, evaluation of the proposed methods under fault and no-fault conditions was required. With a difference that the detection time is not critical for the present monitoring scheme. The evaluations also included the investigated methods of the literature.

The presented results validated reliability of the proposed methods for double wye SCBs under external unbalances. This was explained to be due to equal impact of system unbalances for both of the wye sections. Simulations showed that depending on the type of external unbalance, delays might impact the fault location determination. For single wye SCBs results demonstrated that for ungrounded banks and banks grounded via CTs, the output of fault location should be blocked in case of system faults. Magnitude limits and other protection functions' output signals were suggested for this blocking. Dependability and security of all of the methods were successfully verified with simulations considering pre-existing inherent unbalance in the bank, measurement noise, harmonics, and system voltage unbalance.

The auto calibration property of the proposed methods enables generating internal failure reports that are further than a fault location report, in terms of detecting subsequent failures and live reporting of number of failed capacitor elements, and could be referred to as online monitoring system outputs. To demonstrate this advantage, comparison based on open loop testing of a commercial relay was provided. Fuse saving for externally fused SCBs was also validated as another advantage of the proposed methods.

The following terms summarize the contributions of the present research work:

- Assumptions of relevant methods of the literature were investigated and their performance analysis under external disturbances was presented, which demonstrated

issues such as detection delays due to external disturbances or importance of magnitude criterion

- A novel technique was developed for estimation of the change in reactance using available measurements for unbalance relays. The method was notified as Superimposed Reactance (SR), and a fault location technique based on this was proposed and verified for SCBs protected with neutral voltage unbalance. The proposed SR adopts calibrating factors for element failures online monitoring and inherent within its definition presents a straightforward solution to set reference indexes for estimating number of failed capacitor elements

- The concept of Superimposed Reactance was expanded for fault location of SCBs that use ground current unbalance or grounding capacitor voltage monitoring for unbalance protection

- An enhanced fault location technique was developed for SCBs protected with neutral current unbalance (both grounded and ungrounded). The algorithm enables online monitoring properties and detection of ambiguous failures

- A complete fault location method was developed and verified for an actual and common design of double wye SCBs protected with tapped voltage differential for both sections

- Based on IEEE C37.99 formulas for deriving the perunit magnitude of unbalance quantities for protection purposes, neutral voltage estimation was investigated for asymmetrical double wye SCBs fault location. Results demonstrated that a fault location based on this quantity (measurement and estimation), is not capable of distinguishing between the faulted and healthy sections for the intended configuration

- An open loop testing scheme was developed to demonstrate shortcomings of conventional unbalance relaying with respect to online monitoring. Advantages of the proposed methods were also demonstrated and compared in this respect

All of the developed fault location methods have the following properties, which present comprehensive capabilities for a fault location algorithm:

- Make the best out of the available measurements and can be embedded in unbalance relaying functions

- Deploy k-factor auto-setting and self-tuning concept

- Compensate for pre-existing unbalance in the SCB (manufacturing tolerances) and system unbalance

- Compensate for gradual changes in the capacitance (aging, temperature impacts)

- Determine consecutive failures location

- Overcome ambiguous failures issue

- Determine number of failed elements (live report)

- Verified for reliable operation considering system harmonics, system voltage unbalance, measurement noise, and power system disturbances

7.2   Future Works

There exists potential research topic on application of current sensors, with wireless acquisition and transmission modules for direct monitoring of power system equipments including individual capacitor unit monitoring. Challenges for these monitoring systems includes the following but is not limited to them: selection of the appropriate current sensor, power supply of the modules, safety of the power supply during transients, synchronous acquisition, and the confined space for extra installations. Although commercialization of such an approach is uncertain; however, with the prospective of smart grids the future for such methods could become bright.

In case of access to high voltage laboratories and power capacitors, break down discharge can be analyzed to investigate more applications for monitoring of different type of power capacitors. The breakdown analysis result can be an asset for development of real-time supervision schemes of HV-SCBs.

With integration of intermittent renewable generations, today advanced control systems as mitigation measures for correspondent overvoltage issues are being developed; however, performing research on impact of these integrations on capacitor failures and outage times is also a perceived research area. Such a study would involve both capacitor overvoltage protection functions and unbalance protection functions.

Sensitivity analysis for the proposed methods considering inrush current limiting reactors and investigating fault location for harmonic filter banks could be a potential area for future research.

Bibliography

[1] M. Dhillon and D. Tziouvaras, "Protection of fuseless shunt capacitor banks using digital relays," in *26th Annual Western Protective Relay Conference*, October 1999.

[2] "IEEE Guide for the Protection of Shunt Capacitor Banks," *IEEE Std C37.99-2012 (Revision of IEEE Std C37.99-2000)*, pp. 1–151, March 2013.

[3] *C70 Capacitor Bank Protection and Control System, UR Series Instruction Manual*, GE Digital Energy, August 2013.

[4] E. Price and R. Wolsey, "String current unbalance protection and faulted string identification for grounded-wye fuseless capacitor banks," in *65th Annual Georgia Tech Protective Relaying Conference*, May 2011.

[5] *S&C Potential Devices: 15-Volt-Ampere Models, Instruction Sheet 581-510*, S & C Electric Company, March 2003.

[6] B. Kasztenny, J. Schaefer, and E. Clark, "Fundamentals of adaptive protection of large capacitor banks - accurate methods for canceling inherent bank unbalances," in *Protective Relay Engineers, 2007. 60th Annual Conference for*, March 2007, pp. 126–157.

[7] P. Danfors, N. Fahlen, and O. Nerf, "Protective device for capacitor bank," US Patent 4 219 856, August, 1980.

[8] P. G. Hjertberg and P. Skogby, "Relay protection for capacitor banks," US Patent 3 143 687, August, 1964.

[9] J. A. Zulaski, "Shunt capacitor bank protection methods," *Power Apparatus and Systems, IEEE Transactions on*, vol. PAS-101, no. 6, pp. 1305–1312, June 1982.

[10] M. Becker and K. Renz, "Device for locating internal faults in a high-voltage capacitor battery," US Patent 4 956 739, September, 1990.

[11] H. Santos, J. Paulino, W. Boaventura, L. Baccarini, and M. Murta, "Harmonic distortion influence on grounded wye shunt capacitor banks protection: Experimental results," *Power Delivery, IEEE Transactions on*, vol. 28, no. 3, pp. 1289–1296, July 2013.

[12] N. Hejazi, "Effect of induction on control/signal cables on shunt capacitor bank protective schemes," Master's thesis, The University of Western Ontario, 2009.

[13] J.-U. Lim and T. Runolfsson, "Improvement of the voltage difference method to detect arcing faults within unfused grounded-wye 22.9-kv shunt capacitor bank," *Power Delivery, IEEE Transactions on*, vol. 22, no. 1, pp. 95–100, Jan 2007.

[14] M. Bishop, T. Day, and A. Chaudhary, "A primer on capacitor bank protection," *Industry Applications, IEEE Transactions on*, vol. 37, no. 4, pp. 1174–1179, Jul 2001.

[15] H. Jouybari-Moghaddam and T. S. Sidhu, "A study of capacitor element failures in high voltage capacitor banks," in *IEEE CCECE 2017*, May 2017.

[16] *Power Capacitors and harmonic filters buyer's guide*, ABB, Document No. 1HSM 9543 32-00en, September 2013.

[17] *Distribution Automation Handbook, Section 8.10 protection of capacitor banks*, ABB, Document No. 1MRS757290, March 2011.

[18] K. C. Agrawal, *Industrial Power Engineering and Applications Handbook.* MA, USA: Butterworth-Heinemann, 2001.

[19] R. Moxley, J. Pope, and J. Allen, "Capacitor bank protection for simple and complex configurations," in *Protective Relay Engineers, 2012 65th Annual Conference for*, April 2012, pp. 436–441.

[20] S. R. McCormick, K. Hur, S. Santoso, A. Maitra, and A. Sundaram, "Capacitor bank predictive maintenance and problem identification using conventional power quality monitoring systems," in *Power Engineering Society General Meeting, 2004. IEEE*, June 2004, pp. 1846–1850 Vol.2.

[21] M. Ellis, D. Meisner, and M. Thakur, "Innovative protection schemes for h configuration fuseless grounded shunt capacitor banks," in *Protective Relay Engineers, 2012 65th Annual Conference for*, April 2012, pp. 449–458.

[22] *Forced outage performance of transmission equipment, for the period Jan 1st 1998-31 Dec 2002*, Canadian Electricity Association, 2004.

[23] *Near-Term Measures for the Return-to-Service of two units at Bruce A NGS: Install Seven 230kV Capacitor Banks in South-Western Ontario, IESO REP 0490*, IESO, 2009.

[24] *Richview SC22 Incident- January 30, 2007, IESO REP 0386*, IESO, 2007.

[25] L. Fendrick, T. Day, K. Fender, J. McCall, and A. Chaudhary, "Complete relay protection of multi-string fuseless capacitor banks," in *Pulp and Paper Industry Technical Conference, 2002. Conference Record of the 2002 Annual*, June 2002, pp. 194–198.

[26] S. Samineni, C. Labuschagne, and J. Pope, "Principles of shunt capacitor bank application and protection," in *Protective Relay Engineers, 2010 63rd Annual Conference for*, March 2010, pp. 1–14.

[27] J. Schaefer, S. Samineni, C. Labuschagne, S. Chase, and D. Hawaz, "Minimizing capacitor bank outage time through fault location," in *Protective Relay Engineers, 2014 67th Annual Conference for*, March 2014, pp. 72–83.

[28] J. A. Zulaski, "Device for detecting unbalanced conditions in a polyphase equipment bank," US Patent 4 104 687, August, 1978.

[29] N. R. Clark and S. B. Farnham, "Connection arrangements and protective practices for shunt capacitor banks," *American Institute of Electrical Engineers, Transactions of the*, vol. 68, no. 2, pp. 1226–1231, July 1949.

[30] M. Becker and K. Renz, "Monitoring device for detecting faults in an electrical device, particularly in an lc filter circuit in an ac voltage network," US Patent 4 713 604, December, 1987.

[31] S. Samineni and C. A. Labuschagne, "Apparatus and method for identifying a faulted phase in a shunt capacitor bank," US Patent 8 575 941, November, 2013.

[32] T. R. Day and D. P. Roth, "Device protection using temperature compensation," US Patent 7 990 668, August, 2011.

[33] A. Chaudhary, T. Day, K. Fender, L. Fendrick, and J. McCall, "Pull a few strings [complete protection of multistring fuseless capacitor banks]," *Industry Applications Magazine, IEEE*, vol. 9, no. 6, pp. 34–39, Nov 2003.

[34] S. Samineni, C. Labuschagne, J. Pope, and B. Kasztenny, "Fault location in shunt capacitor banks," in *Developments in Power System Protection (DPSP 2010). Managing the Change, 10th IET International Conference on*, March 2010, pp. 1–5.

[35] S. Samineni, C. Labuschagne, S. Chase, and J. Hawaz, "Fault location in capacitor banks:how to identify faulty units quickly and restore the bank to service," in *CIGRE, 21 rue dArtois F-75008 Paris, France*, 2014, pp. B3–212.

[36] A. Kalyuzhny, J. C. Mccall, and T. R. Day, "Corrective device protection," US Patent 7 973 537, July, 2011.

[37] Z. Gajic, M. Ibrahim, and J. Wang, "Method and arrangement for an internal failure detection in a y-y connected capacitor bank," US Patent 20 130 328 569, December, 2013.

[38] B. Kasztenny, D. McGinn, and I. Voloh, "Enhanced adaptive protection method for capacitor banks," in *Developments in Power System Protection, 2008. DPSP 2008. IET 9th International Conference on*, March 2008, pp. 269–274.

[39] H. Jouybari-Moghaddam, T. S. Sidhu, and P. Parikh, "A study of fault location method in double wye shunt capacitor banks," in *CIGRE Canada, Vancouver, Canada*, October 2016.

[40] Home Guides, "The difference between air temperature in shade and in sun," *SFGATE*. [Online]. Available: http://homeguides.sfgate.com/difference-between-air-temperature-shade-sun-92497.html

[41] "IEEE Standard for Shunt Power Capacitors," *IEEE Std 18-2012 (Revision of IEEE Std 18-2002)*, pp. 1–39, Feb 2013.

[42] N. D. Sadanandan, F. A. Deviney, L. Hollomon, and M. Sendaula, "Microprocessor-based capacitor bank control and protection system," *IEEE Transactions on Power Delivery*, vol. 4, no. 1, pp. 241–247, Jan 1989.

[43] H. Jouybari-Moghaddam, T. S. Sidhu, M. R. Zadeh, and P. Parikh, "Enhanced fault location scheme for double wye shunt capacitor banks," *IEEE Transactions on Power Delivery*, vol. 32, no. 4, pp. 1872–1880, August 2017.

[44] H. Jouybari-Moghaddam, T. S. Sidhu, P. Parikh, and I. Voloh, "Enhanced fault location method for shunt capacitor banks," in *2017 Texas A & M Protective Relaying Conference*, April 2017.

[45] *SEL-487V Relay, Capacitor bank protection, automation, and control- instruction manual*, Schweitzer Engineering Laboratories, INC., August 2012.

[46] G. Scheer, "Roles of annunciators in modern electrical substations," in *13th Annual Western Power Delivery Automation Conference , Spokane, Washington, March, 2011.*

[47] "IEEE Recommended Practice and Requirements for Harmonic Control in Electric Power Systems," *IEEE Std 519-2014 (Revision of IEEE Std 519-1992)*, pp. 1–29, June 2014.

[48] GridSense, Inc., "Voltage and current unbalance," *Application Note*. [Online]. Available: http://www.gridsense.com/wp/wp-content/uploads/2013/09/App-Note-PM-VoltageCurrent-Imbalance.pdf

[49] P. Pillay and M. Manyage, "Definitions of voltage unbalance," *Power Engineering Review, IEEE*, vol. 21, no. 5, pp. 49–51, May 2001.

[50] *Network Protection & Automation Guide.* Levallois-Perret, France: Alstom, 2002.

[51] H. Jouybari-Moghaddam, T. S. Sidhu, M. R. Zadeh, and P. Parikh, "Shunt capacitor banks online monitoring using a superimposed reactance method," *to be published in IEEE Transactions on Smart Grid*, 2017.

[52] T. Ernst, "Fuseless capacitor bank protection," in *Proc. of Minnesota Power Systems Conf.*, 1999, pp. 77–83.

[53] U. Khan, "Modeling and protection of phase shifting transformers," Ph.D. dissertation, The University of Western Ontario, 2013.

[54] *PSCAD/EMTDC V. 4.5.2*, Manitoba HVDC Research Center, Winnipeg, MB, Canada.

[55] "IEEE Guide for the Application of Shunt Power Capacitors," *IEEE Std 1036-2010 (Revision of IEEE Std 1036-1992)*, pp. 1–88, Jan 2011.

[56] *ABB Application Guide for Instrument Transformers*, ABB, Feb. 2015.

[57] Nokian Capacitors, "Unbalance protection current relay NUR-36," *Product Flyer*. [Online]. Available: http:/www.nokiancapacitors.ru

[58] T. Longland, T. W. Hunt, and W. A. Brecknell, *Power Capacitor Handbook*. UK: Butterworths, 1984.

Appendix A

Simulation Settings

The solution time step was $10\mu s$ and the COMTRADE recording time step was selected to be $50\mu s$ [53]; therefore, PSCAD applies interpolation for synchronization between the two $[\mu s]$ [54]. The recorder's low pass filter was not used, instead anti-aliasing filters were considered in PSCAD simulation before recording the signals. The filters were forth order butter-worth low pass filters with cut off frequency of 1536 Hz.

As the time step for recording in PSCAD can only be an integer, a MATLAB function (linear interpolation or resample) must be applied in the processing code to synchronize the resampled data with the original records. Accordingly the mentioned time steps can not be adjusted to be an integer multiple of the final 64×60 data sampling rate. As the resample function in MATLAB again requires a rational fraction between the recording rate and the resampling rate for the relay model, the interp1 function (linear interpolation) was used instead.

Appendix B

Simulated System and Specifications of the SCBs

Figs. B.1 and B.2 illustrate both the bank and unit construction for ungrounded single wye SCBs, they are adapted from [55] and [34], respectively. Figs. B.3 and B.4 illustrate
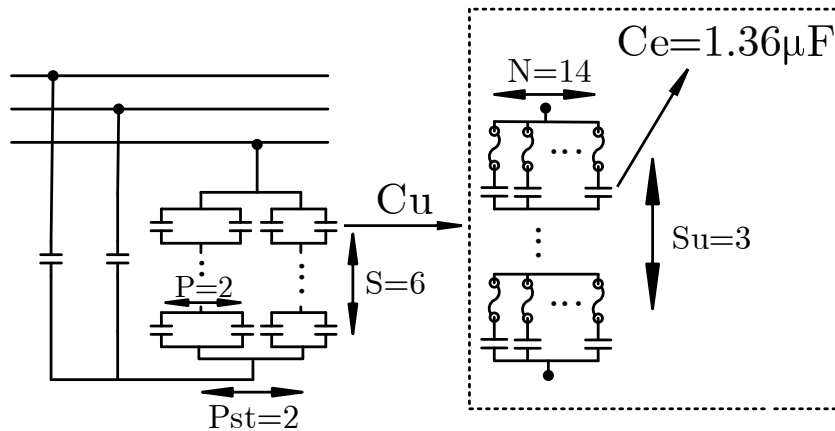
Figure B.1: 230 kV internally fused ungrounded single wye SCB.

both the bank and unit construction for ungrounded double wye SCBs, they are adapted from [27] and [34], respectively. For double wye grounded banks, the right section reactance would be the same as the left section.

For double wye banks with isolated neutrals, if the bank sections are configured identical they are the same as the grounded double wye configurations. If they are configured non-identical they will be configured as the ungrounded double wye configuration.

The schematic of the simulated power system is presented in Fig. B.5. The component parameters and their values are shown in Table B.1. For the existing utility configuration of Section 4.7, a source impedance of $Z_1 = 6.67\angle 84.28°\Omega$ and $Z_0 = 13.34\angle 70°\Omega$ was used for the simulation. The extracted application settings for Fig. 4.8, and Fig. 4.10 are as follows in Table B.2.
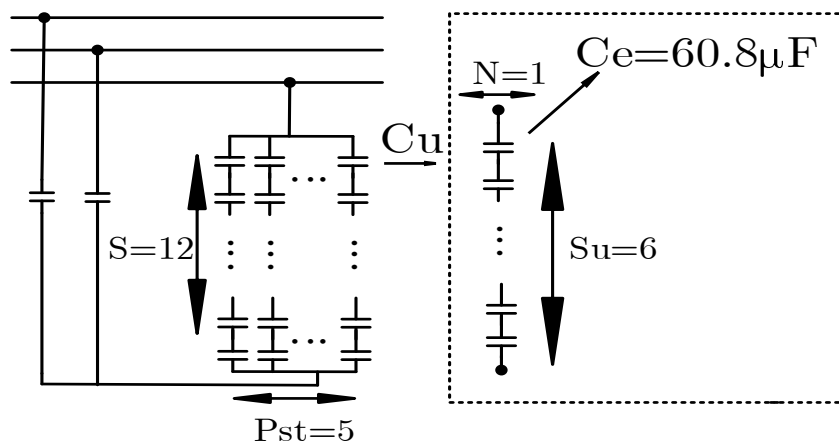
Figure B.2: 230 kV fuseless ungrounded single wye SCB.
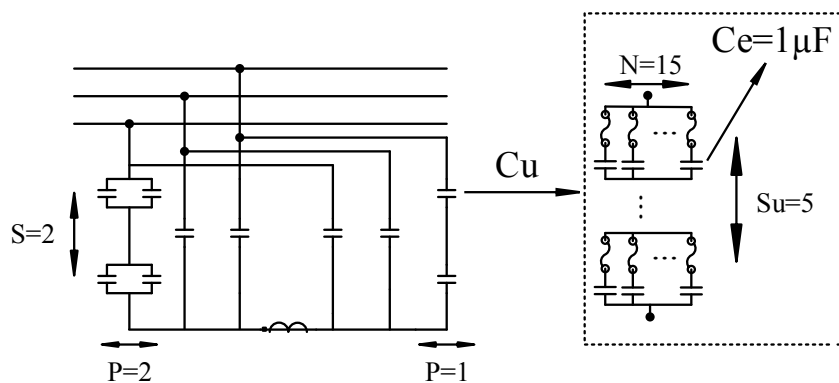
Figure B.3: 230 kV internally fused ungrounded double wye SCB with single string per phase for each section.
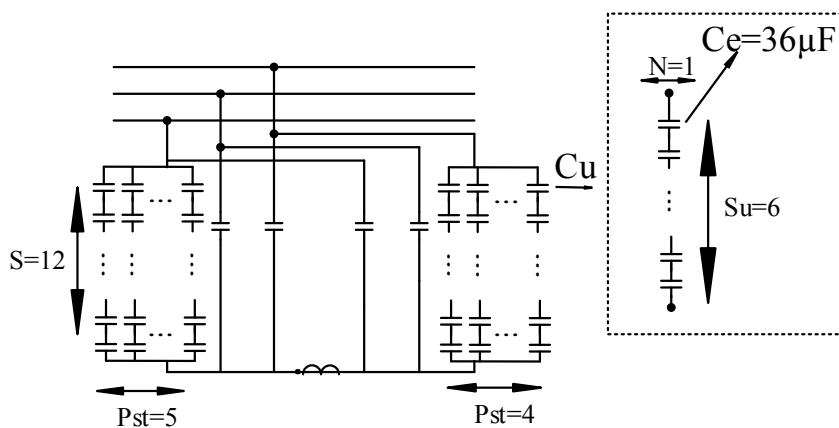
Figure B.4: 230 kV fuseless ungrounded double wye SCB.
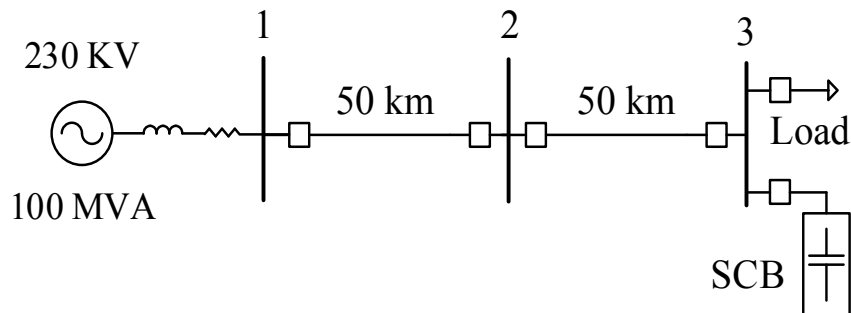
Figure B.5: Schematic of the simulated power system

Table B.1: System Parameters

Parameter	Value
Source Impedance	$Z_1 = 1.5 + j10$ $Z_0 = 15 + j30$
External Impedance	$5 + j50$
Balanced Load	About 40 MW per phase (dependent on the SCB capacity) at 0.9 power factor lagging
Transmission Lines	$Z_1 = 25.45\,\Omega\angle85.9\,\mathrm{deg}$ $Z_0 = 68.76\,\Omega\angle74.6\,\mathrm{deg}$

Table B.2: Utility Banks Construction Data

SCB	Su	N	P	S	Pst-L	Pst-R
Fig. 4.8	11	1	1	8	1	7
Fig. 4.10	11	1	1	5	1	6

The existing utility system discussed in Section 5.10 and the corresponding SCB construction data are shown in Fig.B.6 and Table B.3 , respectively, as follows.
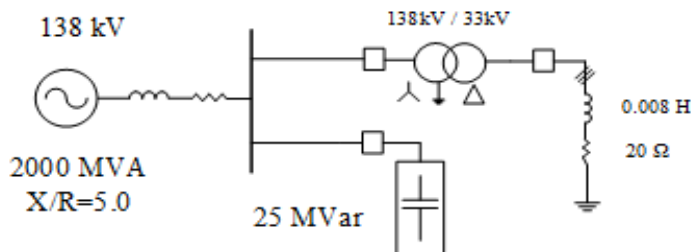
Figure B.6: Single line diagram of the existing utility system.

Table B.3: Construction data for single wye SCB and each bank of the double wye SCB

Protection Element	Ce	Su	N	S	Pst
Neutral Voltage Unbalance	58.936	6	1	6	2
Neutral Current Unbalance	58.936	6	1	6	1

Table B.4 shows the bank construction data for the externally fused SCB, this has been adapted from provided data in [1, 2].

Table B.4: Construction data for the single wye SCB with externally fused units

Ce	Su	N	S	P
3.316	8	3	5	14

Appendix C

Plot of Additional Signals During External Unbalance

Residual and Neutral Voltage for Single Wye SCB

To demonstrate the changes in residual and neutral voltages upon internal and external failures the following scenarios are selected. An internal failure taking place at 0.25 second, in the phase C of a fuseless wye SCB is simulated under three conditions. First, when we have the failure only, second, when we have the failure and a shunt power system fault in the middle of the transmission line with 100 ms clearing time, and last, when we have the failure happening while the same phase is open, in a 360 ms open pole tripping and a subsequent reclosure scenario.

As per equations (4.16)-(4.24) in the SR based proposed method, in addition to phase voltages, the neutral voltage and zero sequence voltage are contributing in the fault location principle definition; therefore, the plots of these two variables in the three aforementioned case studies, are presented here. Figs. C.1-C.3 illustrate the comparison for the three aforestated scenarios, respectively. Simulations include presence of pre-existing SCB unbalance, harmonics, measurement noise, and voltage unbalance.

The effect of internal failure on neutral voltage can be seen in Fig. C.1. In case of external disturbance the results will be different. Affecting both neutral voltage and the zero sequence voltage.

Neutral Current and Compensated Neutral Current for Double Wye SCB

To demonstrate the changes in compensated and uncompensated neutral measurements upon internal and external failures the following scenarios are selected to illustrate the signal variations. An internal failure taking place at 0.25 second, in the phase A of a fused double wye SCB is simulated under three conditions.

First, when we have the failure only, second, when we have the failure and a shunt power system fault in the middle of the transmission line with 100 ms clearing time (includes both phase to phase and phase to ground fault (once phase A another scenario phase B) with 20Ω fault resistance), and last, when we have the failure happening while the same phase is open, in a 360 ms open pole tripping and a subsequence reclosure scenario.
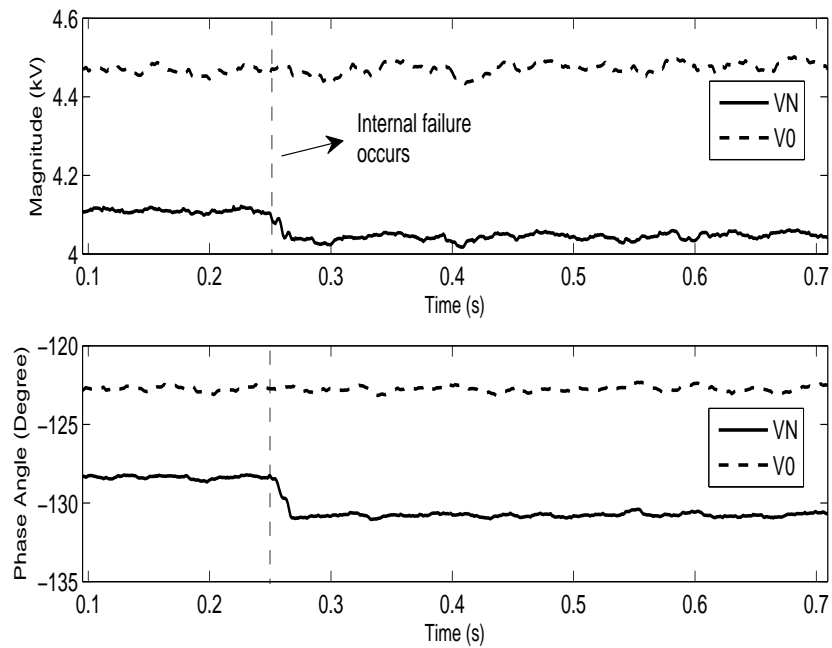
Figure C.1: Neutral voltage and zero sequence voltage, internal failure only (the bank and system have pre-existing unbalance too).
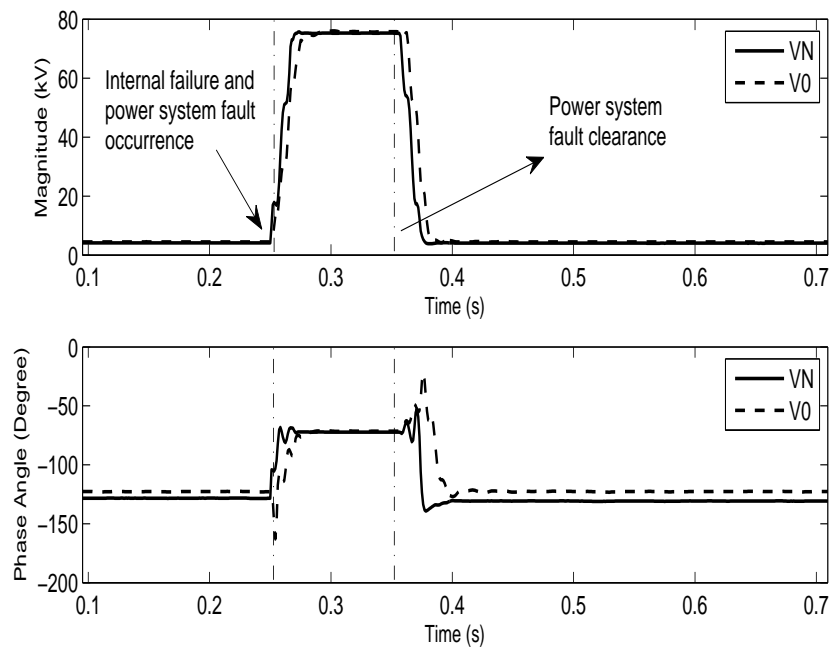

Figure C.2: Neutral voltage and zero sequence voltage, simultaneous internal failure and shunt power system fault.
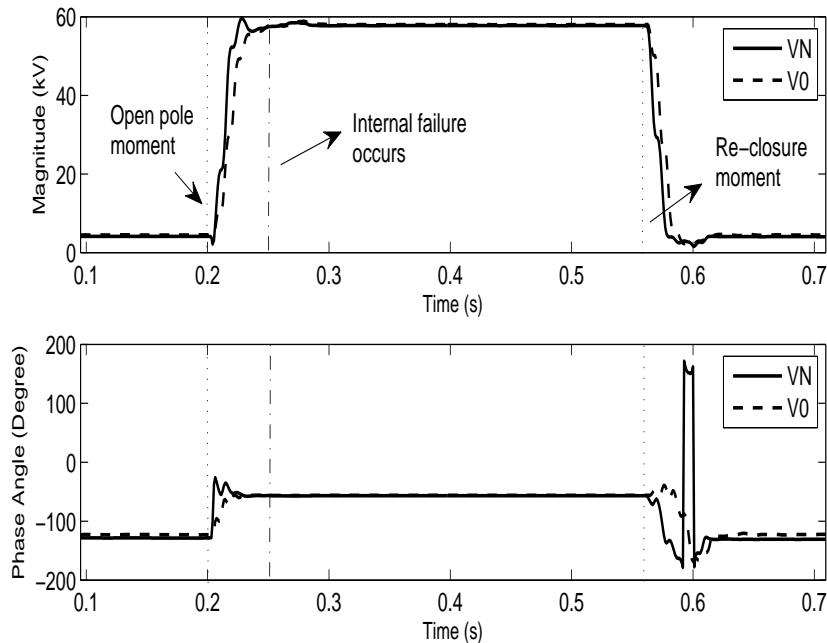
Figure C.3: Neutral voltage and zero sequence voltage, internal failure in one phase of the SCB while the same phase of the line is open.

Figs. C.4-C.13 demonstrate the compensated neutral current, neutral current, and neutral voltage along-with the fault location counter for each of the afore-stated scenarios, respectively.

With reference to Fig. C.5 the internal failure location is determined in less than 50 ms. In addition, Fig. C.4 presents the fact that neutral voltage phase angle variation in case of failure is minimal in double wye SCBs. As can be seen, it takes more than 50 ms to determine the failure location. Also, again the necessity of compensation is apparent in the phase angle plot as the neutral current and voltage phase angles do not follow any special patterns to differentiate an internal failure. Successful fault location determination in various fault resistance and fault clearance times had been validated before, here again we see same results. The only change from the previous scenario is the higher magnitude jump in the neutral voltage. From the figures of both shunt power system faults, and open poles that involve the same phase as the one that includes the internal failure, we conclude that the magnitude of the compensated neutral current does not jump as much as it is expected unless the fault is cleared or the open pole is reclosed. However, for double wye banks in the event of an open pole, the fault location still is reliable and there isn't any need for blocking the fault location function.

For grounded bank, simulations show that there is no need for restraint supervision for fault location. Fault location is not susceptible to external unbalance, except for the introduced detection delays.
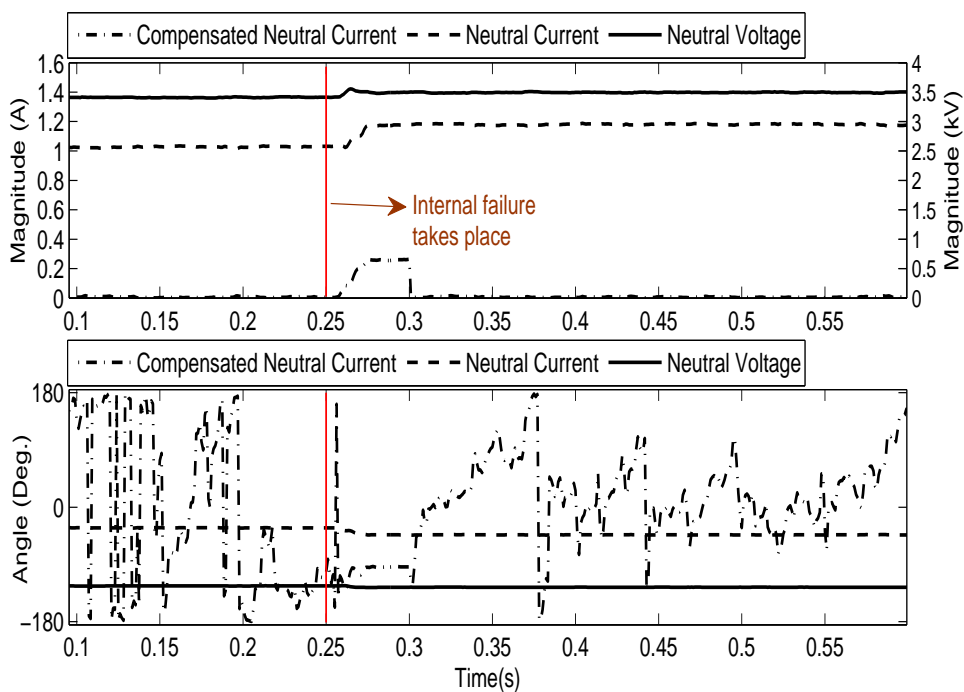
Figure C.4: Neutral measurements for a scenario including an internal failure occurrence

Figure C.5: The proposed fault location counter for an internal failure occurrence

Figure C.6: Neutral measurements for a scenario including an internal failure occurrence during a power system phase to phase fault

Figure C.7: The proposed fault location counter for the scenario of Fig. C.6.

Figure C.8: Neutral measurements for a scenario including an internal failure occurrence during a power system phase to ground fault for the same phase
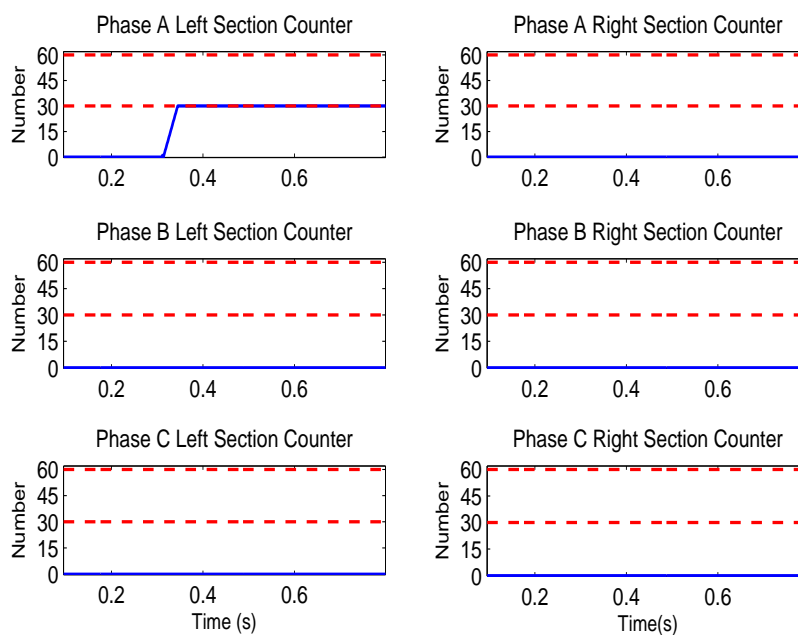
Figure C.9: The proposed fault location counter for the scenario of figure C.8.
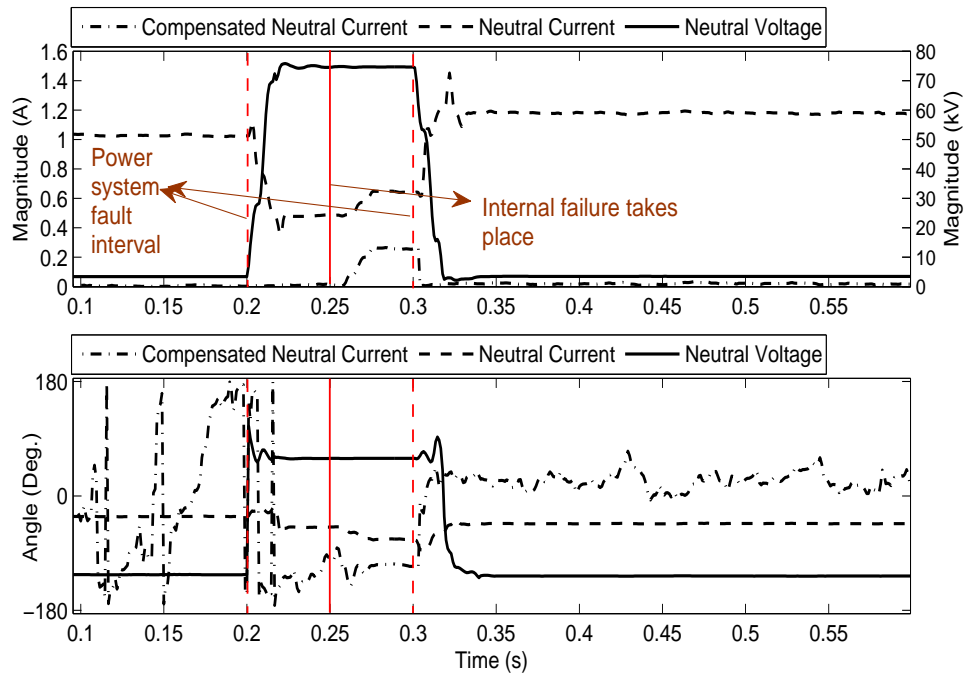
Figure C.10: Neutral measurements for a scenario including an internal failure occurrence during a power system phase to ground fault in another phase
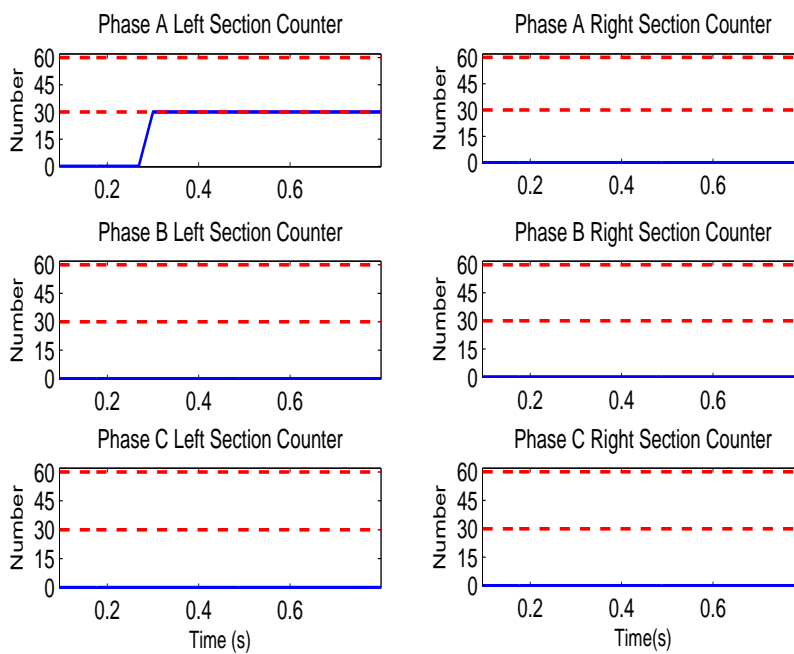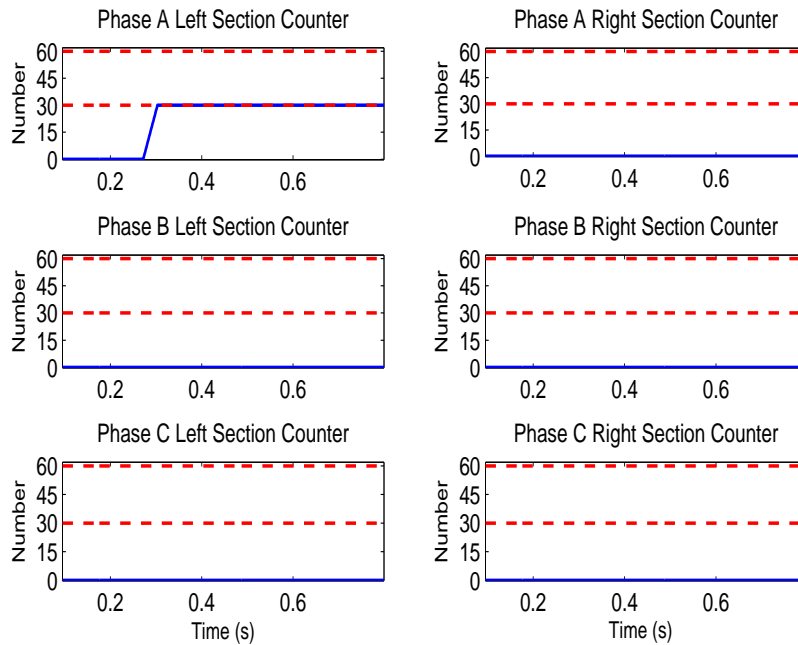

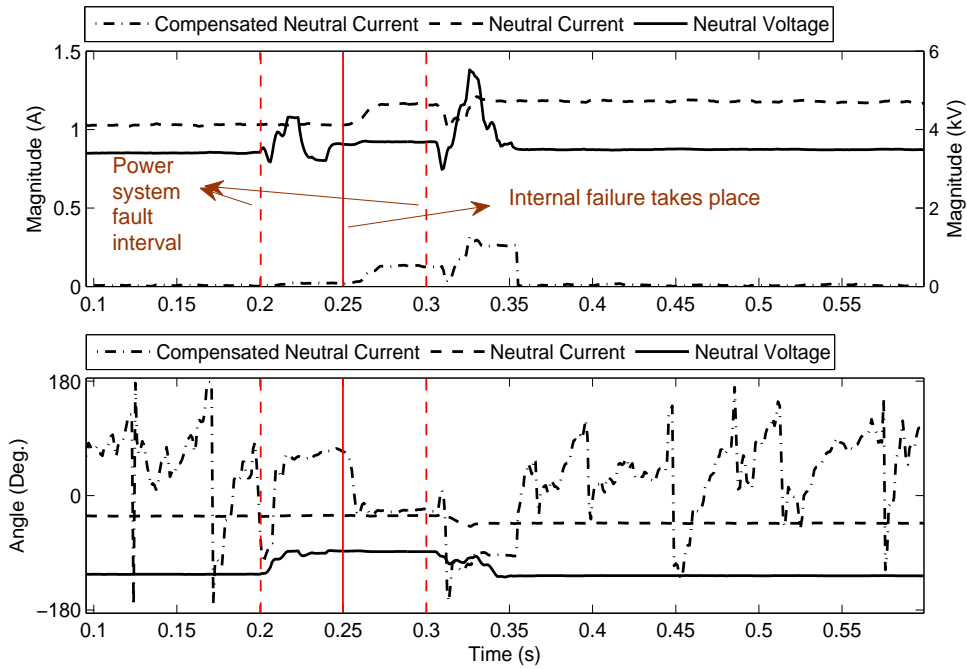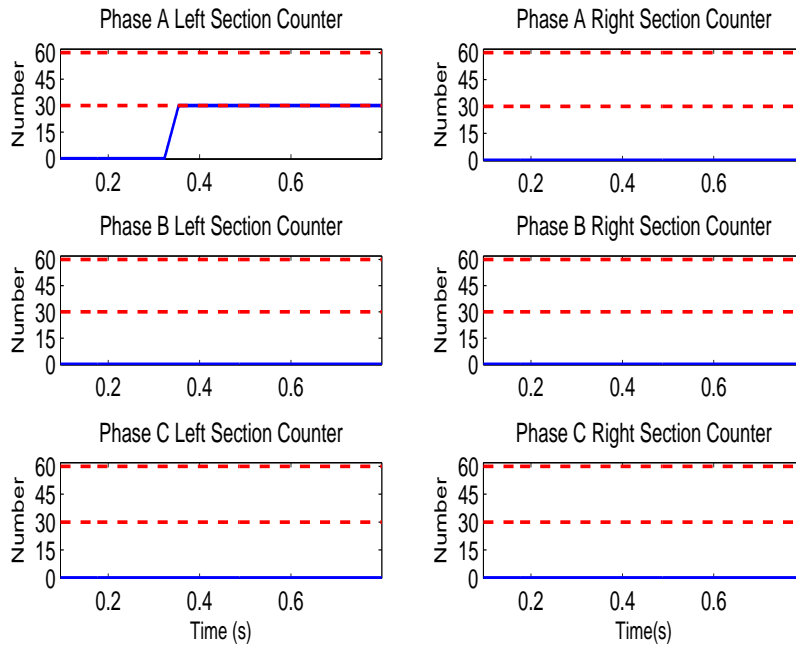Figure C.11: The proposed fault location counter for the scenario of figure C.10.
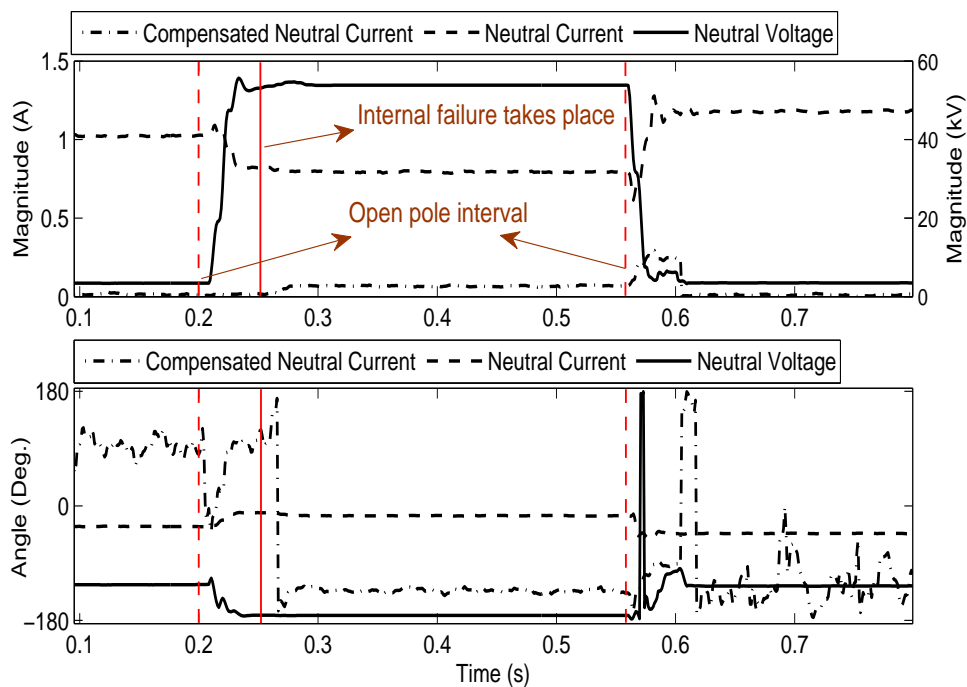
Figure C.12: Neutral measurements for a scenario including an internal failure occurrence during an open pole in the same phase

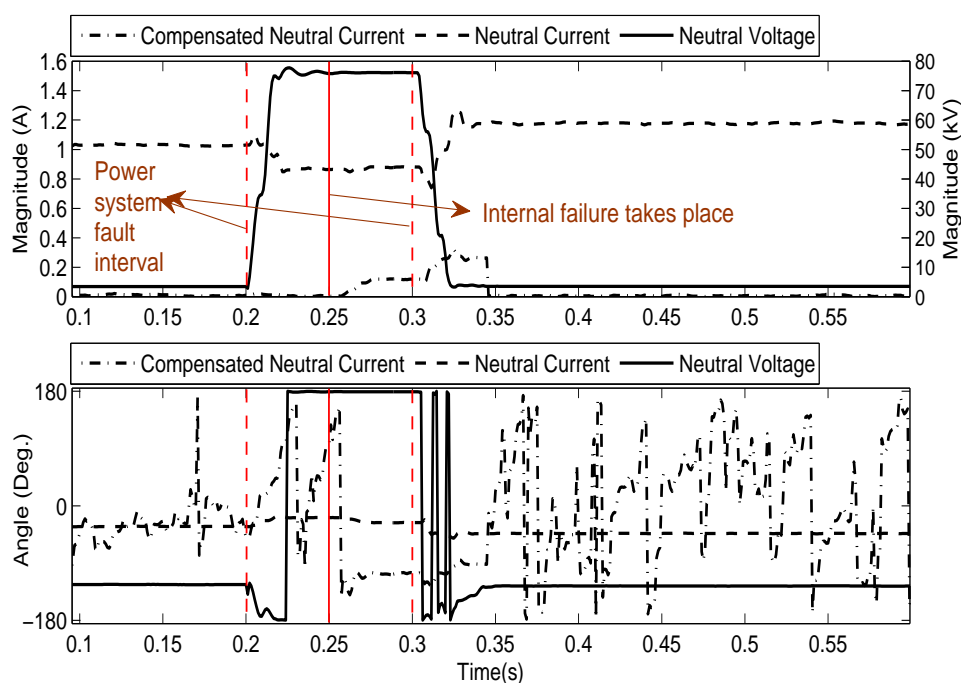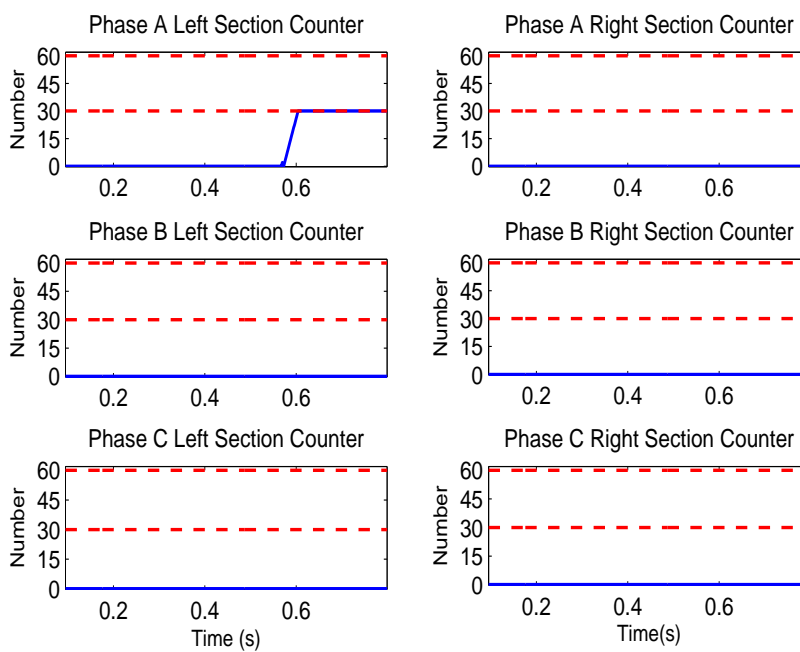Figure C.13: The proposed fault location counter for the scenario of figure C.12.

Figs. C.14, and C.15 show the way that same phase shunt fault and other phase shunt faults, respectively, affect both the fault location principle (compensated value), and the uncompensated measurement.

As can be seen in Figs. C.15, and C.14 unlike the ungrounded bank, Figs. C.8, and C.10, the effect of same phase faults and the faults that do not involve the phase that has the failed element are the same for grounded banks and that is why both of the scenarios for grounded banks result in detection delay.
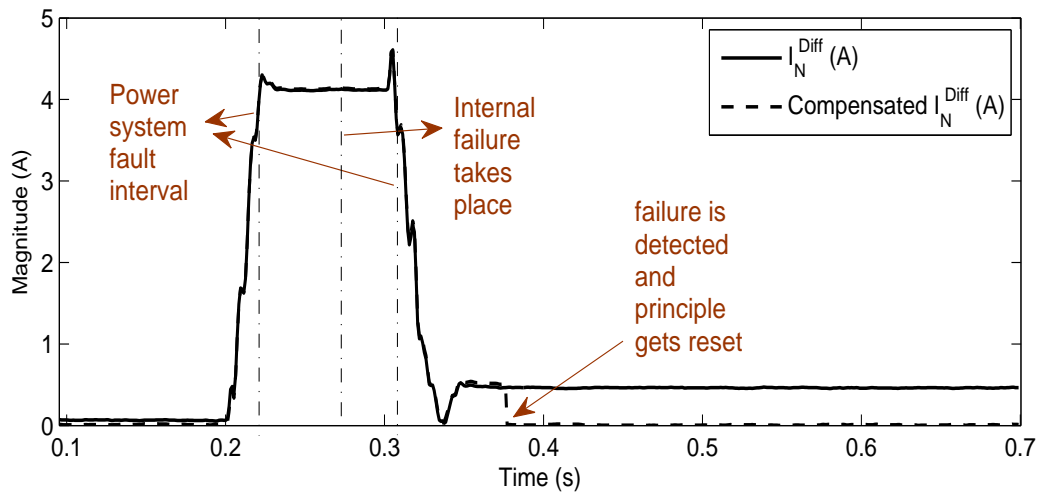
Figure C.14: Compensated and uncompensated neutral current for fault in phase B and internal failure in phase B
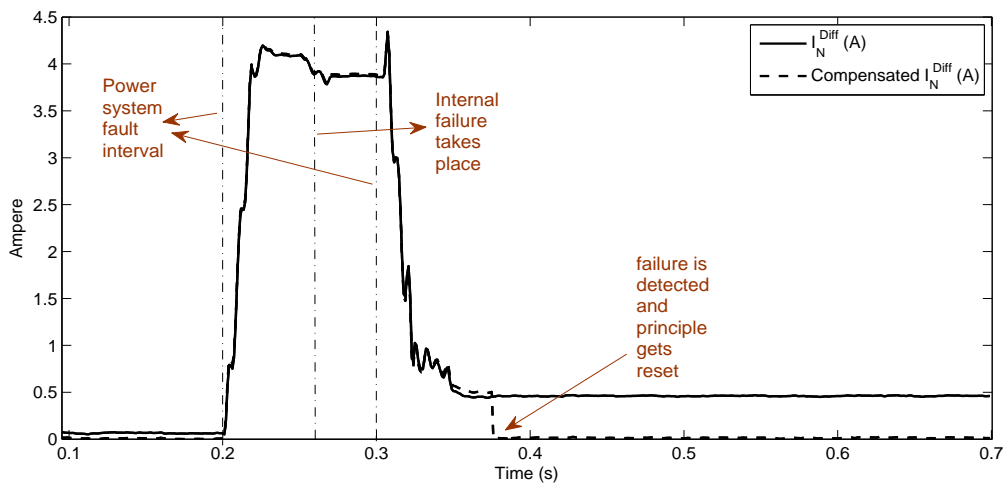
Figure C.15: Compensated and uncompensated neutral current for fault in phase A and internal failure in phase B

Appendix D

Additional Simulation Results on Measurement Accuracy

In this appendix some simulation results which demonstrate the successful performance of the proposed fault location methods considering instrumentation errors, system unbalance, and harmonic rich scenarios, are presented.

Impact of system unbalance, capacitor inherent unbalance, and both of these unbalances on the estimated superimposed reactance quantity is shown in Figure D.1. The simulated failures have been:

- Single element failure in phase A at 0.2 s

- Double element failure in phase B at 0.25 s

- Consecutive failure in phase A at 0.3 s

- Double element failure in phase C at 0.35 s
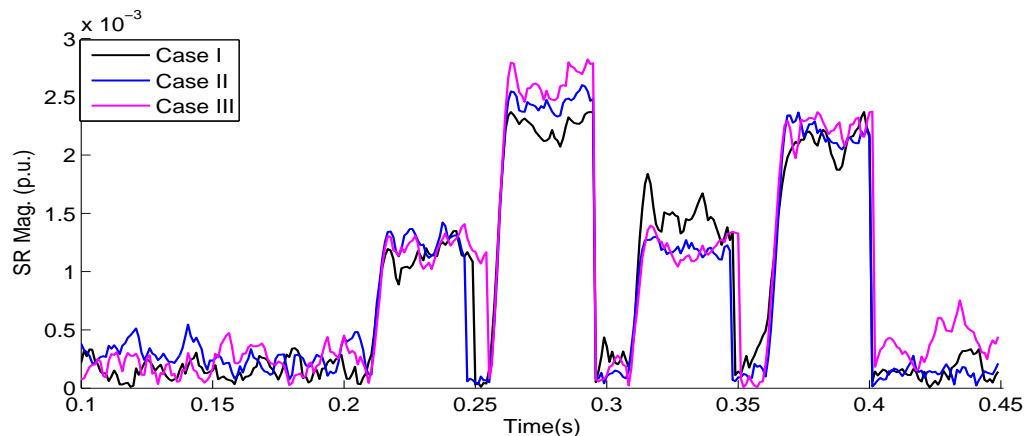
Figure D.1: Superimposed Reactance Magnitude, case I: system unbalance and capacitor unbalance, case II: capacitor unbalance only, case III: system unbalance only.

Simulations have verified the successful fault location report for the simulated cases. This is due to the fact that irrespective of the level of unbalance between three phase phasors, each phase's estimated voltage phasor is accurate. Also the calibrating factors effectiveness ensure reliable online monitoring of the capacitor failures. Our simulations have also validated the performance of the proposed methods for system unbalances of 8 %. In practice voltage unbalance in transmission systems is required to be kept as low as 2 % or less.

With regard to CT/PT errors, we should point out that the proposed methods have differential property and apart from the initial compensation, that negates any pre-existing unbalance measured due to errors, they apply thresholds and zones to account for the remainder of error consequences.
In general by deploying magnitude zones, i.e. upper and lower limits for magnitude thresholds, or blocking by means of time delays or supervision from other protective functions of a capacitor bank multi-functional numerical relay, the proposed method security during system faults is also taken care of. We do block the monitoring function because we do not deal with system faults. This is due to the fact that the monitoring function is dedicated to internal failures that impose minor changes on the measurement channels. As verified in Chapter 5, even in worst case scenarios upon clearance of the disturbance the transient error will vanish and even an internal failure event that might occur during these severe transients will be eventually monitored and recorded in capacitor element failure reports.

Based on reference [56], the errors of a CVT and inductive voltage transformer, change very little for voltage variations and the voltage dependence can for all practical applications be neglected. To investigate ratio errors, a maximum ratio error of 6% from rated values in voltage transformers and CVTs [56] was simulated. Figure D.2 shows the impact of the ratio error on the superimposed reactance. In this figure, no measurement noise case, 50 dB SNR case, and 50 dB SNR plus 6% ratio error are shown for online monitoring of the selected scenario earlier mentioned in this appendix. Simulations have verified successful fault location for these scenarios.
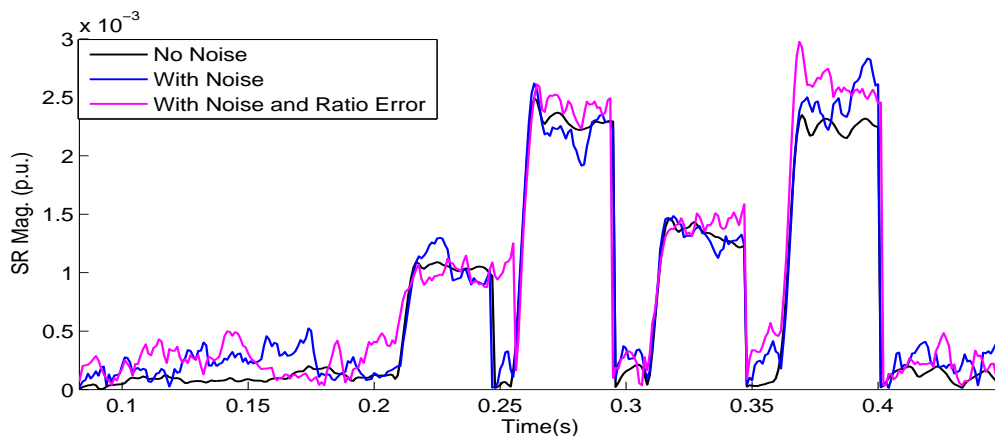

Figure D.2: Superimposed Reactance Magnitude, case I: no measurement noise, case II: 50 dB SNR. case III: 50 dB SNR and 6% ratio error.

For CT errors, we assumed a high ratio error of 10% [56] for another illustrative scenario under system fault for a SCB grounded through CT. The simulation scenario includes the following events:

- A Phase B to Ground Fault at 0.2 s which lasts for 100 ms

- Two elements failure in phase B of the capacitor bank at 0.25 s

As can be seen in Figure D.3, the change in the SR has been negligible. This figure has been zoomed to the time interval in which the decision criteria has been satisfied and the internal failure is detected.
Applying different potential transformer characteristics (B-H curves) or different PSCAD CT models have also verified successful performance of the proposed methods.
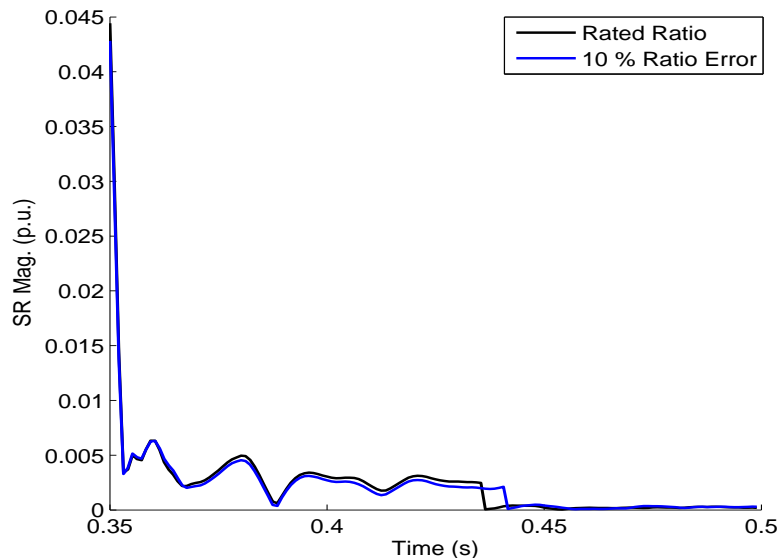
Figure D.3: A closer look at the SR considering Neutral CT ratio error.

As explained, our studies have considered non-ideal scenarios. Power system harmonics, and measurement noise are other factors we have considered. The reason the proposed methods are robust against such factors is the fact that:

- The proposed method does not rely on any new measurement and only requires the actual measurements present in the HV substations today.

- The relay model for the proposed methods deploys the filters that numerical relays deploy in practice and is therefore reliable under non-ideal conditions. These filters include: Anti-Aliasing filter, CVT Transient filter, Decaying DC Removal, and DFT filter (fundamental frequency phasor estimation).

A low pass analog filter is part of the hardware acquisition in commercial numerical SCB protection and control relays [45]. Further, digital filters with half power points of 640

Hz in product [45] or 100 Hz in product [57] are part of the input processing before the phasor calculation is performed.

In our simulations, DFT is applied for fundamental frequency phasor estimation. DFT is a long window phasor estimation algorithm which is generally considered to be immune to noise and harmonics to an acceptable extent. Frequency response of real and imaginary filter of the applied full cycle DFT with 64 samples per power system period are shown in Fig. D.4. The attenuation level for harmonics is effective while the 64 samples per cycle is one that is actually deployed in some commercial relays [3].
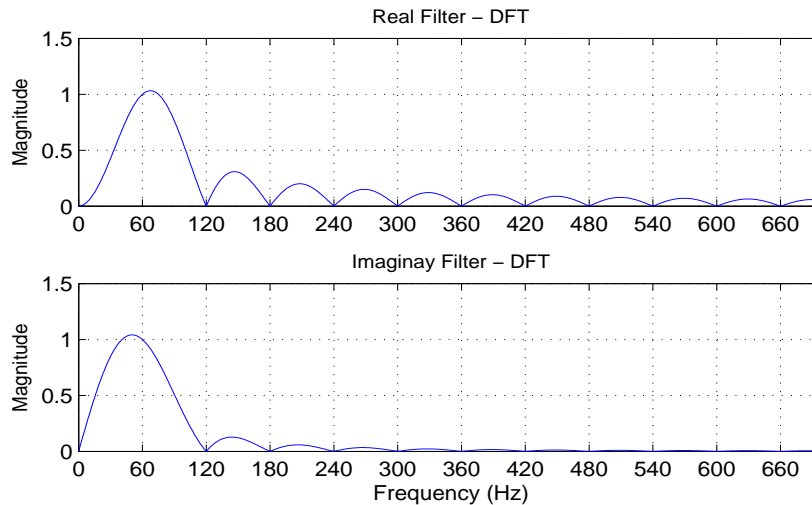
Figure D.4: Full cycle DFT: frequency response.
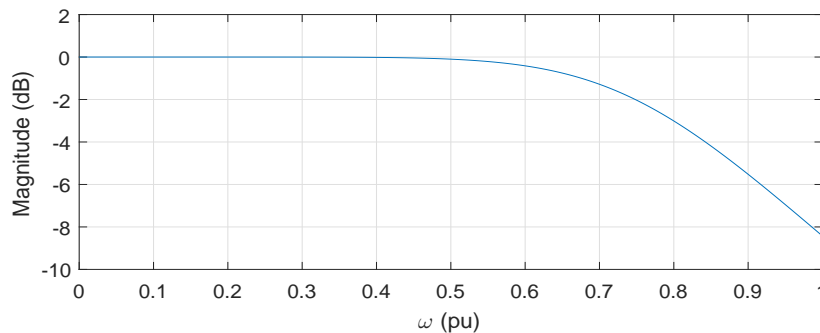
Figure D.5: Frequency response of the applied anti aliasing filter.

Neutral current waveform of a sample scenario in which a single element fails in one of the six possible locations of a double wye bank is selected to show the effectiveness of the low pass filter and the applied DFT filter, see Fig. D.6. Note that the uncompensated neutral current is depicted in this figure, i.e. the signal also carries the system unbalance and pre-existing internal unbalance of the bank besides the noise and harmonics. This demonstrates that the algorithm has been robust and able to extract the fundamental frequency phasor with an acceptable capability. To further validate the proposed method performance we made the harmonic injections 10 times richer and results verified same successful determination of the fault location. The reason is that the fundamental frequency phasor of the phase and neutral currents are estimated accurately. Fig.D.7 shows

the neutral current waveform, and the estimated fundamental frequency phasor for this scenario.

Figure D.6: Low pass filter and DFT filter application on the measured signal.

Figure D.7: Low pass filter and DFT filter application on the measured signal for system with ten times richer harmonic sources.

Appendix E

Further on SCB's Protection and Internal Failures

During this study some useful information from utility practice was learned and here is a summary of the main parts.
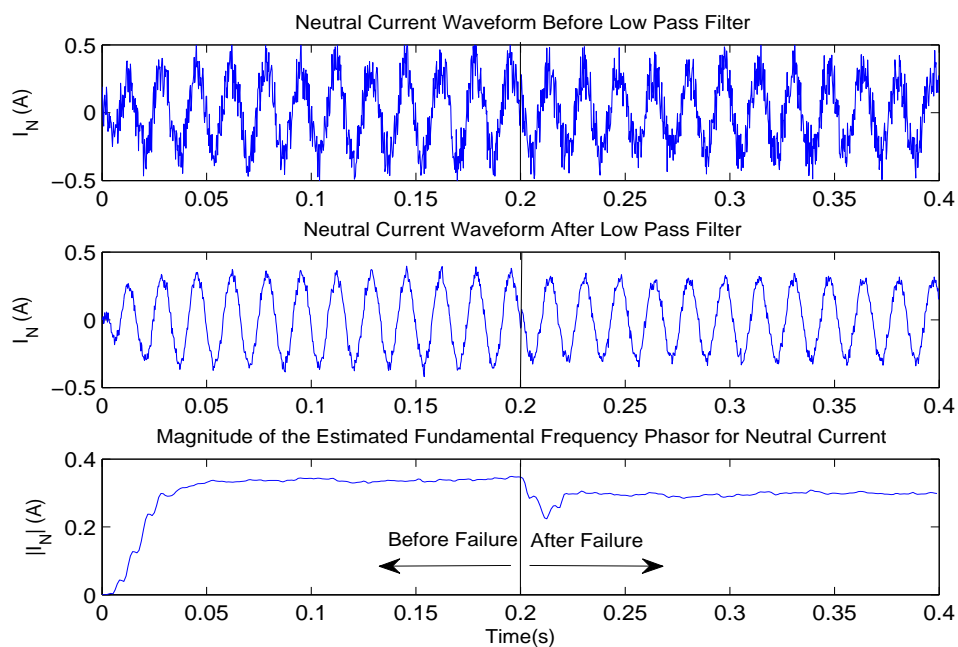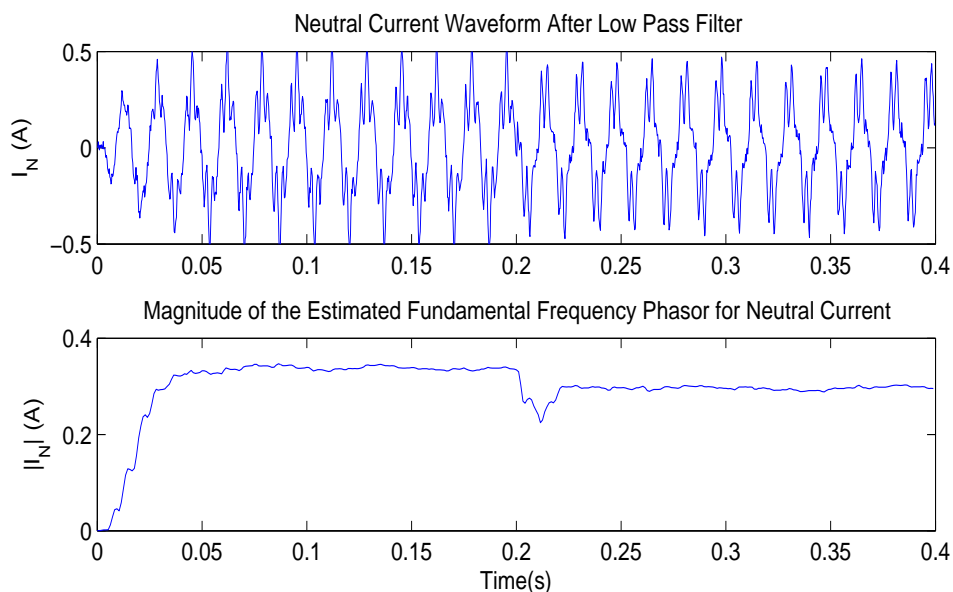
E.1 Other protection functions for SCBs

Apart from fusing, which is the first line of protection against over-current, and unbalance relaying, which is the subject of the present thesis and helps to disconnect the SCB to prevent from cascading failures inside the SCB, HV shunt capacitor banks are protected in various ways by different utilities. Common protection elements include the followings. Applicability of these functions depends on which CTs or VTs are available and the protection philosophy of the utility:

No Volt Protection On supply failure, SCBs should be disconnected and locked out to prevent from automatic switch-on upon resumption of grid supply. Reclosing is only allowed after passing the capacitor's expected safe discharge time. Even sudden voltage dips may cause the charged capacitors discharge into the terminal equipment and damage them [18].

Line and Overvoltage Protection The overall cover for the complete capacitor bank and any ancillary equipment, including cabling, busbars, and other external connections is line and over voltage protection [58]. In particular, this would be overcurrent function sensitive to true rms current and overvoltage protection for prolonged exceeding in the voltage, over 1.1 pu. Principally, the unbalance protection is intended to detect failed elements inside the SCB and prevent from cascading failures by tripping the bank before the stressed elements fail. However, in a healthy bank external problems can still make elements overstressed. Protection from system overvoltages that might cause this overstress is done via overvoltage protection [3].

Overcurrent Protection In order to detect line-to-line faults or bus ground faults outside the shunt capacitor banks, overcurrent relays (OCRs) are applied in connection with current transformers (CTs) [13].

E.2   Resistive Potential Devices (RPDs)

Some utilities employ resistance type voltage sensing devices for voltage monitoring of shunt capacitor banks. A commercial product of this type is S&C 15 Volt Ampere Potential [5]. The 15 VA Resistive Potential Device (RPD) is applicable to neutral to ground connection of ungrounded wye connected SCBs. For intermediate tap point to ground connections on grounded wye SCBs, and for line to ground connections in all other applications 30 VA RPDs are applicable. The RPDs have constant current output like CTs. An adjustable burden resistor is connected across the output terminals and produces an output voltage directly proportional to the voltage applied to the line terminal.

Particularly, the superiority of the 15 VA devices are first that they do not possess resonant characteristics and are immune to ferroresonance, unlike CVTs. Their limited frequency response makes them ideal for locations with high frequency transients. Second, unlike VTs, they do not saturate when subjected to switching overvoltages. As the 15 VA RPDs are immune to these voltage surges they are suitable for neutral voltage monitoring for increased sensitivity since they can be applied in ratings below the system nominal voltage. The output of RPDs has minimal phase shift and excellent linearity at low voltages. Figure E.1 illustrates a simplified diagram for a RPD connected across a low voltage capacitor. Figure E.2 depicts a more detailed schematic for the 15 VA S&C potential device. The high voltage resistor in Figure E.2 is in the range of tens of $M\Omega$.

E.3   Rack bonding

Substation capacitor units are typically mounted in racks that are insulated from the ground. One side of a parallel set of capacitors is connected to the line side of the system. The other side of the capacitors is typically either connected directly to the frame (if aluminum) or to an aluminum bus directly connected to the frame. All rack voltages are anchored at the voltage potentials of some particular capacitor unit terminals by rack bonding, i.e. the rack must be tied to a fixed potential, otherwise the voltage the capacitor bushing will be subjected to cannot be determined.
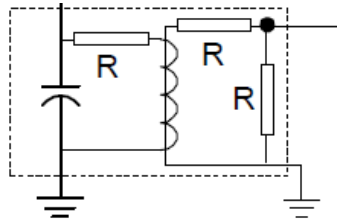
Figure E.1: Resistive divider for voltage sensing in SCBs [1].
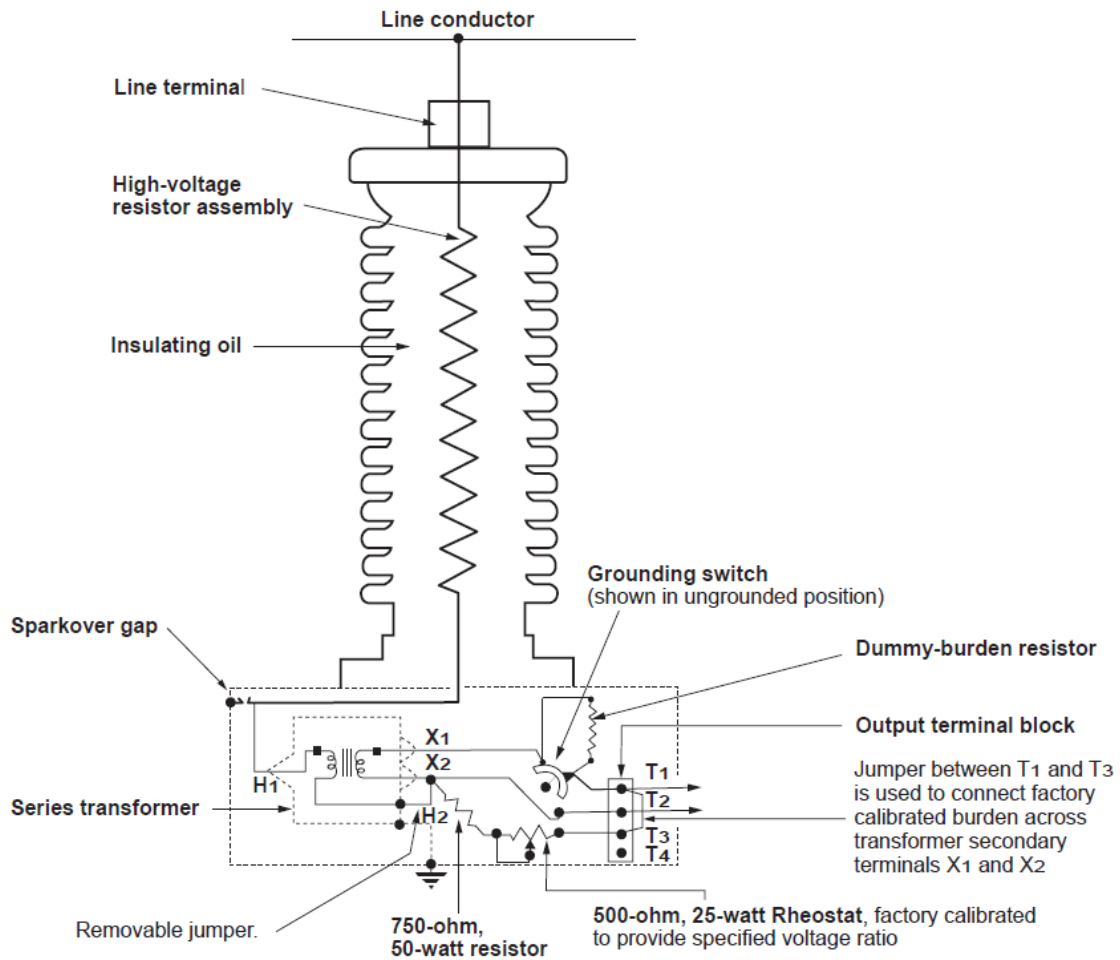
Figure E.2: S&C 15 VA Potential Device Schematic [5].

Curriculum Vitae

Name: Hessamoddin Jouybari Moghaddam

Education: University of Western Ontario
London, ON
2013 - 2017, Ph.D. ECE
GPA: 91.6 %

Tehran Polytechnic (Amirkabir University of Technology)
Tehran, Iran
2010 - 2012 M.Sc. ECE
GPA: 18.02/20

Ferdowsi University of Mashhad
Mashhad, Iran
2006 - 2010 B.Sc. ECE
[Ranked first amongst the power group students]

Honours and Western ECE Graduate Student Award for Excellence in Research
Awards: 2017
Ferdowsi University Academic Foundation Award
2010

Publications:

Journal papers

- H. Jouybari-Moghaddam, T. S. Sidhu, M. R. Dadash Zadeh, P. Parikh, Shunt Capacitor Banks Online Monitoring Using a Superimposed Reactance Method, Accepted for *IEEE Transactions on Smart Grids*.
  http://dx.doi.org/10.1109/TSG.2017.2690643.

- H. Jouybari-Moghaddam, T. S. Sidhu, M. R. Dadash Zadeh, P. Parikh, Enhanced Fault Location Scheme for double wye shunt capacitor banks, *IEEE Transactions on Power Delivery*, vol.32, no.4, pp. 1872 -1880, Aug. 2017.

- H. Jouybari-Moghaddam, S.H. Hosseinian, B. Vahidi, Grid reconnection detection for synchronous distributed generators in stand-alone operation, *International Transactions on Electrical Energy Systems (formerly ETEP)*, John Wiley & Sons. vol.25, no.1, pp. 138 -154, Jan. 2015.

- H. Jouybari-Moghaddam, B. Vahidi, S.H. Hosseinian, Rotational Invariance Technique for Evaluation of Perturbed Lightning Impulses, *IEEE Transactions on Power Delivery*, vol. 28, no. 1, pp. 531-533, Jan. 2013..

- H. Jouybari-Moghaddam, A. Alimardani, S.H. Hosseinian, Influence of Electric Vehicle Charging Rates on Transformer Derating in Harmonic-rich Battery Charger Applications , *Archives of Electrical Engineering*, Polish Academy of Sciences, vol. 61, no. 4, pp. 483-497, Dec. 2012.

- H. Jouybari-Moghaddam, G. B. Gharehpetian, S.H. Hosseinian, Performance of power-line-signaling based detection algorithms for islanding protection of distributed generators in interharmonic polluted systems, *Renewable Energy & Power Quality Journal*, Paper 272, No. 10, Apr. 2012.

Conference Papers

- H. Jouybari-Moghaddam, T. S. Sidhu, I. Voloh, M. R. Dadash Zadeh "New Method of Capacitors Failure Detection and Location in Shunt Capacitor Banks", Accepted for 2017 Western Protective Relay Conference, Spokane, WA, USA, October 17-19, 2017.

- H. Jouybari-Moghaddam, T. S. Sidhu "A Study of Capacitor Element Failures in High Voltage Capacitor Banks", IEEE CCECE 2017, Windsor, ON, Canada, 30 April-3 May, 2017.

- H. Jouybari-Moghaddam, T. S. Sidhu, P. Parikh, I. Voloh "Enhanced Fault Location Method for Shunt Capacitor Banks", Texas A&M 70th Annual Conference for Protective Relay Engineers, College Station, TX, USA, April 3-6, 2017.

- H. Jouybari-Moghaddam, T. S. Sidhu, P. Parikh, "A Study of Fault Location Method in Double Wye Shunt Capacitor Banks", CIGRE Canada Conference, Vancouver, Canada, October 17-19, 2016.

- H. Jouybari-Moghaddam, S.H. Hosseinian, B. Vahidi, Active distribution networks islanding issues: An introduction, in proc. 11th International Conference on Environment and Electrical Engineering, EEEIC12, Venice, Italy, 18-25 May, 2012.

- H. Jouybari-Moghaddam, S.H. Hosseinian, B. Vahidi, Automatic Local State Detection for Synchronous Distributed Generators, in proc. 11th International Conference on Environment and Electrical Engineering, EEEIC12, Venice, Italy, 18-25 May, 2012.

- H. Jouybari-Moghaddam, S.H. Hosseinian, A. Alimardani, Application of a Probabilistic Approach to Distribution Transformer Derating Calculation, in proc. 17th Electric Power Distribution Conference, EPDC12, Tehran, Iran, May 1-2, 2012.

- H. Jouybari-Moghaddam, S.H. Hosseinian, B. Vahidi, M. Ghiasi Rad, Smart Control Mode Selection for proper operation of Synchronous Distributed Generators, 2nd Iranian Conference on Smart Grids (ICSG 2012), Tehran, Iran, May 24-25, 2012.

- H. Jouybari-Moghaddam, H. Javidi, Genetic Algorithm Based Optimal Sizing and Sitting of Different Distributed Generators for Voltage Profile Improvement and Active Loss Minimization , 13th Iranian Student Conference on Electrical Engineering (ISCEE), Tehran, Iran, Sep. 2010 (in Persian).